ISOLATION AND ELUCIDATION OF STRUCTURES OF BIOLOGICALLY ACTIVE SECONDARY METABOLITES FROM VARIOUS ORGANISMS, INCLUDING CYANOBACTERIA, SPONGES AND *ARECA CATECHU*

A DISSERTATION SUBMITTED TO THE OFFICE OF GRADUATE EDUCATION OF THE UNIVERSITY OF HAWAI‘I AT MĀNOA IN PARTIAL FULFILLMENT OF THE REQUIREMENTS FOR THE DEGREE OF

DOCTOR OF PHILOSOPHY

IN

CHEMISTRY

DECEMBER 2017

By

Ram Prasad Neupane

Dissertation Committee:

Philip G. Williams, Chairperson
Marcus A. Tius
Joseph T. Jarrett
Ho L. Ng
Qing X. Li

In most likelihood, I would not have taken off on this academic journey without the selfless involvement of my primary school teacher Mr. Ganga Prasad Shrestha many years ago. This dissertation is dedicated to him.

ACKNOWLEDGMENTS

The work described in this dissertation has been possible because of the contributions of many key figures. I am deeply indebted to Professor Philip Williams for his support, guidance, teaching and endless patience over the last several years. I have been extremely fortunate to find an adviser like you. I am also very grateful to the entire dissertation committee for their unwavering support during the course of this academic journey. Thank you, Professors Marcus Tius, Joseph Jarrett, Ho Ng and Qing Li! Professor John Head's help with computational chemistry has been extremely invaluable. My gratitude also goes to the rest of the faculty and the support structure in the chemistry department at the University of Hawai‘i at Mānoa and I would like to especially acknowledge Wesley Yoshida for his incredible help with NMR spectroscopy.

A lot of the work described here was made possible by the efforts of coworkers and collaborators. I am appreciative of the help and data provided by Casey Philbin, Dr. Stephen Parrish, Dr. Jingqiu Dai, Zhibin Liang, Joshua Gurr, Professor Reinhold Penner, Dr. Malika Faouzi, members of the Turkson group and the Matter group at the University of Hawai‘i Cancer Center, and Professor Alison Sherwood. Thank you to my current and former lab mates and fellow graduate students for important conversations throughout my time here.

This journey would not come this far without my family. I cannot find words to express my deepest appreciation to my parents and siblings for their love and support even in the most difficult times. Jayanti, thank you for the unconditional support I have received from you over the last five years that we have spent together.

ABSTRACT

Investigation of extracts of several biological specimens, including cyanobacteria, sponges and Areca nut, for activity in various biological assays led to the isolation of several known and new secondary metabolites. Sesquiterpene quinones and hydroquinones isolated from the sponge *Dactylospongia elegans* Thiele (Thorectidae) showed strong to moderate cytotoxicity (CC_{50} between 2.4 and 22.6 μM) against human glioblastoma (U251MG) and human pancreatic carcinoma (Panc-1) cell lines. Furthermore, ilimaquinone (IC_{50} 65 μM) and smenospongine (IC_{50} 78 μM) exhibited moderate inhibition of BACE1, an enzyme implicated in the pathogenesis of Alzheimer's disease. The aqueous fractions of the extracts of *Areca catechu* L. (Arecaceae) displayed Ca-signaling effects in immune (Jurkat, U937 and RBL-2H3) cell lines and the components responsible for this activity may be oligomeric or polymeric flavonoids. The utility of prediction of ^{1}H and ^{13}C NMR chemical shifts using density functional theory computations was demonstrated in the elucidation of structures of three new molecules.

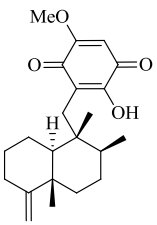

2.3

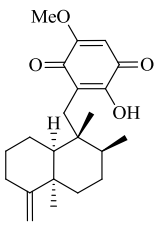

2.4

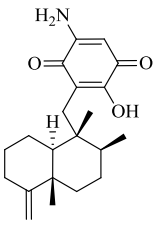

2.5

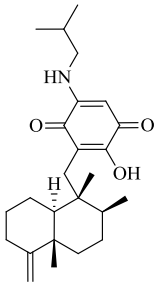

2.6

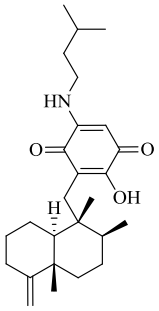

2.7

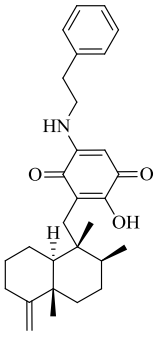

2.8

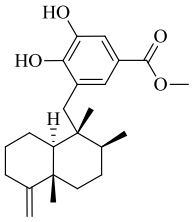

2.9

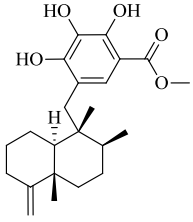

2.10

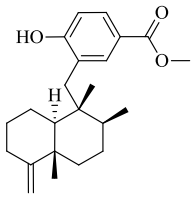

2.11

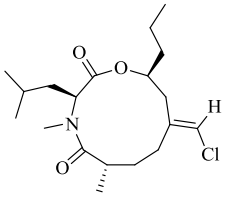

2.12

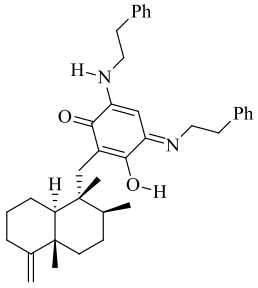

2.24

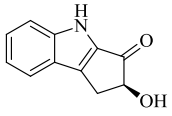

3.6

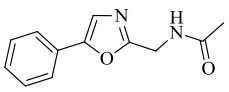

3.7

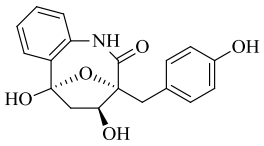

3.8

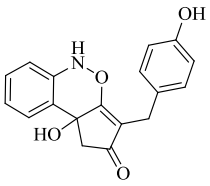

3.9

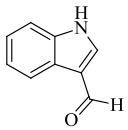

3.10

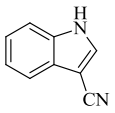

3.11

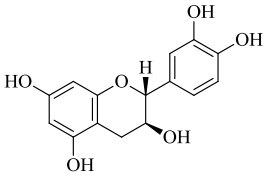

4.5

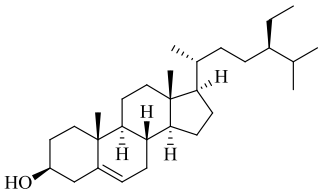

4.18

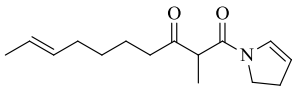

5.6

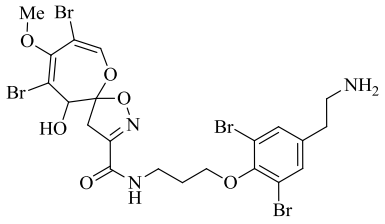

5.2

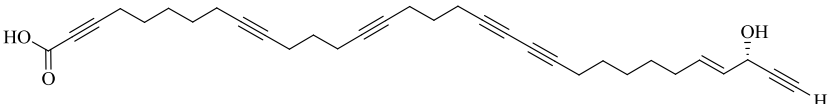

5.1

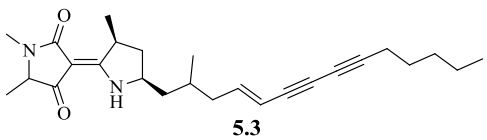

5.3

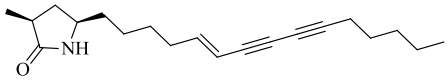

5.4

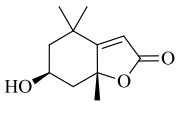

5.5

TABLE OF CONTENTS

LIST OF TABLES

LIST OF FIGURES

LIST OF SCHEMES

LIST OF ABBREVIATIONS

6-31+G	basis set in density functional theory calculations
6-311+G	basis set in density functional theory calculations
$[\alpha]_D^T$	specific rotation at 589 nm and temperature T in ºC
Aβ	beta amyloid protein
A$\beta_{40/42}$	beta amyloid protein fragments containing 40 or 42 amino acids
ACH	amyloid cascade hypothesis
amu	atomic mass unit
ANE	Areca nut extract
APP	amyloid precursor protein
Ara-A	arabinosyladenine
Ara-C	arabinosylcytosine
aug-cc-pVDZ	basis set in density functional theory calculations
AZT	azidothymidine
B3LYP	Becke, 3-parameter, Lee-Yang-Parr (an energy functional)
BACE1	beta-site of amyloid precursor protein cleaving enzyme one
BCE	before common era
BG-11	blue green growth medium
BGM	blue green growth medium with MOPS (*vide infra*) buffer
BLAST	basic local alignment search tool
brd	broad doublet
brs	broad singlet

BuOH	butanol
c	concentration in g/100 mL
°C	degrees in Celsius
C8	octylsilyl (chromatography resin)
C18	octadecylsilyl (chromatography resin)
Ca^{2+}	calcium ion
Ca-signaling	calcium-signaling
calcd	calculated
CC_{50}	50% cytotoxicity concentration
CD	circular dichroism (spectroscopy) or a compact disc (storage device)
$CDCl_3$	deuterated chloroform
CD_3OD	fully deuterated methanol
CIP	Cahn-Ingold-Prelog priority rules for stereochemical description
^{13}C NMR	nuclear magnetic resonance of carbon isotope with mass 13 Daltons
COSY	correlation spectroscopy
δ	chemical shift
d	doublet
1D	one dimensional
2D	two dimensional
Da/kDa	dalton/kilodalton
δ_C	carbon chemical shift
DCM	dichloromethane

dd	doublet of doublets
ddd	doublet of doublet of doublets
dddd	doublet of doublet of doublet of doublets
ddt	doublet of doublet of triplets
Decne.	Joseph Decaisne
δ_H	proton chemical shift
DMSO	dimethyl sulfoxide
DMSO-d_6	fully deuterated dimethyl sulfoxide
DNA	deoxyribonucleic acid
DP4/DP4+	statistical probabilities to compare experimental and predicted data
dq	doublet of quartets
dt	doublet of triplets
E	entgeggen (descriptor in the Cahn-Ingold-Prelog system)
EA	enzyme acceptor fragment
ECD	electronic circular dichroism
ED	enzyme donor fragment
EDTA	ethylenediaminetetraacetic acid
EFC	enzyme fragment complementation
EGTA	ethylene glycol-bis(*β*-aminoethyl ether)-*N*,*N*,*N*',*N*'-tetraacetic acid
EIC	extract ion chromatogram
ESI	electrospray ionization
FDA	Food and Drug Administration

FITC	fluorescein isothiocyanate
Fura-2	calcium-indicating fluorescent dye
Fura-2 AM	calcium-indicating fluorescent dye, acetoxymethyl ester version
GIAO	gauge-independent atomic orbital
GNPS	global natural products social molecular networking
GTPase	enzyme which binds to and hydrolyzes guanosine triphosphate
HL-60	human promyelocytic leukemia cell line
HMBC	heteronuclear multiple bond coherence
HP-20	polystyrene/polydivinylbenzene resin
^{1}H NMR	nuclear magnetic resonance of hydrogen isotope with mass 1 Dalton
HPLC	high pressure liquid chromatography
HREIMS	high resolution electron impact mass spectrometry
HRESIMS	high resolution electrospray ionization mass spectrometry
HRMS	high resolution mass spectrometry
HSQC	heteronuclear single quantum coherence
Hz	hertz
IC_{50}	inhibitor concentration of 50%
ID	identification
IP_3	inositol triphosphate
IR	infrared
^{n}J	coupling constant via n bonds
L.	Carl Linnaeus

LC-ESIMS	liquid chromatography electrospray ionization mass spectrometry
LC-MS	liquid chromatography mass spectrometry
m	multiplet
M-062X	basis set in density functional theory calculations
MAE	mean absolute error
MALDI-MS	matrix assisted laser desorption ionization mass spectrometry
MAPK	mitogen-activated protein kinases
MCMM	Monte-Carlo multiple minimum
MDA-MB-231	human breast cancer cell line
MeOH	methanol
$[M+H]^+/[M+Na]^+$	protonated molecule/sodium adduct
$[M–H]^-$	deprotonated molecule
m/*z*	mass to charge ratio
MHz	megahertz
MOPS	*N*-morpholinopropanesulfonic acid
MRM	multiple reaction monitoring
MS	mass spectrometry
MS/MS	mass spectrometry/tandem mass spectrometry
MW	molecular weight
MWCO	molecular weight cutoff
NIH	National Institutes of Health
NMR	nuclear magnetic resonance

NOE/nOe	nuclear Overhauser effect
Nutt.	Thomas Nuttall
[O]	oxidation
opc	oligomeric procyanidins
p	pentet
Panc-1	human pancreatic carcinoma cell line
PCM	polarizable continuum model
PCR	polymerase chain reaction
PMCA	plasma membrane calcium ATPase pump
PMN	polymorphonuclear leukocytes
ppm	parts per million
q	quartet
qC	quaternary carbon
Qd	quartet of doublets
QQQ	triple quadrupole
R	rectus (stereochemical descriptor in the Cahn-Ingold-Prelog system)
RBL-2H3	rat mast cell line
RBL-M1	rat mast cell line overexpressing the M1 muscarinic receptor
RNA	ribonucleic acid
ROESY	rotating frame Overhauser effect spectroscopy
RP HPLC	reversed phase high performance liquid chromatography
R-Ras	protein coding gene

s	singlet
S	sinister (stereochemical descriptor in the Cahn-Ingold-Prelog system)
sAPP	soluble amyloid precursor protein
SCRF	self-consistent reaction field
SCUBA	self-contained underwater breathing apparatus
SDS	sodium dodecyl sulfate
SERCA	sarco-endoplasmic reticulum calcium ATPase
Si	silica (chromatography resin)
SI	supplementary information
SOCE	store operated calcium entry
sp.	species
$sp/sp^2/sp^3$	$sp/sp^2/sp^3$ hybridization states
spp.	species, plural
16S rRNA	16S ribosomal ribonucleic acid sequencing
STAT	signal transducer and activator of transcription
STAT3	signal transducer and activator of transcription 3
t	triplet
tdd	triplet of doublet of doublets
TDDFT	time dependent density function theory
TNF_{α}	tumor necrosis factor alpha
TOCSY	total correlation spectroscopy
U/mL	units per milliliter

UV	ultraviolet rays
UV-Vis (UVs)	ultraviolet-visible spectroscopy
VEGF-A	vascular endothelial growth factor A
xs	excess

CHAPTER 1

Introduction

1.1 A Brief History of Natural Products

Throughout history, mankind has depended on Nature for medicinal agents to combat a wide variety of diseases and illnesses. While it is extremely difficult to trace the precise origin of traditional medicine, several ancient documents describe the use of formulations from various plant extracts to cure illnesses. Some of the earliest descriptions were documented in the "Ebers Papyrus" in Egypt, the Chinese Materia Medica, the Charaka and the Sushruta and Samhitas from the Indian subcontinent, all of which came before the Common Era.[1] Many of the formulations used in ancient civilizations, such as oils of *Cedrus* spp. (cedar), *Cupresses sempervirens* L. (Cupressaceae) (cypress) and *Glycyrrhiza glabra* L. (Fabaceae) (licorice), which were originally documented in Mesopotamia before 2500 BCE, are used in many parts of the world even today to fight illnesses ranging from cough to infections and inflammations.[1]

Nature has remained an important source of pharmaceutical agents, even in modern medicine. The switch from complex medicinal formulations to single components, i.e. the advent of modern pharmacognosy, in the nineteenth century led to the isolation and characterization, followed by synthesis, of biologically active natural products derived from plants. The earliest single agents described were the alkaloids, including morphine[2] **1.1** (by Derosne and Sertuerner in the early 1800s), strychnine[3] **1.2** (Pelletier and Caventou, 1817), quinine[4] **1.3** (Pelletier and Caventou, 1820), codeine[5] **1.4** (Robiquet, 1832) and atropine[6] **1.5** (Mein, 1833). Ladenburg's synthesis of coniine[7] **1.6** in 1886[8] marked the first instance of a complete set of isolation,

structure elucidation and synthesis of a plant natural product. Synthesis has ever since been an integral arm of natural product research, often serving as the only avenue for delivering enough supply of bioactive molecules and generating analogues for various stages of pharmacological testing.

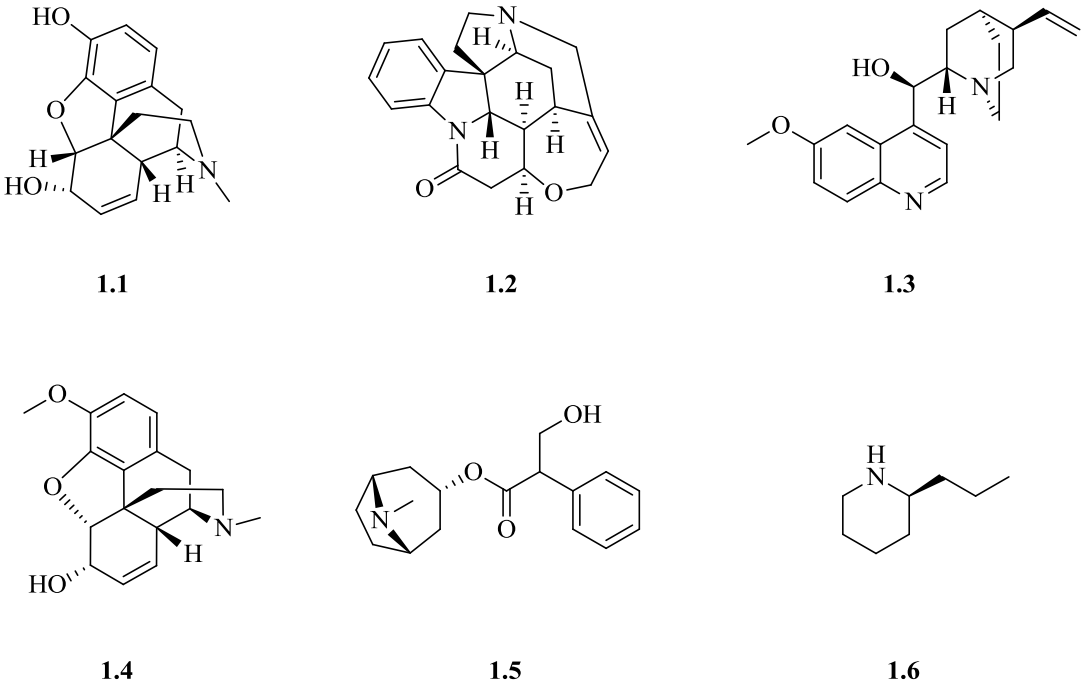

1.1 **1.2** **1.3**

1.4 **1.5** **1.6**

Figure 1: Alkaloid natural products of medicinal importance

In the twentieth century, discovery of drugs and drug leads from Nature intensified and various classes of drugs, including antibacterial, antifungal, anticancer and antiviral agents, were introduced in relatively quick time. Following Alexander Fleming's isolation and recognition of the activity of penicillin G **1.7** in the late 1920s,[9] it saw widespread use as a life-saving antibiotic, particularly during the later stages of the Second World War, and ushered in the era of antibiotics.

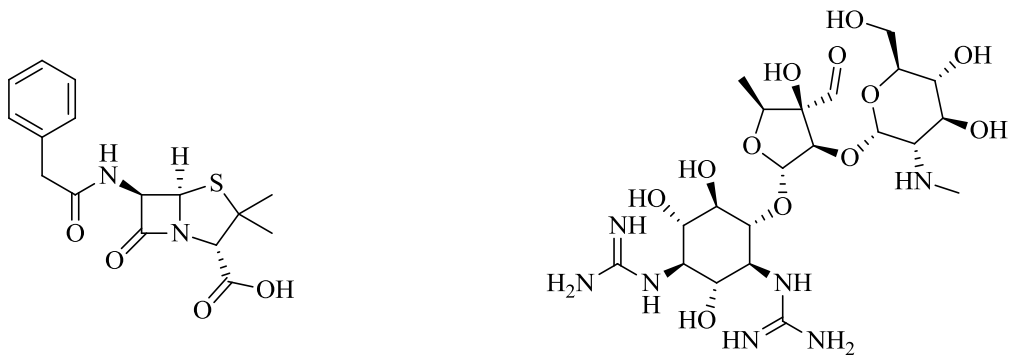

1.7 **1.8**

Figure 2: Penicillin G and streptomycin, antibiotic natural products

The successful implementation of penicillins and streptomycin[10] **1.8** as antibiotics paved the way for the discovery of new classes of drugs from microbial sources. Antifungal agents amphotericin B[11] **1.9** and nystatin (fungicidin)[12] **1.10** were isolated in the 1950s from *Streptomyces nodosus* Trejo (Streptomycetaceae) and *Streptomyces noursei* Brown (Streptomycetaceae), respectively, and their structures were elucidated in the 1970s.

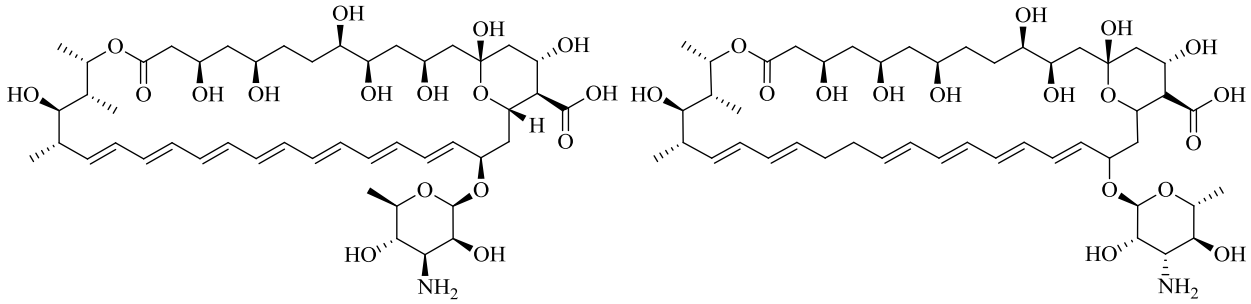

1.9 **1.10**

Figure 3: Polyene antifungal natural products amphotericin B and nystatin

More than half of anticancer agents in clinical use come from natural sources or are inspired by natural products.[13] Among the first natural product anticancer agents were the vinca

alkaloids, vinblastine **1.11** and vincristine **1.12**, which were isolated from the Madagascar periwinkle, *Catharanthus roseus* (L.) G. Don (Apocynaceae), in the 1950s.[14] These were followed by taxanes and camptothecins, which are also plant-derived natural products. Paclitaxel **1.13**, a promoter of tubulin polymerization, was originally isolated from the bark of the Pacific Yew, *Taxus brevifolia* Nutt. (Taxaceae),[15] but is also present, along with its analogs, in leaves of several *Taxus* species. Camptothecin **1.14**, which was isolated from the Chinese plant *Camptotheca acuminata* Decne. (Nyssaceae),[16] was abandoned in clinical trials due to severe toxicity to the bladder. Semisynthetic analogues of camptothecin, such as irinotecan **1.15**,[17] however, are currently in clinical use.

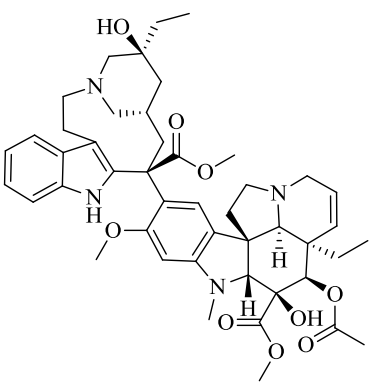

1.11

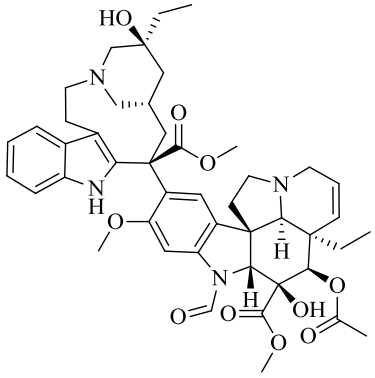

1.12

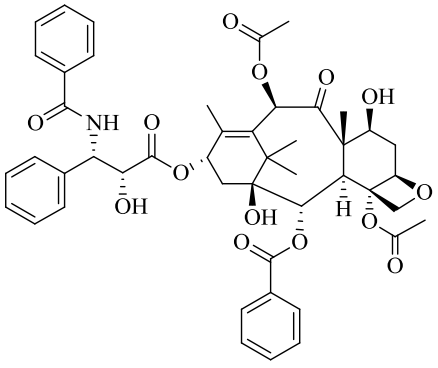

1.13

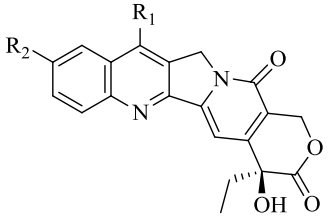

1.14 $R_1, R_2 = H$

1.15 $R_1 = Et$, $R_2 =$ 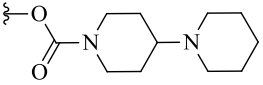

Figure 4: Anticancer agents, and a semisynthetic analogue, derived from plants

Many of the antiviral drugs and drug leads in clinical use today are synthetic. However, it is important to note the work done by Werner Bergmann as his discovery of spongonucleosides[18] – spongouridine **1.16** and spongothymidine **1.17** – from the sponge *Cryptotethya crypta* de Laubenfels (Tethyidae) in 1951 led to the realization that biologically active natural products could have sugars other than ribose and deoxyribose. Consequently, many analogues containing unnatural sugars were synthesized, including arabinosyladenine (vidarabine or Ara-A) **1.18**, arabinosylcytosine (cytarabine or Ara-C) **1.19**, acyclovir **1.20** and azidothymidine (AZT) **1.21**. Many of them have been approved as clinical antiviral and antitumor agents.

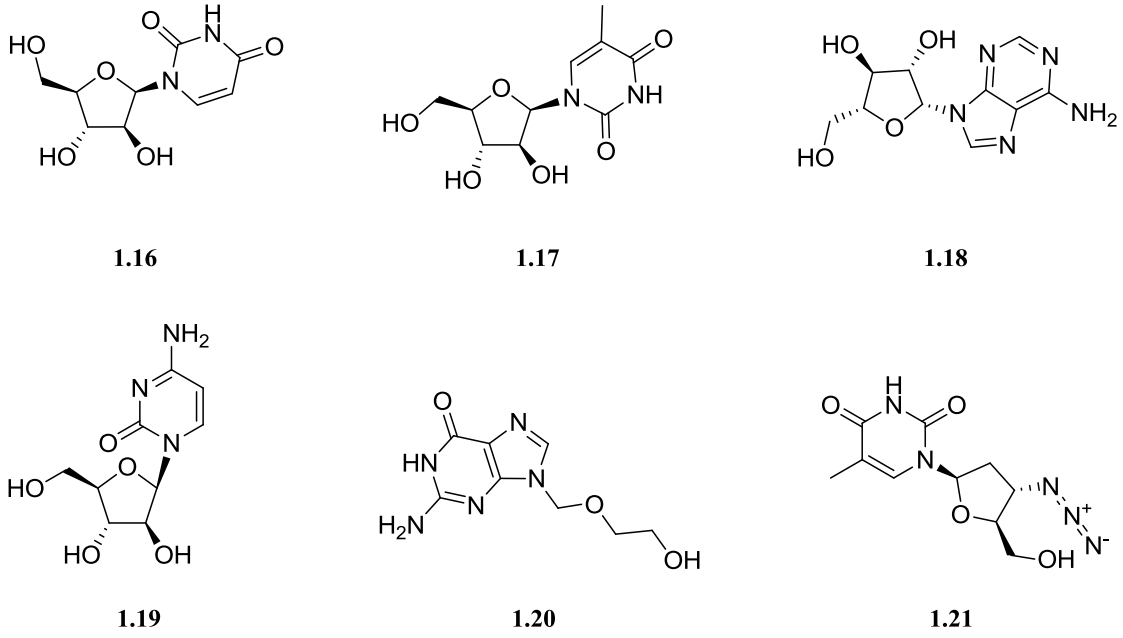

1.16 **1.17** **1.18**

1.19 **1.20** **1.21**

Figure 5: Spongonucleosides and their synthetic derivatives

Bergmann's pioneering work on marine sponges also led to a surge in investigations of the organisms from the marine environment for the discovery of new classes of biologically active secondary metabolites and drug leads. In the latter half of the twentieth century, aided by

advances in SCUBA, researchers began to scour the seas and oceans for novel pharmaceutical agents from sponges, mollusks, tunicates, corals, algae, fungi and bacteria. The marine habitat proved to be a prolific source of biologically active compounds with diverse structural features, such as manzamine A[19] **1.22**, trabectedin[20] **1.23** (originally called ET-743 by Rinehart), ziconotide[21] **1.24**, salinosporamide A[22] **1.25**, dolastatin 10[23] **1.26**, and bryostatin 1[24] **1.27**. Trabectedin and ziconotide are FDA approved drugs as anticancer and pain management agents.

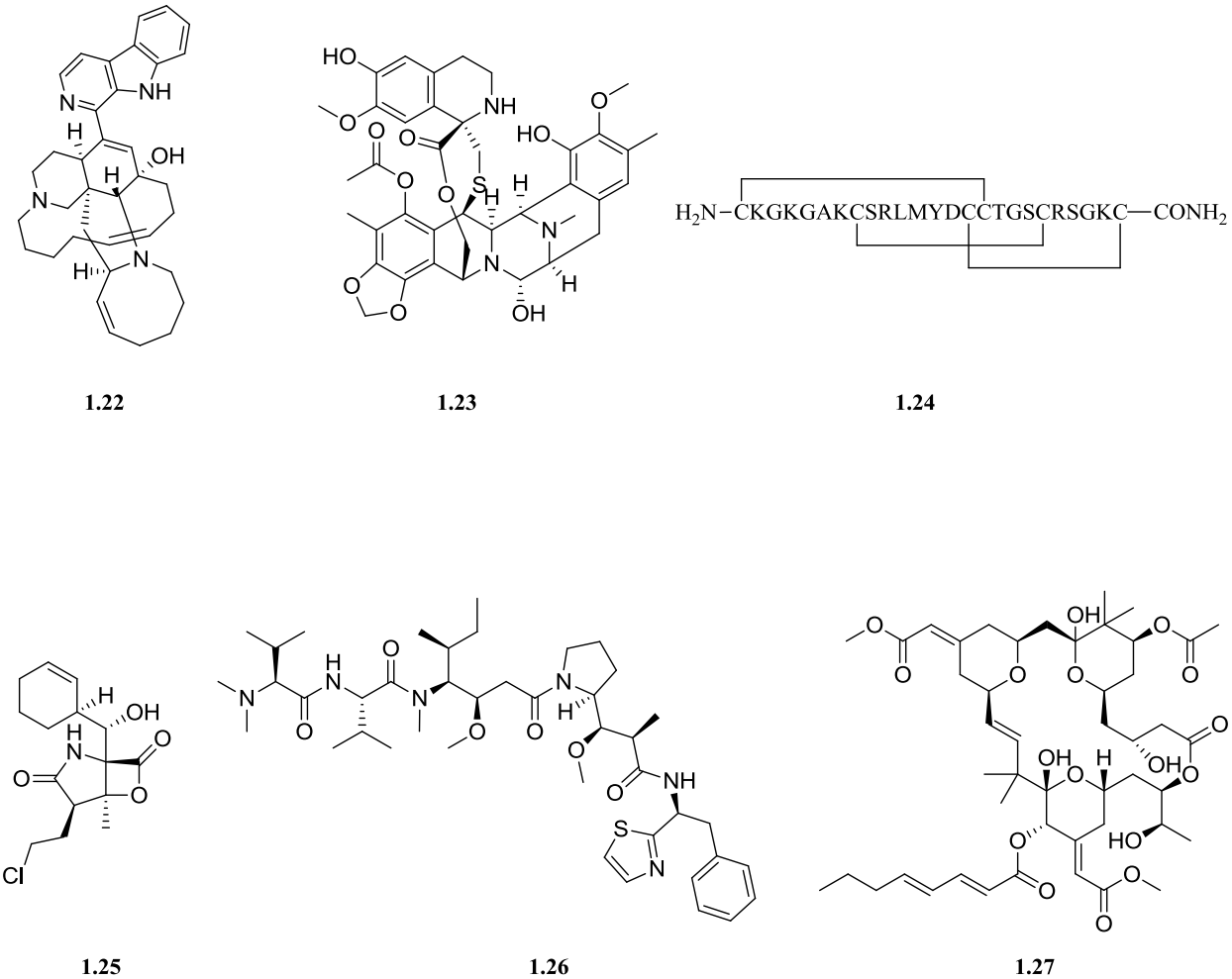

1.22 **1.23** **1.24**

1.25 **1.26** **1.27**

Figure 6. Diverse natural products isolated from organisms found in the marine habitat

Dolastatin 10 was one of the most potent anticancer agents at the time of its discovery, when it was originally isolated from the sea hare *Dolabella auricularia* Lightfoot (Aplysiidae). Further research, however, revealed that the compound was in actuality produced by the cyanobacterium *Symploca* sp.[25] Bryostatin 1, a potent protein kinase C activator currently in clinical trials for various forms of cancer, was initially isolated from the bryozoan *Bugula neritina* L. (Bugulidae) but its biosynthetic origin was traced to the symbiont bacterium *Candidatus* Endobugula sertula Haygood (Cellvibrionaceae).[26] These revelations illustrate the role of cohabitating microorganisms in the biosynthesis of biologically active secondary metabolites, sometimes in symbiosis with the host organism. Importantly, a significant percentage of these microbes are amenable to culturing, allowing for large-scale production of secondary metabolites of interest as well as discovery of new classes of natural products. Additionally, there have been reports of induction of bioactive secondary metabolites when organisms are co-cultured[27] or introduced to chemical entities from foreign organisms,[28] likely in competition for resources or as part of a defense mechanism. These approaches relying on complex interactions between organisms have been identified as possible routes toward discovery of new classes of bioactive natural products.

1.2 Significance of Natural Products Research

Natural products remain the most reliable sources of drugs and drug leads, as illustrated by Newman and Cragg in their serial reviews of new chemical entities as drugs.[13, 29] In the most recent review, they highlight that more than half of all new small molecule drugs approved in the timeframe 1981–2014 are natural products, close mimics or synthetic derivatives with natural product pharmacophores (Figure 7).[13] This, unequivocally, highlights the occupation

of a unique chemical space by natural products, one that correlates well to the chemical space of drugs.

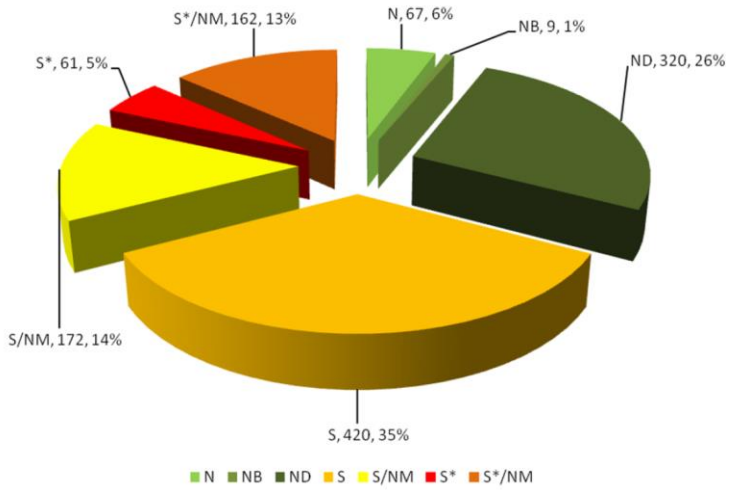

Figure 7. Distribution of all small molecule approved drugs between 1981 and 2014.

Key: N: Natural product, NB: botanical drug, ND: natural product derivative, S: synthetic, S*: synthetic molecule with a natural product pharmacophore, NM: mimic of natural product. Figure obtained from Ref. 13.

Despite a strong push by pharmaceutical companies away from natural products based drug discovery in favor of combinatorial synthetic libraries over the past few decades, the latter has not reaped success as initially predicted. One of the major issues with synthetic libraries is their inability to replicate the structural complexity, diversity, and drug-like properties of natural products. Molecular scaffold analysis shows that combinatorial libraries are farther away than natural products from the chemical space occupied by drugs.[30] Nature, owing to its complex biosynthetic machinery comprising numerous enzymes, has the ability to efficiently synthesize complex molecules with defined stereochemical configurations which are not always readily accessible by synthesis. The continued successes of natural products as new drugs or drug

leads and the failure of combinatorial approaches amplify the importance of natural products based drug discovery processes.

The similarities between the chemical spaces of drug molecules and natural products has been attributed to closely related protein fold topologies during the interaction of drugs with target proteins and the interaction of natural products with their biosynthetic enzymes.[31] A modeling study showed that flavonoid biosynthetic enzymes and their kinase targets share similar secondary structures, i.e. protein fold topology around the active site.[32] This study suggests that natural products have a built-in advantage of being recognized by target proteins because of favorable major secondary structures and topological arrangements.

The Dictionary of Natural Products[33] and the Dictionary of Marine Natural Products[34] contain over 290,000 and 55,000 natural products, respectively. However, only a fraction of the natural products in the database have been investigated thoroughly in drug discovery campaigns.[35] While 15% of drugs in clinical trials listed at ClinicalTrials.gov are plant natural products, the majority (~60%) of these come from only 10 taxonomic families,[36] despite the fact that natural products from plants have been studied far longer than from other sources. It illustrates continued opportunities for drug discovery from natural products. A renewed focus on investigating natural products for novel drugs and drug leads is certainly warranted.

1.3 Challenges in Natural Products Research

Limited supply and extremely low yields from isolation procedures often impede drug discovery research on bioactive natural products. In the absence of an easily accessible

synthetic route, enough material for testing may not be generated without serious detriment to the environment and without incurring significant labor and monetary costs. Often, the miniscule amount of natural product obtained precludes researchers from determining the structure and carrying out rigorous biological assessments in spite of a promising early outlook. Synthesis of natural products is often impractical because of their complex structures and difficulty in efficiently installing the correct stereochemistry. Moreover, a modular synthesis of natural product derivatives is not always possible, preventing effective structure-activity relationship studies. New approaches toward sustainable production and modification of natural products are essential.

We also often rely on a needle in a haystack approach, i.e. a trial and error approach, toward finding new classes of natural products and drug leads. A more strategic, target oriented discovery of new natural products is necessary.

Rediscovery of known secondary metabolites is a chronic problem facing researchers. In absence of a robust database for reliable dereplication, natural products researchers have to rely on traditional practices and often isolate known compounds with known biological activity. In recent years, encouraging advances in automated high throughput screening, computational methods, and molecular networking platforms have been made. We need to continue to make crucial advances in technological innovations for the growth of the field.

1.4 Current Areas of Research in Natural Products

A group of leading researchers in marine natural products chemistry from the United States and Japan convened for the 8th US-Japan Symposium under the theme of 21st Century

Innovations in Natural Products in Honolulu in November 2016. A wide range of topics were presented and discussed, highlighting the state-of-the-art of natural products research.[37] At the conclusion of the symposium, William Gerwick highlighted the contemporary areas of focus in the field and summarized the direction the broader natural products research community is headed in. These are briefly described in the following paragraphs.

In recent years, there have been increasing reports of microbial resistance in humans to pharmaceutical agents used in treatment of bacterial[38] and viral[39] infections. Since the efficacy of several existing drugs is diminishing, discovery of new classes of drugs and molecular scaffolds to combat these resistances are of utmost clinical importance. There continues to be a strong push to discover novel classes of natural products from new organisms, particularly from sparsely investigated habitats and regions. Additionally, the advances in instrumentation have resulted in high throughput screening systems that allow for testing of large batches of known natural products against various targets, creating the possibility for discovery of new biological activity from existing natural product libraries.

As the cases of dolastatins and bryostatins have revealed, many natural products isolated from macro-organisms have biosynthetic origins in cohabitating organisms. This works to our advantage as the microbes producing the natural products may be cultured, giving access to a sustainable supply of natural product drug candidates. Newman and Cragg point out that "the interface between the microbial interactions with their hosts and commensals" has the greatest potential for the discovery of novel structures from natural sources.[40] Another advantage of culturing microbes is targeted production of natural products by means of functional genomics and genetic engineering. Combinatorial biosynthesis,[35, 41] in which biosynthetic genes from different gene clusters or organisms are mixed together to produce compounds with desired

pharmacophores or functionalities, is emerging as a viable route to new natural products, new analogues of existing ones,[42] or toward increasing production of known high value compounds.

Advances in DNA sequencing have the ability to shift the paradigm on isolation of natural products. Ready access to biosynthetic genome sequences now facilitates a bottom-up approach toward discovery of novel natural products.[43] The traditional top-down approach, in which organisms are collected or cultured and natural products are isolated based on desired biological activity or spectroscopic profiles and then characterized, is very suitable for compounds that are produced in abundance and survive the traditional extraction and isolation methods. Genome sequence driven bottom-up approach allows one to predict the structures of natural products and selectively focus on the novel ones. Several studies show that there are far more biosynthetic gene clusters in organisms than those accounted for the production of secondary metabolites,[44] suggesting a vast potential for new discoveries.

The genomic approach to discovery of natural products, coupled with sensitive spectroscopic techniques, is amenable toward detection of novel chemical scaffolds; however, for applications in medicine, sufficient quantities still need to be isolated. We can only fully take advantage of the prospects of the genomic approach when advances in isolation, spectroscopy and dereplication allow for routine analysis of compounds produced in miniscule amounts. That ability has already been demonstrated in the case of the phorbasides, aided by cryo-microprobe NMR spectroscopy.[45] The global natural product social (GNPS) molecular networking project[46] is a collaborative project aimed at quick dereplication of natural products and discovery of novel scaffolds based on MS/MS libraries. Natural product chemistry has the ability to bounce back in a major way when advances of this nature come to fruition.

1.5 Research Objectives

Multitudes of medical challenges exist today. Despite significant advances in biomedical research over the last several decades, there remain pressing issues that need to be tackled. Many diseases still have no cure and microbial drug resistance in humans is increasing.

Alzheimer's stands alone as the only disease among the ten leading causes of deaths in the United States that cannot be cured, slowed down or prevented.[47] An estimated $236 billion was spent on dementia care in the United States in 2016, incurring a huge socioeconomic burden. In 2015, nearly 47 million cases of dementia were estimated worldwide and this number is projected to double every twenty years.[47] The lack of a single drug to slow down, prevent or cure this disease presents a pressing need toward discovery of anti-Alzheimer's drug leads. While the root cause of Alzheimer's is not fully understood, there are a few strategic approaches toward discovery of anti-Alzheimer's drugs. One of the approaches relies on finding inhibitors of the β-site of amyloid precursor protein cleaving enzyme (BACE1), implicated in the formation of signature neurotoxic amyloid plaques in the neural cells of Alzheimer's patients, as described in the amyloid cascade hypothesis.[48] While there are small molecule BACE1 inhibitors in clinical trials for efficacy against Alzheimer's, there is a concern that these may cause various mechanism-based side effects.[49] Hence, discovery of viable inhibitors of BACE1 is very much needed. A major objective of this research was to identify extracts from cyanobacteria, marine algae, sponges and other invertebrates that showed BACE1 inhibitory activity and to carry out bioactivity-guided isolation and structure elucidation of active components. Efforts toward discovery of BACE1 inhibitors are discussed in both chapters 2 and 3.

In collaboration with researchers at the University of Hawai'i Cancer Center, many of the extracts were screened against other relevant targets. These include cytotoxicity assays

involving cancer cell lines, such as glioma and breast cancer, that show elevated levels of the activated signal transducer and activator of transcription 3 (STAT3) protein.[50] Tumor cells secrete vascular permeability factors, such as vascular endothelial growth factor A (VEGF-A), increasing permeability in the cells and releasing toxins in the blood stream.[51] This deadly condition is known as sepsis and accounts for nearly a tenth of all cancer related deaths.[52] Our objectives from these collaborations were to find inhibitors of STAT3 activation and vascular permeability for potential therapeutic uses. These are described in chapters 2 and 5, respectively.

Areca catechu L. (Arecaceae), commonly known as betel nut, is the fourth most used psychoactive substance in the world. Betel nut chewing has been implicated in various oral cancers, such as oral squamous cell carcinoma.[53] It is not clear what components of *Areca catechu* are responsible for oral cancer incidences nor is anything known about the mechanism of action. A recent study suggested that incubation of polymorphonuclear leukocytes with areca nut extracts resulted in Ca^{2+} mobilization and release of pro-inflammatory agents such as leukotriene B4.[54] However, it was not clear where the Ca^{2+} was mobilized from or which leukocytes were responsive to the areca nut extracts. In collaboration with Dr. Reinhold Penner's team at the Queen's Medical Center in Honolulu, we sought to identify components of *Areca catechu* that were responsible for the Ca^{2+} mobilization in immune cells and to understand the mechanism behind the mobilization. Details on this investigation are provided in chapter 4.

In addition to these major objectives, this dissertation describes various aspects of structure elucidation of natural products. Computational studies, in which ^{1}H and ^{13}C NMR shifts were calculated based on density functional theory, have played an integral role in determining planar structures and stereochemical configurations of some of the molecules discussed herein.

1.6 Work Flow and Biological Evaluation

Extraction and fractionation. Samples are either collected in the field (marine species by snorkeling or SCUBA-diving) or cultured in the laboratory. A voucher specimen for each unique field-collected sample is preserved in alcoholic solution for taxonomic identification. Field collected samples, or culture harvests, are typically freeze-dried prior to extraction. The general extraction and fractionation scheme of biological material is outlined in Figure 8. Compounds from the broth of cell cultures (cyanobacteria) are extracted separately, using HP-20 resin, which is then filtered, re-suspended in organic solvent (methanol), filtered again before removal of solvent to afford a crude media extract. Initial fractionation on a small scale is carried out for preliminary biological evaluation against various targets. Samples considered hits in various assays are then subjected to a large scale extraction and purification process, followed by re-evaluation of biological activity and elucidation of structure of purified secondary metabolites with the aid of modern spectroscopic tools. On some occasions, samples lacking activity against the specific biological targets are also advanced to further processing based on a few criteria. These criteria include detection of chlorinated or brominated species by mass spectrometry as these halogens are likely to be found in secondary metabolites and not primary metabolites. Likewise, if an initial dereplication of a sample leads to no obvious hits based on the mass of the molecular ion of the compound and features present in its ^{1}H NMR spectrum, it may indicate the discovery of an as yet unreported secondary metabolite and that sample is also given priority for further processing.

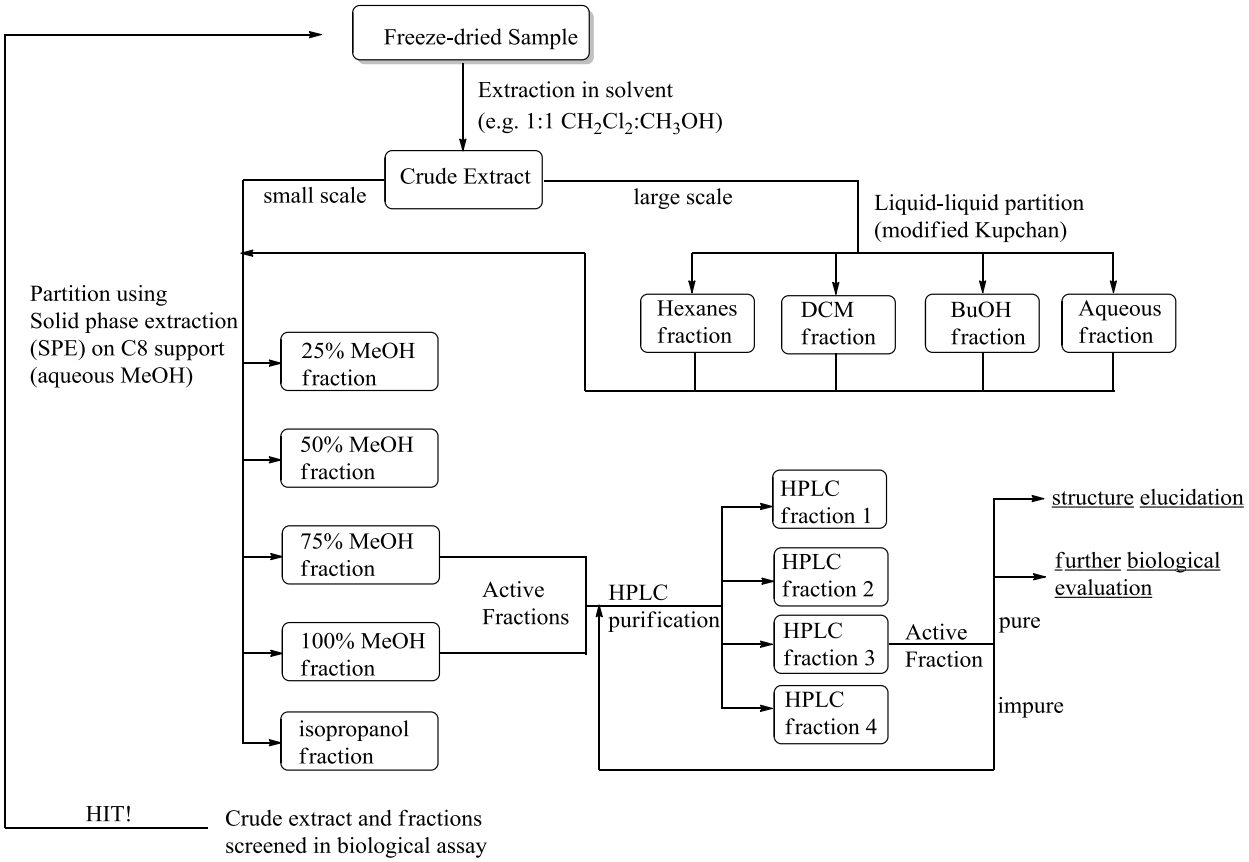

Figure 8. Bioactivity-guided extraction and fractionation workflow

Dereplication and structure elucidation. SciFinder[55] is the most comprehensive database of chemistry journals, patents and other scientific literature with a massive repository of chemical substances and their reactions. More specialized but less comprehensive natural product libraries include the MarinLit[56], AntiBase[57] and AntiMarin[58] databases. All of these databases offer dereplication tools using experimental and predicted data. Mass spectrometric and NMR spectroscopic data are most commonly utilized to search for prior occurrences of a natural product in the literature. Absence of a match in any of these databases would suggest that a natural product may be unreported, unless it was discovered recently and/or not yet indexed in the databases.

When a metabolite appears to be novel, including a new analogue of an existing natural product, its structure is elucidated using the modern spectroscopic tools at our disposal. The full complement of spectral data – mass spectrometry, infrared spectroscopy, ultraviolet-visible spectroscopy, one-dimensional and two-dimensional NMR spectroscopy, optical rotation and the like – are obtained in efforts to deduce structural information of the metabolite. Occasionally, synthetic and computational methods are necessary to confirm the proposed structure of a secondary metabolite. Finally, each purified metabolite is evaluated for a wide range of biological activities that may be available.

Biological evaluation. The primary goals of our research, as stated previously, is to identify potential inhibitors of BACE1, STAT3 and vascular permeability from the extracts of marine invertebrates, algae, cyanobacteria as well as cyanobacteria cultured in the laboratory. A brief description of these targets and the assays involving these targets follows. Additionally, we continue to pursue the identity of Ca-mobilizing components of *Areca catechu* and details on the fluorimetric Ca-signaling assay are provided in Chapter 4.

BACE1 as a therapeutic target in Alzheimer's disease. Alois Alzheimer described the presence of neurofibrillary tangles and senile plaques as signature pathological features of presenile dementia.[59] Detailed studies on the senile plaques led to the widely used Amyloid Cascade Hypothesis (ACH), which was first proposed by Hardy and Higgins in 1992.[48a] The ACH proposes the beta-amyloid protein (Aβ), the main component of the senile plaques, as the chief causative agent in the pathogenesis of Alzheimer's disease. The neurofibrillary tangles, cell degeneration and dementia have been claimed to be consequences of the deposition of Aβ. This hypothesis implies that the buildup of Aβ is a result of the initial cleavage of the amyloid precursor protein (APP) by the protease β-secretase (BACE1) (Figure 9).[60]

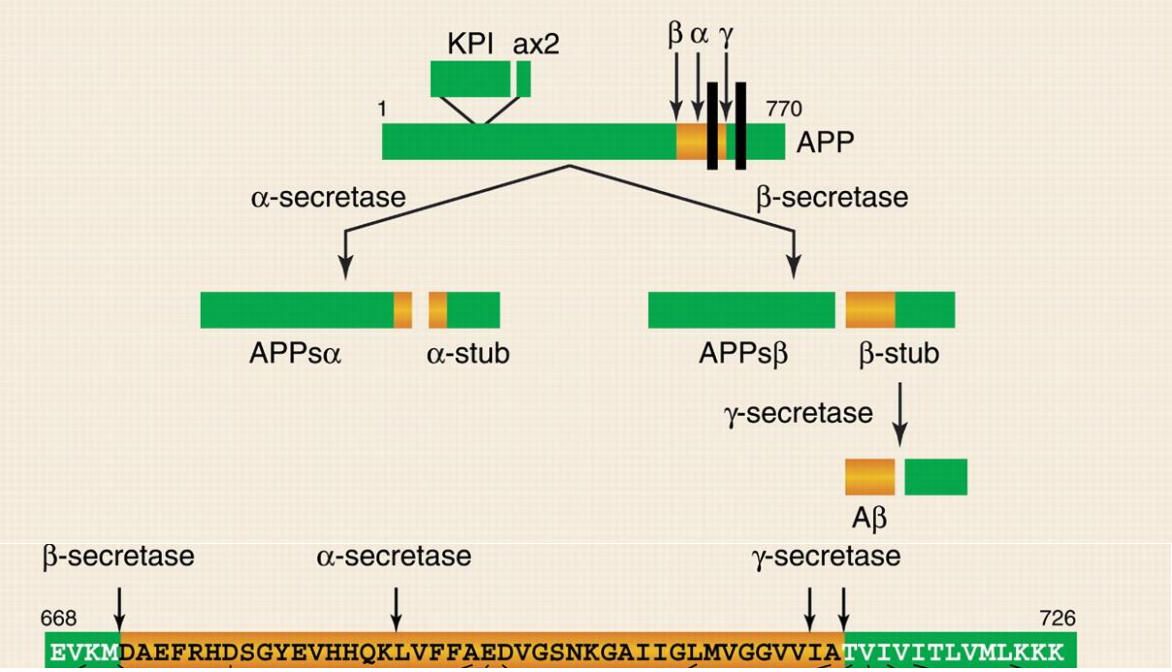

Figure 9. Formation of Aβ_{40} and Aβ_{42}, according to the Amyloid Cascade Hypothesis

Image reproduced from Ref. 60.

Neurofibrillary tangles, the other physiological markers of Alzheimer's disease, are mainly composed of hyperphosphorylated tau protein.[61] These tau filaments are also present in other cognitive disorders, such as Pick's disease and Parkinson-dementia complex, in which the plaques are absent.[60] Hence, the ACH remains controversial because no definitive link has been established between Aβ and hyperphosphorylated tau-protein. Nevertheless, significant research on Alzheimer drug discovery is geared toward prevention of the deposition of Aβ through inhibition of BACE1. BACE1 inhibitors, in theory, should slow down Alzheimer's disease, an action that falls outside the capabilities of the current treatment methods. The existing United States Food and Drug Administration (FDA) approved Alzheimer drugs, which are mostly acetylcholinesterase inhibitors, slow down symptoms of the disease and provide short-term relief to the patients but do not stop or slow down the disease itself (Figure 10).[62]

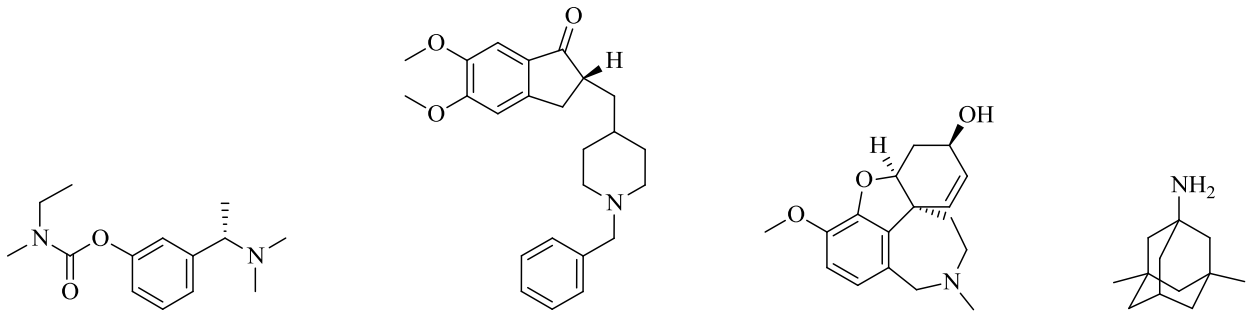

1.28 **1.29** **1.30** **1.31**

Figure 10. Current FDA approved medications for Alzheimer's disease

Key: **1.28** rivastigmine (Exelon), **1.29** donepezil (Aricept) and **1.30** galantamine (Razadyne) are acetylcholinesterase inhibitors; **1.31** memantine (Namenda) is an N-methyl-D-aspartate receptor antagonist

BACE1 assay. The preliminary screen for BACE1 inhibitors relies on an enzyme fragment complementation (EFC) assay (Figure 11).[63] A cyclic peptide containing an enzyme donor (ED) fragment is cleaved by BACE1 before the ED fragment can complement with an enzyme acceptor (EA) fragment to form an active β-galactosidase enzyme. The β-galactosidase enzyme cleaves off galactose from the Galacton-Star substrate **1.32**, triggering chemiluminescence, which is measured using a plate reader. Compounds that inhibit BACE1 cannot trigger this series of events, resulting in the absence of chemiluminescence. The calculated percent activity is proportional to the concentration of the protease and lower percent activity equates to stronger inhibition of BACE1. Samples that appear to contain potent inhibitors of BACE1 are then evaluated under a secondary screen. A secondary assay is essential as the enzyme fragment complementation assay could lead to false positives if the components in the extract inhibit complementation of the enzyme donor and enzyme acceptor fragments or the active β-galactosidase itself.

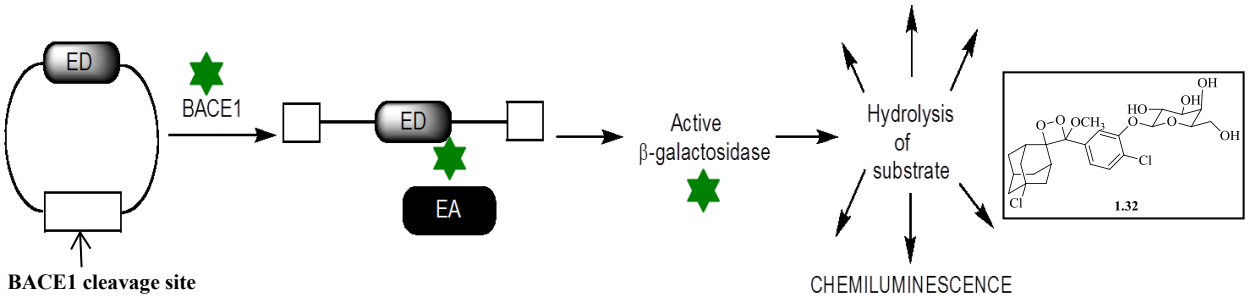

Figure 11. The primary BACE1 enzyme fragment complementation assay

A homogeneous affinity assay constitutes the secondary screen of this two-step protocol (Figure 12).[64] Prioritized samples are incubated overnight with BACE1 and the inhibitor-protease complex is then separated from the crude mixture using a micro spin column. The inhibitor is directly analyzed by liquid chromatography-mass spectrometry (LC-MS) following dissociation from the protease. This method provides the retention time and the molecular weight of a potential inhibitor, which is information that can simplify the process of isolation of the inhibitor from a complex mixture.

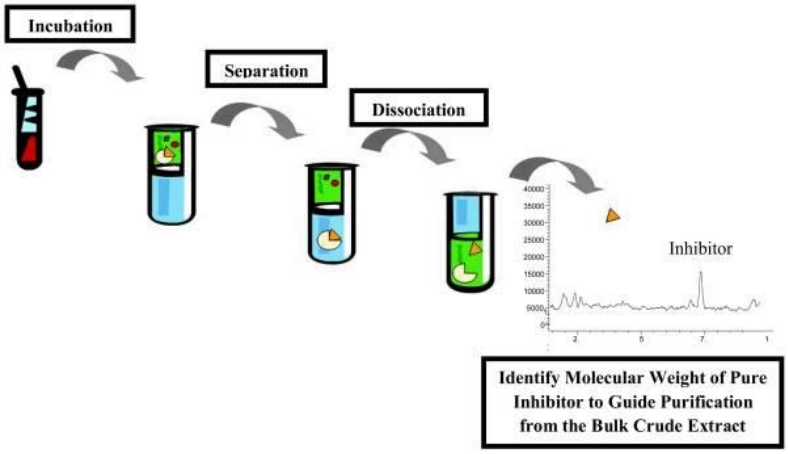

Figure 12. The secondary homogeneous BACE1 affinity assay

STAT3 as a therapeutic target in cancer cell lines. The signal transducer and activator of transcription (STAT) family of proteins are latent in the cytoplasm until activated, via phosphorylation, by extracellular-signaling proteins such as cytokines and growth factors (Figure 13).[65] The cytokines and growth factors can activate tyrosine kinases in the cell, which in turn can phosphorylate STAT proteins. Activated STAT proteins can dimerize, disengage from receptor proteins and accumulate in the nucleus to regulate transcription.[65] STAT3, specifically, regulates the expression of genes related to cell cycle, cell survival, and immune response associated with cancer progression and malignancy in a number of cancer types.[66] Elevated levels of activated STAT3 are among the common features of a variety of cancers, including leukemia, glioma, breast cancer, lung cancer, melanoma and pancreatic adenocarcinoma.[67] Poor prognosis for many of these cancers has been attributed to elevated levels of activated STAT3.[68] Therefore, inhibition of the STAT3 signaling pathway is a promising strategy for the development of anticancer therapeutics.

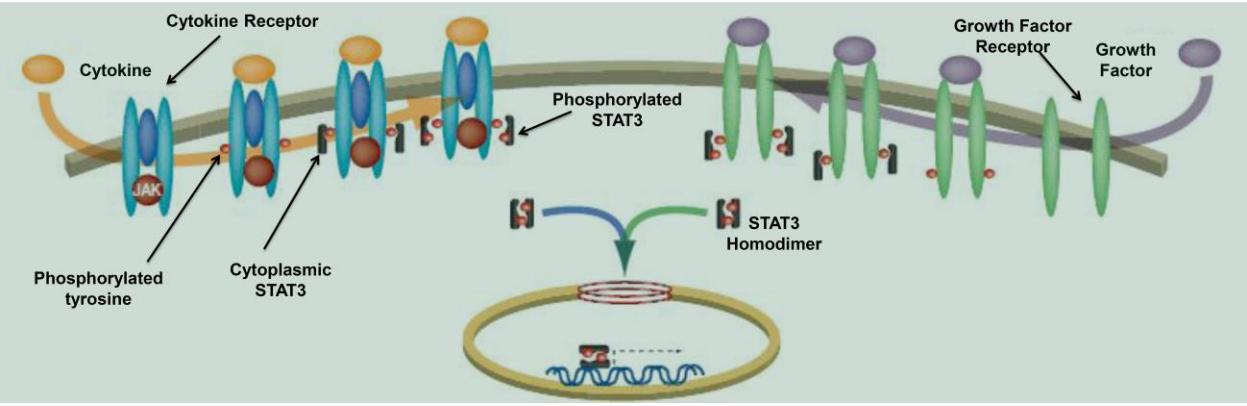

Figure 13. STAT3 signaling pathways in cells

Figure reproduced from Ref. 67

A large number of STAT3 inhibitors, several of which are small synthetic molecules or natural products derived from herbal sources, are in clinical trials for effects on patients with cancer.[69] These inhibitors act at various sites of action in the STAT3 signaling pathway. However, most of them suffer from toxicities and lack of efficacy, potency or specificity to STAT3. While STAT3 remains an attractive target in cancer therapy, there is a need for development of novel inhibitors of STAT3 that can overcome the deficiencies observed with current therapeutic candidates. Marine natural products have not been investigated thoroughly for their ability to inhibit activation of STAT3, hence the collaboration with Prof. James Turkson at the University of Hawai‘i Cancer Center is aimed at discovering new classes of STAT3 inhibitors from marine organisms. As part of the collaboration, various marine natural product extracts and fractions are first screened for cytotoxicity against cancer cell lines with elevated levels of activated STAT3, such as human glioblastoma (U251MG), human breast adenocarcinoma (MDA-MB-231) and human pancreatic adenocarcinoma (Panc-1). Recently, the Panc-1 assay has also been set up to be performed in-house. Compounds with promising activity are then advanced for further biological evaluation.

Pursuit of inhibitors of vascular permeability from marine organisms. Hyperpermeability of the endothelial membrane and resulting microvascular failure are a hallmark of sepsis and linked to multiple organ failures and increased mortality in humans.[70] Currently, there are no clinical drugs for the treatment of sepsis. The mechanisms of vascular hyperpermeability are not fully understood but the interaction between the GTPase R-Ras and Filamin A has been found to be critical in maintaining endothelial barrier.[71] Deficiency of R-Ras or Filamin A has been found to increase leakage in the endothelial barrier. R-Ras, unlike other Ras proteins known to cause malignant transformations, promotes endothelial cell survival.[72]

Agonists of R-Ras are therefore suitable therapeutic targets against vascular leakage. In collaboration with Prof. Michelle Matter at the University of Hawai‘i Cancer Center, we pursued the discovery of novel vascular permeability inhibitors from marine organisms.

The scheme of the vascular permeability assay is shown in Figure 14. Endothelial cells are seeded on a semipermeable membrane pre-coated with collagen to form a monolayer in the permeability insert (Figure 14A), which is then treated with an extract from marine organisms as well as tumor necrosis factor alpha (TNFα), a cytokine that enhances permeability of the monolayer (Figure 14B). After replacement of the media, fluorescence indicator FITC-Dextran is added and allowed to pass through the permeable monolayer (Figure 14C-D). The permeability insert is then removed and fluorescence in the receiver plate well is measured to evaluate the degree of permeability. Extracts or samples that block vascular permeability lead to reduced fluorescence readings in the assay.

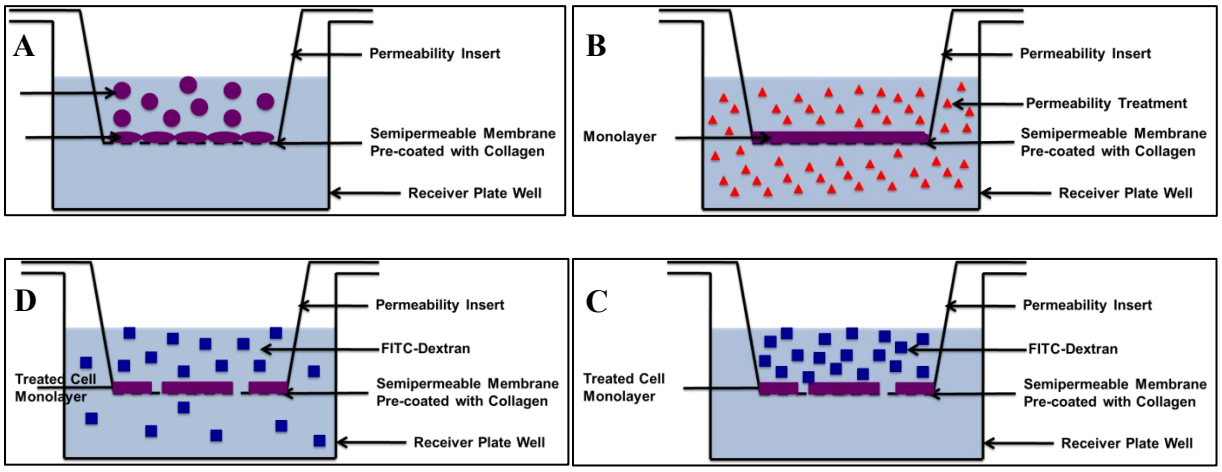

Figure 14. Schematic representation of the vascular permeability assay

CHAPTER 2

Biologically Active Secondary Metabolites from *Dactylospongia elegans*

2.1 Sponges as Rich Sources of Secondary Metabolites

Bergmann's original discovery of spongonucleosides from a sponge (*vide supra*) initiated a wide-spread investigation of the marine habitat for biologically active secondary metabolites. There are over 10,000 species of sponges (porifera)[73] and they are among the most interesting sources of bioactive natural products because these primitive filter-feeding marine organisms have survived and thrived for over hundreds of millions of years[74] despite lacking physical defense features (shells, spines, etc.) or an immune system. Organisms without an immune system or physical defense features are known to be prolific producers of secondary metabolites, presumably as their chemical defense against predation and competition for resources.[75] In support of the chemical defense argument, sponges that grow exposed have been observed to be more toxic than those that grow unexposed.[75b]

In a five-decade timeframe between 1963 and 2013, almost 25,000 new compounds were discovered from the marine environment, with sponges producing a third of them.[76] Furthermore, the majority of the novel natural product chemotypes reported from sponges occupy a unique space and have no close analogs in terrestrial plant and microbial natural products or in natural products isolated from other marine organisms.[77] The prolificacy and diversity of sponge natural products is complemented by their activity in a wide array of biological targets. Therefore, sponges continue to attract significant interest in natural product chemistry. Currently, there are three sponge natural product-inspired drugs in clinical use and

many others are in clinical trials or that have potent biological activities.[78] In addition to the aforementioned vidarabine **1.18** and cytarabine **1.19**, eribulin mesylate **2.1** is a clinically approved drug for the treatment of metastatic breast cancer. Eribulin mesylate is a synthetic analogue of halichondrin B **2.2**, a polyether macrolide isolated from the sponge *Halichondria okadai* Kadota (Halichondriidae) (Figure 15).[79]

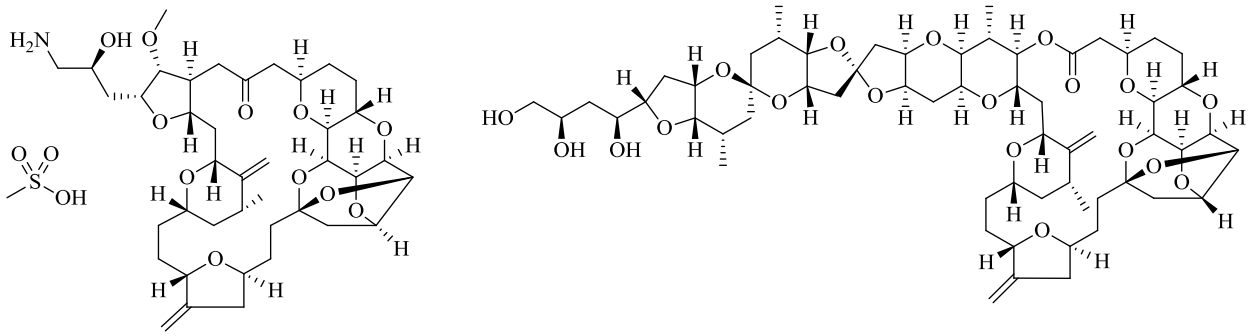

2.1 **2.2**

Figure 15. Eribulin mesylate is a synthetic analogue of halichondrin B, a sponge metabolite

2.2 Collection Details and Identification of *Dactylospongia elegans*

A sponge specimen (ID: 10-Kauai-08) was collected by SCUBA diving from a depth of 55 feet below sea level at the Sheraton Caverns dive site off the coast of Kaua‘i (coordinates: 21° 51.920 N and 159° 27.097 W) on June 09, 2010. In a subsequent recollection trip, another sponge specimen (ID: 11-Kauai-80) believed to be an identical organism was collected from the same location at a depth of 55 feet below sea level on May 29, 2011. LC-MS analysis showed identical metabolic profiles for the extracts of both samples. A voucher sample of 10-Kauai-08 was preserved in alcoholic solution for future taxonomic identification. In 2016, Mary Kay

Harper (University of Utah) identified the 10-Kauai-08 specimen as *Dactylospongia elegans* Thiele (Thorectidae). We inferred that 11-Kauai-80, based on similarities in collection site, appearance and LC-MS profiles of the two specimens, belonged to the same species.

Both sponges (Figure 16) were collected as encrusting yellow sponges, which were heavily fouled with various growths, exuded red solution, and turned brown on standing.

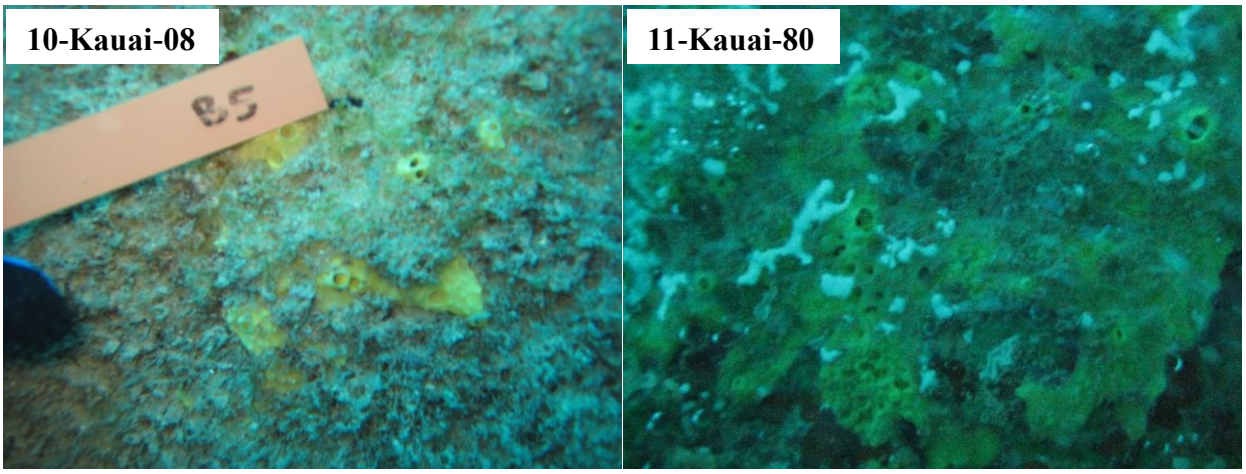

Figure 16. Photos of sponge samples collected from Kaua‘i

2.3 Isolation of Secondary Metabolites from *Dactylospongia elegans*

In our quest to discover new inhibitors of BACE1 from marine organisms, an extract of *Dactylospongia elegans* displayed activity against the enzyme in the *in vitro* assay described in section 1.6. Bioactivity-guided purification of the extract led to the isolation of ilimaquinone[80] **2.3**, a sesquiterpene quinone containing a 4,9-friedo-rearranged drimane skeleton. Other sesquiterpene quinones and hydroquinones isolated from the extract included 5-*epi*-ilimaquinone[81] **2.4**, smenospongine[82] **2.5**, smenospongorine[82] **2.6**, smenospongiarine[82] **2.7**, smenospongidine[82-83] **2.8**, dictyoceratin A[82, 84] **2.9**, dictyoceratin B[84] **2.10** and dictyoceratin C[85]

2.11 (Figure 17). The structures of these compounds were confirmed, except in one instance, by comparison of experimental spectroscopic data with the values reported in the literature. We discovered and confirmed by simple synthesis that the ^{1}H and ^{13}C NMR literature data for smenospongidine **2.8** contained obvious errors or omissions, which are discussed in depth in section 2.6.

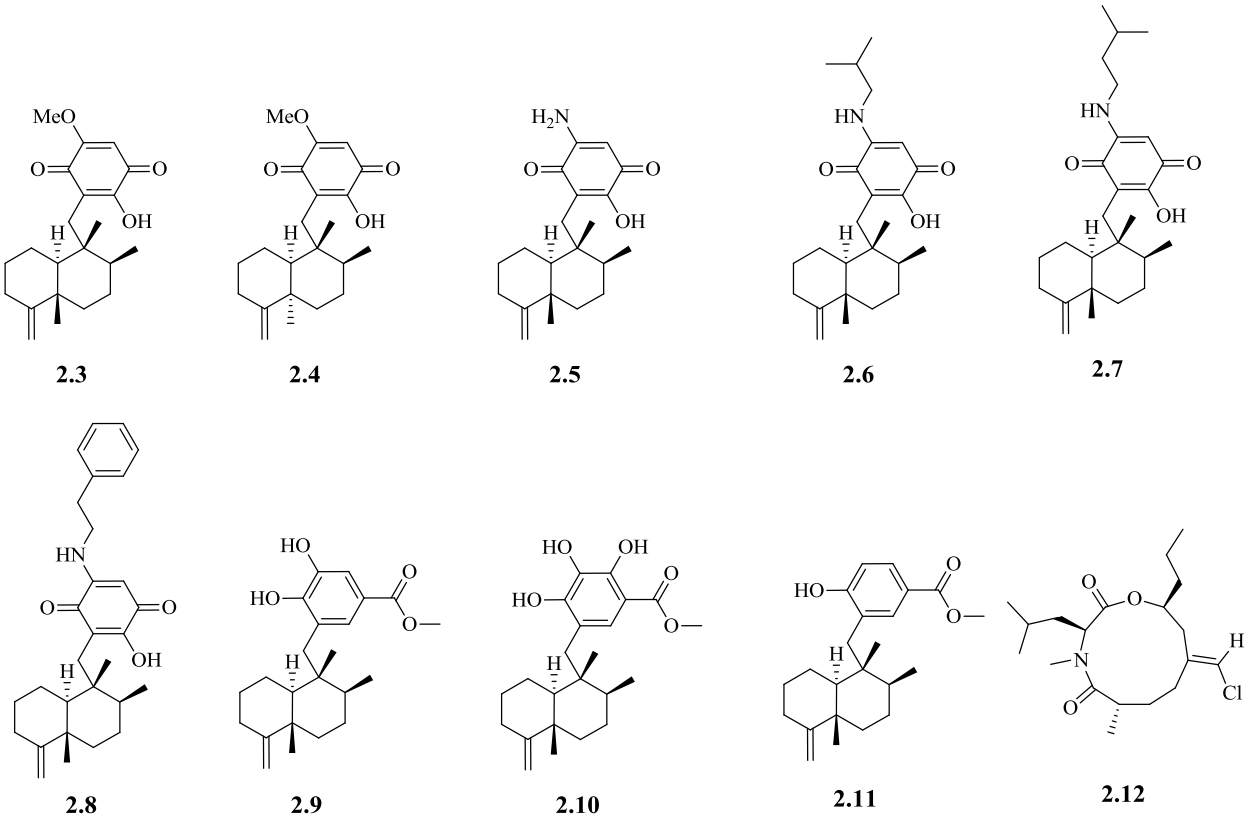

Figure 17. Natural products isolated from *Dactylospongia elegans*

In addition to these compounds, which have previously been isolated from sponges of the genus *Dactylospongia*, a new chlorinated compound **2.12** with a rare 11-membered heterocyclic framework was also isolated. The description of structure elucidation of this compound is presented in sections 2.4 and 2.5.

2.4 Planar Structure of Kauamide

The chlorinated compound **2.12** was present in an inactive fraction but we nonetheless pursued the isolation and purification of this metabolite, which we have named kauamide. Herein, we describe the elucidation of the structure of kauamide based on spectroscopic, chemical and computational methods. We also demonstrate the utility of computational tools in addressing questions of stereochemical configuration when the availability of sample may be too low to employ conventional methods.

High resolution mass spectrometry of kauamide suggested the molecular formula of $C_{19}H_{32}ClNO_3$, with four degrees of unsaturation. Two carbonyl units - an amide and an ester – were inferred from the ^{13}C NMR shifts at 177.4 ppm and 171.1 ppm as well as the infrared signals at 1734 cm^{-1} and 1653 cm^{-1}. The appearance of two additional sp^2 type signals in the ^{13}C NMR spectrum at 138.9 ppm and 116.7 ppm indicated the presence of an olefin and implied that a ring fulfilled the degrees of unsaturation in the molecule.

From the ^1H, ^{13}C and HSQC NMR data of kauamide (Table 1), five methyl groups, including one bonded to a nitrogen atom (δ_C 30.3, δ_H 2.84), six methylene units and four methine fragments were identified. Furthermore, the tri-substituted nature of the olefin was confirmed, as only one sp^2 carbon was connected to a single hydrogen atom. The majority of the planar structure was put together based on the COSY and HMBC data (Figure 18), paving way for the placement of the chlorine atom on the terminal carbon of the exocyclic olefin. The *E*-olefin geometry was determined from the presence of nOe correlations between H-15 and H-10 and the absence of such correlations between H-15 and H-8.

Table 1. NMR Spectroscopic Data of Kauamide (**2.12**) in $CDCl_3$ (500 MHz)

Position	δ_C, type	δ_H (J in Hz)	COSY	HMBC[a]
2	171.1, C			
3	55.7, CH	5.49, dd (11.5, 4.9)	15	2, 5, 16, 18
5	177.4, C			
6	36.0, CH	3.11, m		
7	26.5, CH_2	1.68, m		
		2.07, m	6, 8	5
8	26.1, CH_2	2.50, m		
		1.86, t (12.0)		9, 10
9	138.9, C			
10	40.2, CH_2	2.36, dd (14.5, 4.2)	11	9, 20
		2.28, dd (14.6, 2.8)		
11	73.5, CH	4.98, m		2, 10, 13
12	34.6, CH_2	1.52, m (15.6, 13.5, 6.9)	11, 13	
		1.43, m		
13	19.0, CH_2	1.26, m		
14	13.8, CH_3	0.92, t (7.3)	13	12
15	116.7, CH	5.83, s		8, 10
16	14.3, CH_3	1.14, d (6.7)	6	5
17	30.3, CH_3	2.84, s		3, 5
18	35.7, CH_2	1.79, m (14.8, 10.1, 4.9)		
		1.68, m		2
19	24.7, CH	1.58, m	18, 20, 20’	
20/20’	23.3, CH_3	0.97, d (6.7)		18
20’/20	21.1, CH_3	0.95, d (6.7)		18

a HMBC correlations, optimized for 7 Hz, are from proton(s) stated to the indicated carbon.

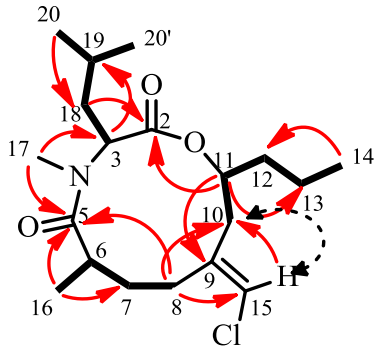

Figure 18. Depiction of COSY (bold lines), HMBC (red solid arrows) and NOE (black dashed arrows) correlations in kauamide (**2.12**)

2.5 Stereochemical Assignment of Kauamide

With three stereogenic centers of kauamide separated from each other by quaternary carbons and heteroatoms in a non-rigid ring structure, we were unsuccessful in determining the relative stereochemical configuration in the molecule using empirical NMR methods. The absolute configuration of each stereogenic center could be assigned individually using irreversible (for practical purposes) chemical modifications of the compound – advanced Marfey's method[86] (C-3), Mosher's method[87] (C-11) and Kusumi's method[88] (C-6) – but the latter two require a considerable amount of sample for unambiguous determination with the aid of standard NMR equipment. We had isolated only 2 mg of kauamide which was going to be insufficient to carry out these chemical modifications. Therefore, we turned to a protocol that relies on density functional theory-based computations of ^{1}H and ^{13}C NMR chemical shifts and the use of statistical tools to assign the experimental data to the correct isomer of a compound.[89] Similar approaches, sometimes in conjunction with synthesis, have been successfully employed toward assignment of stereochemical configurations of complex natural products, such as cernupalhine A[90] **2.13**, leiodermatolide[91] **2.14** and gambierone[92] **2.15**, and revision of incorrectly assigned structures of nobilisitine A[93] **2.16** mandelalide A[94] **2.17**, and hexacyclinol[95] **2.18** to name a few (Figure 19). Recently, Grimblat and Sarotti have reviewed the role of GIAO NMR calculations on the structural assignment of complex molecules.[96]

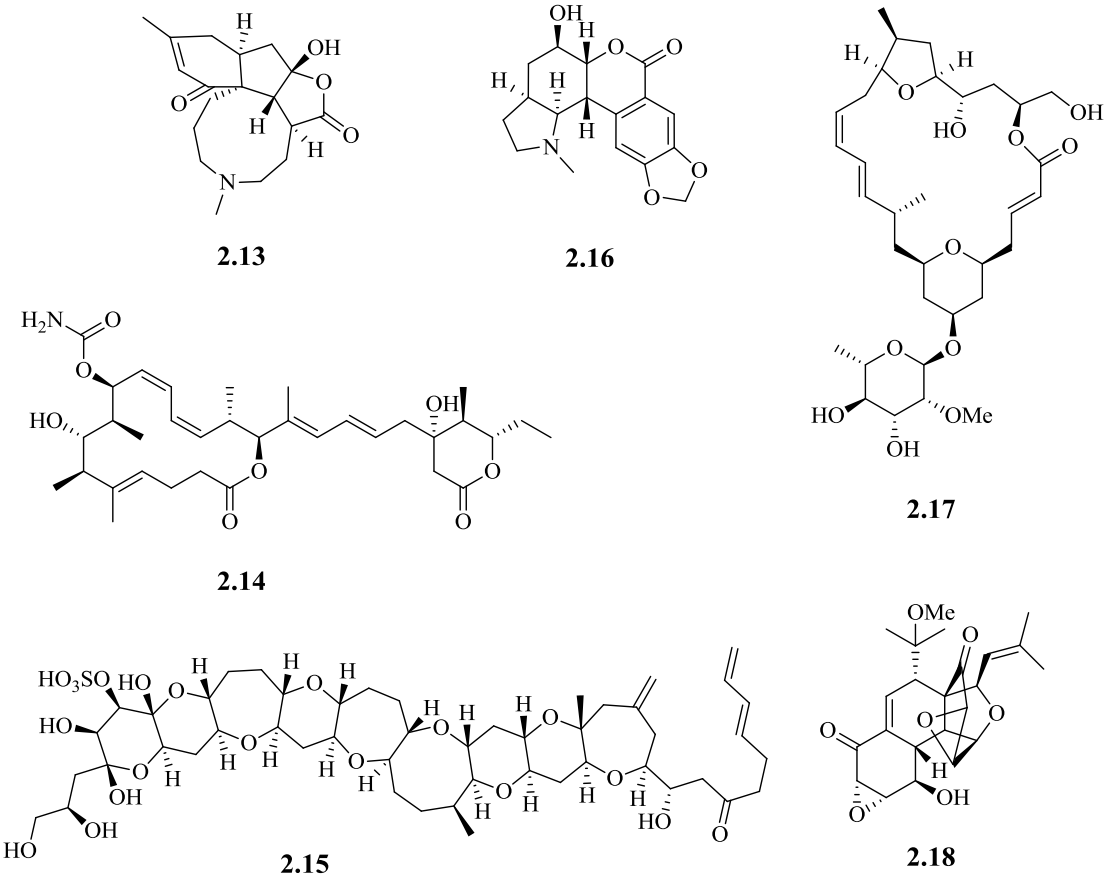

Figure 19. Examples of natural product structures that were established or revised based on DFT predictions of NMR chemical shifts

On our hands, the floppy nature of the two alkyl groups at C-3 and C-11 would amass a high computational cost because each diastereomer of kauamide resulted in more than two hundred and fifty conformers within 5 kcal/mol of the lowest energy conformer. To simplify the computational operations, we truncated the alkyl groups at those positions to methyl groups, as shown in the structure of **2.19** (Figure 20), which resulted in an approximately ten-fold reduction in the number of conformers.

An unambiguous match between the experimentally obtained ^{1}H and ^{13}C shifts of kauamide and the predicted values of the (3*S*,6*S*,11*S*)-diastereomer of **2.19** (Table 2) was established from various statistical comparisons between empirical and computed data. The chemical shifts of this diastereomer had the best fit to the ^{1}H and ^{13}C data of kauamide by any statistical measure, including mean absolute error (MAE), DP4[97] and DP4+[98] probabilities (Figure 20). From these studies, we propose that kauamide bears the (3*S*,6*S*,11*S*) relative configuration. The absolute configuration, (3*S*,6*S*,11*S*) and as drawn on **2.12**, was established after hydrolysis of kauamide and subsequent confirmation of the L-configuration of leucine residue by advanced Marfey's analysis.

Table 2. ^{1}H and ^{13}C NMR shifts of kauamide **2.12** (experimental) and all four diastereomers of **2.19** (predicted by DFT computations)

Key: *SRR* = (3*S*,6*R*,11*R*)-**2.19**; *SSR* = (3*S*,6*S*,11*R*)-**2.19**; *SRS* = (3*S*,6*R*,11*S*)-**2.19**; *SSS* = (3*S*,6*S*,11*S*)-**2.19**

		Computed						Computed			
H	**Experimental**	***SRR***	***SSR***	***SRS***	***SSS***	**C**	**Experimental**	***SRR***	***SSR***	***SRS***	***SSS***
15	5.83	5.73	6.04	5.94	**5.86**	9	138.9	145.1	142.0	145.2	**144.1**
11	4.98	5.13	5.31	4.60	**4.82**	8	26.1	26.7	28.7	29.3	**26.9**
10a	2.36	1.98	2.10	2.19	**2.43**	7	26.5	32.1	31.6	29.8	**26.2**
10b	2.28	2.79	2.59	2.39	**2.18**	6	36.0	38.1	37.0	37.5	**37.1**
8a	1.86	2.12	1.82	1.81	**1.98**	5	177.4	174.8	174.8	173.1	**174.3**
8b	2.50	2.68	2.77	2.73	**2.52**	3	55.7	60.1	57.0	56.6	**52.9**
7a	2.07	1.74	1.88	1.91	**2.12**	2	171.1	170.4	170.7	172.0	**171.4**
7b	1.68	1.54	1.50	1.54	**1.67**	11	73.5	68.0	69.4	74.4	**69.9**
6	3.11	2.78	2.15	2.72	**3.07**	10	40.2	39.1	39.3	42.4	**42.2**
3	5.49	3.42	4.20	4.38	**5.36**	15	116.7	116.5	121.2	119.5	**119.3**
16	1.14	1.01	1.14	1.13	**1.09**	16	14.3	15.4	15.7	15.6	**12.7**
17	2.84	3.05	3.15	2.80	**2.74**	17	30.3	34.6	30.8	27.4	**28.8**

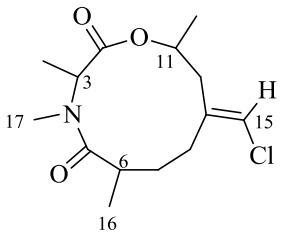

2.19

Isomer	DP4 probability	DP4+ probability
(3*S*,6*R*,11*R*)-**2.19**	0.00	0.00
(3*S*,6*S*,11*R*)-**2.19**	0.00	0.00
(3*S*,6*R*,11*S*)-**2.19**	0.00	0.00
(3*S*,6*S*,11*S*)-**2.19**	**1.00**	**1.00**

Figure 20. Relative configuration of kauamide **2.12** was established by statistical analyses of the computed and experimental ^{1}H and ^{13}C NMR shifts of all possible diastereomers of **2.19**

Kauamide, which is a mixed polyketide-peptide natural product, has a structural framework, including the vinyl chloride motif, which suggests that it may have been produced by a marine cyanobacterium. The 11-membered ring, however, is very rare in this class of molecules and natural products in general. The closest structural similarities are observed in jamaicamides A-C[99] **2.20**-**2.22**, which were isolated from *Moorea producens* Engene (Oscillatoriaceae),[100] a cyanobacterium formerly identified as *Lyngbya majuscula* and in kanamienamide[101] **2.23**, which was isolated from the cyanobacterium *Moorea bouillonii* Engene (Oscillatoriaceae) (Figure 21). These precedents strongly suggest that kauamide was produced by cyanobacteria cohabitating in the heavily fouled specimen of *Dactylospongia elegans*. The polyketide fragment in kauamide has the same carbon framework and identical olefin geometry as in the C1-C10 segment of jamaicamides A-C, whereas the 11-membered ring including the leucine residue is present in kanamienamide. Kanamienamide, however, lacks the vinyl chloride motif and has opposite configuration at C6, the carbon alpha to the amide carbonyl in the ring. The ^{1}H and ^{13}C NMR data for kanamienamide were acquired in benzene-d_6, precluding a direct comparison with

kauamide of the chemical shifts for protons and carbons in the 11-membered ring. Nevertheless, there is a reasonable match between the predicted ^{1}H NMR chemical shifts of (3*S*,6*R*,11*S*)-diastereomer of **2.19** and the experimental values reported for kanamienamide **2.23**, which bears the same configuration at the specified stereogenic centers. This provides further support to the assignment of relative configuration of kauamide through prediction of NMR chemical shifts.

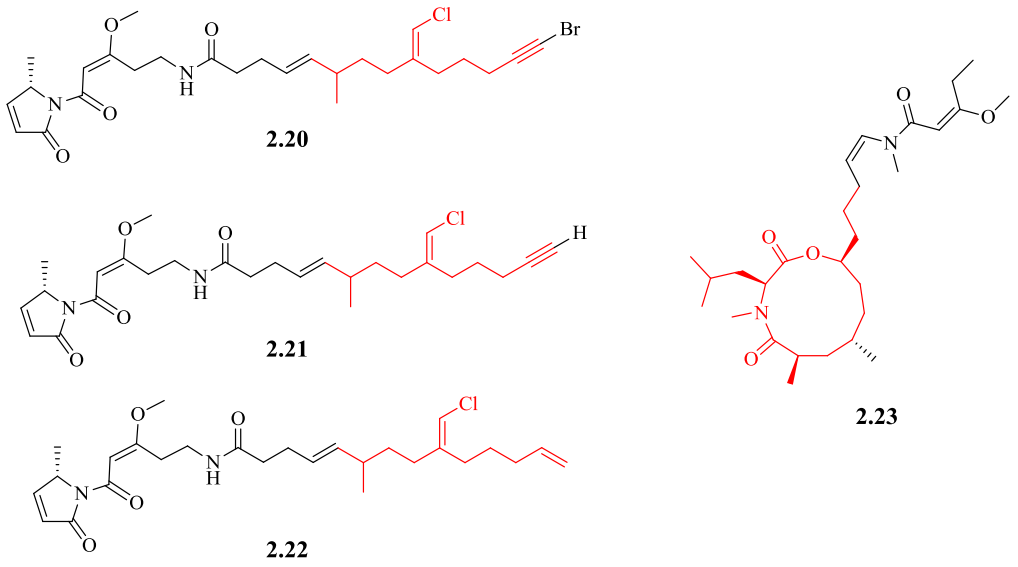

Figure 21. Cyanobacterial metabolites with partial structural similarity with kauamide **2.12**

2.6 Detailed Analysis of ^{1}H and ^{13}C NMR Data of Smenospongidine

Smenospongidine **2.8**, which is a biologically active quinone sesquiterpenoid, was first isolated from the sponge *Smenospongia* sp. by Kondracki and Guyot in 1989.[82] The authors proposed the structure of **2.8** based on analysis of HRMS, ^{1}H NMR and ^{13}CNMR data, but omitted carbon chemical shift data from the manuscript. In 1992, Rodríguez *et al.* published the first tabulated ^{13}C NMR data of **2.8**.[83] In the intervening years, **2.8** has been isolated from various sponge sources[102] with each reporting close agreement to the published data. In 2002,

Theodorakis and coworkers reported an enantioselective total synthesis of **2.8**, which, in addition to the usual statement about good agreement with published data, was accompanied by supplementary information with ^{1}H and ^{13}C NMR spectra of the synthesized molecule.[103] Recently, we also isolated **2.8** from *Dactylospongia elegans* and found significant discrepancies between our spectral data, and previous reports. Herein, we summarize the discrepancies and report corrected data for **2.8**. This case story demonstrates the value of depositing raw NMR data by showing how errors (omission, assignment, typographical, etc.) propagate through the literature when we are forced to rely on reproduced, tabulated, or listed data. This story also highlights the difficulties in locating original NMR data decades after publication of the original work. While **2.8** is a specific example, the problems are nonetheless widespread and persistent in the literature.

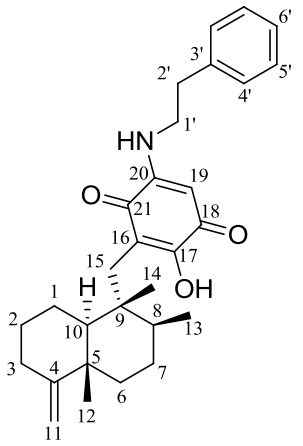

2.8

Figure 22. Structure of smenospongidine **2.8**, annotated with atom numbers.

The spectral data of smenospongidine obtained from this study are tabulated (Table 3) against those reported by Rodríguez *et al*. Rodríguez *et al.* did not report signals for the quaternary carbons C-10, C-16 and C-18 in **2.8** (Figure 22). Aside from that, the only major difference (> 2

ppm) between the two ^{13}C NMR data sets occurs at C-20 (150.0 vs. 154.7 ppm), with our value of 150.0 being more consistent with their data for the C-5 epimer of **2.8**. The partial ^{1}H NMR data reported in that manuscript has two main inconsistencies. First, a singlet reported at 5.41 ppm assigned as the hydroxyl proton may instead be the vinyl proton H-16 in the quinone ring. Second, a doublet at 0.77 ppm assigned to methyl protons (H-13) is more appropriate for H-10, an axial methine proton at the *trans*-decalin junction in quinone-containing analogues of **2.8** with identical stereochemical configuration.[82] With access to the original spectra, these issues of unreported or possibly misassigned signals are easy to resolve. For example, the last issue (H-10 vs H-13) could possibly be distinguished by the integrals, multiplicity (d vs dd) or the magnitude of observed coupling as the axial methine H-10 should display a larger *J* value (> 10 Hz), due to coupling with the neighboring axial proton (H-1), than the typical 7 Hz observed from methyl doublets. It should be noted that it is highly unlikely that even modern day spectra submitted as SI would possess adequate resolution or sufficient peak-picked expansions to resolve the matter.

To resolve these issues and clarify the identity of our sample of **2.8** with only proton and carbon data, we turned to the reported synthesis. As is typical, no specific proton or carbon assignments are reported in the manuscript describing the synthesis of **2.8** for the listed chemical shifts, so we have assigned them to the best of our ability for this comparison (Table 3) with the major differences highlighted in gray. Unfortunately, this data raised more questions. The listed ^{1}H NMR data on S19 does not include the signal for H-10, the proton at the A/B ring juncture possibly misassigned by Rodríguez *et al.*, but does include a signal at δ 0.97 (3H, d, J = 6.0 Hz) that we have assigned to H-13, a signal missing altogether from Rodríguez *et al*. Despite the inclusion of ^{1}H NMR spectra in the SI, the presence of these signals could not be conclusively confirmed because of the unavailability of an appropriate expansion of the spectrum. Other

Table 3. Comparison of ^{1}H and ^{13}C NMR Data of Smenospongidine **2.8** in $CDCl_3$.

	Data from this study		Data from Rodríguez *et al.*		Data from Ling *et al.*	
No.	δ_C	δ_H (500 MHz)	δ_C	δ_H (250 MHz)	δ_C‡	δ_H‡(400 MHz)
1	23.2	2.08, m	23.4		24.5	
		1.43, m				
2	27.9	1.38, m	27.8		29.3	
3	33.0	2.32, m	33.7		33.7	
		2.06, m				
4	160.5		161.9		167.7	
5	40.4		41.3		39.1	
6	36.6	1.51, m	37.8		35.6	
		1.35, m				
7	28.6	1.83, m	30.4		29.9	
		1.11, m				
8	37.8	1.18, m	38.3		37.9	
9	42.9		43.3		44.2	
10	49.8	0.77, dd (11.9, 2.0)			51.1	
11	102.5	4.44, brs	102.6	4.45, brs	103.7	4.44, d (5.2)
		4.45, brs				
12	20.5	1.06, s	21.0	1.05, s	21.9	1.04, s
13	17.9	0.97, d (6.5)	18.7	0.77, d	19.3	0.95, d (6.8)
14	17.3	0.84, s	17.7	0.82, s	18.7	0.82, s
15	32.4	2.39, d (14.0)	34.0	2.48, m	32.1	2.38, d (14.0)
		2.49, d (14.0)				2.51, d (14.0)
16	113.6					
17	157.0		155.3		161.5	
OH		8.35, brs		5.41, s		
18	178.3				180.2	
19	91.8	5.40, s	91.7		93.0	5.39, s
20	150.0		154.7			
NH		6.47, brs		6.53, brs		6.47, s
21	182.7		184.3		182.8	
1’	44.0	3.42, q (6.8)	44.6		45.3	3.42, m
2’	34.3	2.95, t (7.0)	34.0	2.95, m	34.3	2.94, m
3’	137.4		139.1			
4’	128.6	7.18, d (7.0)	129.5	7.27, m (H-4’ – H-6’)	129.7	7.10-7.40, m (H-4’ – H-6’)
5’	128.9	7.33, t (7.3)	129.5		130.0	
6’	127.0	7.26, m	127.5		128.2	

‡ Assignments were made by matching the proton and carbon nuclei with the closest reported chemical shift values. No chemical shift values could be assigned to C-16, C-20 and C-3’; signals at 69.0, 65.9 and 31.0 ppm were extra.

issues apparent from the listed ^{1}H NMR values are the mischaracterization of resonances that we have assigned to the terminal exocyclic alkene H-11 (reported as δ 4.44 (2H, d, J = 5.2 Hz)) and H-2 (reported as δ 2.94 (2H, m)). The latter resonance should be a triplet as the protons responsible for the signal are adjacent to only two equivalent protons, while the characterization of the δ 4.44 (2H, d, J = 5.2 Hz) resonance is clearly erroneous – as a J value of 1.2 Hz, typical of the coupling between two non-equivalent protons of the exocyclic terminal alkene, can be calculated from peak picking in the SI.

The ^{13}C NMR spectrum provided in the supplementary information and the chemical shift values extracted from the spectrum raise further questions on the interpretation of the NMR spectral data. Twenty-seven unique ^{13}C NMR resonances are expected for **2.8**. The SI of Ling *et al*. lists 25 signals for **2.8**, omitting two carbonyl signals. Of these 25 signals, only 7 out of the 12 required sp^2 carbon signals are reported and the list includes signals at δ 69.0 and 65.9 clearly inconsistent with the proposed structure, as it lacks oxygenated sp^3 carbons. The ^{13}C NMR spectrum with the poor signal-noise included in their SI sheds some light on the situation, but also raises questions as it includes the two carbonyl signals omitted from their list. The two carbonyl signals are labeled at 182.8 and 180.2 ppm but both appear between the chemical shifts of 181 and 182 ppm in the ^{13}C NMR spectrum perhaps due to peak picking errors.

There is little question smenospongidine was isolated or synthesized, as published in these articles. We have in fact synthesized smenospongidine from ilimaquinone using the method described by Ling *et al.*, and independently confirmed the structure (Scheme 1). Throughout the process the corresponding authors of those reports graciously offered assistance and searched for their original data at our request, but decades later were unsurprisingly unable to locate it. The difficulties of individual labs or departments maintaining NMR records over 40 years are

significant. Our laboratory (Prof. Philip Williams) receives frequent requests for copies of NMR data generated by the late Paul Scheuer and Richard Moore with a success rate of less than 50%. Most recently, we were unable to fulfill a request for data on the cyanobacterial compound micromide due to degradation of the CD backups. The fact remains that our community's reliance on tabulated or summarized data introduces the possibility of a litany of errors into the literature. Availability of raw NMR data would undoubtedly play a major role in curbing the propagation of these errors.

Scheme 1. Synthesis of smenospongidine **2.8** from ilimaquinone **2.3**

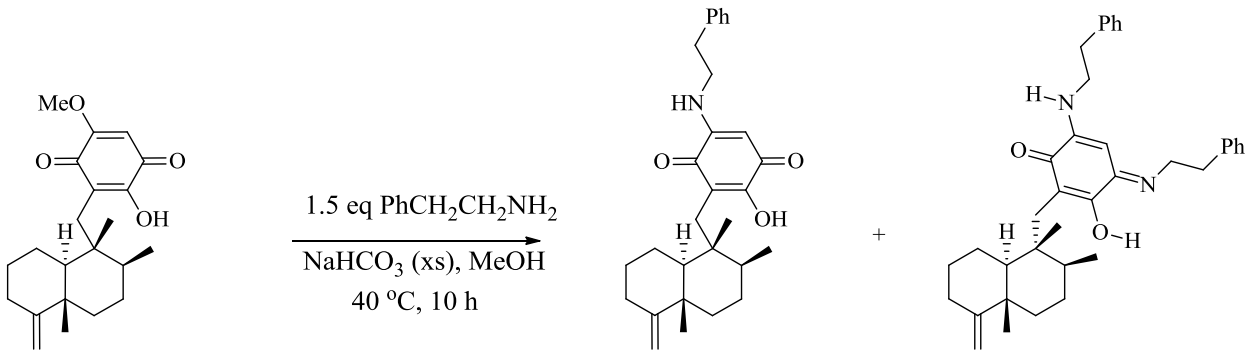

2.3

2.8 (53% yield)

2.24 (27% yield)

2.7 Structure of Smenospongidinimine

In replicating the one-step synthesis of smenospongidine from ilimaquinone and phenethylamine,[103] we also discovered smenospongidinimine **2.24**, a previously unreported side product. Smenospongidinimine, which was produced in a 3:5 ratio with smenospongidine because of the presence of excess phenethylamine, displays symmetry in the quinone ring of the molecule because of the equilibrium between two rapidly interconverting tautomers (Figure 23).

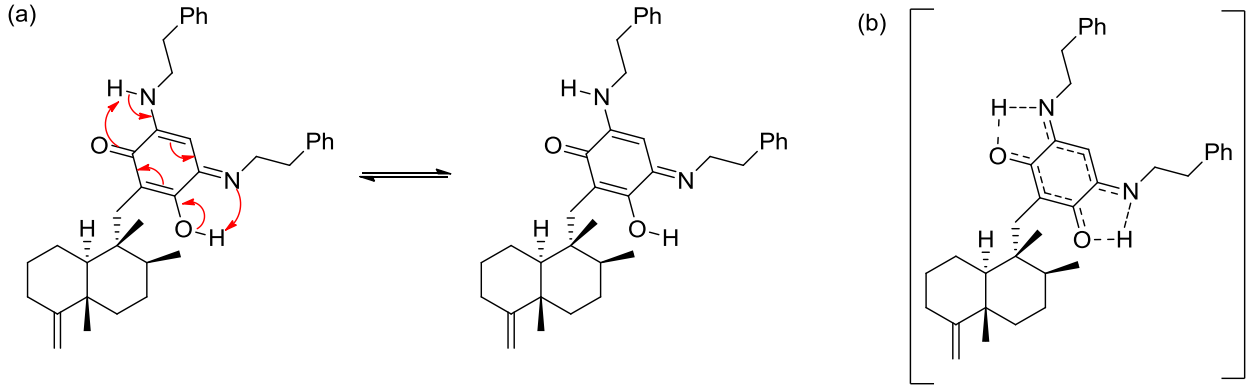

Figure 23. (a) The two tautomeric forms and (b) the resonance hybrid of smenospongidinimine

2.8 Evaluation of Biological Activity

Ilimaquinone **2.3** and smenospongine **2.5** displayed moderate inhibition of BACE1, whereas the other analogs showed weak or no activity (Table 4). Sesquiterpene quinones and hydroquinones are known to be cytotoxic to a variety of cancer cell lines, which was reaffirmed when we screened these compounds against human glioblastoma (U251MG) and human pancreatic carcinoma (Panc-1) cell lines. Compounds **2.3**-**2.11** all exhibited considerable cytotoxicity toward U251MG cells, with smenospongine **2.5** and dictyoceratin A **2.9** showing the most potent effects. Furthermore, compounds **2.3** and **2.6**-**2.9** were significantly cytotoxic toward Panc-1 cells as well. Kauamide showed no biological activity in any of the three assays but will be examined in antimicrobial and other assays.

Table 4. Biological activity of metabolites isolated from *Dactylospongia elegans*

Compound	IC_{50} (BACE1)	CC_{50} (U251MG)	CC_{50} (Panc-1)
2.3	65 μM	19.3 μM	20.4 μM
2.4		19.4 μM	
2.5	78 μM	2.4 μM	
2.6		19.4 μM	22.6 μM
2.7		4.5 μM	15.1 μM
2.8		4.0 μM	12.6 μM
2.9		2.8 μM	21.7 μM
2.10		8.4 μM	
2.11		4.1 μM	
2.24[b]		19.3 μM	

b Synthesized from ilimaquinone **2.3**

2.9 Conclusions

Nine known cytotoxic sesquiterpene quinones and quinols and kauamide, a new 11-membered heterocycle, were isolated from the extracts of *Dactylospongia elegans*. Ilimaquinone and smenospongine also exhibited moderate BACE1 inhibition. A detailed study of ^{1}H and ^{13}C NMR spectral data of smenospongidine revealed errors in the literature data. During the process, a previously unreported side-product smenospongidinimine was also isolated and characterized.

CHAPTER 3

Isolation and Characterization of Secondary Metabolites from the Culture Broth of HCC1088, *Nostoc* sp.

3.1 Significance of Cyanobacteria and their Metabolites

Cyanobacteria are among the oldest and the most successful microorganisms on earth. They were the first organisms to utilize photosynthesis for energy, thereby releasing oxygen into the earth's atmosphere.[104] Also known as blue-green algae, these Gram-negative bacteria have been found to inhabit a variety of environments, including marine and fresh water, hot springs, ice, soil, rocks, plants, and animals.[105] Their long and successful history – spanning approximately three billion years – has attracted immense interest as scientists try to uncover the reasons why these organisms have been able to flourish in various environments across different geological and biological eras.[106]

One of the factors that keep cyanobacteria successful is their ability to produce a variety of secondary metabolites that serve specific purposes.[107] Toxins help them ward off grazers whereas UV-screening agents and antifreeze compounds protect them from severe environmental elements.[108] In addition to serving these functions, many of the metabolites have shown powerful bioactivity. Consequently, several cyanobacterial secondary metabolites and their analogues have been developed as small molecule drug targets.[109]

Cyanobacteria have been known to produce a variety of structurally diverse secondary metabolites, such as alkaloids, polyketides, peptides, terpenes and combinations thereof.[105b] The biosynthetic machinery of the blue-green algae allows for the incorporation of

the structural features of peptides and lipids, and additional functionalizations, such as unusual oxidations, methylations and halogenations.[110] While natural products from terrestrial cyanobacteria have been reported as early as the 1930s, work on marine cyanobacteria began in the 1970s. The late professor Richard Moore of the University of Hawaii pioneered the research on natural products from marine cyanobacteria and continued his work until the 2000s.[110a, 111]

The studies carried out by Moore and others to date have revealed that marine and terrestrial cyanobacteria produce a rich collection of metabolites with neurotoxic, anti-infective, anti-proliferative and anti-inflammatory properties.[112] Many of these molecules, such as cryptophycin 1[113] **3.1**, dolastatin 10[25, 114] **1.26** and curacin A[115] **3.2**, have shown potent biological activity and are of interest for the development of pharmaceuticals (Figure 24). Dolastatin 10 and cryptophycin 52[116] **3.3** (a synthetic analog of cryptophycin 1), which are microtubule-binding agents, entered clinical trials for breast cancer and solid tumors, respectively, but have been abandoned due to ineffectiveness and adverse side effects.[117] Analogues of dolastatin 10 have already been approved as drugs or are currently in clinical trials.[117] The active component in brentuximab vedotin, which is an FDA approved monoclonal antibody-drug conjugate for the treatment of Hodgkin lymphoma,[118] is monomethyl auristatin E **3.4**, a synthetic analogue of dolastatin 10 (Figure 24). Romidepsin **3.5**, which was originally isolated as FR901228 from the broth culture of *Chromobacterium violaceum* Bergonzini (Neisseriaceae),[119] is a cyclic depsipeptide analogue that has been approved by the FDA for the treatment of cutaneous T-cell lymphoma.[120]

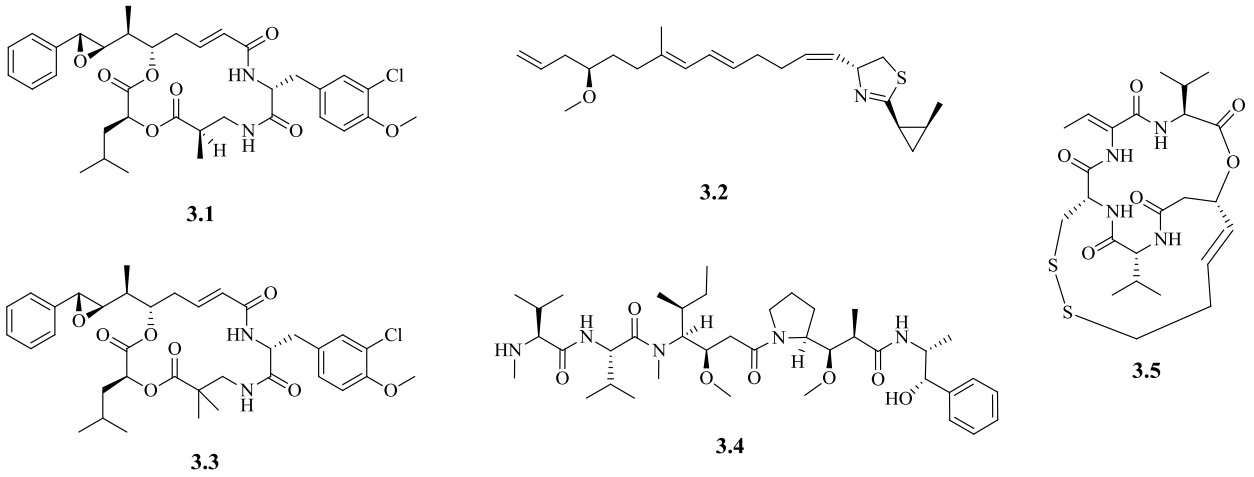

Figure 24. Cyanobacterial natural products and synthetic analogues of pharmaceutical interest

The unique structural features coupled with powerful bioactivity make metabolites from marine and terrestrial cyanobacteria attractive targets in the development of drug leads against other diseases as well, including Alzheimer's. Moreover, many of these microbes are amenable to laboratory cultures using existing techniques,[112a] potentially allowing for large-scale production and harvesting. However, the application of cyanobacterial cultures for industrial-scale synthesis of compounds and products of interest is technologically challenging and needs further development.[121] As part of our studies to isolate novel bioactive molecules, we cultured several cyanobacterial strains and screened their extracts for activity against various targets. The culture broth of HCC1088 showed initial activity against BACE1; hence, we pursued the isolation of potential BACE1 inhibitors from this strain.

3.2 Culture Details, Appearance and Phylogenetic Information of HCC1088

HCC1088 is a cyanobacterial strain obtained from the cryogenically preserved Patterson cyanobacteria collection housed at the University of Hawai‘i at Manoa. The strain, tentatively identified as a species of the genus *Nostoc*, was acquired from the Mitsui-Miami collection (ID: 102201) and its original collection location is unknown. A cryovial of HCC1088 was thawed and cultured in a 10 mL tube containing the BGM cyanobacterial growth medium (BG-11 prepared with 3-(*N*-morpholino)propanesulfonic acid (MOPS) buffer). The culture, through a series of propagation steps in various sized flasks, was eventually grown in multiple 20 L carboys with aeration. The timeframe for the growth of cyanobacteria from a preserved cryovial to 20 L cultures is typically 6-9 months. HCC1088 is a filamentous cyanobacterium with short to medium strands which grows from light green to dark green as cell density increases in the culture medium (Figure 25). Microscopic imaging showed that the culture contained fungal and possibly bacterial contaminants.

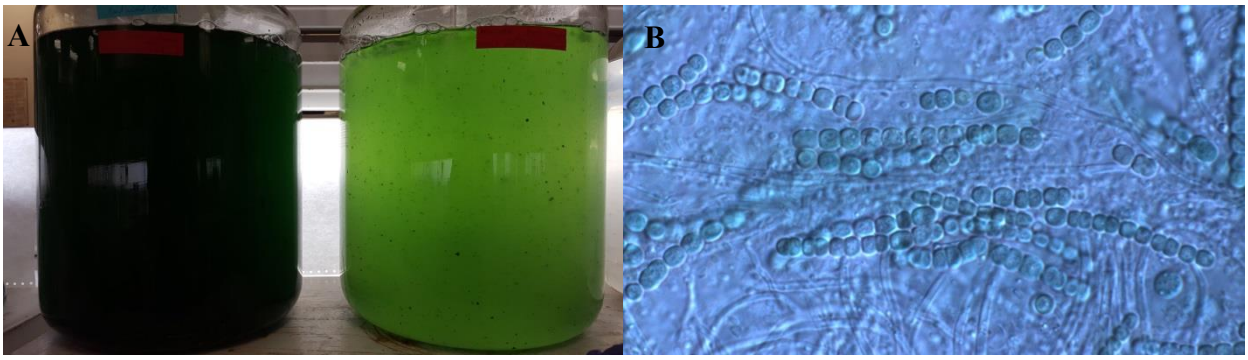

Figure 25. (a) Photographs of 20 L cultures of HCC1088 at various stages of growth (b) microscopic image of the culture

In efforts to determine phylogeny of the strain HCC1088, genomic DNA was isolated from the cells and its 16S ribosomal RNA gene sequence was obtained. The sequence was then searched for close matches in the 16S rRNA gene sequence database and the nucleotide collection database using NCBI's basic local alignment search tool (BLAST). The sequences with the most similar alignments were then subjected to a molecular phylogenetic analysis using available bioinformatics tools. The evolutionary history, as depicted in Figure 26, was inferred by using the Maximum Likelihood method based on the Tamura-Nei model.[122]

The phylogenetic analysis of the closely matched gene sequences obtained from the 16S rRNA sequence database revealed no obvious phylogenetic match for the strain HCC1088; however, the most analogous sequences were found in the nucleotide collection database (Figure 26). These sequences belong to uncultured cyanobacteria with no phylogenetic information, precluding us from making any inference on the phylogeny of the strain HCC1088. While morphological evaluation was consistent with a *Nostocalean* strain, no firm conclusions could be reached.

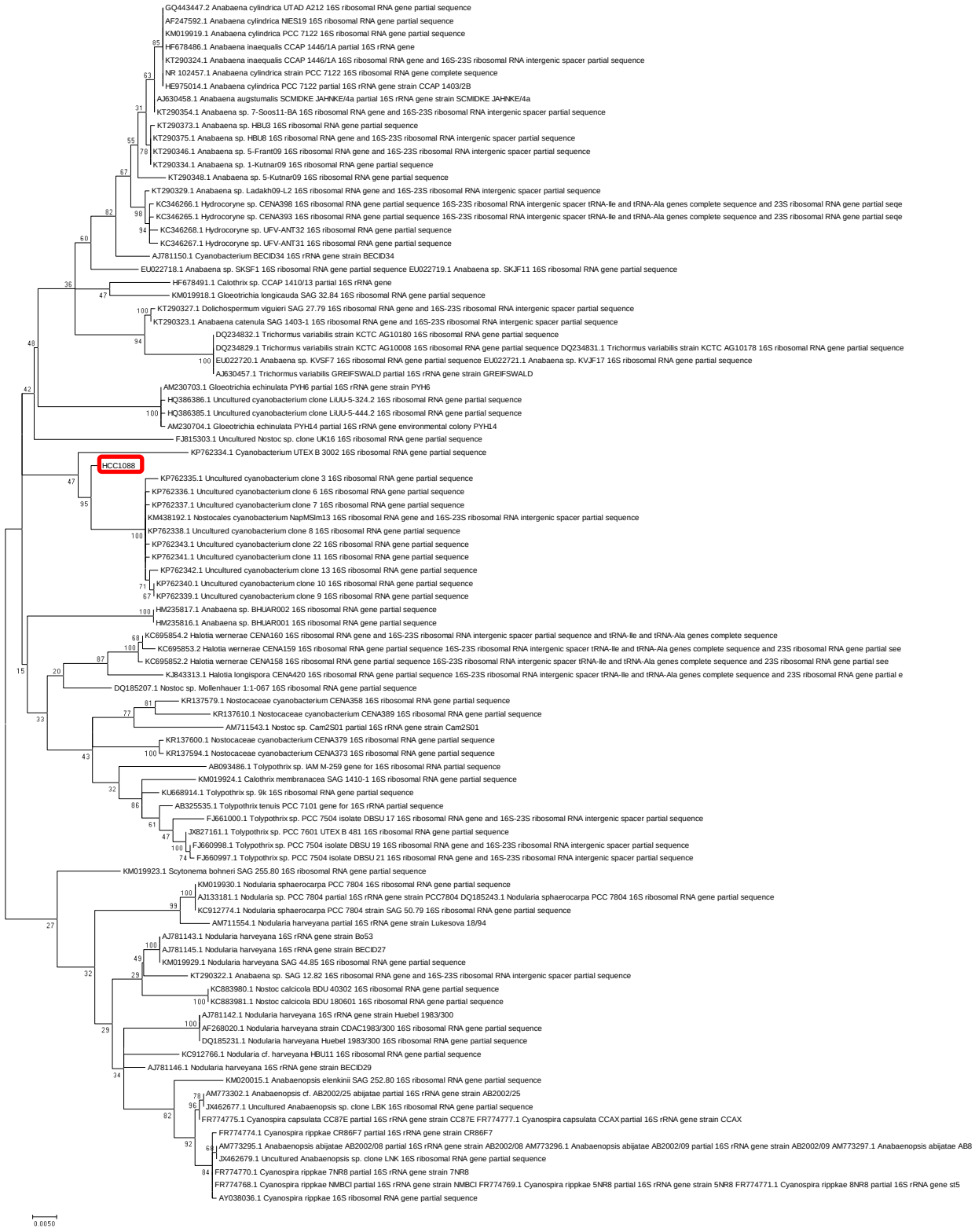

Figure 26. Molecular phylogenetic analysis by maximum likelihood method, using MEGA7

3.3 Isolation of Secondary Metabolites from HCC1088, *Nostoc* sp.

Secondary metabolites from the culture broth of HCC1088 were of interest because its extract showed significant inhibitory activity in the BACE1 enzyme fragment complementation assay. Extraction of compounds from the broth using HP-20 resin, followed by purification by HPLC, led to the isolation of several compounds.

Four new compounds **3.6-3.9** and two previously known metabolites 3-formylindole[123] **3.10** and 3-cyanoindole[124] **3.11** were isolated from the culture broth extract of HCC1088 (Figure 27). Compound **3.7** was identified as the molecule potentially responsible for the BACE1 inhibitory activity in the enzyme fragment complementation assay as well as the homogeneous affinity assay based on prior work by former members of the Williams research group.

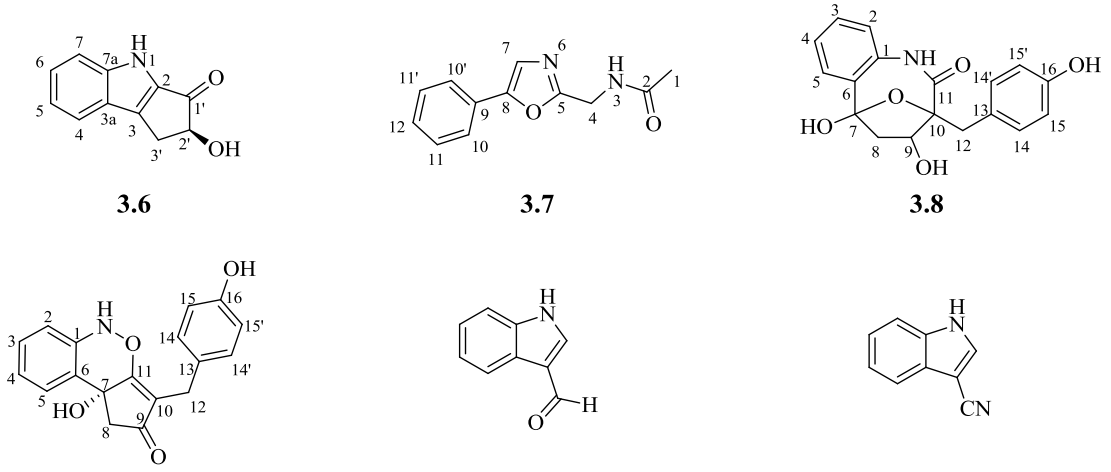

3.6 **3.7** **3.8**

3.9 **3.10** **3.11**

Figure 27. Structures of metabolites isolated from the culture broth of HCC1088

3.4 Elucidation of Structures of Metabolites of HCC1088

Structure elucidation of 3.6. The molecular formula of compound **3.6**, which was isolated as optically active ($[\alpha]_D^{21}$ +15 (*c* 0.2, CH_3OH)) yellow crystalline needles, was established as $C_{11}H_9NO_2$ from its HRESIMS signal at *m*/*z* 210.0525 $[M+Na]^+$. The infrared stretches at 3303 cm^{-1} and 3210 cm^{-1} were indicative of the presence of O-H and N-H bonds, whereas the stretch at 1678 cm^{-1} suggested that **3.6** contained an α,β-unsaturated carbonyl (ketone) unit. The latter conclusion was supported by the signal at 194.4 ppm in the ^{13}C NMR spectrum. A total of eleven carbon signals were observed, including two sp^3 carbons and eight sp^2 carbons in addition to the conjugated ketone, and they were classified into methine, methylene and quaternary carbons using the HSQC spectrum (Table 5). The ^1H NMR signals at δ_H 4.53, 3.48 and 2.69 constitute an AMX pattern, indicating the presence of an isolated $CH\text{-}CH_2$ fragment bearing an oxygen atom on the methine carbon. The splitting patterns of the four aromatic proton signals, i.e., δ_H 7.65, 7.41, 7.31 and 7.08, show the presence of a 1,2-disubstituted benzene ring, which accounts for six of the eight unassigned sp^2 carbons. The benzene ring was proposed to be a part of a 2,3-disubstituted indole ring based on the remaining atoms, which included two quaternary sp^2 carbons, one nitrogen and two exchangeable protons, one of which was assigned as the hydroxyl proton. This satisfied all but one degree of unsaturation, which suggested the presence of a third ring in the molecule. The HMBC resonances from δ_H 3.48 and 2.69 (3') to δ_C 123.2 (3a) were used as the key evidence in establishing the planar structure of compound **3.6** (Figure 28).

Table 5. NMR Spectroscopic Data of Compound **3.6** in DMSO-d_6 (500 MHz)

Position	δ_C, type	δ_H (J in Hz)	COSY	HMBC[a]
1 (NH)		11.60, brs		
2	136.3, C			
3	141.0, C			
3a	123.2, C			
4	121.6, CH	7.65, dt (8.1, 1.0)	5	3, 3a, 6, 7a
5	120.3, CH	7.08, ddd (8.0, 7.0, 1.0)	4, 6	3a, 6, 7
6	127.1, CH	7.31, ddd (8.2, 6.9, 1.2)	5, 7	4, 7a
7	113.8, CH	7.41, dt (8.3, 0.9)	6	3a, 5
7a	143.9, C			
1’	194.4, C			
2’	77.0, CH	4.53, dd (6.3, 2.6)	3’	1’, 3, 3’
3’	30.7, CH_2	3.48, dd (16.2, 6.4)	2’	1’, 2, 2’, 3, 3a
		2.69, dd (16.2, 2.8)	2’	2, 2’, 3, 3a
2’-OH		5.85, brs		

a HMBC correlations, optimized for 7 Hz, are from proton(s) stated to the indicated carbon.

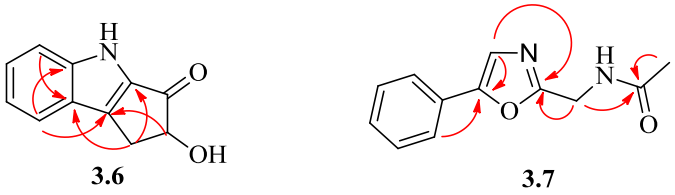

3.6 **3.7**

Figure 28. Important HMBC correlations that were used to establish the planar structures of compounds **3.6** and **3.7**

Mosher’s method[125] is an established protocol in determining the absolute configuration of a chiral secondary alcohol, however, the $\Delta\delta$ ($\delta S - \delta R$) values cannot be used to conclusively assign the absolute configuration at C-2’ of compound **3.6** because of the lack of proximal non-exchangeable protons on one side of the secondary alcohol (Figure 29a). Subsequent reductions of the MTP-esters of compound **3.6** (**3.12** and **3.13**) using the Luche

protocol[126] to compounds **3.14** and **3.15** introduce an additional proton at C-1', allowing for a more definitive assignment of absolute configuration at C-2' (Scheme 2). In each reduction, **3.14** or **3.15** is formed as a single diastereomer, which may be rationalized by a chelation model in which cerium coordinates to both the ketone and the ester carbonyls, facilitating a hydride attack from one face. While the relative stereochemistry of this single diastereomer was not determined, it likely has the *syn* configuration.[127] Formation of a single diastereomer in each reduction is not critical to the success of Mosher's analysis, but it results in a cleaner spectrum, eliminates the need for difficult separation and makes the analysis straightforward. The $\Delta\delta$ ($\delta S - \delta R$) values computed from the ^{1}H NMR spectra of compounds **3.14** and **3.15** suggest an *S*-configuration at C-2' of compound **3.6** (Figure 29b). This assignment is further supported by density functional theory (DFT) calculations. The computed specific rotation of compound **3.6** ($[\alpha]_D^{25}$ +19, MeOH solvation) at the B3LYP/6-311+G(d,p) level was a close match with the experimental value.

Scheme 2. Mosher esterification of compound **3.6** and subsequent reductions.

NOTE: Based on CIP rules, the *S*-ester **3.12** is synthesized from the *R*-acid chloride. Likewise, the *R*-ester **3.13** is synthesized from the *S*-acid chloride

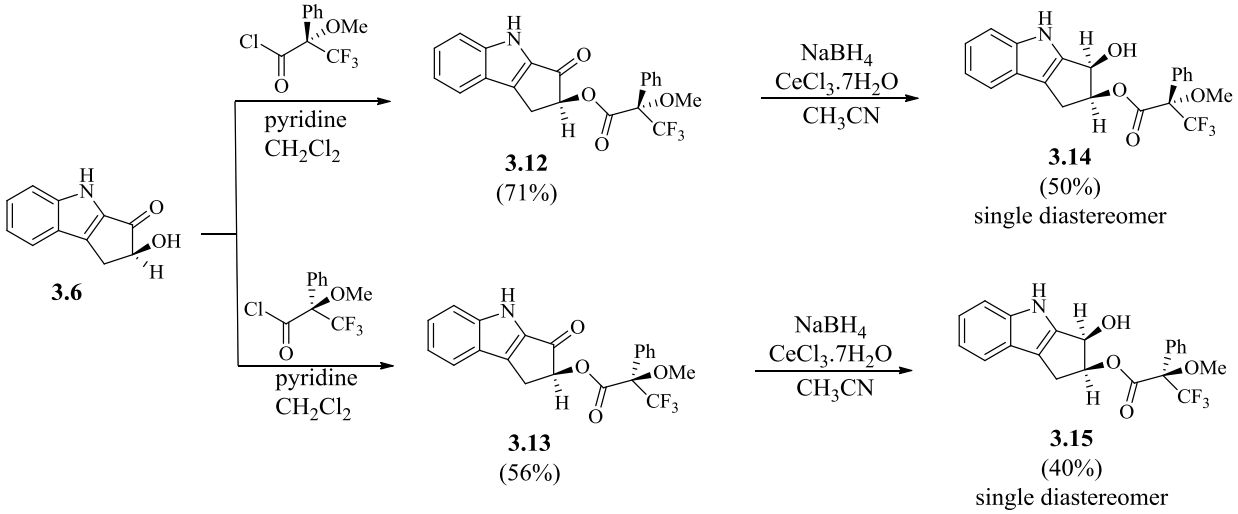

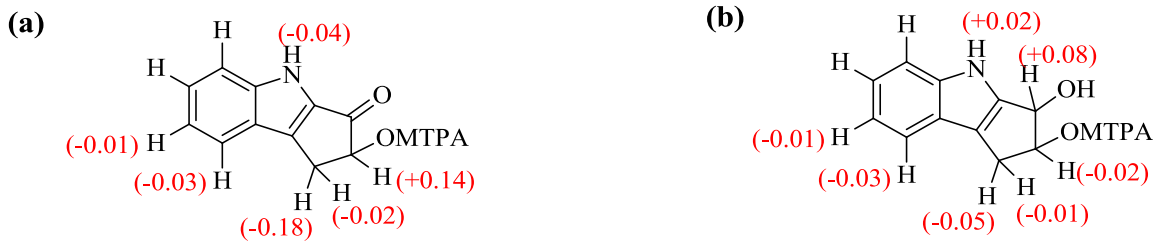

Figure 29. $\Delta\delta$ ($\delta S - \delta R$) values for (a) Mosher's esters and (b) reduced Mosher's esters of compound **3.6** suggest an (*S*)-configuration at the carbinol stereogenic center.

The octant rules[128] predict compound **3.6** to exhibit a positive Cotton effect in its electronic circular dichroism (ECD) spectrum (Figure 30a). A positive Cotton effect was also observed in the ECD spectrum generated by SpecDis[129] using the data obtained from TDDFT calculations (see experimental section) at the B3LYP/6-311+G(d,p) level as well as the B3LYP/aug-cc-pVDZ level (Figure 30b). However, the experimental ECD spectrum of **3.6** showed a negative Cotton effect, implying an anti-octant behavior (Figure 30b). Anti-octant behavior is not an uncommon phenomenon and is often observed with compounds containing axial substituents and, particularly, fluorine.[130] Moreover, compounds with oxygen- and nitrogen-containing substituents have been identified as capable of exhibiting either octant or inverse octant behavior and the roles of the substituents are not clear.[131] In compound **3.6**, the presence of a hydroxyl group on the lone stereogenic center (C-2') of an otherwise planar and rigid molecule may be deemed responsible for the apparent anti-octant behavior seen in its ECD spectrum.

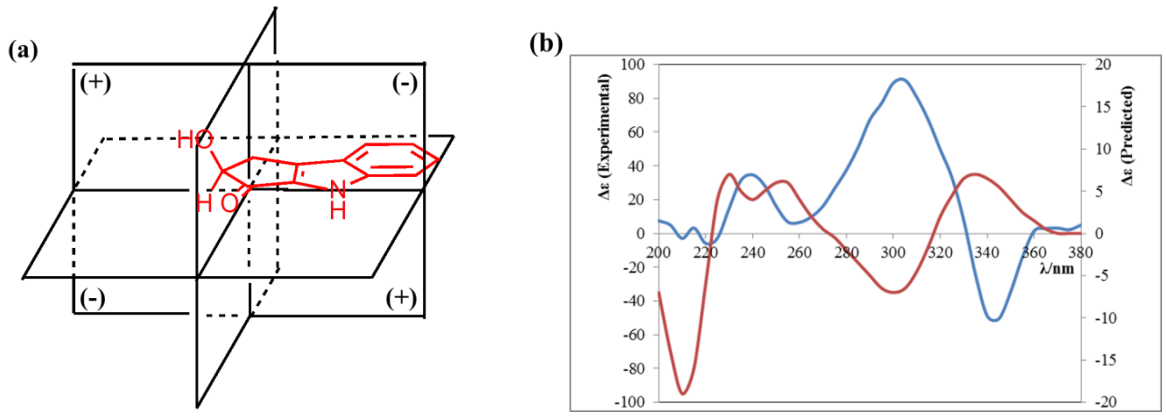

Figure 30. (a) Compound **3.6** is predicted to show a positive Cotton effect based on octant rules; (b) Calculated (red) and experimental (blue) ECD spectra of compound **3.6** show positive and negative Cotton effects, respectively.

A plausible biosynthetic route of compound **3.6** involves an intramolecular electrophilic aromatic substitution (Friedel-Crafts acylation) of tryptophan, transamination to a dione, and subsequent reduction to the α-hydroxy ketone moiety. It must be noted that Friedel-Crafts alkylation is a common occurrence in biological systems[132] but acylation is quite rare.[133] While compound **3.6** is reported here for the first time, a close analogue, in which the hydroxyl group is substituted by an amino group, has been prepared by synthesis and is known to be an anti-inflammatory agent and a central nervous system drug.[134]

Structure elucidation of 3.7. Compound **3.7** was isolated as an amorphous white solid and its molecular formula was determined to be $C_{12}H_{12}N_2O_2$ from its HRESIMS signal at *m*/*z* 239.0782 $[M+Na]^+$. The ^{13}C NMR spectrum of **3.7** indicated the presence of ten unique carbons, which were classified into four quaternary sp^2 carbons, four sp^2 methines, one sp^3 methylene group, and one methyl group using the HSQC spectrum (Table 6). The signal at δ_C 170.1 (C-2) was assigned to the carbonyl carbon of an amide or an ester. Analysis of the HMBC

spectrum helped establish both the identity of the amide functional group and its connectivity with the methyl group (C-1) based on the correlations from the singlet methyl at δ_H 2.10 (H-1) to δ_C 170.1 (C-2) and 37.1 (C-4). These resonances ruled out the possibility of a direct connectivity of C-1 with the methylene C-4 or of C-4 with an oxygen atom, the latter based on the chemical shift of the carbon. The relative integrations and multiplicities of the signals at δ_H 7.61, 7.42 and 7.33 suggested that a mono-substituted benzene ring was present in the molecule. The proton signal at δ_H 7.26 (H-6) did not show resonances in the HSQC spectrum (optimized for 140 Hz) but its connectivity to C-7 was established from the HMBC spectrum, which was also used to extract the $^1J_{C\text{-}H}$ value of 194 Hz, indicating that this methine was part of a heteroaromatic ring. An oxazole ring was speculated based on the remaining fragments, and the structure of compound **3.7** was proposed following analysis of chemical shifts and some key HMBC resonances (Figure 28). These included correlations from δ_H 7.26 (H-6) to δ_C 152.0 (C-8), 160.1 (C-5) and 37.1 (C-4), and from δ_H 4.65 (H-4) to δ_C 160.1 (C-5), 170.1 (C-2), 152.0 (C-8), 121.6 (C-7) and 23.1 (C-1). Since several of these are four-bond correlations, an alternate structure **3.16** was also considered (Figure 31b). The HMBC resonances were more in line with **3.16**, however, chemical shifts and examination of biosynthetic routes suggested that **3.7** was the more likely structure. While compound **3.7** has plausible biosynthetic precursors in phenylethanolamine and *N*-acetylglycine (or glycine and an acetate unit), there is no straightforward pathway for compound **3.16** (Figure 31a). Nevertheless, the presence of ambiguous data necessitated the confirmation of the structure via other methods.

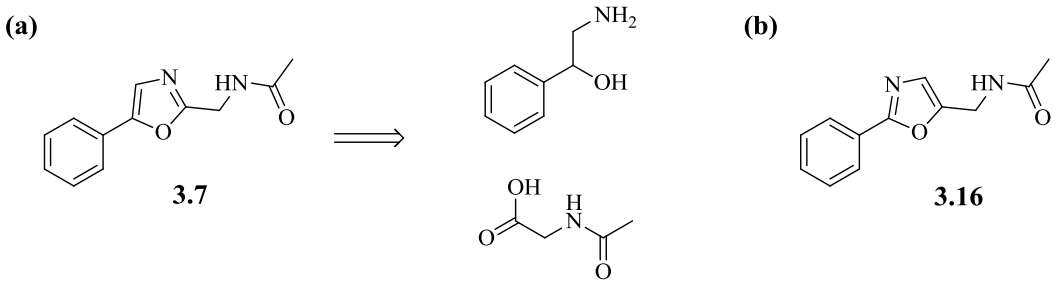

Figure 31. (a) Biosynthetic precursors of compound **3.7** and (b) an alternate structure **3.16**

Due to degradation of the compound during the analysis steps, which precluded us from carrying out further characterization and biological evaluation, compound **3.7** was synthesized through acetylation of its commercially available amine hydrochloride precursor, **3.17** (Scheme 3). The ^{1}H and ^{13}C NMR data of synthetic **3.7** were nearly identical to those acquired from natural product isolated from the culture broth of the cyanobacterium, confirming the structure of compound **3.7**.

Table 6. NMR Spectroscopic Data of Compound **3.7** in $CDCl_3$ (500 MHz)

Position	δ_C, type	δ_H (*J* in Hz)	COSY	HMBC
1	23.1, CH_3	2.10, s		2, 4
2	170.1, C			
3 (NH)		6.19, brs		
4	37.1, CH_2	4.65, d (5.4)	3	1, 2, 5, 7, 8
5	160.1, C			
6 (N)				
7	121.6, CH	7.26[a], s		5, 8
8	152.0, C			
9	127.5, C			
10, 10’	124.2, CH	7.61, d (7.8)		8, 12[b]
11, 11’	128.9, CH	7.42, t (7.7)	10, 10’, 12	10, 10’, 9[b]
12	128.6, CH	7.33, t (7.4)		10, 10’

a C-H connectivity established from HMBC experiment ($^{1}J_{C\text{-}H}$ = 194 Hz)

b Observed when optimized for 7.0 Hz and recorded in CD_3OD (other HMBC signals observed when optimized for 4.0 Hz and recorded in $CDCl_3$)

Scheme 3. Preparation of compound **3.7** via acetylation of **3.17**

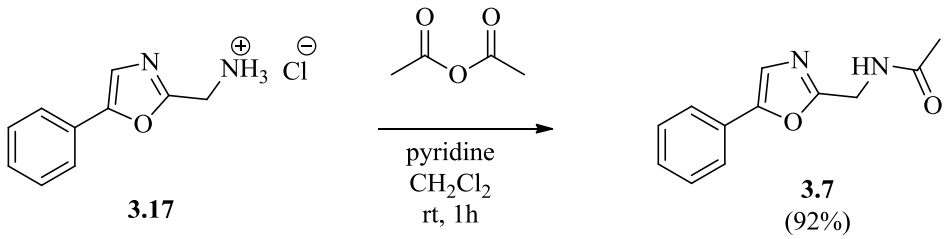

Structure elucidation of 3.8. The molecular formula of compound **3.8** was determined to be $C_{18}H_{17}NO_5$ based on its HRESIMS signal at *m*/*z* 328.1184 $[M+H]^+$. Two benzene rings, *ortho*- and *para*-disubstituted, were identified from the coupling patterns of the proton signals in the aromatic region. Analysis of the ^1H, ^{13}C, and HSQC NMR spectra of compound **3.8** further revealed the presence of a CH-CH_2 fragment with oxygenation at the methine, and an isolated CH_2 fragment (Table 7). A carbonyl moiety – an amide or an ester – was established from the signal at 175.5 ppm in the ^{13}C NMR spectrum. Also observed in the ^{13}C NMR spectrum were two downfield quaternary carbons, at 104.3 ppm and 91.3 ppm, indicative of sp^3 carbons connected to oxygen atoms and/or other deshielding atoms or functional groups.

The carbon framework of compound **3.8** was completed on the basis of various HMBC resonances (Figure 32). The correlation from δ_H 7.49 (H-5) to δ_C 104.0 (C-7) established C-7, assigned as a ketal or a hemiketal carbon based on its chemical shift, as a substituent on the 1,2-disubstituted benzene ring. Correlations from δ_H 2.38, 2.18 (H-8) and δ_H 4.31 (H-9) to δ_C 104.0 (C-7), and from δ_H 2.38, 2.18 (H-8) to δ_C 136.0 (C-6), helped connect C7, C8 and C9 in order. Likewise, the HMBC resonances from δ_H 4.31 (H-9) to δ_C 91.3 (C-10), 175.5 (C-11) and 40.3 (C-12) extended the framework as shown on the structure. C-12 was connected to the 1,4-disubstituted benzene ring based on HMBC signals from δ_H 7.17 (H-14) to δ_C 40.3 (C-2). The

hydroxyl substituent on C-16 of the 1,4-disubstituted benzene ring was inferred from its ^{13}C shift of 157.2 ppm.

Table 7. NMR Spectroscopic Data of Compound **3.8** in CD_3OD (500 MHz)

Position	δ_C, type	δ_H (*J* in Hz)	COSY	HMBC[a]
1	136.9, C			
2	120.0, CH	6.94, dd (8.0, 0.9)	3	4, 6
3	129.6, CH	7.16, m		1, 5
4	123.3, CH	6.97, td (7.6, 1.1)	3, 5	2, 3, 6
5	125.8, CH	7.49, dd (7.8, 1.5)		1, 3, 7
6	136.0, C			
7	104.0, C			
8	47.8, CH_2	2.38, dd (13.7, 8.7)	9	6, 7, 9, 10
		2.18, dd (13.7, 8.7)	9	6, 7, 9, 10
9	78.0, CH	4.31, t (8.8)		7, 8, 10, 11, 12
10	91.3, C			
11	175.5, C			
12	40.3, CH_2	3.30, d (14.2)		9, 10, 11, 13, 14
		3.05, d (14.3)		9, 10, 11, 13, 14
13	128.4, C			
14, 14’	133.0, CH	7.17, d (8.6)	15, 15’	12, 14, 15, 16
15, 15’	115.6, CH	6.64, d (8.6)		13, 15, 16
16	157.2, C			

a HMBC correlations, optimized for 7 Hz, are from proton(s) stated to the indicated carbon.

With the carbon framework completed, the remaining planar structure of compound **3.8** was deduced based on a few key evidences. In addition to the ketal/hemiketal at C-7, oxygen atoms were connected to C-9 and C-10, based on their ^{13}C shifts. Moreover, one of the oxygen atoms on C-7, C-9 and C-10 had to be connected to two of the carbon atoms, based on the molecular formula. An ether linkage between C-7 and C-10 was thus established. The nitrogen was then determined to be part of an anilide moiety, as opposed to an aniline as shown in structure **3.18**, because closer inspection of ^{13}C NMR signals of C-1 (136.9 ppm), C-2 (120.0

ppm) and C-6 (136.0 ppm) revealed that the chemical shift values were more reasonable with the placement of an amide substituent at C-1 instead of an amine moiety.[135] Computations of NMR shifts using the gauge-independent atomic orbital (GIAO) method also agreed with the conclusion that compound **3.8** contained an anilide moiety instead of aniline.

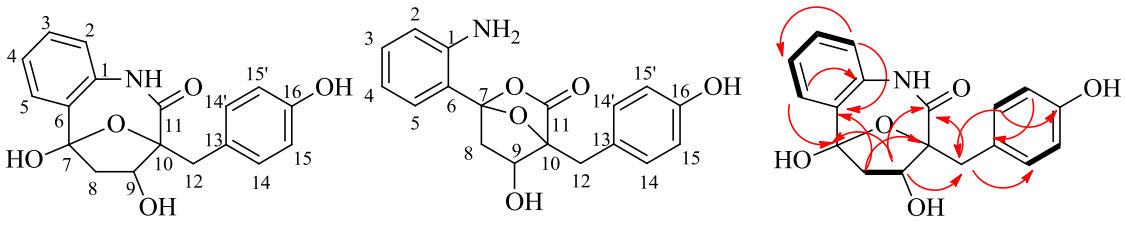

Figure 32. Two structures were proposed (**3.8** and **3.18**), based on the COSY (bold lines) and the HMBC (red arrows) correlations shown on the right.

In our computational studies, which we adopted from the protocol published by Willoughby *et al.*,[89] we constructed all possible diastereomers, *i.e.* four each, of compounds **3.8** and **3.18**, and conducted a global search for conformers of each diastereomer within 5 kcal/mol of the respective lowest energy conformer. For each non-redundant conformer within the energy windows, GIAO NMR shifts were computed at the B3LYP/6-311+G//M06-2X/6-31+G levels. Statistical comparisons of the computed ^{1}H and ^{13}C NMR shifts and the experimental values, using both the DP4[97] and the sDP4+[136] probability methods, support the anilide structure, including the relative configuration as shown (Figure 33).

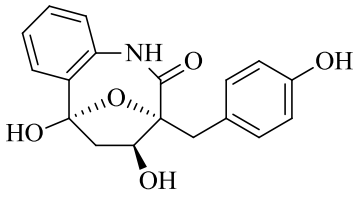

(7*S*,9*S*,10*R*)-**3.8**

Isomer	DP4 probability	sDP4+ probability
(7*S*,9*R*,10*S*)-**3.8**	0.00	0.00
(7*S*,9*S*,10*R*)-**3.8**	0.97	0.98
(7*S*,9*R*,10*R*)-**3.8**	0.03	0.02
(7*R*,9*R*,10*R*)-**3.8**	0.00	0.00
(7*S*,9*R*,10*S*)-**3.18**	0.00	0.00
(7*S*,9*S*,10*R*)-**3.18**	0.00	0.00
(7*S*,9*R*,10*R*)-**3.18**	0.00	0.00
(7*R*,9*R*,10*R*)-**3.18**	0.00	0.00

Figure 33. Relative configuration of compound **3.8**, as suggested by statistical analyses of the computed and experimental ^{1}H and ^{13}C NMR shifts of all possible diastereomers of **3.8** and **3.18**.

Compound **3.8**, which has been reported for the first time here, has plausible building blocks in anthranilic acid, both a precursor to and a degradation product of tryptophan,[137] an acetate unit, and tyrosine (Scheme 4). We propose that a series of transformations, including cyclization, epoxidation and nucleophilic attack on the epoxide, eventually results in the biosynthesis of compound **3.8**. While we have neither carried out rigorous mechanistic studies nor isolated the intermediates, LCMS analysis of the culture broth extract does show components with *m*/*z* values of 294 and 310 $[M+H]^+$, which may represent the proposed intermediates.

Scheme 4. A sketch of a possible biosynthetic route to compound **3.8**.

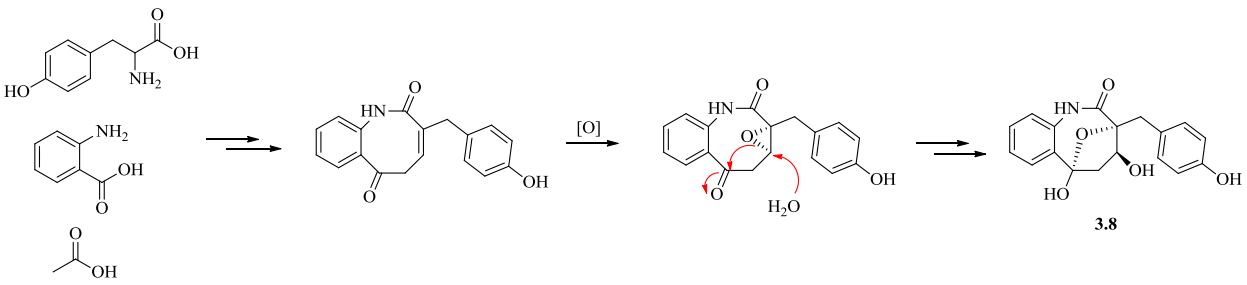

Structure elucidation of 3.9. Compound **3.9**, which had an HRESIMS signal at *m*/*z* 310.1062 $[M+H]^+$, suggesting a molecular formula of $C_{18}H_{15}NO_4$, appeared to be structurally

related to compound **3.8** based on the similarities in the NMR spectra of the two compounds (Table 8). Notable differences include the presence of a ketone functional group, as indicated by the signal at 207.7 ppm in the ^{13}C NMR spectrum, and the lack of an oxygenated methine signal in compound **3.9**, suggesting that an alcohol functional group in compound **3.8** was oxidized to a carbonyl unit in compound **3.9**. An additional quaternary sp^2 carbon resonance at 112.4 ppm, coupled with signals at 207.7 ppm and 180.0 ppm, suggested the presence of a cyclopentane-1,3-dione core in a non-interconverting keto enol ether form. Both compounds **3.8** and **3.9** possessed similar carbon frameworks, however, the molecular formula of compound **3.9** contained one oxygen atom and two hydrogen atoms fewer than that of compound **3.8**. This necessitated the placement of an additional ring, which was proposed to connect the nitrogen atom to the oxygen atom of the enol ether to form a 1,2-oxazine ring. The chemical shifts of carbon and proton nuclei in the *ortho*-disubstituted benzene rings of compounds **3.8** and **3.9** suggest difference in electronic properties of the nitrogen substituents of these compounds, i.e. more electron donating in the latter, and the placement of the oxazine ring in **3.9** in place of the lactam ring in **3.8** is consistent with these observations. The 1,2-oxazine motif, albeit very rare and unusual, is present in the natural products trichodermamide A[138]/penicillazine A[139] **3.19**, aspergillazine A[140] **3.20** and paeciloxazine[141] **3.21**, which were all isolated from fungi (Figure 35). It is unclear at this point whether these metabolites, particularly compounds **3.8** and **3.9**, are synthesized by cyanobacteria, fungal or bacterial contaminants, or via symbiotic efforts of these cohabitating organisms.

Table 8. NMR Spectroscopic Data of Compound **3.9** in CD_3OD (500 MHz)

Position	δ_C, type	δ_H (J in Hz)	HMBC[a]
1	148.2, C		
2	112.3, CH	6.93, d (7.9)	4, 6
3	131.1, CH	7.24, td (7.8, 1.3)	1, 5
4	123.0, CH	6.96, t (7.5)	2, 6
5	125.7, CH	7.41, d (7.5)	1, 3, 7
6	133.3, C		
7	81.7, C		
8	48.0, CH_2	2.77, d (15.7)	6, 7, 9, 10, 11
		2.72, d (15.7)	6, 7, 9, 10, 11
9	207.7, C		
10	112.4, C		
11	180.0, C		
12	27.9, CH_2	3.30, d (15.3)	9, 10, 11, 13, 14
		3.05, d (15.3)	9, 10, 11, 13, 14
13	131.6, C		
14, 14’	130.3, CH	7.07, d (8.5)	12, 14, 16
15, 15’	116.1, CH	6.67, d (8.5)	13, 15, 16
16	156.6, C		

a HMBC correlations, optimized for 7 Hz, are from proton(s) stated to the indicated carbon.

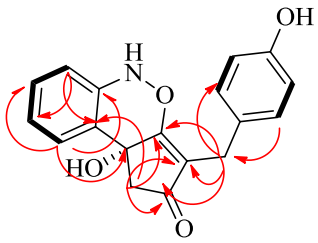

3.9

Figure 34. Key COSY (bold lines) and HMBC (red arrows) correlations used in establishing the structure of compound **3.9**.

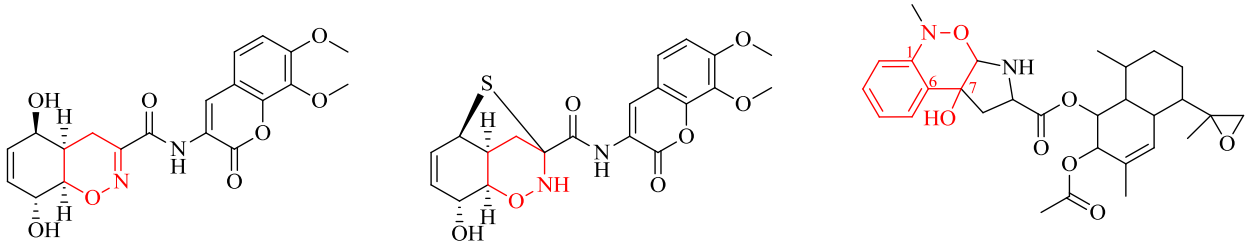

3.19 **3.20** **3.21**

Figure 35. Oxazine containing fungus-derived natural products

Computed NMR shifts of **3.9** using the gauge-independent atomic orbital (GIAO) method at the B3LYP/6-311+G//M06-2X/6-31+G levels are in reasonable agreement with the observed shifts. The mean absolute error of 0.15 ppm between the observed and computed ^{1}H NMR shifts of the compound is within the 0.20 ppm window desired for the correct structure.[89] Furthermore, the ^{1}H and ^{13}C chemical shifts in the aromatic ring of the benzoxazine fragment of **3.9** are in close agreement with the corresponding shifts of paeciloxazine,[141] providing additional support to the proposed structure (Table 9).

Table 9. Comparison of relevant NMR shifts between paeciloxazine **3.21** and compound **3.9**

Position	δ_C, **3.9**	δ_H, **3.9**	δ_C, **3.21**	δ_H, **3.21**
1	148.2		148.2	
2	112.3	6.93	112.1	6.71
3	131.1	7.24	128.3	7.21
4	123.0	6.96	121.9	6.97
5	125.7	7.41	127.2	7.43
6	133.3		129.3	

The metabolites 3-formylindole **3.10** and 3-cyanoindole **3.11** were identified from their ^{1}H NMR spectra and ESIMS data. The ^{1}H NMR data are in close agreement with the data found in the literature.[123-124]

3.5 Evaluation of Biological Activity of Metabolites of HCC1088

The main objective of growing this strain of cyanobacteria and isolating the metabolites found in the culture broth was to discover novel BACE1 inhibitors. While the natural product believed to be active against BACE1, **3.7**, was isolated early on during the course of the research, its structure was proposed and confirmed by synthesis much later. In an unfortunate turn, the in-house BACE1 assay that we relied upon for much of our research was no longer available as the commercial vendor stopped supplying the assay kit. Efforts to validate other commercial BACE1 assay kits have been unsuccessful to date.[142] In that context, the evaluation of the intended primary biological activity remains incomplete until a robust assay becomes available.

Nonetheless, compounds **3.6**, **3.7**, **3.10** and **3.11** were evaluated for activity in other assays available to us. These compounds failed to show any promising activity in cytotoxicity assay against Panc-1 and U251MG cell lines, Ca-signaling assay or the vascular permeability assay run by our collaborators. Evaluation of antimicrobial properties of these metabolites has been planned.

3.6 Producers of the HCC1088 Metabolites

The microscopic image shown in Figure 25b revealed the strong presence of fungal contaminants in the culture of the cyanobacterial strain, and it naturally begs the question as to whether the metabolites described in this chapter are produced by the cyanobacterium, fungus or even a bacterium, which are likely contaminants as well. Cyanobacterial secondary metabolites typically accumulate in the biomass and it is unusual for them to be found in the culture medium.

The only known instances are a few, such as the antifungal compounds tolybyssidin A and B[143] from *Tolypothrix byssoidea* (Hass) Kirchm. (Scytonemataceae), antibacterial compounds noscomin[144] and comnostin A-E[145] from *Nostoc commune* Vaucher (Nostocaceae), and an algicidal *β*-carboline from various species of cyanobacteria of the Nostocaceae family.[146] Furthermore, the rare oxazine moiety, as present in **3.9**, has been reported primarily in fungus-derived natural products. Combination of these evidences certainly gives rise to the possibility that a fungus is the main producer of these natural products. Other questions remain to be answered, such as, could these compounds be produced by the cyanobacteria in defense against the other organisms in the culture? We set out on conducting a series of experiments to reveal more about the production of these metabolites.

In efforts to isolate the fungi from the cyanobacteria, we attempted two experiments. The heavily contaminated HCC1088 cellular suspension was inoculated with nitrate absent BGM media, in order to deprive the heterotrophs of a nitrogen source and to eventually get rid of fungi and bacteria that cannot fix nitrogen. Likewise, colonies of contaminated cyanobacteria/fungi composites were grown on an agar plate containing chloramphenicol, an antibiotic, to induce a pure culture of fungus. Remarkably, both experiments succeeded in achieving the intended goals.

The cyanobacterial culture in nitrate absent BGM media was free of fungal strains, as observed by light microscopy (Figure 36a). Meanwhile, the fungal strain thrived and the cyanobacterial strain vanished on the agar plate laden with antibiotic (Figure 36b). Following these encouraging observations, the axenic cultures of both cyanobacterium and fungus were grown in appropriate media with the purpose of monitoring the formation of metabolites in each.

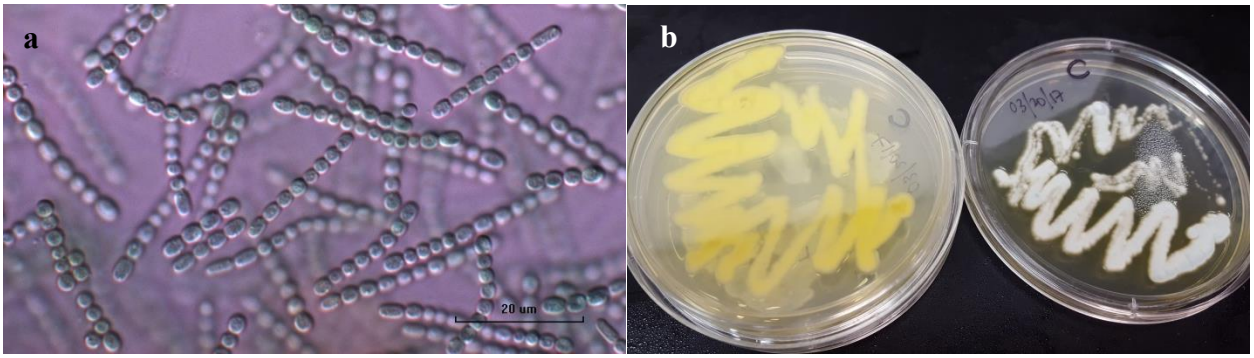

Figure 36. (a) Microscopic image of HCC1088 culture grown in nitrate absent BGM medium (b) Fungal colonies isolated from the HCC1088 culture growing on an agar plate

Extraction of the fungal cell mass and its culture medium at different time intervals (5, 10, 30 d) showed no presence of the metabolites **3.6**-**3.9**. Likewise, these compounds were not detected in the cell extract of HCC1088 over an extended period of time (30 d). The oxazole **3.7** was detected in the culture broth but not in the cell extract of the axenic HCC1088 culture grown in nitrate absent medium, suggesting that it is indeed produced by the cyanobacterium and released in the culture medium. The oxazine **3.9**, presumed to be a fungal metabolite based on the occurrences in fungal strain, was not detected in either culture. These observations suggest that the oxazine **3.9** is produced by either the fungus or the cyanobacterium in presence of the other organism, or by unknown bacterial contaminants.

Next, we propagated a portion of this axenic culture to a large 20 L culture containing regular BGM medium (with nitrate present) to monitor any metabolic changes using LC-MS methods. [Note: It is extremely difficult to keep a culture of this size axenic, especially when aliquots are removed in periodic intervals. Therefore, contaminants are likely to populate this culture over time.] Compounds **3.6**, **3.7**, **3.8**, and **3.9** were monitored by their extract ion chromatogram (EIC) signals at *m*/*z* 188 (ESI+), 217 (ESI+), 326 (ESI-) and 308 (ESI-),

respectively. Compound **3.6**, which is the most abundant of these metabolites, was monitored by its prominent UV absorption at 280 nm as well. The LC-MS analysis of the aliquots of this culture in regular time intervals (2 or 4 days) revealed some notable trends.

Compound **3.7**, which was produced by the cyanobacterium in the nitrate absent medium, showed a gradual and consistent growth starting day 20 and continuing this trend through the end of the study, i.e. 54 days (Figure 37b). The compounds **3.6**, **3.8** and **3.9**, however, appeared to follow mirroring trends of increased production beginning on day 30 and plateaued growth around day 50 (Figure 37a, d, c). Furthermore, in an observation that may be relevant or entirely coincidental, growth of white fungus under the rubber stopper of the culture vessel was observed on day 28. [This was confirmed to be fungus following development of the culture on an agar plate and inspection by light microscopy.] Remarkably, the cyanobacterial culture medium did not show presence of fungal strains under the light microscope. These are interesting observations that suggest that compounds **3.6**, **3.8** and **3.9** may be produced as antifungal agents, but must not be interpreted as definite trends in the absence of further supporting evidence and more robust analytical methods. It is also very plausible that bacterial contamination in the cultures may be driving the production of these metabolites.

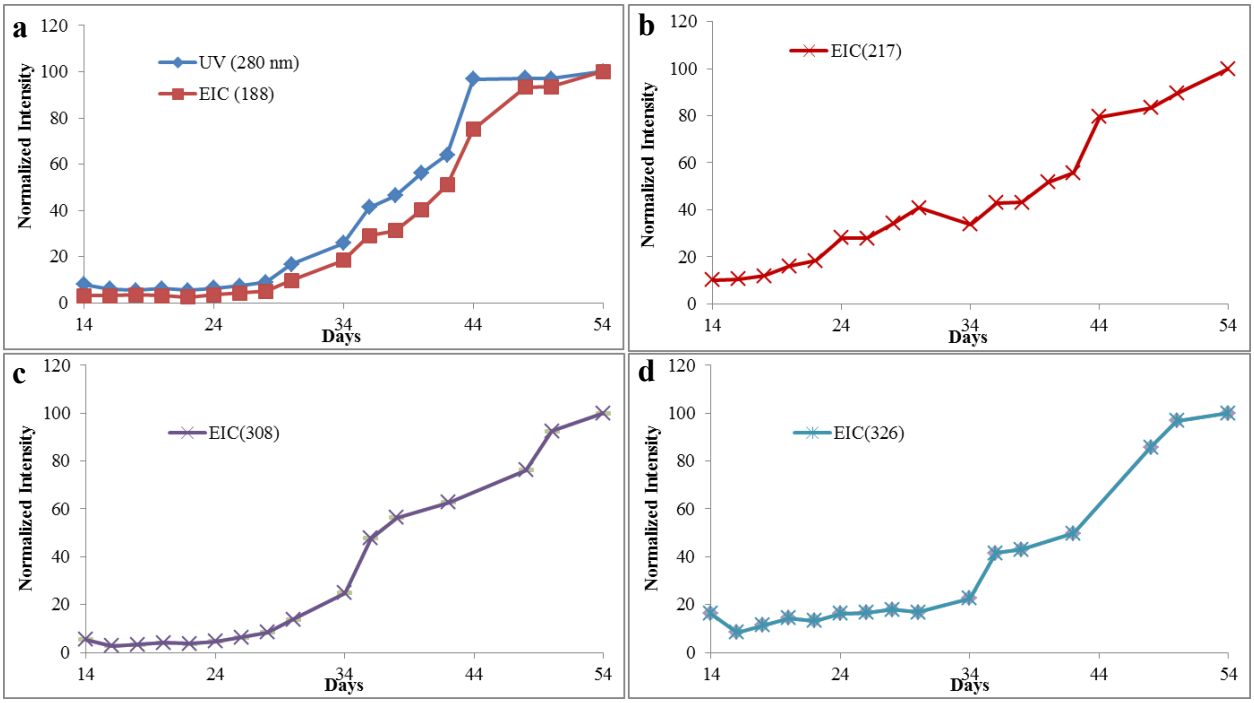

Figure 37. LC-MS monitoring of HCC1088 metabolites in periodic intervals

Efforts to determine whether these compounds are produced by the cyanobacteria as an antifungal response are underway. Four cultures of HCC1088, two of which were inoculated with fungal cell matter, are being sampled in periodic intervals and the culture broth is extracted with HP-20 to monitor the levels of compounds **3.6-3.9**. Multiple reaction monitoring (MRM) methods are being employed to get a more accurate quantitation of these metabolites.

3.7 Conclusions and Outlook

Four new metabolites (**3.6-3.9**) and two known compounds (**3.10** and **3.11**) were isolated from the extract of the culture broth of HCC1088, an as yet unidentified cyanobacterium. Computations of NMR chemical shifts using density functional theory methods

have been central to the elucidation of the structures of **3.8** and **3.9**. Isolation of fungus from the cyanobacterial culture has revealed that metabolites **3.6**, **3.8** and **3.9** are not produced by either the cyanobacterium or the fungus alone. Work is underway to determine whether the cyanobacterium HCC1088 produces these compounds as a defense mechanism in response to the detection of fungal cells. This concept has prior precedence, as demonstrated by Patterson and Bolis, who established enhanced production of the antifungal compound tolytoxin when fungal cell wall preparations containing chitin oligomers were introduced into the cultures of *Scytonema ocellatum* Lyngby (Scytonemataceae).[28] Moreover, cyanobacterial oligopeptides such as microcystins, microviridins, anabaenopeptins have been widely regarded as allelochemicals. A recent study shows that oligopeptide knockout mutant cyanobacterial strains of the genus *Planktothrix* are more susceptible to fungal infections than the wildtype strains, further suggesting the involvement of oligopeptides in defense mechanisms.[147]

CHAPTER 4

Investigation of *Areca catechu* for Ca-Signaling Activity in Immune Cells

4.1 Significance of *Areca catechu*

Areca catechu L. (Arecaceae), commonly known as betel nut (also referred to as Areca nut), is consumed by approximately 700 million people worldwide,[148] ranking fourth among the most commonly used psychoactive substances, behind caffeine, nicotine and alcohol. It is chewed in various forms – ripe, unripe, fresh, dried – and often as "betel quid" in combinations with slaked lime, aromatic spices, tobacco and other ingredients wrapped in *Piper betle* leaf.

The most frequent practice of betel nut consumption is found in South and South East Asia, East Africa and the Western Pacific, areas where the nut has sociocultural significance.[149] In many countries in these regions, betel nut is a common offering at ceremonies, including engagements, weddings, and funerals. Social pressure is a significant reason for consumption of betel nut in various islands of the Western Pacific as it is viewed as a socializing activity identifiable with those communities.[149a] Some unusual practices involving the Areca nut include formal pronunciation of a divorce when a North Sumatran Muslim man hands his wife three pieces of the nut, one at a time.[149b] In many rural communities of Nepal, acceptance of a dried Areca nut is a formal acceptance of an invitation to a religious or a social function, such as a wedding. Many other accounts of sociocultural significances are provided in a book written by Henry Brownrigg.[150]

4.2 Health Benefits and Concerns from Consumption of Betel Quid

Sushruta, the historical medical text in Sanskrit, claimed as early as the first century that betel nut tends to 'cleanse the mouth, impart a sweet aroma to it, enhance its beauty and cleanse and strengthen the voice, tongue and teeth, the jaws and the sense organs'.[150] It is, to date, used as a digestive remedy and a mouth freshener in populations across the Indian subcontinent that cater to the Ayurvedic medicine. Modern medicinal research, however, portrays betel quid consumption in a decidedly negative light as a global health issue and links its usage to various systemic diseases.

Chewing of betel quid has been established as a cause of oral lesions and pathological epidermal changes within the oral cavity that increase the likelihood of malignant transformations and development of esophageal and oral cancers.[151] A clear causal relationship has been established between betel quid chewing and diseases such as leukoplakia and oral submucous fibrosis.[152] Various other studies have implicated betel quid consumption to numerous diseases, including liver cirrhosis, hepatocellular carcinoma, obesity, hypertension, type 2 diabetes, chronic kidney disease, hyperlipidemia, metabolic syndrome, cardiovascular disease, aggravation of asthma, and complications in reproductive health.[152a, 153] In Pacific islands, including Hawai'i, betel nut consumption is more prevalent in minority groups such as the Chamorros and the Micronesians. In light of health disparities between these groups and the rest of the populations, betel nut consumption has attracted scrutiny from the health community.[154]

4.3 Molecular Components of *Areca catechu* and their Effects on Human Health

Despite the strong association of betel quid consumption with various oral diseases and cancer, the identity of the responsible components and the underlying mechanisms are not fully understood. *Areca catechu* is known to contain different classes of molecules, including alkaloids, tannins, flavones, triterpenes, steroids, and fatty acids. The major alkaloids of Areca nuts are arecoline **4.1**, arecaidine **4.2**, guvacine **4.3** and guvacoline **4.4**, with arecoline the most abundant, whereas catechin **4.5** and *epi*-catechin **4.6** are the most dominant flavonoids (Figure 38). Oligomeric and polymeric proanthocyanidins (polyflavonoids) found in Areca nuts primarily comprise these two monomers. Steroids such as 5,8-epidioxyergosta-6,22-dien-3β-ol (ergosterol peroxide), stigmast-4-en-3-one, β-sitosterol, and cycloartenol have also been isolated from *Areca catechu*.[155]

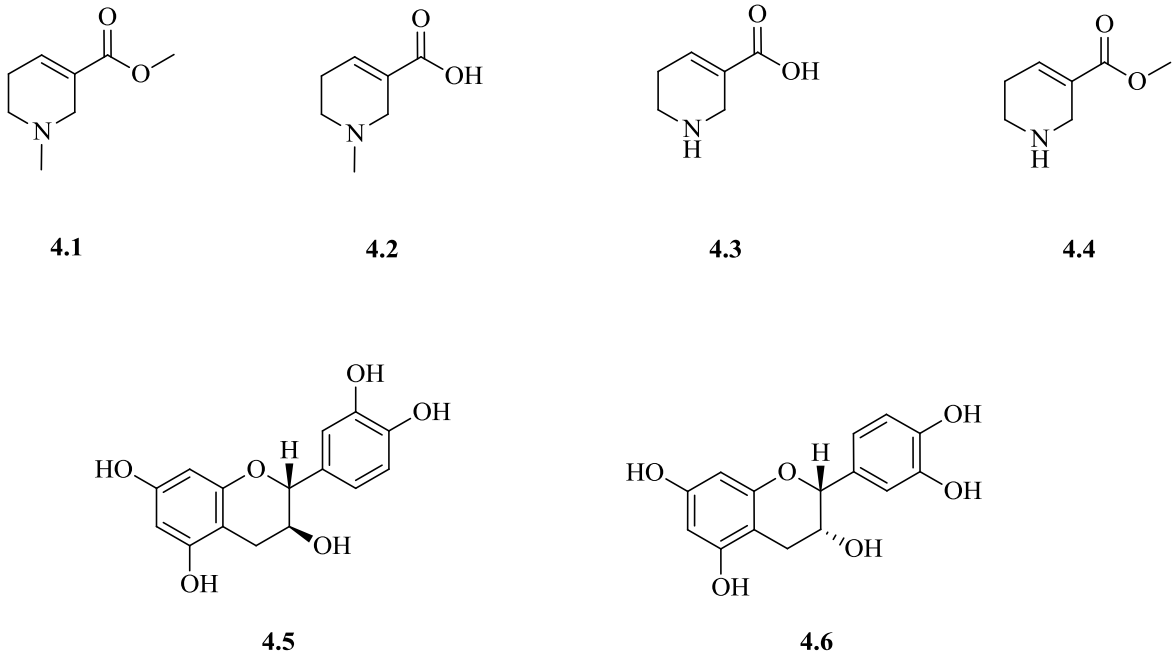

Figure 38. Major alkaloids and flavonoids from *Areca catechu*

Many pharmacological effects, ranging from beneficial medicinal purposes to serious health risks, have been identified from extracts or compounds isolated from Areca nut.[156] Areca nut components have been most frequently studied for their potential carcinogenic effects using both *in vitro* and *in vivo* assays.[152a, 156-157] Polyphenols and tannins isolated from Areca nuts have been reported to behave as both carcinogenic and anti-carcinogenic agents.[152c, 157a, 158] Areca alkaloids show mutagenic and genotoxic effects in many short-term assays, [152c, 156, 159] but genotoxicity to oral fibroblasts and keratinocytes, the target cells of betel quid, has not been clearly established.[157a] These reports do not provide an unambiguous picture and hence the toxicity from Areca nuts cannot be attributed specifically to polyphenols, tannins or alkaloids but rather suggest that additional factors may be involved.

4.4 *Areca catechu* and Inflammation

An important observation in the context of the study described in this chapter is that Areca nut consumption triggers release of various mediators from host cells that contribute to a chronic inflammatory microenvironment in the oral cavity,[160] thus promoting the development of oral lesions and tissue damage. It is now widely acknowledged that chronic inflammation plays an important role in carcinogenesis,[161] but the biological mechanisms that link Areca nut metabolites to immune cell activation, cytokine production, inflammation, and cancer remain underexplored and are the focus of this study.

There are two types of inflammation – acute and chronic. The process of acute inflammation is a short-lived response that is commonly initiated by resident mast cells, dendritic cells, and monocytes/macrophages, and followed by the infiltration of polymorphonuclear leukocytes (PMN).[162] Over time, usually 1 to 2 days, monocytes predominate and begin to

differentiate into macrophages, which then attract lymphocytes.[162-163] Persistence of this process can lead to chronic inflammation and severe tissue damage. During chronic inflammation, there is an abundance of monocytes, macrophages, and lymphocytes, and a favorable environment for the release of pro-inflammatory cytokines[164] and reactive oxygen species, which in turn facilitates an environment for the growth of cancer cells.[165]

Despite some reports of anti-inflammatory effects of Areca nut extracts,[166] there is a general consensus, driven by several scientific observations, that consumption of betel nut and betel quid leads to an increased risk of periodontal diseases, oral submucous fibrosis, and oral squamous cell carcinoma.[152a, 153c, 157b, 167] The components in Areca nut may trigger immune responses to establish an inflammatory environment in the oral cavity that can initiate and/or contribute to these diseases. This was shown in a previous study in which the treatment of polymorphonuclear leukocytes with Areca nut extracts resulted in phosphorylation of p38 mitogen-activated protein kinase (MAPK) and Ca^{2+} mobilization, resulting in the release of pro-inflammatory lipid mediators such as leukotriene B4.[54] However, it remains unclear what the source of calcium is and which leukocytes (neutrophils, basophils, eosinophils, mast cells) are responsive to the extracts. Furthermore, questions like whether Areca nut extracts activate other immune cells, including those found in the adaptive immune system, remain unanswered. In this study, we demonstrate that Areca nut extracts are capable of mobilizing Ca^{2+} in various cells of the innate and adaptive immune system (T lymphocytes, mast cells, and monocytes), which may cause chronic inflammation and play a potentially important role in oral diseases seen in betel quid chewers.

4.5 Calcium Regulation in Cells and Ca-Signaling Assay

Cytosolic calcium is regulated by various pumps and receptors (Figure 39). Calcium efflux from the cytosol is caused by the actions of plasma membrane calcium ATPase (PMCA), sarco-endoplasmic reticulum calcium ATPase (SERCA), sodium-calcium exchanger, and mitochondrial uptake, whereas influx mechanisms include store operated calcium entry (SOCE) through the calcium channels in the plasma membrane, and release of calcium through the ryanodine receptor channel and the inositol 1,4,5-triphosphate (IP_3) receptor channel across the endoplasmic reticulum membrane. The receptor operated calcium channels are known to be activated by metal cations and small molecules.[168]

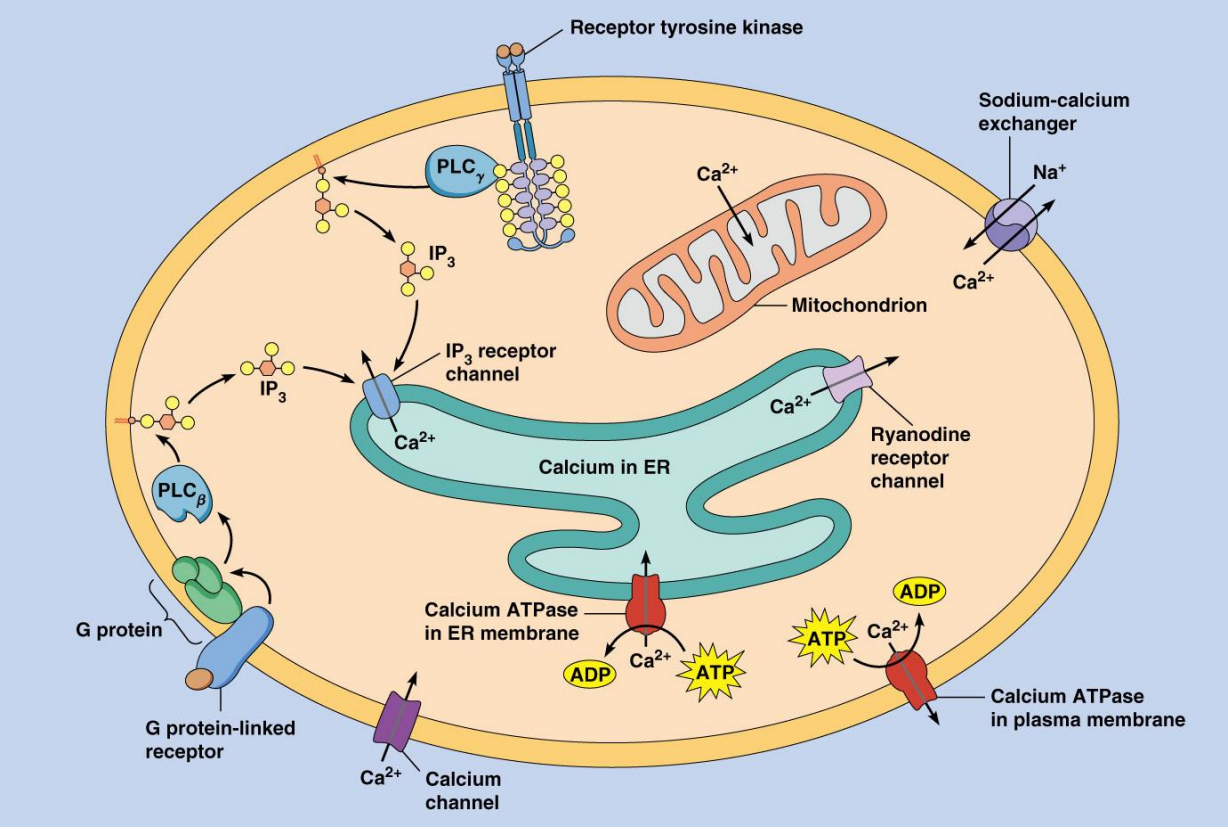

Figure 39. Calcium regulation mechanisms in cells.

Image obtained from Pearson Education, Inc. (2012).

Cellular calcium concentration was measured using a fluorimetric assay depicted in Figure 40. A calcium indicator dye, Fura-2 acetoxymethyl ester (Fura-2 AM) **4.7** is introduced into the cell medium in a 96-well plate and incubated for 1 hour. The culture medium is then substituted for the standard Ringer's solution with known calcium concentrations. A high throughput instrument (Hamamatsu FDSS 7000 EX) equipped with scientific camera detects [Ca^{2+}] based on the ratio of fluorescence signals at 340 nm and 380 nm. In a typical assay, the basal levels of calcium are measured for 30 – 60 seconds before a stimulus of a control or an extract is introduced into the wells. A continuous measurement of the ratio of fluorescence signals at the two wavelengths generates calcium response curves as shown in the bottom left of Figure 40. Thapsigargin **4.8**, a SERCA pump inhibitor originally isolated from *Thapsia garganica* L. (Apiaceae),[169] is used as a positive control while ethylene glycol-bis(2-aminoethylether)-*N*,*N*,*N*′,*N*′-tetraacetic acid (commonly abbreviated as EGTA and also known as egtazic acid) **4.9**, an inhibitor of the store operated calcium entry across the plasma membrane, blocks the influx of Ca^{2+} in the cytosol.

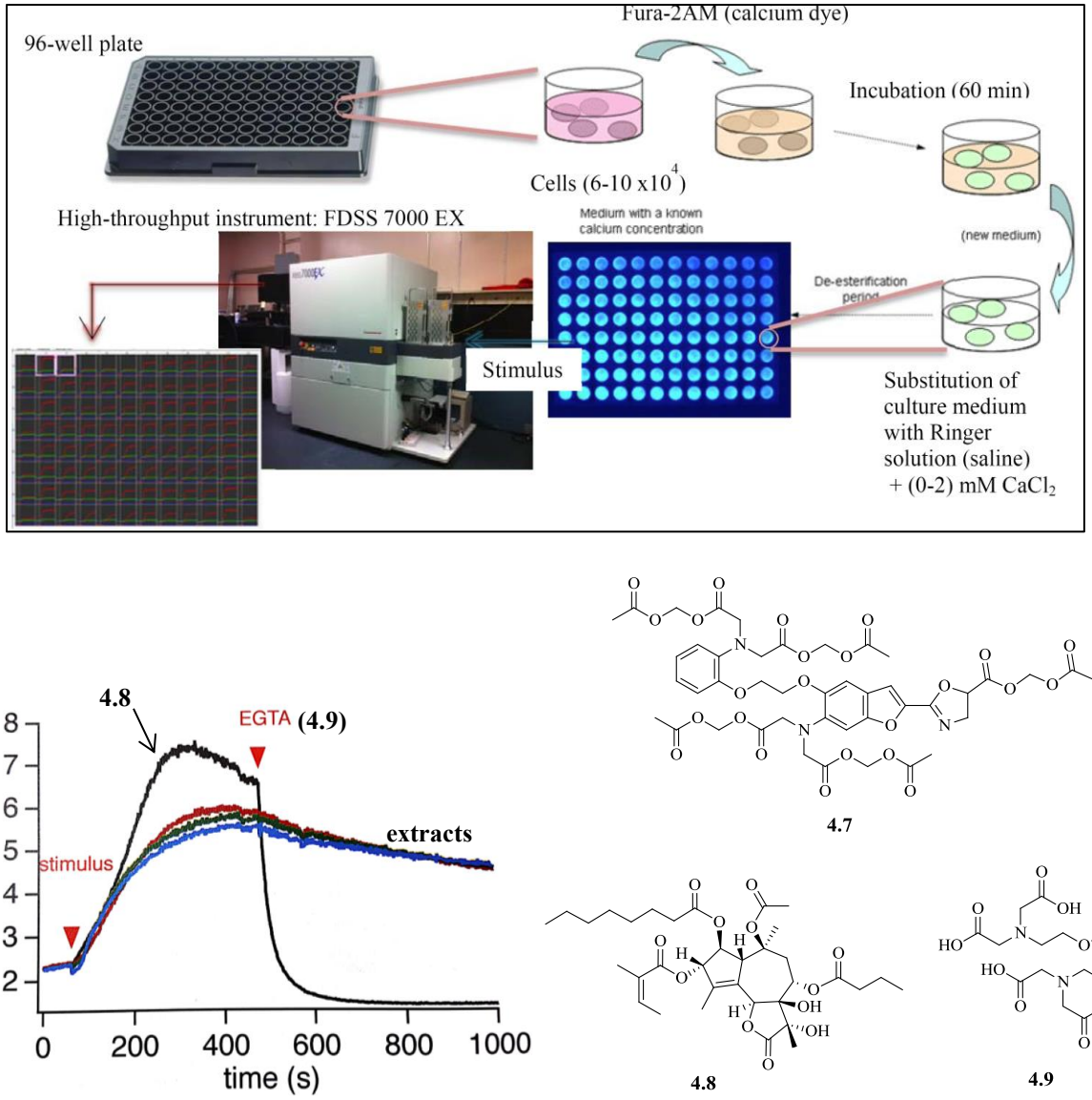

Figure 40. Schematic representation of the Ca-signaling assay

4.6 Ca-Signaling Activity from Components of *Areca catechu*

Calcium mobilization in immune cells by areca nut extracts. To assess the Ca^{2+} mobilizing activity of the components of betel nut, we treated the rat mast cell line RBL-2H3 to extracts of the betel leaf, Areca nut and areca husk (Figure 41). Each component (kernel and husk) was extracted using a mixture of chloroform ($CHCl_3$), methanol (MeOH) and water (12:5:3), a solvent system known to generate the highest mass of extracts from certain plant specimens.[170] Areca nut extract (ANE) increased intracellular Ca^{2+} concentrations in RBL-2H3 cells at 50 µg/mL (Figure 42a), while Areca husk and betel leaf extracts failed to induce any significant Ca^{2+} signals at the same concentrations (Figure 42b,c). This finding indicates that *Areca catechu* is indeed capable of mobilizing cytosolic calcium in immune cells and that the Ca^{2+}-mobilizing components are localized in the Areca nut kernels.

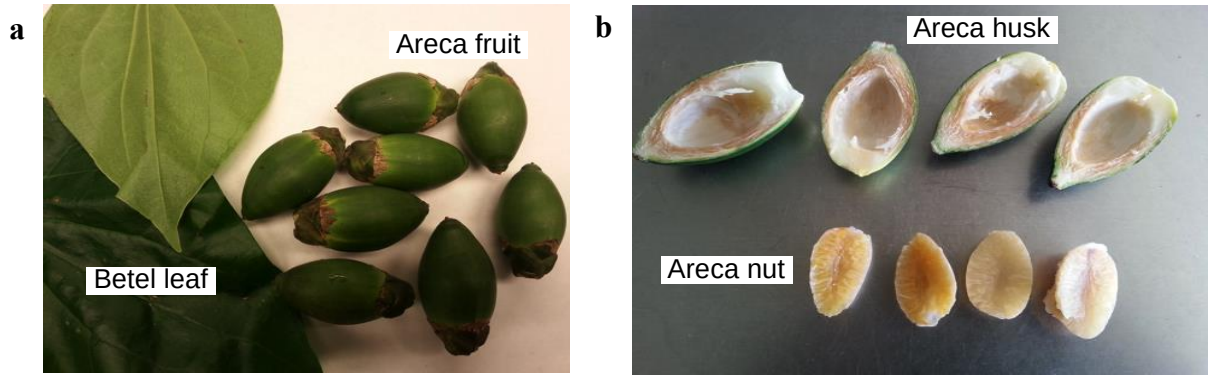

Figure 41. Betel leaf and Areca nut obtained from a local market

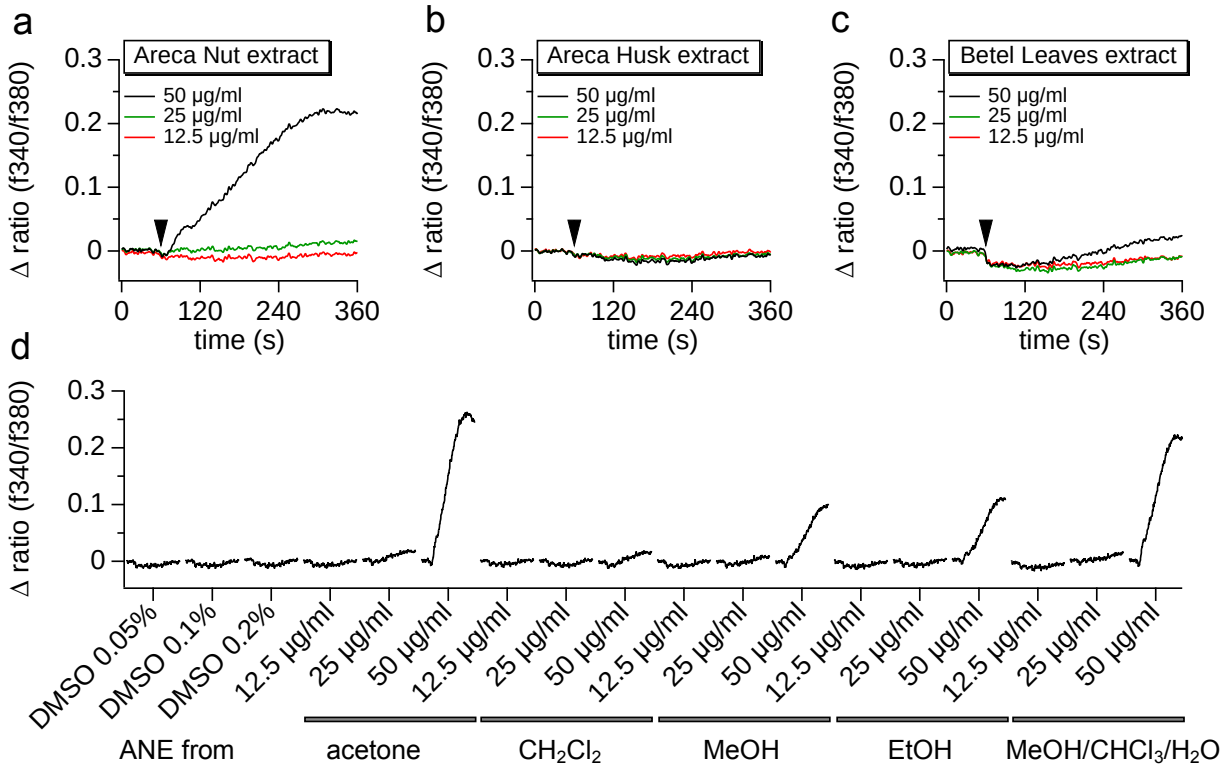

Figure 42. Calcium mobilization in RBL-2H3 cells by betel quid components.

We then sought to optimize the extraction protocol of Areca nuts. Extracts of Areca nut obtained from acetone, dichloromethane, methanol, and ethanol were tested using the Ca-signaling assay in the same cell line and the response was compared to the signals obtained from the use of a mixture of chloroform, methanol and water. While the ethanol and methanol extracts showed considerable Ca^{2+} signals, extracts obtained from acetone (2.5-fold increase in response) and methanol/chloroform/water mixture (2-fold increase in response) were more potent (Figure 42d). The dichloromethane extract was inactive in the assay. Furthermore, extractions performed in acidic (pH 4), neutral (pH 7) and basic (pH 10) aqueous ethanolic solutions offered no improvement in Ca-signaling activity. Based on these findings, we used acetone as the standard solvent in the extraction protocol throughout the entire study.

Following the observations of calcium mobilization in immune cells by the whole extract of *Areca catechu* nut, we sought to identify the fractions or components responsible for the activity. A liquid-liquid partitioning of the extract in chloroform and water, and subsequent tests on various immune cell lines, unequivocally demonstrated that the Ca-signaling activity of the Areca nut extract arises from the components present in the water soluble fraction. ANE and its aqueous fraction increased intracellular Ca^{2+} concentrations in the rat mast cell line RBL-2H3 (Figure 43a), the human T lymphocyte line Jurkat (Figure 43b), the human monocyte line U937 (Figure 43c), but not in the human neutrophil line HL-60 (Figure 43d). The lipophilic fraction, however, shows little to no effect on calcium concentrations in these cell lines. These data indicate that water soluble ANE components are capable of mobilizing Ca^{2+} in various important pro-inflammatory immune cell types. The lack of response from the HL-60 cells is a surprising observation which may suggest that these cells may lack the signaling mechanism responsible for the Ca^{2+} mobilization observed in human primary neutrophils.[171] However, the selectivity may also suggest that the Ca-signaling activity is due to some specific mechanisms.

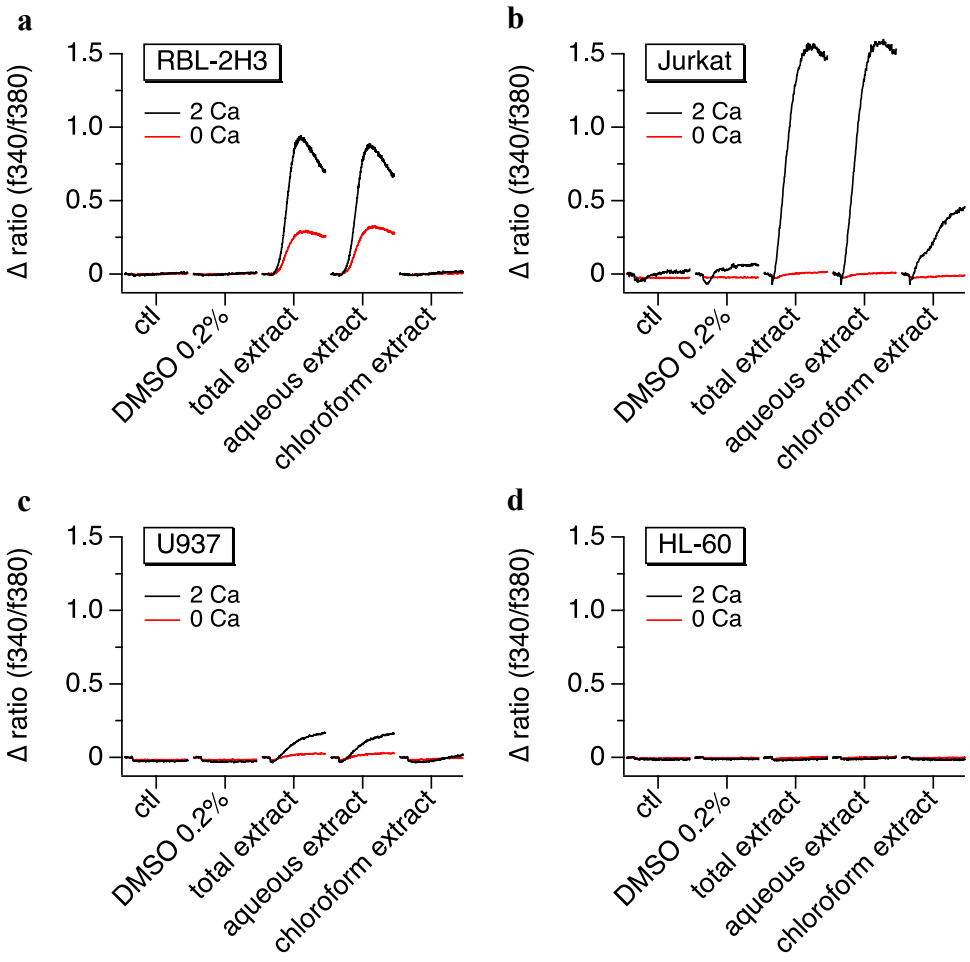

Figure 43. Ca-signaling responses generated by *Areca catechu* extracts in various immune cells.

The following cell lines were used: (a) RBL-2H3, rat mast cells, (b) Jurkat, human T cells, (c) U937, human monocytes and (d) HL-60, human neutrophils.

In order to identify the source of elevated calcium in the immune cells in the presence of Areca nut extracts, we applied the cells with the extracts dissolved in standard Ringer's solution containing 2 mM Ca^{2+} or no calcium. Figure 43a shows that elevated levels of calcium are observed in the mast cell line RBL-2H3 treated under both conditions, suggesting that both intracellular release and entry of extracellular Ca^{2+} contribute to the ANE-induced calcium signal. The differences in the shapes of the Ca^{2+} signals observed under the two conditions

indicate that several mechanisms may be involved. Interestingly, the responses in Jurkat T lymphocytes and U937 monocytes appear to be caused primarily by influx mechanisms.

Fractionation of Areca nut extract for identification of active components. In attempts to isolate the active component(s) responsible for Ca-signaling activity in immune cells, the aqueous fraction of the Areca nut extract was separated by reversed phase high performance liquid chromatography on a Phenomenex C18 Gemini column (Figure 44). Fractions were collected at regular time intervals (1.5 min) and each fraction was subjected to the fluorimetric Ca-assay.

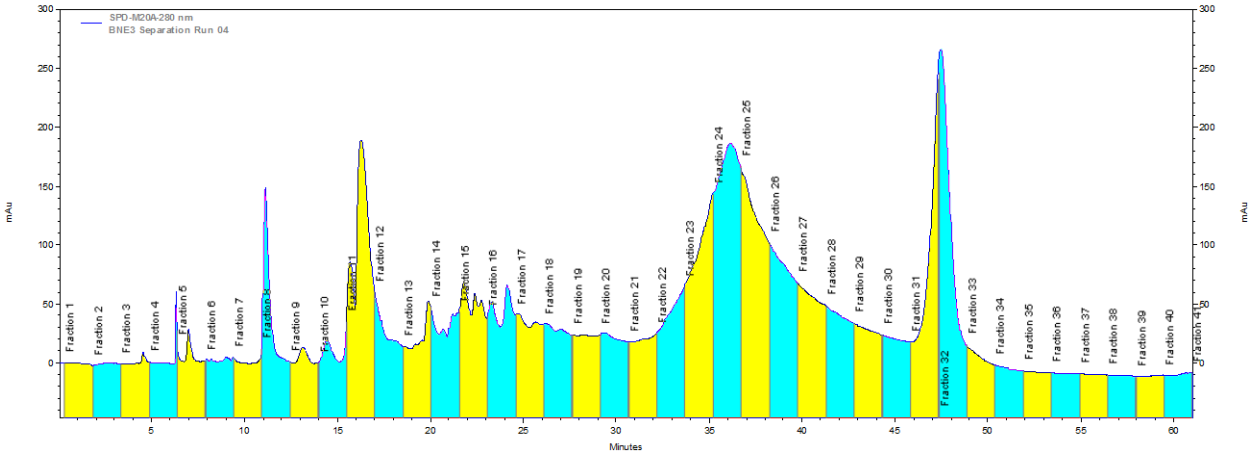

Figure 44. HPLC fractions of aqueous fraction of young Areca nut extract.

Detection at 280 nm (UV); separation conditions are outlined in the experimental section.

Various fractions showed Ca-mobilizing effects in the U937 (Figure 45a) and Jurkat (Figure 45b) cell lines but no activity in the HL-60 cell line, consistent with our previous observations. Activity from the fractions was observed primarily in three regions – fractions 14-20, 22-28 and 31-32.

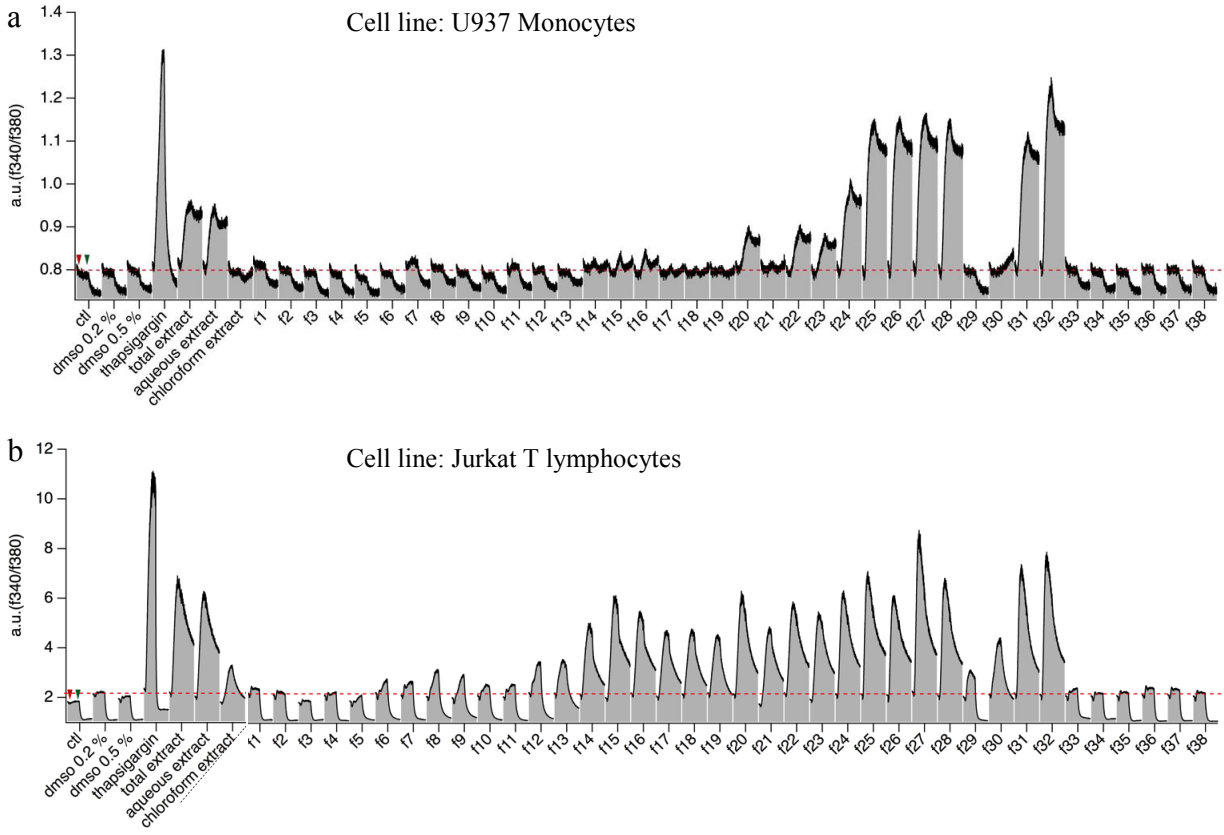

Figure 45. HPLC fractions of Areca nut extract show Ca-signaling in immune cells.

Spectroscopic characterization of the active fractions, e.g. fraction 16, proved challenging, as high resolution mass spectrometry failed to generate readily discernible signals whereas ^{1}H NMR spectra were very poorly resolved. Closer inspection of the signals in the ^{1}H NMR spectra showed close resemblances, in terms of chemical shifts, to those observed from fraction 11, which lacked Ca-signaling activity in human immune cells but was identified as catechin **4.5** from its spectroscopic data. Distinct differences were seen in the δ 2-3 ppm region, indicating that the active component may have been formed after a chemical transformation at the 4 position of catechin (Figure 46).

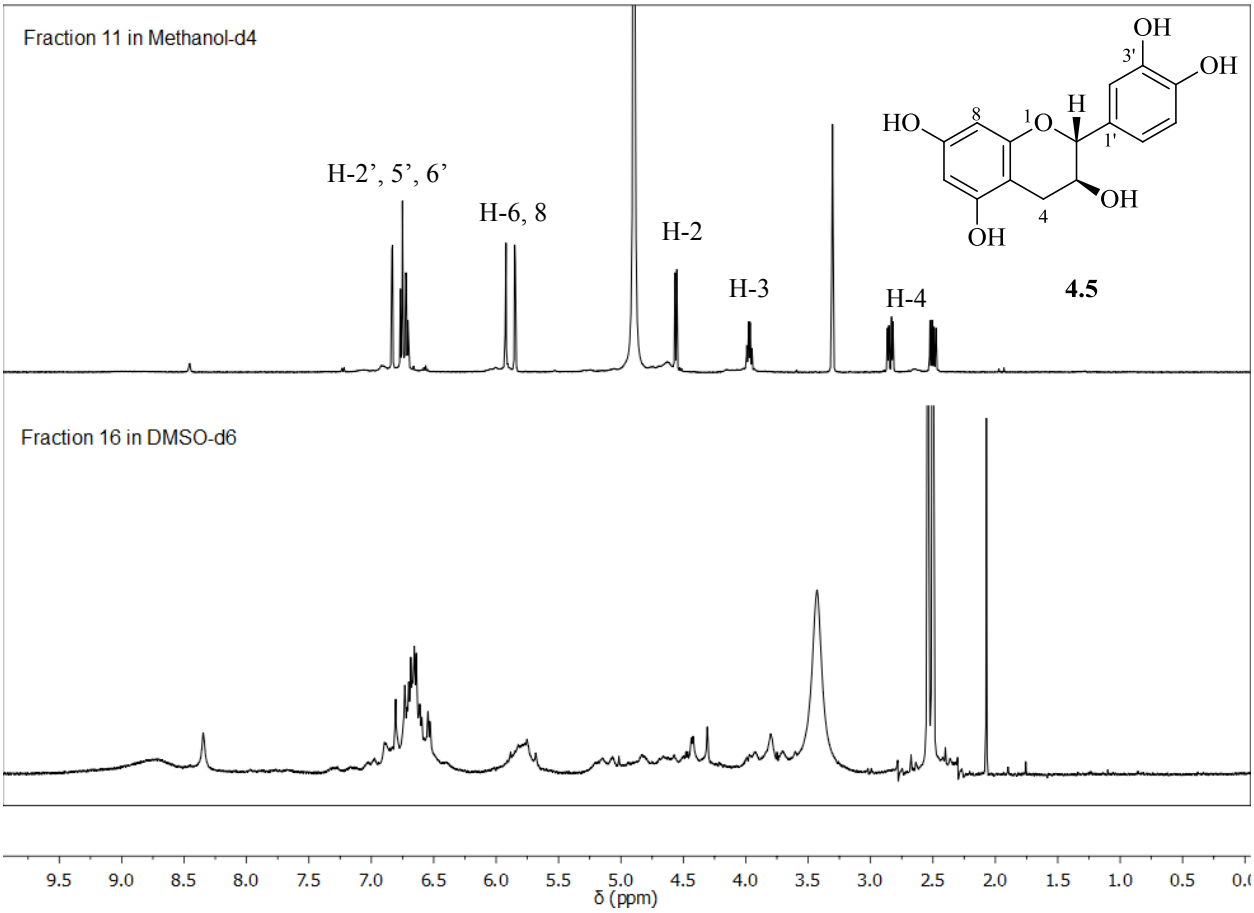

Figure 46. Comparison of ^{1}H NMR spectra of HPLC fractions 11 and 16

The poor resolution in the ^{1}H NMR signals of the active fractions may be attributed to a number of factors, such as, presence of paramagnetic impurities, multiple compounds with similar spectroscopic profile, or material that is highly oligomeric or polymeric. In the latter case, it would also mean the possibility of a presence of a complex mixture of components. Various ion exchange filtration experiments, aimed at removing paramagnetic impurities, did not afford improved resolution. The nature of the ^{1}H NMR signals and the difficulty in obtaining discernible mass spectrometry signals by LC-ESIMS suggested that the fractions that mobilized

Ca^{2+} in immune cells may be oligomeric or polymeric flavonoid in nature. Flavonoids polymerize primarily in two ways – an A-type linkage in which bonds are formed between C4 and C8' as well as between C2 and O7', as shown in **4.10**, or a more common B-type linkage between C4 and C8' with α or β configuration, as present in **4.11** and **4.12**, respectively (Figure 47). B-type linkage between C4 and C6' is also prevalent in some plant polyflavonoids. In absence of resolved NMR spectra, it is difficult to ascertain which linkages are present in the Areca polyflavonoids. Nonetheless, each linkage involves transformation at C4 of the flavonoid monomer, causing a downfield shift in the ^{1}H NMR chemical shift of H-4. The absence of signals in the δ 2-3 ppm region of the ^{1}H NMR spectra of the active fractions is likely tied to polymerization of these molecules.

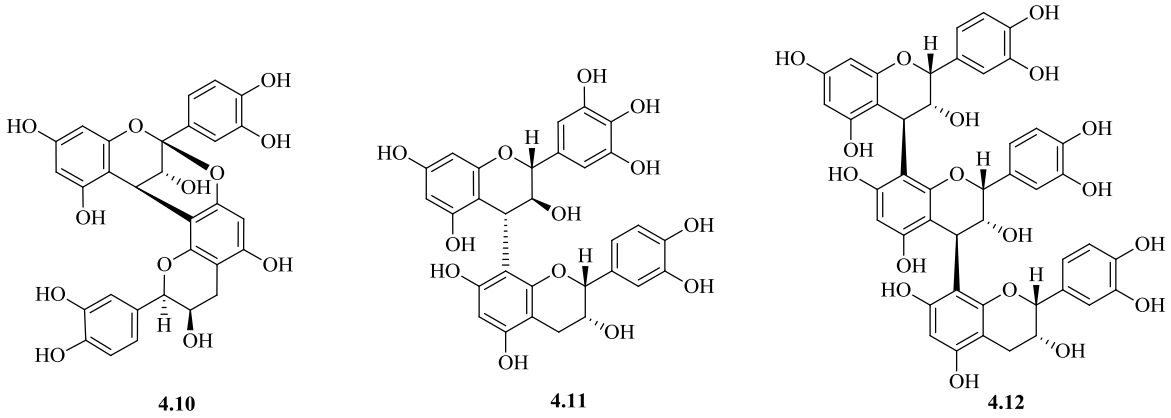

Figure 47. Different types of linkages in flavonoid oligomers and polymers

To further explore the possibility of attributing the Ca-signaling activity to polymeric flavonoids, we turned to dialysis of the aqueous extract and the active fractions using cellulose membranes with nominal molecular weight cutoff (MWCO) values of 3,500 Da and 10,400 Da. Interestingly, the activity remained with the higher molecular weight fraction after each dialysis experiment (Figure 48). Basic hydrolysis or methylation of an active fraction resulted in loss of

all Ca-signaling activity, lending credence to our preliminary assessment that oligomeric or polymeric flavonoids may be responsible for elevated intracellular calcium in immune cells. The loss of activity from methylation suggests that the hydroxyl moieties may be essential for the pharmacological effects of the polymeric flavonoids, whereas, hydrolysis under basic conditions depolymerizes these molecules into monomers and lower order oligomers, which appear inactive in this assay.

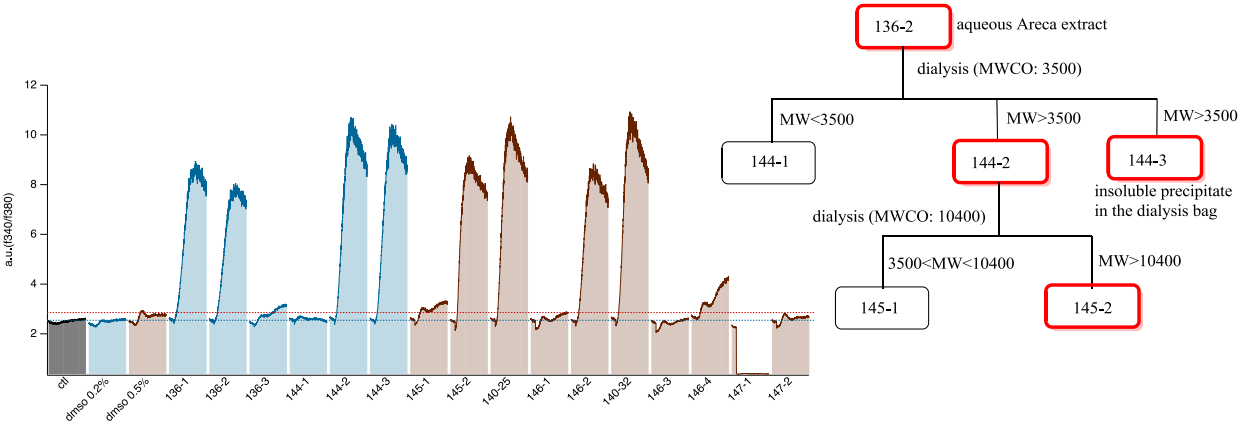

Figure 48. Ca-signaling responses in Jurkat T lymphocytes using dialyzed samples

Key: The x-axis labels refer to the sample ID. 136-1: whole extract; 136-2: aqueous fraction; 136-3: chloroform fraction. 140-25 and 140-32 are active fractions obtained from HPLC (see Figure 44). 146-1 (MW<3500) and 146-2 (MW>3500) are dialysis fractions of 140-25. 146-3 (MW<3500) and 146-4 (MW>3500) are dialysis fractions of 140-32. 147-1 and 147-2 are organic and aqueous fractions obtained from hydrolysis of 144-2. Active fractions are highlighted in bold and red in the flowchart.

Ca^{2+} signals are not caused by known small molecule Areca nut metabolites. While the results discussed thus far strongly hinted at oligomeric or polymeric flavonoids being the components responsible for Ca-mobilization in immune cells, we could not readily discount the possibility of an extremely active Areca nut metabolite being present in miniscule quantities.

To that end, we screened various commercially available Areca nut alkaloids, flavonoids and steroids to assess their ability to mobilize Ca^{2+} in RBL-2H3, Jurkat, U937, and HL-60 cells. Areca alkaloids are not known to mobilize Ca^{2+} in immune cells but arecoline and guvacoline have been reported as agonists of the muscarinic receptor[172] and they could potentially exhibit signaling effects in cells that overexpress this receptor. Therefore, we tested these alkaloids and carbachol, a known agonist used as a positive control, against the RBL-2H3 mast cell overexpressing muscarinic acetylcholine receptor M1 (RBL-M1) as well. Our results were consistent with the fact that Areca alkaloids are unlikely to exhibit Ca-signaling effects as none of the four alkaloids, when tested at 100 μM, led to any significant Ca^{2+} signals to appear in the four cell lines (Fig. 49). This excludes these alkaloids from being responsible for the Ca^{2+} elevation induced by the Areca nut extract. Furthermore, as expected, the RBL-M1 cells were responsive to 100 μM carbachol as well as arecoline and guvacoline, both of which are known agonists of muscarinic receptors (Fig. 49a). RBL-M1 also showed a small Ca^{2+} response when perfused with the chloroform extract. The response observed in the organic fraction is likely caused by arecoline, the most abundant Areca nut alkaloid, typically constituting 0.1-0.63% of the dry weight of the nut.[173]

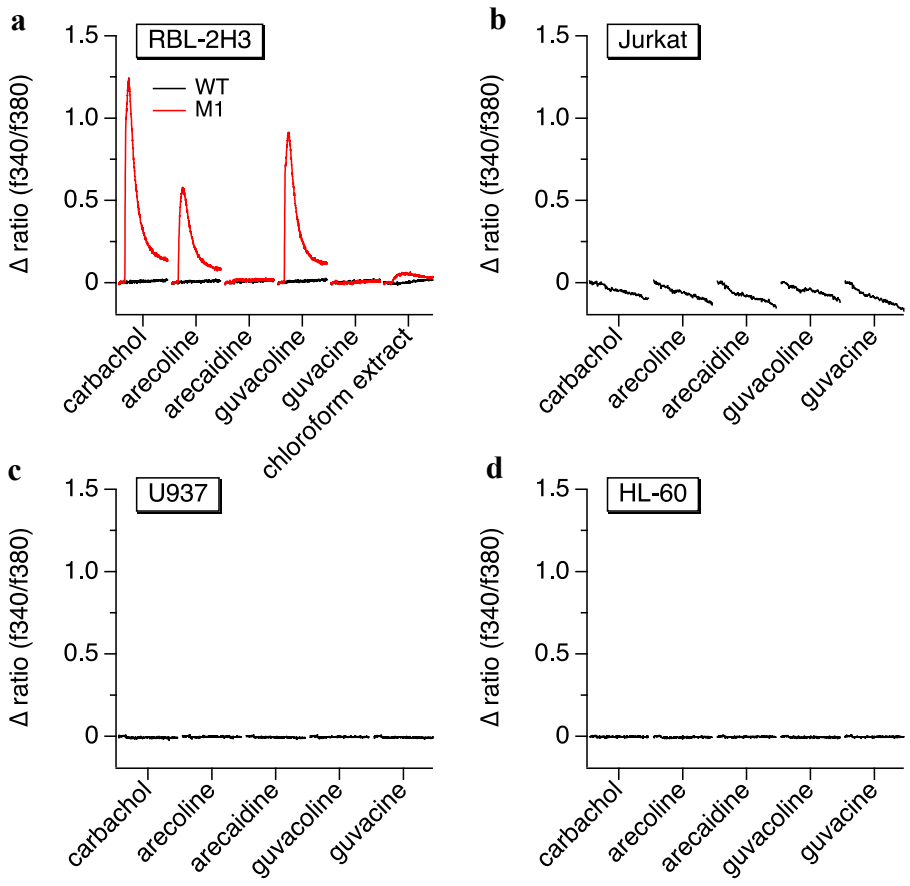

Figure 49. Ca-signaling responses of Areca alkaloids on immune cell lines

After eliminating the alkaloids as the constituents responsible for inducing the observed Ca^{2+} signals, we considered and tested other chemical constituents that have been identified in Areca nuts. Several commercially available flavonoids (catechin **4.5**, quercetin **4.13**, liquiritigenin **4.14**, isorhamnetin **4.15**), other phenolic metabolites (*trans*-resveratrol **4.16**, ferulic acid **4.17**, vanillic acid **4.18**) and steroids (ergosterol peroxide **4.19**, stigmast-4-en-3one **4.20**, *β*-sitosterol **4.21**) were acquired for these purposes (Figure 50).

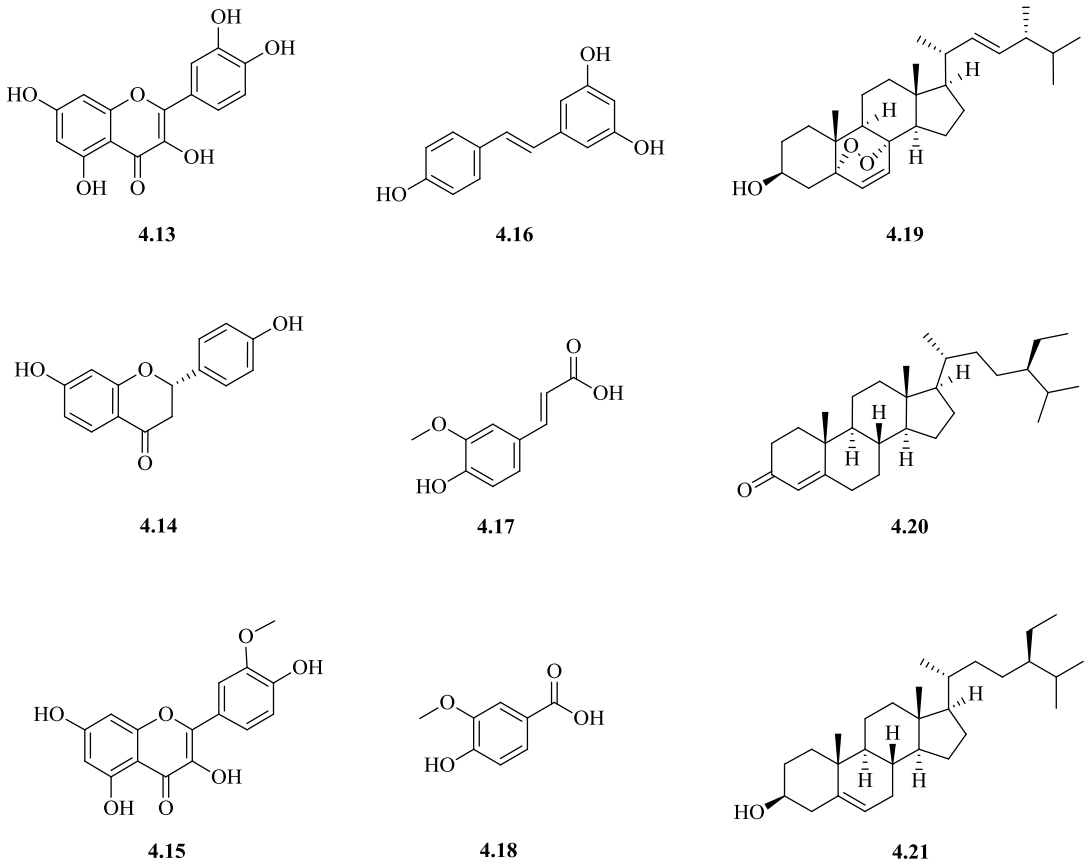

Figure 50. Some commercially available Areca nut metabolites

None of these commercially available metabolites were observed to induce significant calcium signals at concentrations of 10 μM (Figure 51). Quercetin **4.13** showed a small biphasic change in Ca^{2+} response with a transient initial spike followed by a decrease (Figure 51b), consistent with previous reports that describe its ability to bind to ryanodine receptor in Jurkat cells and release Ca^{2+} from intracellular stores.[174]

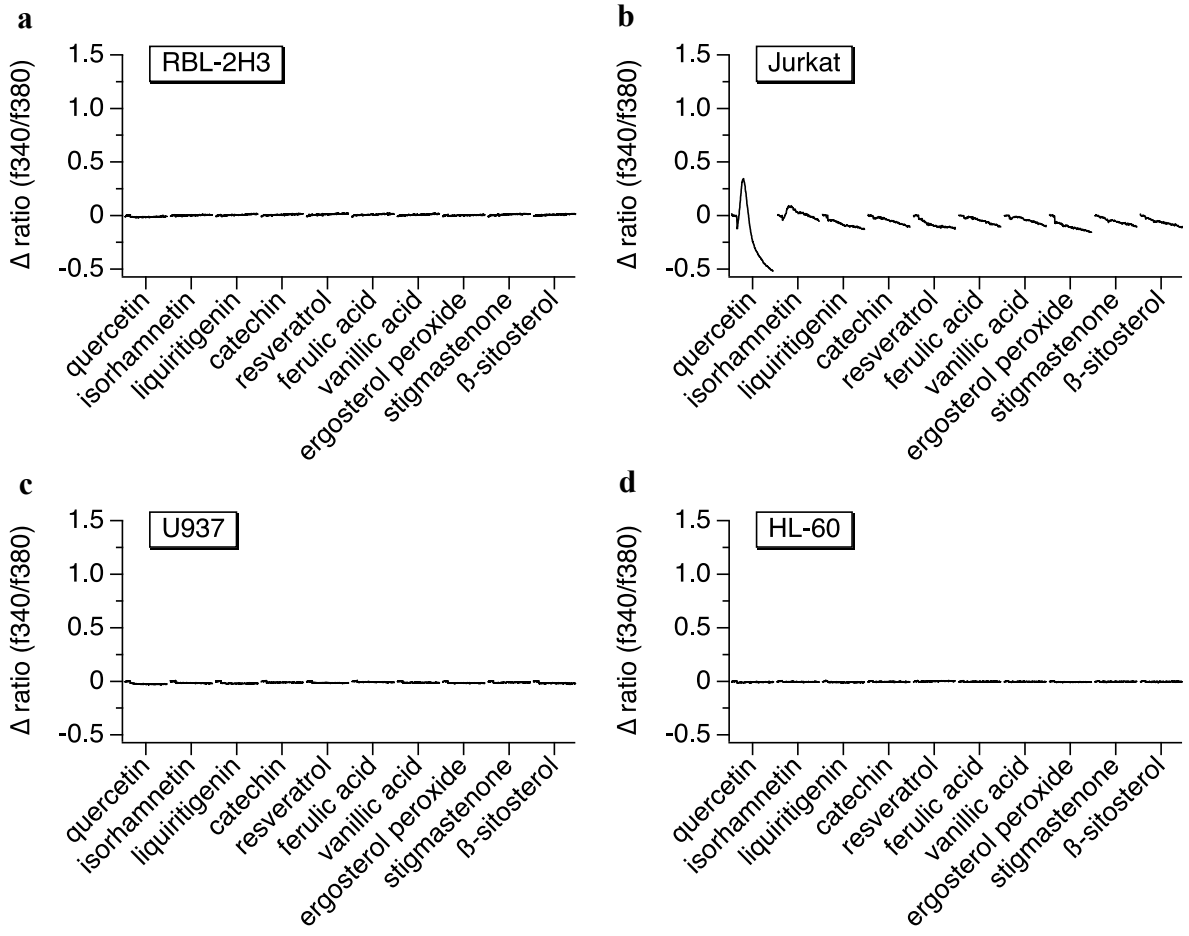

Figure 51. Ca-signaling profiles from selected Areca nut metabolites in immune cells

4.7 Characterization, Purification and Activity of Polymeric Flavonoids

The preponderance of evidence suggesting that proanthocyanidins (oligomeric and polymeric flavonoids; procyanidins belong to a subgroup with only catechin and *epi*-catechin as monomers) are responsible for the Ca-signaling effects in immune cells led us to work toward obtaining more specific structural information on the active component(s) present in Areca nut extract. Proanthocyanidins have been described in a litany of literature reports and they exist in various sizes, from dimers to higher order oligomers (n > 10). A study estimated the average molecular weight of the peracetate derivatives of proanthocyanidins derived from various plant sources to be in the 1600-5500 Da range.[175] Lower order procyanidin oligomers (dimers and trimers) from various plant sources have been isolated, purified and characterized[176] but there is little to no information on higher order polymers. In this context, the results from our dialysis experiments, which implied that the molecular weights of the active polyflavonoids isolated from *Areca catechu* may be higher than 10 kDa, were unusual because receptor-operated calcium channels are not known to be activated by large polymers. This could stem from two reasons, i.e., higher order polymers from *Areca catechu* have not been properly characterized or the dialysis membranes in our experiments have retained a majority of the components with molecular weights lower than the MWCO. Literature on dialysis membranes shows that MWCO is not a sharply defined value and more than 50% of molecules with molecular weights much smaller than the MWCO could be retained in the membranes.[177] Consequently, dialysis experiments are not suitable gauges for estimation of molecular weights of components. Therefore, we sought to address the questions regarding the size of the molecules and the number of components present in the active sample by employing MALDI mass spectrometry and chromatographic methods.

MALDI-MS of the dialyzed aqueous Areca extract fraction (RPN-3-145-2) retained in the dialysis membrane with MWCO of 10 kDa showed a cluster of signals at *m*/*z* values in the 2900-3000 range (Figure 52). Many species present in this cluster appear to be singly charged and, therefore, have molecular weight values around 3 kDa. This suggests that the polymeric procyanidins comprise of approximately 10 monomer units (molecular weights of catechin and *epi*-catechin are 290 Da). However, there is also indication that other species may be triply charged (based on *m*/*z* spacing of 0.3 between peaks), which would imply that their molecular weights are in the neighborhood of 9 kDa. The latter value is a little surprising as it is not consistent with literature reports that describe quantification and estimation of various plant-derived procyanidins.

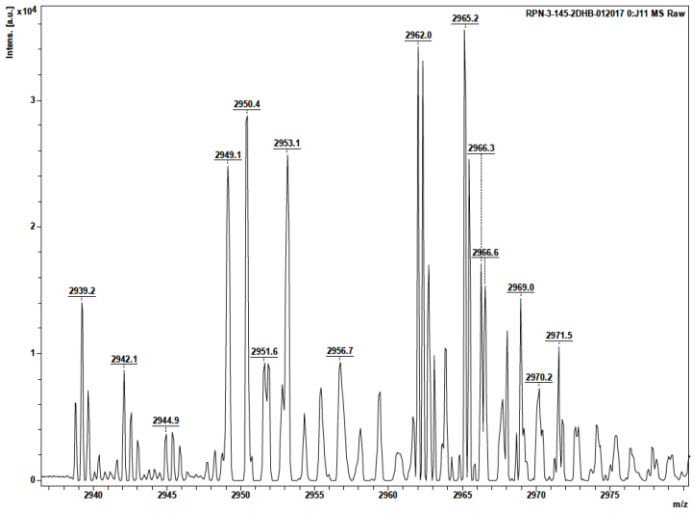

Figure 52. MALDI mass spectrum of Areca extract fraction retained in dialysis (MWCO: 10.4 kDa)

We turned to gel permeation (size exclusion) chromatography to provide additional evidence to corroborate the information obtained from MALDI-MS. Based on the size exclusion

chromatographic separation of protein standards and methyl cobalamin (Figure 53, top), the highest molecular weight of the earliest eluting component (Figure 53, bottom) in the dialyzed Areca extract sample (RPN-3-145-2) appeared to be approximately 3.1 kDa, which is in close agreement to the MALDI-MS data. The resolution, however, was pretty poor, indicating that these components may not be separated easily by gel permeation chromatography.

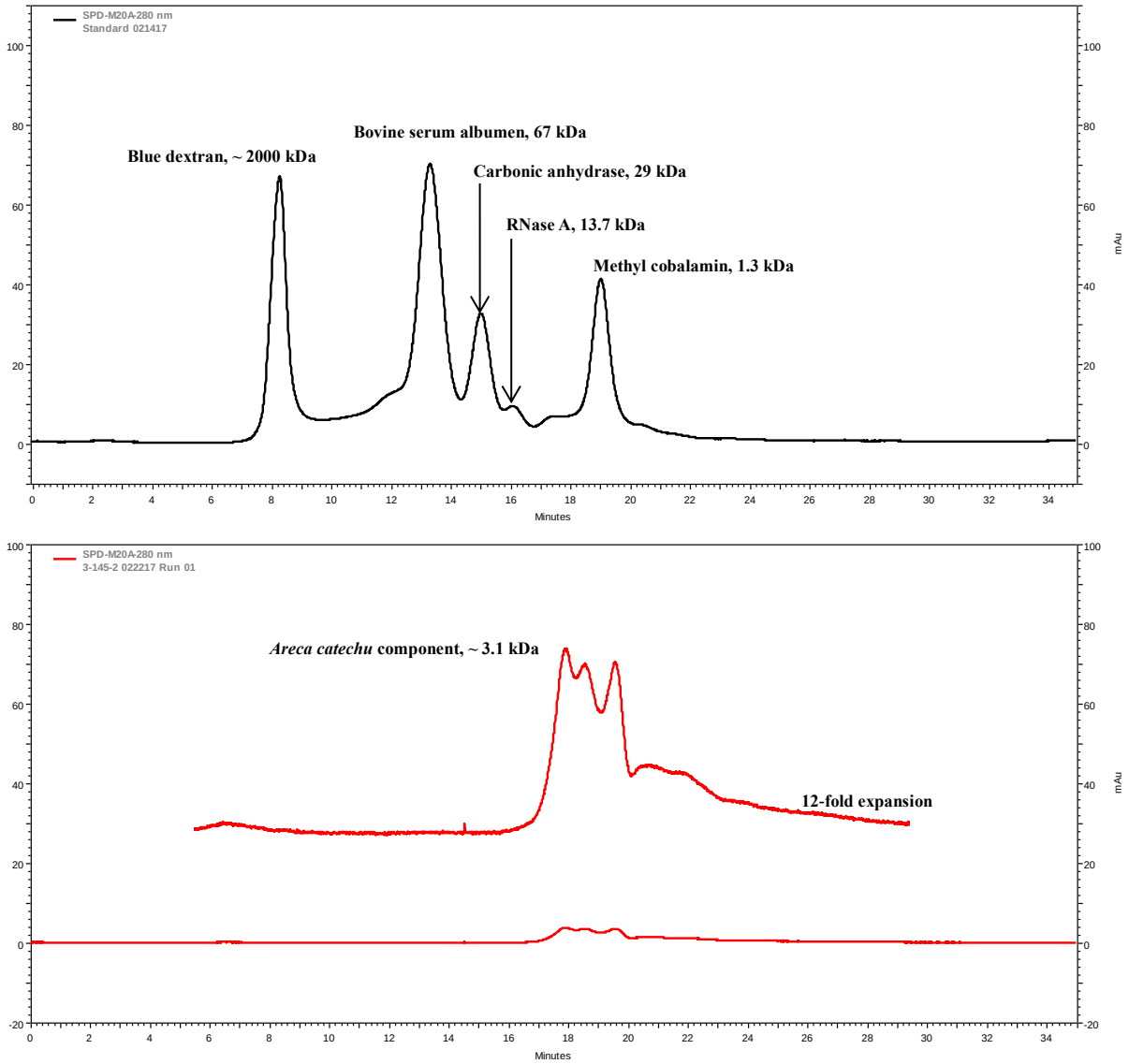

Figure 53. Size exclusion chromatograms of standards (top) and Areca sample (bottom)

The most common method of chromatographic separation of procyanidin samples utilize the reversed phase solid support, however, normal phase HPLC has been found to be better suited at resolving higher oligomeric forms of procyanidins.[178] Several studies have adopted this strategy in purifying procyanidin oligomers isolated from *Areca catechu*[179] and other plant sources.[180] We resorted to an identical approach in efforts to purify polymeric procyanidin components from the active dialyzed sample (RPN-3-145-2) for further biological evaluation. The active dialyzed sample appeared to be comprised primarily of polymers (> 10 monomers) of flavonoids based on the analysis by Gu *et al.*[180] (Figure 54). In Gu *et al.*'s and our chromatographic separations, the polymers eluted as a single peak after 54 min. Approximately 700 µg of the polymeric sample was obtained from purification of 2 mg of the dialyzed fraction.

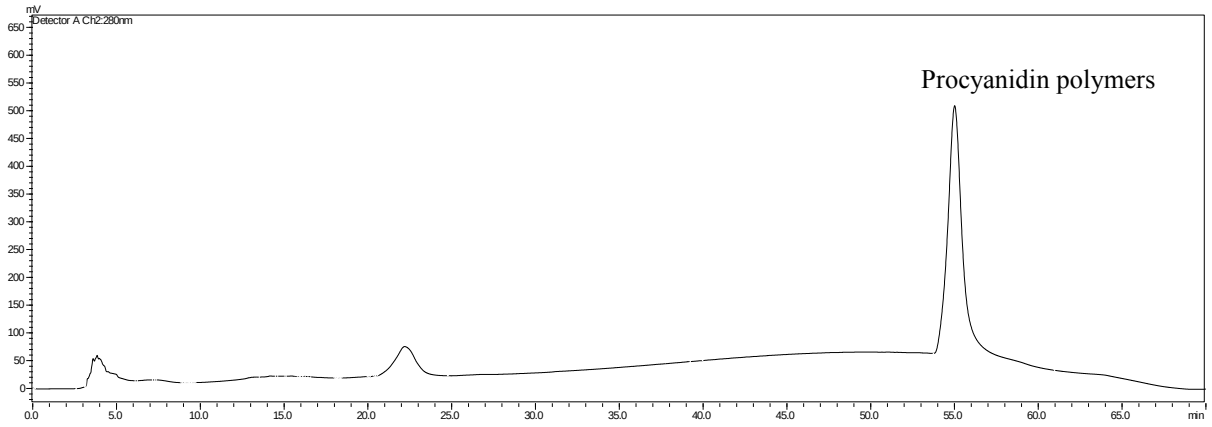

Figure 54. Normal phase HPLC trace of dialyzed Areca extract fraction, detected at 280 nm

The polymeric procyanidins purified from Areca nut extract (ANE opc) were unable to induce Ca-signals in the immune cells, whereas, commercially available oligomeric procyanidins isolated from grape seeds (GS opc) showed activity resembling those exhibited by the active Areca nut extracts (Figure 55a). Moreover, the activity from the grape seed procyanidin oligomers persists even after addition of EGTA, an inhibitor of SOCE, akin to how it

responds with the active Areca nut extracts (Figure 55b). These results show that Areca nut extracts have the same active components as oligomeric procyanidins obtained from grape seeds. Additionally, there were no discernible differences between the ^{1}H NMR spectra of oligomeric procyanidins obtained from grape seeds and active Areca fractions. However, the inactivity of polymeric procyanidins obtained from purification of Areca extract is inconsistent, which may be a result of a few different scenarios. The amount of the polymers obtained from purification by HPLC may have been much less than 700 μg, due to errors in weighing sub-milligram quantities of material. Alternatively, lower order oligomers, which look to be present in the Areca extract (Figure 54, t_R 21-23 min) but were not collected during the purification, may be responsible for the Ca-signaling activity. The possibility that the active oligomers may have polymerized over time, losing activity in the process, was considered but appears unlikely. Catechin, one of the two monomers of procyanidins, was not observed to polymerize in acetonitrile-water solutions (with or without 0.1% formic acid) when monitored by ^{1}H NMR spectroscopy over a period of 10 days. Overall, the results obtained from these studies indicate strong likelihood that procyanidin oligomers or polymers are responsible for Ca-mobilization in immune cells. Further work is necessary to identify the molecular structure of the active component. Specifically, the normal phase HPLC purification of the aqueous Areca extract and its dialyzed fraction on a larger scale to obtain appreciable quantities of purified flavonoid components, i.e. monomers, oligomers and polymers, for rigorous characterization and biological evaluation is crucial for the identification of the active component. MALDI-MS must be incorporated in the characterization methods for an accurate assessment of the molecular weights of the components. Additionally, access to commercially available natural or synthetic standards of oligomers and polymers would support the findings from our experiments.

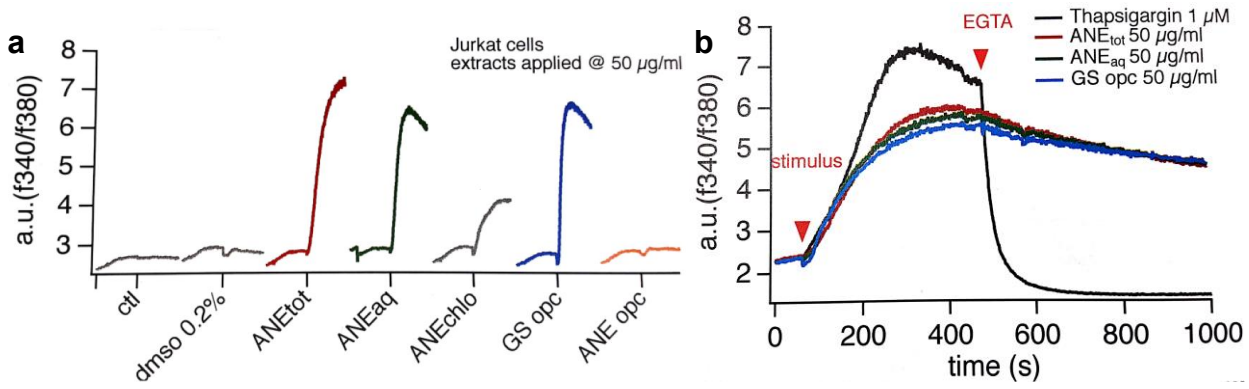

Figure 55. Ca-signaling activity from Areca nut extracts and commercially obtained grape seed oligomeric procyanidins

4.8 Conclusions and Outlook

Areca nut extracts are capable of mobilizing intracellular calcium in immune cell lines and may be responsible for inflammation-mediated carcinogenesis in oral cancers. Preliminary research suggests that oligomeric or polymeric procyanidins may be responsible for the Ca-signaling observed in these cells. Further purification and isolation of oligomeric and polymeric procyanidins is necessary to unambiguously identify the specific active component(s) present in *Areca catechu*. Dr. Reinhold Penner and Dr. Malika Faouzi, the lead collaborators, are also conducting various studies to determine the mechanism of action triggered by these components to induce Ca-signaling activity.

CHAPTER 5

Isolation of Known Natural Products from Other Organisms

Bioactivity-guided isolation of active natural products may not come to fruition very often because of several reasons. Firstly, an extract may contain compounds that are ineffective against the target of a particular assay but could show biological effects in other assays. These extracts would be considered inactive but in reality they may not have been screened against the most suitable targets, in most cases due to lack of access. Secondly, an organism may produce a biologically active natural product but in such small quantities that it is very difficult to isolate enough for full characterization of the molecule. Lack of availability of enough biomass of the organism producing an active natural product may also lead to similar issues. This is a chronic problem faced by many natural product researchers. Sometimes, an active natural product may be unstable in the laboratory settings and could decompose during the course of the investigation because of its exposure to solvents, acids and bases that could cause chemical transformations. Likewise, a lack of a robust screening method would lead to conflicting biological assessment due to inherent variations associated with the screening method. For example, in cell-based assays that have not been previously optimized, it is difficult to get uniformity in the behavior of the cells across various replications. In many instances of these unsuccessful ventures, natural product researchers resort to spectroscopy-guided isolation of natural products. Very often, this simply leads to re-isolation of known natural products. Some of those examples are discussed briefly in this chapter, organized by the producing organism.

5.1 Sponge 12-Maui-38

12-Maui-38, a very hollow lavender/pink sponge (Figure 56a) tentatively identified as *Callyspongia* sp., was collected from a depth of 28 feet off Black Rock Point in Maui (Coordinates: 20°55'35.85" N; 156°41'49.40" W) on July 12, 2012. Lyophilization of the sample resulted in 1 g of dry biomass.

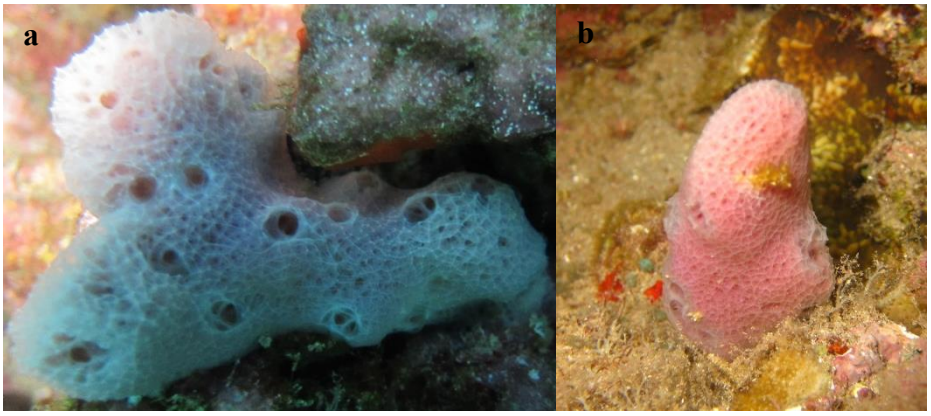

Figure 56. Photographs of (a) 12-Maui-38 and (b) 13-Maui-75, sponges collected from Black Rock Point, Maui

The 75% methanol fraction obtained from the solid phase extraction of the crude extract of 12-Maui-38 showed significant inhibition (88%) of BACE1 in the chemiluminescent assay. Purification by HPLC led to the isolation and characterization of callyspongynic acid[181] **5.1** (Figure 57).

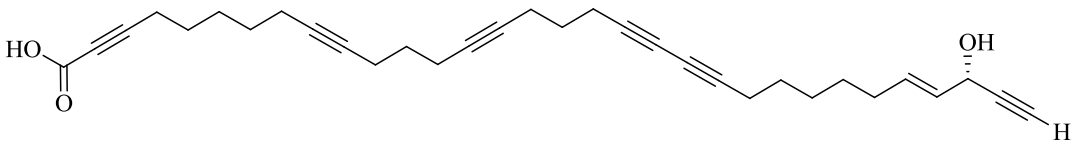

5.1

Figure 57. Structure of callyspongynic acid

Callyspongynic acid was originally isolated from *Callyspongia truncate* Lindgren (Callyspongiidae), which was collected off the Kii Peninsula, 450 km west of Tokyo. It displayed potent selective inhibition of *α*–glucosidase but was inactive against *β*–glucosidase and *β*-galactosidase.[181]

In this study, callyspongynic acid was evaluated for activity against BACE1 following its full structural characterization and, surprisingly, was found to be inactive in the chemiluminescent assay. Further examination revealed degradation of the compound into unknown components. This led to a repeat collection trip to Maui. 13-Maui-75 was collected from the same location and identified as the same sponge (Figure 56b). Work on this specimen, which was carried out by Dr. Stephen Parrish, led to the isolation of callyspongynic acid and its decarboxy analogue.[142] Callyspongynic acid displayed 96% inhibition of BACE1 at 64 μM but no IC_{50} value was obtained because of the discontinuation of the assay kit by the commercial vendor, as stated in Chapter 3. Callyspongynic acid was cytotoxic to Panc-1 cells, with a CC_{50} value of 15 μM.[142]

5.2 Sponges 13-Maui-52 and 14-Maui-05

An assay plate containing extracts of various organisms collected from Maui in 2013 was screened against the vascular permeability assay run by our collaborators, as described in section 1.6. The extracts in the following wells (A5, B9, C4 and F10) exhibited reduced permeability relative to the DMSO control (Figure 58). The extracts were identified as follows: A5 – isopropanol fraction of the extract of the algae 13-Maui-01; B9 – isopropanol fraction of the extract of the sponge 13-Maui-52; C4 – isopropanol fraction of the extract of the algae 13-Maui-08; F10 – 75% methanol fraction of the extract of the sponge 13-Maui-04.

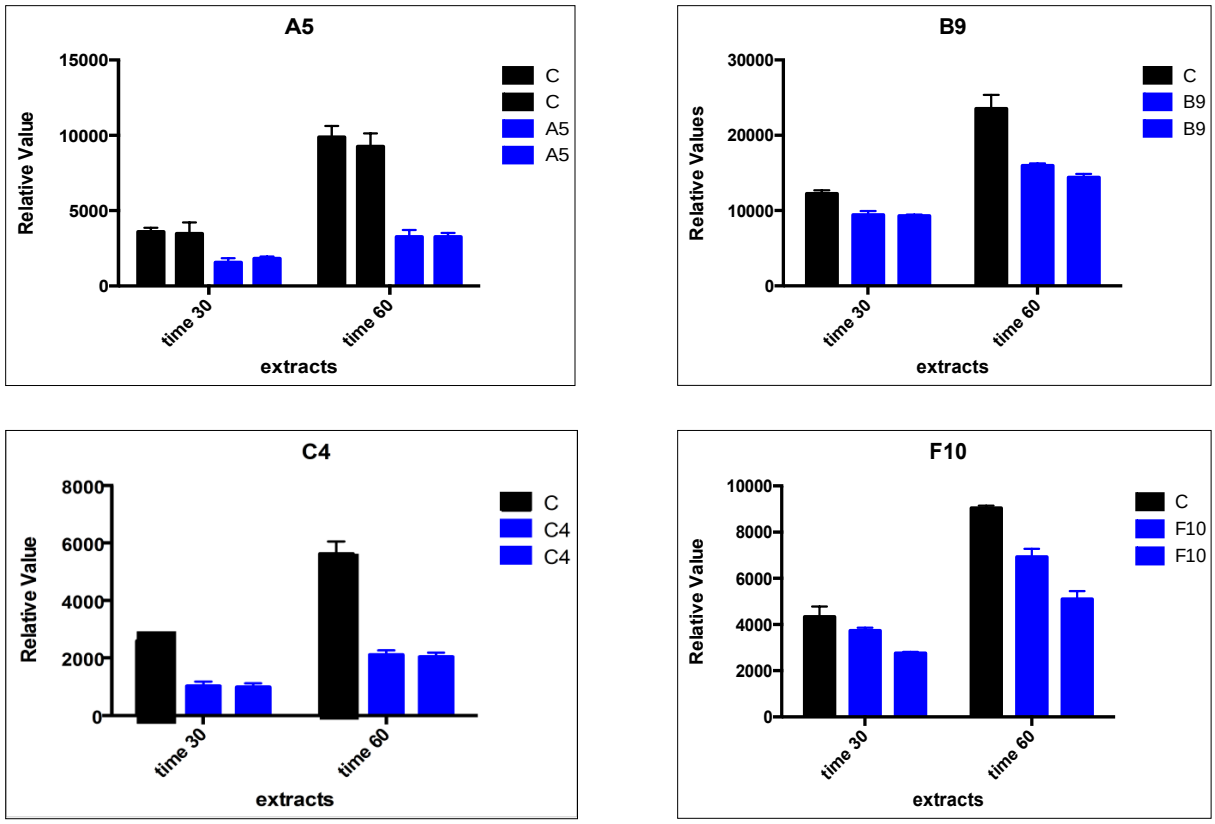

Figure 58. Inhibition of vascular permeability by various extracts

Attempts to isolate inhibitors of vascular permeability from these extracts were unsuccessful primarily because of two reasons – the activity data from the assay was inconsistent with noticeable fluctuations even when the same sample was run multiple times and in some instances, chromatograms from HPLC separations were also inconsistent. The latter could be because of operator error or other chromatographic issues. Furthermore, the bioassay portion of the project was carried out by multiple users and there was lack of consistency in the results obtained by different users. Cell-based assays generally need careful optimizations and consistent handling, and it is not ideal for the assay to be run by different users over short periods of time. Moreover, there was no obvious way to validate the assay because a positive control was

not available. Typically, assays are validated based on their z-factors, which depend on the mean and standard deviation values of readings obtained from the positive and negative controls.

Nonetheless, two sponge samples were investigated further and their extracts were purified by HPLC. 13-Maui-52 (Figure 59a) is an undescribed cave sponge species of the genus *Myrmekioderma*, which was collected at a depth of 40-60 feet near the second cathedral dive site off the south shore of Lanaʻi (coordinates: 20°44'05.0" N, 156°55'25.7" W). 14-Maui-05 (Figure 59b) was a re-collection sample of the sponge 13-Maui-04, which was taken from a depth of 10 feet near the Ulua beach dive site in Maui and identified as *Hyrtios* sp.

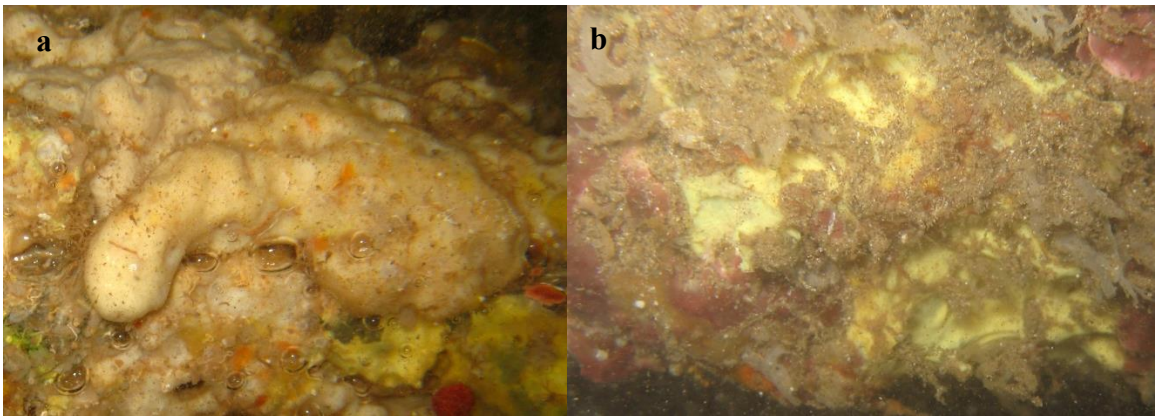

Figure 59. Photographs of (a) 13-Maui-52 and (b) 14-Maui-05, sponges collected from Maui county

β-Sitosterol **4.18**, a ubiquitous sterol found in many plants and sponges, was isolated from the sponge 13-Maui-52 and psammaplysin A **5.2**, a tetrabrominated alkaloid originally discovered from the Palauan sponge *Psammaplysilla purpurea* Carter (Pseudoceratinidae),[182] was isolated from the sponge 14-Maui-05 (Figure 60). Additionally, other sterol derivatives were identified from 13-Maui-52 by Dr. Stephen Parrish.[142]

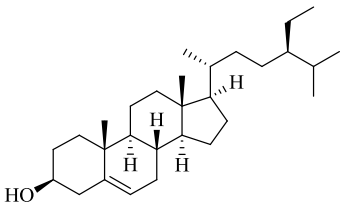

4.18

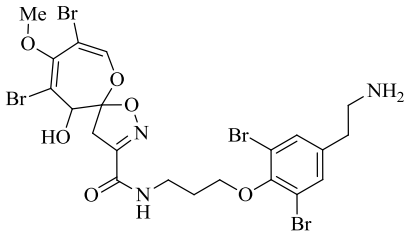

5.2

Figure 60. β-sitosterol and psammaplysin A

5.3 Cyanobacterium CN-16-1

CN-16-1 is a cyanobacterial strain, obtained from the Patterson collection, which was originally collected from the Western Caroline Islands in Palau and identified as *Hapalosiphon* sp. Extracts of CN-16-1 were tested against BACE1 in our in-house chemiluminescent assay and determined to be inactive. Further purification of the hexanes and the dichloromethane fractions (obtained from modified Kupchan partitioning) led to the isolation of Fischerellin A[183] **5.3**, Fischerellin B[184] **5.4** and loliolide[185] **5.5** (Figure 61). Fischerellin A, which has antifungal and herbicidal properties, and Fischerellin B, an algicidal natural product, were isolated from the cyanobacterium *Fischerella muscicola* (Thuret) Gomont (Hapalosiphonaceae). Loliolide is an ant repellent[186] originally isolated from the English ryegrass *Lolium perenne* L. (Poaceae).

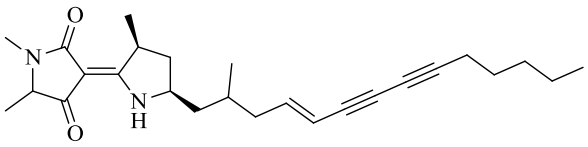

5.3

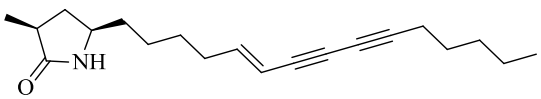

5.4

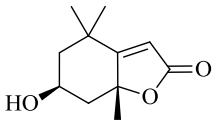

5.5

Figure 61. Compounds isolated from the cyanobacterium CN-16-1

5.4 Fungus Isolated from the HCC1088 Culture

Previously, we showed that the compounds **3.6-3.9** were not produced by the fungus present in the culture of the cyanobacterium HCC1088. Extraction of the fungal cell mass from an axenic culture and subsequent separation by HPLC yielded several compounds, including **5.6** (Figure 62). Compound **5.6** was isolated from the fungi *Penicillium brevicompactum* Dierckx (Trichocomaceae)[187] and *Penicillium citrinum* Thom (Trichocomaceae)[188] and reported to exhibit anti-juvenile hormone activity.[187a] Preliminary ^{1}H NMR and LCMS analyses suggest that some of the other compounds in the extract are structurally related to **5.6** and have molecular weight values in the same vicinity. For example, one of the compounds with molecular weight that is 34 units higher than that of **5.6** may have been produced by dihydroxylation of the olefin in the hydrocarbon chain of **5.6**. The elucidation of these compounds is in progress. Work is also underway toward obtaining a taxonomic identification of this fungal strain.

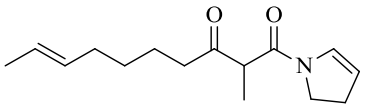

5.6

Figure 62. A metabolite isolated from the culture of a fungus separated from HCC1088 culture

CHAPTER 6

Conclusions and Significance

Chemical investigations of several organisms toward the discovery of biologically active secondary metabolites led to the isolation of several known and new natural products. Nine known sesquiterpene quinones and hydroquinones **2.3** – **2.11** isolated from the sponge *Dactylospongia elegans* showed strong to moderate cytotoxicity against the human glioma (U251MG) cancer cell line. Additionally, four of these compounds exhibited moderate cytotoxicity against the human pancreatic carcinoma (Panc-1) cell line. Furthermore, ilimaquinone and smenospongine displayed moderate inhibition of BACE1, an enzyme implicated in the pathogenesis of the Alzheimer's disease. The significance of these findings is that they represent new reports of biological activity of the known compounds against previously untested targets. A new 11-membered heterocycle, kauamide **2.12**, was also isolated from the sponge extract. Literature reports of isolation of structurally similar metabolites from cyanobacteria of the genus *Moorea*, however, suggest that kauamide is in most likelihood biosynthesized by a cyanobacterium. Regardless, the discovery of kauamide illustrates the potential in the discovery of new natural products from the marine environment.

Investigation of the extract from the broth of the culture of an as yet unidentified cyanobacterium (HCC1088) led to the isolation of four new molecules **3.6** – **3.9**. Compound **3.7** was identified in the early stages of the investigation as a probable BACE1 inhibitor. However, due to discontinuation of the assay kit by the commercial vendors, further biological assessment of the compound against the BACE1 target has not been completed yet. Early suggestions that

compounds **3.6**, **3.8** and **3.9** may be produced by the cyanobacterium in defense against fungal invasion remain unverified but experiments to determine the legitimacy of these indications are ongoing. Nonetheless, the finding that these compounds may be produced by the cyanobacterium and released into the growth medium is in itself unusual, as there are not many accounts of the isolation of cyanobacterial metabolites from the culture broth. Isolation of compounds with rare functional groups and structural features from the culture broth of HCC1088 show that the cyanobacterial culture medium may be an untapped source for the discovery of novel classes of polar natural products.

Mobilization of intracellular calcium by the extracts of *Areca catechu* in immune cell lines (Jurkat, U937, RBL-2H3) has been attributed to the presence of oligomeric or polymeric flavonoids found in the nuts of the plant. Furthermore, the extracts of grape seeds and other plant specimens (not described in this dissertation) showed similar mobilization of intracellular calcium in immune cells. While the identity of the specific component(s) responsible for this activity may be revealed by future experiments, the current findings may provide a breakthrough in our quest to gain important insights into the role of *Areca catechu* in oral diseases, including inflammation and cancer. Further investigations are necessary before we can reach firm conclusions but these discoveries are significant in that they may demonstrate the ability of the ubiquitous flavonoids to activate pathways in humans that have not yet been described.

Finally, prediction of ^{1}H and ^{13}C NMR chemical shifts by density functional theory computation has been demonstrated to be a viable strategy for the determination of the planar structure and the relative configuration of new molecules. This is an especially advantageous approach in the structure elucidation of molecules isolated in very low yields because, unlike conventional methods, it does not require irreversible chemical modifications.

CHAPTER 7

Experimental Section

7.1 General Experimental Procedures

General experimental procedures. Optical rotations were measured on a JASCO DIP-370 polarimeter at 589 nm using a sample cell of path length 0.1 dm. UV spectra were obtained on a Varian Cary 50 Bio UV-Visible spectrophotometer. IR spectra of the compounds, as thin films on CaF_2 discs, were recorded using a Shimadzu IRAffinity-1 Fourier Transform spectrophotometer. NMR spectra were acquired on a Varian Inova 500 MHz spectrometer operating at 500 (^{1}H) or 125 (^{13}C) MHz using the residual solvent signals as internal references (CD_3OD δ_H 3.30, δ_C 49.0; DMSO-d_6 δ_H 2.50, δ_C 39.5; $CDCl_3$ δ_H 7.26, δ_C 77.0). Samples were placed in 3-mm Shigemi NMR tubes as necessary. HRMS data were obtained from Agilent 6210 LC/TOF and Agilent 6545 LC/QTOF instruments using electrospray ionization in positive and negative modes. ESIMS data were also obtained using Agilent 6410 QQQ instrument. Samples were purified using a combination of chromatographic techniques, including high performance liquid chromatography. Purity of the compounds was assessed from their UV absorptions at appropriate wavelengths, or from their ^{1}H NMR spectra. Percent yields of natural products were based on the amount of freeze-dried biological material or crude extract from the culture broth.

Chemicals and reagents. Assays were performed according to manufacturer's instructions. The BACE1 assay kit was purchased from DiscoveRx. ACS grade solvents were distilled and filtered before use. HP-20 resin, flash column stationary phases, and HPLC columns were purchased from Supelco, Sorbent Technologies, and Phenomenex, respectively. The amine

hydrochloride precursor **3.17** was obtained from Enamine Limited and used as received. Mosher's acid chlorides (*R* and *S*), sodium borohydride, cerium(III) chloride heptahydrate, and other chemical reagents were obtained from Sigma-Aldrich and Acros, and used as received.

BACE1 assay. The HitHunter BACE1 enzyme fragment complementation chemiluminescence assay was purchased from DiscoveRx. The proteolytic cleavage of amyloid precursor protein was assayed as described by Naqvi.[63] Test compounds were solubilized in DMSO at the desired concentration and incubated with the enzyme in triplicates for 16 h in 96-well plates. A DMSO control (1.5 μL) and an inhibitor standard (β-secretase inhibitor IV from Calbiochem used as a positive control) were also tested in triplicates. The chemiluminescence signal was read using a Fluostar Optima spectrophotometer. Data were analyzed using GraphPad Prism. BACE1 activity was calculated as a percent of the positive control using a nonlinear regression analysis function that corresponded to a best one-fit model.

Cytotoxicity assays. Human glioblastoma (U251MG) cell lines were maintained in RPMI 1640 Medium (Gibco, REF: 11875-093) supplemented with 10% premium fetal bovine serum (Atlanta biological, Cat. No.: S11150) and 100 U/mL penicillin and 100 µg/mL streptomycin (Gibco, REF: 15140-122). A day prior to treatment, cancer cells were seeded at 4,000 cells per well into a 96-well tissue culture plate. Twenty hours post seeding, the serially diluted compounds were added to the cells for the cytotoxicity assay, and co-incubated with 5% CO_2 at 37 ^{o}C for 72 h. Then the medium with compounds were replaced with 1 × dye binding solution prepared according to the manufacturer's instruction (CyQuant NF Cell Proliferation Assay Kit [C35006, Invitrogen]) and incubated with 5% CO_2 at 37 ^{o}C for 60 minutes. After that, cell viability data were collected with a PerkinElmer Multimode Plate Reader according to the manufacturer's instruction. CC_{50} curves were generated using GraphPad Prism 5.

Human pancreatic carcinoma (Panc-1) cell lines were maintained in DMEM media supplemented with 10% premium fetal bovine serum and 50 U/mL penicillin and 50 μg/mL streptomycin. One day before treatment, cancer cells were seeded at 5,000 cells per well into a 96-well tissue culture plate. Twenty four hours post seeding, the serially diluted compounds were added to the cells for the cytotoxicity assay, and incubated at 37 ^{o}C with 5% CO_2 for 72 h. Then 40 μL MTS dye (CellTiter aqueous One Solution Cell Proliferation Assay) was added to each well and incubated with 5% CO_2 at 37 ^{o}C for 90 minutes. Cell viability data were collected with a Modulus Microplate Reader and CC_{50} curves were generated using GraphPad Prism 5.

NMR shift computations. Conformers within 5 kcal/mol of the lowest energy conformer were searched using the Monte Carlo multiple minimum (MCMM) method and the OPLS-2005 force field in MacroModel (Schrodinger Inc.). Each conformer within 5 kcal/mol of the lowest energy conformer was optimized in Gaussian09[189] at the M06-2X/6-31+G level and the geometries of all conformers with similar energies were checked for redundancy. NMR shielding tensors of all unique conformers within the energy window were computed using the gauge-independent atomic orbital (GIAO) method at the B3LYP/6-311+G level and ^{1}H and ^{13}C chemical shifts were obtained after applying appropriate scaling factors (^{1}H: intercept = 31.9477, slope = -1.0767; ^{13}C: intercept = 181.2412, slope = -1.0522). Statistical comparisons of the computed shifts with the experimental data were carried out using the applet provided by Goodman[97] and the spreadsheet provided by Sarotti[136].

Computations of ECD and optical rotation. Density functional theory (DFT) was used to perform calculations, which were carried out in Gaussian 09.[189] All ground-state geometries were optimized at the B3LYP/6-31+G level. The same DFT level was employed to evaluate the effects of solvation in methanol using the SCRF/PCM method.[190] TDDFT[191]

calculations at the B3LYP/6-31+G and the B3LYP/aug-cc-pVDZ levels were conducted to calculate the electronic excitation energies and rotational strengths in methanol.

7.2 Extraction and Isolation of Metabolites from *Dactylospongia elegans*

Biological material. A specimen of the sponge *Dactylospongia elegans* (Sample ID: *10-Kauai-08*) was collected from a depth of 40 feet at the Sheraton Caverns, Kauai by SCUBA diving on June 09, 2010. The sponge was fouled green in its natural habitat and exuded red solution in the collection bag. Recollection of the same sponge (Sample ID: *11-Kauai-80*) from the same location on May 29, 2011 was confirmed upon comparison of collection details, sample description and pictures, and LC-MS profiles of their crude extracts. The biological material was freeze-dried and stored in a freezer prior to extraction. A voucher sample of *10-Kauai-08* was preserved in aqueous alcohol and deposited with Mary Kay Harper (University of Utah) for taxonomic identification.

Extraction and isolation of metabolites from *Dactylospongia elegans*. The freeze-dried sponge sample (40 g) was extracted three times in a 1:1 mixture of methanol and dichloromethane to yield 6.82 g of crude extract, which was then partitioned with hexanes, dichloromethane, butanol and aqueous methanol.

The fraction obtained from the partition with hexanes (1.32 g) was subjected to solid phase extraction on C8 support, in which the extracts were eluted sequentially with an increasing concentration of methanol in water, followed by isopropanol. The extract obtained from the elution with methanol (0.45 g) was divided into six fractions by Flash chromatography (Silica, 250 x 50 mm, eluted in the following order: 0:10, 1:9, 2:8, 3:7, 10:0 mixtures of ethyl acetate to hexanes, and isopropanol.) The second fraction (52 mg) was purified by RP-HPLC (Phenomenex

Luna C18, 150 x 4.6 mm, 5 μm particle size, 100 Å; eluted with MeCN/H_2O at 0.7 mL/min using a gradient of 70% to 100% MeCN over 20 min followed by a wash with MeCN for 10 min) to afford kauamide (**2.12**, t_R 16.0 min, 2.0 mg, 0.005 % yield, >95% purity by ^{1}H NMR). The third fraction (110 mg) was purified by RP-HPLC (Phenomenex Luna C18, 250 x 10 mm, 5 μm particle size, 100 Å; eluted with MeCN/H_2O at 2.5 mL/min using the following gradient: 70% to 90% MeCN over 15 min, held at that composition for 10 min, then increased to 100% MeCN over 5 min and washed with MeCN for an additional 15 min) to afford dictyoceratin C (**2.11**, t_R 26.7 min, 3.5 mg, 0.009 % yield, >90% purity by ^{1}H NMR), dictyoceratin B (**2.10**, t_R 29.3 min, 4.0 mg, 0.01 % yield, >99% purity at 272 nm), smenospongorine (**2.6**, t_R 38.0 min, 3.5 mg, 0.009 % yield, >99% purity at 313 nm) and smenospongiarine (**2.7**, t_R 41.3 min, 5.5 mg, 0.014 % yield, 99% purity at 313 nm). The fifth fraction (27 mg) obtained from the Flash chromatographic separation was subjected to an identical purification scheme to afford dictyoceratin A (**2.9**, t_R 24.1 min, 4.5 mg, 0.011 % yield, >99% purity at 260 nm).

The fraction obtained from partition with dichloromethane (0.98 g) was also subjected to solid phase extraction on C8 support, in which the extracts were eluted sequentially with an increasing concentration of methanol in water, followed by isopropanol. The extract obtained from the elution with 75% methanol (0.28 g) was purified by RP-HPLC (Phenomenex Luna C18, 150 x 4.6 mm, 5 μm particle size, 100 Å; eluted with MeCN/H_2O at 2.5 mL/min using a gradient of 90% to 100% MeCN over 25 min followed by a wash with MeCN for 10 min) to afford 5-*epi*-ilimaquinone (**2.4**, t_R 20.1 min, 10.0 mg, 0.025 % yield, 78% purity by ^{1}H NMR), ilimaquinone (**2.3**, t_R 21.7 min, 98.0 mg, 0.245 % yield, >99% purity at 310 nm), smenospongine (**2.5**, t_R 22.5 min, 3.5 mg, 0.009 % yield, 95% purity at 310 nm) and smenospongidine (**2.8**, t_R 29.8 min, 6.5 mg, 0.016 % yield, >99% purity at 310 nm).

Synthesis of smenospongidine 2.8 from ilimaquinone 2.3. This protocol was adapted from Ling *et al*.[103] To a solution of 13 mg (36 μmol, 1 equiv.) of ilimaquinone **2.3** in 6.5 mL methanol in a round bottomed flask were added a solution of 1.3 mL methanol containing 7 μL (54 μmol, 1.5 equiv.) of phenethylamine, followed by 6 mg $NaHCO_3$. The contents of the flask were stirred for 10 h at 40 ^oC. After cooling the purple-colored reaction mixture to room temperature, a few drops of 1N HCl were added to slightly acidify the solution, which turned red. The solvent was removed *in vacuo* and the crude mixture was dissolved in 4 mL *tert*-butyl methyl ether and extracted with 4 mL of water. The organic layer was separated and after removal of solvent *in vacuo*, 16.3 mg of a crude red solid was obtained. Purification by HPLC (Silica, 250 x 10 mm, 3.0 mL/min flow, elution with ethyl acetate/hexanes using the following gradient: 15% – 30% ethyl acetate over 15 min, held at that composition for 10 min, followed by a wash with ethyl acetate for an additional 10 min) afforded synthetic smenospongidine (**2.8**, t_R 11.7 min, 8.6 mg, 52.8 % yield, >95% purity by ^1H NMR) and smenospongidinimine (**2.24**, t_R 31.0 min, 5.3 mg, 26.7 % yield, >95% purity by ^1H NMR).

Hydrolysis of kauamide 2.12 and advanced Marfey's analysis. A solution of 200 μg (0.6 μmol, 1 equiv.) of kauamide **2.12** in 0.5 mL 6N HCl in a capped reaction vial was stirred for 24 h at 110 ^oC. Solvent was removed by streaming N_2 (g) over the reaction mixture and the residue was analyzed by ESIMS in negative mode to confirm the presence of signals at *m*/*z* 247 and 249. To the dried hydrolysate in the vial were added a solution of 500 μg (1.6 μmol, 2.7 equiv.) 1-fluoro-2,4-dinitrophenyl-5-L-leucinamide (L-FDLA) in acetone (160 μL), H_2O (100 μL) and 1N solution of $NaHCO_3$ (50 μL). The contents in the vial were warmed to 40 ^oC for 1 h, cooled to room temperature, and analyzed by LC-MS (EclipsePlus C18 column, 2.1 x 50 mm, 1.8 μm particle size; eluted with acetonitrile and water (+0.1% formic acid in each) at 0.4

mL/min flow using the following gradient: 20-50% acetonitrile (0-10 min), 50-100% acetonitrile (10-12 min), 100% acetonitrile (12-16 min); detection at 340 nm). The LC-MS data was compared to the data obtained from similar protocols on the standard amino acids DL-*N*-methylleucine and L-*N*-methylleucine, which were obtained from the amino acid standards collection in the Williams laboratory. The retention times for the LL-adduct and the DL-adduct were 9.2 min and 10.3 min, respectively.

Ilimaquinone 2.3: yellow, crystalline solid; $[\alpha]_D^{22}$ -25 (*c* 1.12, $CHCl_3$); UVs (CH_3OH) λ_{max} (log ε) 286 (4.21), 214 (4.06) nm; ^{1}H NMR ($CDCl_3$, 500 MHz) δ 5.84 (1H, s), 4.44 (1H, brs), 4.42 (1H, brs), 3.86 (3H, s), 2.53 (1H, d, *J* = 13.7 Hz), 2.46 (1H, d, *J* = 13.7 Hz), 2.31 (1H, tdt, *J* = 13.8, 5.5, 1.8 Hz), 2.11-2.04 (2H, m), 1.86 (1H, m), 1.52-1.28 (5H, m), 1.20-1.10 (2H, m), 1.03 (3H, s), 0.97 (3H, d, *J* = 6.4 Hz), 0.84 (3H, s), 0.75 (1H, dd, *J* = 11.9, 2.2 Hz) ppm; ^{13}C NMR ($CDCl_3$, 125 MHz) δ 182.3, 182.0, 161.7, 160.5, 153.3, 117.3, 102.5, 102.0, 56.9, 50.1, 43.3, 40.4, 38.0, 36.6, 32.9, 32.3, 28.6, 27.9, 23.1, 20.5, 17.8, 17.4 ppm; HRESIMS *m*/*z* 359.2206 $[M+H]^+$ (calcd for $C_{22}H_{31}O_4$, 359.2217); HREIMS *m*/*z* 358.2128 (calcd for $C_{22}H_{30}O_4$, 358.2144). All spectroscopic data were consistent with literature reports.[80b, 82-83] (Notebook ID: RPN-2-56-1 and RPN-2-100-1)

5-*epi*-Ilimaquinone 2.4: yellow, amorphous solid; ^{1}H NMR ($CDCl_3$, 500 MHz) δ 5.87 (1H, s), 4.70 (1H, brs), 4.67 (1H, brs), 3.88 (3H, s), 2.59 (1H, d, *J* = 13.7 Hz), 2.49 (1H, d, *J* = 13.7 Hz), 2.46-2.40 (1H, m), 2.17-2.08 (2H, m), 2.03-1.99 (1H, m), 1.90-1.72 (2H, m), 1.22-1.06 (4H, m), 1.05 (3H, s), 0.94 (3H, d, *J* = 6.3 Hz), 0.88 (3H, s) ppm; HRESIMS *m*/*z* 359.2211 $[M+H]^+$ (calcd for $C_{22}H_{30}O_4$, 359.2217). ^{1}H NMR data were consistent with literature reports.[83] (Notebook ID: RPN-2-88-7 and RPN-2-91-1)

Smenospongine 2.5: red, amorphous solid; ^{1}H NMR ($CDCl_3$, 500 MHz) δ 5.64 (1H, s), 4.46 (1H, brs), 4.45 (1H, brs), 2.51 (1H, d, J = 13.9 Hz), 2.42 (1H, d, J = 13.9 Hz), 2.34 (1H, td, J = 13.8, 5.5 Hz), 2.13-2.06 (2H, m), 1.86 (1H, m), 1.54-1.35 (5H, m), 1.21-1.15 (2H, m), 1.06 (3H, s), 0.98 (3H, d, J = 6.4 Hz), 0.88 (3H, s), 0.79 (1H, dd, J = 11.9, 2.2 Hz) ppm; HRESIMS m/z 344.2210 $[M+H]^+$ (calcd for $C_{21}H_{30}NO_3$, 344.2226). ^{1}H NMR data were consistent with literature reports.[82-83] (Notebook ID: RPN-2-91-2)

Smenospongorine 2.6: red, amorphous solid; ^{1}H NMR ($CDCl_3$, 500 MHz) δ 6.52 (1H, brs), 5.36 (1H, s), 4.44 (1H, brs), 4.43 (1H, brs), 2.98 (2H, t, J = 6.5 Hz), 2.48 (1H, d, J = 13.8 Hz), 2.40 (1H, d, J = 13.8 Hz), 2.40-2.28 (2H, m), 2.12-1.82 (7H, m), 1.46-1.32 (2H, m), 1.04 (3H, s), 0.99 (3H, d, J = 6.7 Hz), 0.98 (3H, d, J = 6.7 Hz), 0.97 (3H, d, J = 6.4 Hz), 0.83 (3H, s), 0.78 (1H, dd, J = 11.8, 2.0 Hz) ppm; ^{13}C NMR ($CDCl_3$, 125 MHz) δ 182.8, 178.0, 160.5, 157.3, 150.3, 113.5, 102.5, 91.5, 49.8, 42.9, 41.2, 40.4, 37.8, 36.8, 36.6, 33.0, 32.4, 28.6, 27.9, 25.9, 23.2, 22.3, 20.5, 17.9, 17.3 ppm; HRESIMS m/z 400.2851 $[M+H]^+$ (calcd for $C_{25}H_{38}NO_3$, 400.2846). All data were consistent with literature reports.[82] (Notebook ID: RPN-3-25-3)

Smenospongiarine 2.7: red, amorphous solid; ^{1}H NMR ($CDCl_3$, 500 MHz) δ 6.42 (1H, brs), 5.38 (1H, s), 4.46 (1H, brs), 4.45 (1H, brs), 3.18 (2H, td, J = 6.7, 6.5 Hz), 2.49 (1H, d, J = 13.9 Hz), 2.41 (1H, d, J = 14.0 Hz), 2.34 (1H, td, J = 13.8, 5.5 Hz), 2.13-2.06 (3H, m), 1.87 (1H, m), 1.78-1.12 (9H, m), 1.06 (3H, s), 0.99-0.93 (9H, overlapping d, d, d), 0.84 (3H, s), 0.79 (1H, dd, J = 11.8, 2.0 Hz) ppm; ^{13}C NMR ($CDCl_3$, 125 MHz) δ 182.8, 178.0, 160.5, 157.2, 150.3, 113.4, 102.5, 91.4, 49.8, 42.9, 41.2, 40.4, 37.8, 36.8, 36.6, 33.0, 32.4, 28.6, 27.9, 25.9, 23.2, 22.4, 22.3, 20.5, 17.9, 17.4 ppm; HRESIMS m/z 414.2999 $[M+H]^+$ (calcd for $C_{26}H_{40}NO_3$, 414.3003). All spectroscopic data were consistent with literature reports.[82-83] (Notebook ID: RPN-2-89-2)

Smenospongidine 2.8: red, amorphous solid; $[\alpha]_D^{22}$ +125 (*c* 0.1, $CHCl_3$); UVs (CH_3OH) λ_{max} (log ε) 488 (2.91), 323 (4.04), 248 (3.65) nm; IR (CaF_2 disc) ν_{max} 3269, 2922, 1642, 1589 and 1581 cm^{-1}; ^1H NMR ($CDCl_3$, 500 MHz) δ 8.35 (1H, brs), 7.33 (2H, t, *J* = 7.3 Hz), 7.26 (1H, m), 7.18 (2H, d, *J* = 7.0 Hz), 6.47 (1H, brs), 5.40 (1H, s), 4.45 (1H, brs), 4.44 (1H, brs), 3.42 (2H, q, *J* = 6.8 Hz), 2.95 (2H, t, *J* = 7.0 Hz), 2.49 (1H, d, *J* = 14.0 Hz), 2.39 (1H, d, *J* = 14.0 Hz), 2.32 (1H, m), 2.08 (1H, m), 2.06 (1H, m), 1.83 (1H, m), 1.51 (1H, m), 1.43 (1H, m), 1.38 (2H, m), 1.35 (1H, m), 1.18 (1H, m), 1.11 (1H, m), 1.06 (3H, s), 0.97 (3H, d, *J* = 6.5 Hz), 0.84 (3H, s), 0.77 (1H, dd, *J* = 11.9, 2.0 Hz) ppm; ^{13}C NMR ($CDCl_3$, 125 MHz) δ 182.7, 178.2, 160.5, 157.0, 150.0, 137.4, 128.9, 128.6, 127.0, 113.6, 102.5, 91.8, 49.8, 44.0, 42.9, 40.4, 37.8, 36.6, 34.2, 33.0, 32.4, 28.6, 27.9, 23.2, 20.5, 17.9, 17.3 ppm; HRESIMS *m*/*z* 448.2846 $[M+H]^+$ (calcd for $C_{29}H_{38}NO_3$, 448.2846). (Notebook ID: RPN-2-91-5 and RPN-2-99-1)

Dictyoceratin A 2.9: white, amorphous solid; ^1H NMR ($CDCl_3$, 500 MHz) δ 7.50 (1H, d, *J* = 1.9 Hz), 7.39 (1H, d, *J* = 1.9 Hz), 6.56 (1H, brs), 5.98 (1H, brs), 4.41 (1H, brs), 4.36 (1H, brs), 3.86 (3H, s), 2.68 (1H, d, *J* = 14.3 Hz), 2.65 (1H, d, *J* = 14.4 Hz), 2.34 (1H, td, *J* = 13.8, 5.3 Hz), 2.09 (2H, m), 1.92 (1H, m), 1.57 (1H, qd, *J* = 13.2, 3.3 Hz), 1.50-1.19 (6H, m), 1.06 (3H, s), 1.03 (3H, d, *J* = 6.4 Hz), 0.95 (1H, dd, *J* = 12.1, 1.7 Hz), 0.87 (3H, s) ppm; ^{13}C NMR ($CDCl_3$, 125 MHz) δ 167.6, 160.1, 148.7, 142.3, 127.3, 125.1, 120.3, 113.9, 102.7, 52.0, 48.0, 42.1, 40.2, 36.9, 36.5, 36.3, 33.0, 27.8, 27.7, 23.1, 20.6, 17.6, 17.6 ppm; HRESIMS *m*/*z* 373.2375 $[M+H]^+$ (calcd for $C_{23}H_{33}O_4$, 373.2373). All spectroscopic data were consistent with literature reports.[84] (Notebook ID: RPN-3-30-1)

Dictyoceratin B 2.10: white, amorphous solid; ^1H NMR ($CDCl_3$, 500 MHz) δ 10.71 (1H, brs), 7.14 (1H, s), 5.87 (1H, brs), 5.42 (1H, brs), 4.42 (1H, dd, *J* = 1.8, 1.8 Hz), 4.38 (1H, brs), 3.90 (3H, s), 2.60 (1H, d, *J* = 14.3 Hz), 2.57 (1H, d, *J* = 14.4 Hz), 2.34 (1H, td, *J* = 13.9, 5.4

Hz), 2.08 (2H, m), 1.90 (1H, m), 1.59-1.50 (1H, m), 1.47 (1H, dt, *J* = 12.4, 3.2 Hz), 1.42-1.20 (5H, m), 1.06 (3H, s), 1.00 (3H, d, *J* = 6.4 Hz), 0.94 (1H, dd, *J* = 11.9, 2.1 Hz), 0.84 (3H, s) ppm; ^{13}C NMR ($CDCl_3$, 125 MHz) δ 170.6, 160.2, 148.9, 147.0, 130.3, 124.6, 117.1, 104.4, 102.7, 52.0, 47.8, 41.8, 40.1, 36.6, 36.2, 36.2, 33.1, 27.8, 27.7, 23.0, 20.6, 17.6, 17.5 ppm; HRESIMS *m*/*z* 411.2142 $[M+Na]^+$ (calcd for $C_{23}H_{32}O_5Na$, 411.2142). All spectroscopic data were consistent with literature reports.[84] (Notebook ID: RPN-3-25-2)

Dictyoceratin C 2.11: white, amorphous solid; ^{1}H NMR ($CDCl_3$, 500 MHz) δ 7.76 (2H, m), 6.73 (1H, d, *J* = 9.0 Hz), 5.22 (1H, brs), 4.41 (1H, dd, *J* = 1.8, 1.8 Hz), 4.36 (1H, brs), 3.86 (3H, s), 2.67 (1H, d, *J* = 14.5 Hz), 2.62 (1H, d, *J* = 14.3 Hz), 2.34 (1H, td, *J* = 13.6, 5.4 Hz), 2.08 (2H, m), 1.93 (1H, m), 1.59-1.17 (7H, m), 1.06 (3H, s), 1.03 (3H, d, *J* = 6.5 Hz), 0.95 (1H, dd, *J* = 12.0, 2.0 Hz), 0.88 (3H, s) ppm; HRESIMS *m*/*z* 357.2423 $[M+H]^+$ (calcd for $C_{23}H_{33}O_3$, 357.2424). ^{1}H NMR data was consistent with literature reports.[85b] (Notebook ID: RPN-3-25-1)

(3*S*,6*S*,11*S*,9*E*)-9-(chloromethylene)-3-isobutyl-4,6-dimethyl-11-propyl-1-oxa-4-azacycloundecane-2,5-dione **(kauamide) 2.12**: white, amorphous solid; $[\alpha]_D^{22}$ +20 (*c* 0.1, $CHCl_3$); UVs (CH_3OH) λ_{max} (log ε) 201 (4.08) nm; IR (CaF_2 disc) ν_{max} 2958, 2927, 2870, 1734, 1653 and 1641 cm^{-1}; ^{1}H NMR ($CDCl_3$, 500 MHz) and ^{13}C NMR ($CDCl_3$, 125 MHz) see Table 1; HRESIMS *m*/*z* 358.2140 $[M+H]^+$ (calcd for $C_{19}H_{33}ClNO_3$, 358.2143). (Notebook ID: RPN-2-89-1 and RPN-3-7-1)

Smenospongidinimine 2.24: blue, amorphous solid; $[\alpha]_D^{22}$ +126 (*c* 0.1, $CHCl_3$); UVs (CH_3OH) λ_{max} (log ε) 354 (4.33), 254 (3.91) nm; IR (CaF_2 disc) ν_{max} 3185, 2923, 2857, 1635 and 1591 cm^{-1}; ^{1}H NMR ($CDCl_3$, 500 MHz) δ 8.40 (2H, brs), 7.32 (4H, t, *J* = 7.7 Hz), 7.25 (2H, m), 7.18 (4H, d, *J* = 7.9 Hz), 4.79 (1H, s), 4.44 (1H, brs), 4.43 (1H, brs), 3.51 (4H, t, *J* = 7.3 Hz), 2.95 (4H, t, *J* = 7.3 Hz), 2.45 (1H, d, *J* = 13.8 Hz), 2.40 (1H, d, *J* = 13.7 Hz), 2.32 (2H, m), 2.05

(1H, m), 1.83 (1H, m), 1.50 (1H, m), 1.42-1.10 (6H, m), 1.04 (3H, s), 1.03 (3H, d, J = 6.7 Hz), 0.88 (1H, dd, J = 11.8, 2.2 Hz), 0.80 (3H, s) ppm; ^{13}C NMR ($CDCl_3$, 125 MHz) δ 171.2, 161.8, 156.6, 137.2, 129.0, 128.6, 127.1, 109.1, 101.6, 80.1, 49.7, 44.6, 42.6, 40.5, 37.8, 37.0, 34.8, 33.4, 33.2, 29.0, 28.1, 23.4, 20.7, 18.1, 17.4 ppm; HRESIMS m/z 551.3635 $[M+H]^+$ (calcd for $C_{37}H_{47}N_2O_2$, 551.3632). (Notebook ID: RPN-2-99-3)

7.3 Extraction and Purification of Metabolites from HCC1088 *Nostoc* sp.

Biological material. HCC1088 (*Nostoc* sp.), originally a part of the Mitsui-Miami collection (Mitsui 102201), was obtained from the cyanobacterial collection housed at the University of Hawaii at Manoa. The strain was cultured in twelve 20 L carboys containing 18 L BG-11 media with MOPS buffer, under continuous illumination and aeration (no CO_2 added; 3-4 L air/min; without shaking) for 4 weeks. HCC1088 was also cultured in flasks containing 1 L or 4 L of BG-11 media with MOPS buffer but lacking sodium nitrate. Cultures in nitrate absent media were not aerated and grown for 2 – 6 months.

16S rRNA gene sequencing. About 100 mg of cell mass was pre-treated with 10 mM Tris.HCl, 0.1 M EDTA, 0.5% SDS, 10 μg/mL RNase A and 1 mg/mL lysozyme for 30 min at 37 ^{o}C. Genomic DNA was extracted from the cells and cleaned up using MoBio's PowerPlant DNA Isolation Kit. The 16S rRNA gene was PCR amplified by the primer pair 27F/1492R, and the amplicon was purified using QiaQuick column. The purified PCR products were sequenced using ABI3730XL with four primers (27F, 533R, 981R and 1492R). The sequences were then assembled to a full 16S rRNA gene using DNAStar SeqMan.

16S rRNA gene sequence of HCC1088. ACGGTGTCTTAGGACATAGTGGCGGACGGGTGAGTAACGCGTg
AgAATCTGGCTTCAGGTCGGGGACAACCATTGGAAACGGTGGCTAATACCGGATATGCCGAGAGGTGA
AAGATTTATTGCCTGAAGATGAGCTCGCGTCTGATTAGCTAGTTGGGAGTGTAAGAGACTACCAAGGC
GACGATCAGTAGCTGGTCTGAGAGGATGATCAGCCACACTGGGACTGAGACACGGCCCAGACTCCTA
CGGGAGGCAGCAGTGGGGAATTTTCCGCAATGGGCGAAAGCCTGACGGAGCAATACCGCGTGAGGGA
GGAAGGCTCTTGGGTTGTAAACCTCTTTTCTCAAGGAAGAAAAAAATGACGGTACTTGAGGAATAAGC
ATCGGCTAACTCCGTGCCAGCAGCCGCGGTAATACGGAGGATGCAAGCGTTATCCGGAATGATTGGGC
GTAAAGCGTCCGCAGGTGGCTGTGAAAGTCTGCTGTTAAAGAGTGAGGCTCAACCTCATAAGAGCAGT
GGAAACTACACGGCTAGAGTGCGTTCGGGGTAGAGGGAATTCCTGGTGTAGCGGTGAAATGCGTAGA
TATCAGGAAGAACACCGGTGGCGAAGGCGCTCTACTAGGCCGCAACTGACACTGAGGGACGAAAGCT
AGGGGAGCGAATGGGATTAGATACCCCAGTAGTCCTAGCCGTAAACGATGGATACTAGGCGTGGCTT
GTATCGACCCGAGCCGTGCCGTAGCTAACGCGTTAAGTATCCCGCCTGGGGAGTACGCACGCAAGTGT
GAAACTCAAAGGAATTGACGGGGGCCCGCACAAGCGGTGGAGTATGTGGTTTAATTCGATGCAACGC
GAAGAACCTTACCAAGACTTGACATGTCGCGAATCTGCCTGAAAGGGGAGAGTGCCTTCGGGAGCGC
GAACACAGGTGGTGCATGGCTGTCGTCAGCTCGTGTCGTGAGATGTTGGGTTAAGTCCCGCAACGAGC
GCAACCCTCGTTTTTAGTTGCCAGCATTAAGTTGGGCACTCTAAAGAGACTGCCGGTGACAAACCGGA
GGAAGGTGGGGATGACGTCAAGTCAGCATGCCCCTTACGTCTTGGGCTACACACGTACTACAATGCTA
CGGACAAAGGGCAGCTACACAGCGATGTGATGCAAATCTCAGAAACCGTAGCTCAGTTCAGATCGCA
GGCTGCAACTCGCCTGCGTGAAGGAGGAATCGCTAGTAATTGCAGGTCAGCATACTGCAGTGAATTCG
TTCCCGGKCCTTGTACACACCGCCCGTCACACCATGGAAGCTGGCAACGCCCGAAGTCATTACTCCAA
C

Phylogenetic tree. The tree with the highest log likelihood (-3158.6529) is shown in Figure 26 (Section 3.2). The percentage of trees in which the associated taxa clustered together is shown next to the branches. Initial tree(s) for the heuristic search were obtained automatically by applying Neighbor-Join and BioNJ algorithms to a matrix of pairwise distances estimated using the Maximum Composite Likelihood (MCL) approach, and then selecting the topology with superior log likelihood value. A discrete Gamma distribution was used to model evolutionary rate differences among sites (5 categories (+G, parameter = 0.6264)). The rate variation model allowed for some sites to be evolutionarily invariable ([+I], 70.1785% sites). The tree is drawn to scale, with branch lengths measured in the number of substitutions per site. The analysis involved 92 nucleotide sequences. All positions containing gaps and missing data were eliminated. Evolutionary analyses were conducted in MEGA7.[192]

Extraction and isolation of metabolites from the culture broth of HCC1088. Upon termination of aeration in the culture vessels, HP-20 resin (1g/L) was added to the culture

broth and allowed to sit overnight. The resin was then separated from the culture broth by filtration and soaked in CH_3OH (5 mL/g resin; extracted once; shaken on a mechanical shaker) for 1 h. Filtration and removal of solvent *in vacuo* generated the crude media extract. A concentrated solution of 198 mg crude media extract in methanol was filtered using a Whatman syringe filter and purified by RP HPLC (Phenomenex Luna C_{18}, 250 x 10 mm, 5 µm particle size, 100 Å; eluted with H_2O/CH_3OH at 2.75 mL/min using the following gradient: 35% CH_3OH for 5 min, increased to 50% CH_3OH over the next 30 min and to 100% CH_3OH over the subsequent 5 min, washed with 100% CH_3OH for 20 min.) The compounds **3.8** (t_R 24.4 min, 0.8 mg, 0.4% yield, > 95% purity by LC-UV detection at 280 nm), (3-formylindole **3.10** (t_R 26.8 min, 3.5 mg, 1.8 % yield, ~75% purity by ^{1}H NMR), **3.7** (t_R 36.9 min, 0.9 mg, 0.5 % yield, ~90% purity by ^{1}H NMR), 3-cyanoindole **3.11** (t_R 41.7 min, 2.1 mg, 1.1 % yield, ~85% purity by ^{1}H NMR), **3.9** (t_R 44.2 min, 0.8 mg, 0.4% yield, > 90% purity by ^{1}H NMR), and **3.6** (t_R 45.8 min, 21.2 mg, 10.7% yield, > 95% purity by LC-UV detection at 230 nm) were isolated and characterized.

Compound 3.6: pale yellow, crystalline solid; $[\alpha]_D^{21}$ +15 (*c* 0.2, CH_3OH); UVs (CH_3OH) λ_{max} (log ε) 304 (4.26), 235 (4.11), 204 (4.18) nm; ECD (c 0.1, CH_3OH) λ_{max} (Δε) 304 (+90.7), 345 (-50.5) nm; IR (CaF_2 disc) ν_{max} 3303, 3210 and 1678 cm^{-1}; ^{1}H NMR (CD_3OD, 500 MHz) δ 7.69 (1H, dt, *J* = 8.2, 1.1 Hz), 7.46 (1H, dt, *J* = 8.4, 1.0 Hz), 7.37 (1H, ddd, *J* = 8.3, 7.1, 1.2 Hz), 7.14 (1H, ddd, *J* = 8.1, 7.1, 1.1 Hz), 4.67 (1H, dd, *J* = 6.3, 2.8 Hz), 3.62 (1H, dd, *J* = 16.4, 6.3 Hz), 2.83 (1H, dd, *J* = 16.4, 2.8 Hz) ppm; ^{1}H (DMSO-d_6, 500 MHz) and ^{13}C NMR (DMSO-d_6, 125 MHz), Table 5; HRESIMS *m*/*z* 210.0525 $[M+Na]^+$ (calcd for $C_{11}H_9NO_2Na$, 210.0531). (Notebook ID: RPN-1-38-1 and RPN-1-41-4)

Synthesis of compound 3.7. To 15 mg (71 μmol) of **3.17** in a reaction vial, under N_2 atmosphere, were added 2 drops of pyridine, 10 μL acetic anhydride, and 1 mL dry CH_2Cl_2. The mixture was stirred at room temperature for 1 h. An additional 1 mL of CH_2Cl_2 was added to the vial and the contents were washed with 2 mL sat. $NaHCO_3$ and 2 mL brine. The resultant organic layer was dried over anhydrous $MgSO_4$. Upon removal of the solvent using a stream of N_2 (g), 15.7 mg of crude product was obtained, 85% of which was purified by RP HPLC (Phenomenex Luna C_{18}, 250 x 10 mm, 5 μm particle size, 100 Å; eluted with H_2O/CH_3CN at 3.0 mL/min using the following gradient: 10-60% CH_3CN over 10 min, maintained an isocratic 60% CH_3CN composition for the next 5 min, increased to 100% CH_3CN over the next 5 min, and washed at 100% CH_3CN for 10 min) to obtain compound **3.7** (t_R 11.0 min, 12.0 mg, 55 μmol, 92% yield) as white, crystalline needles.

Compound 3.7: white amorphous solid; ^1H ($CDCl_3$, 500 MHz) and ^{13}C NMR ($CDCl_3$, 125 MHz), Table 6; HRESIMS *m/z* 239.0782 $[M+Na]^+$ (calcd for $C_{12}H_{12}N_2O_2Na$, 239.0791). **Compound 3.7 (synthetic)**: white crystalline needles; UVs (CH_3OH) λ_{max} (log ε) 272 (4.23), 266 (4.24), 204 (4.19) nm; IR (CaF_2 disc) ν_{max} 3273, 3085, 1659, 1645, 1564 cm^{-1}; ^1H NMR ($CDCl_3$, 500 MHz) δ 7.62 (2H, d, J = 7.3 Hz), 7.43 (2H, t, J = 7.6 Hz), 7.35 (1H, t, J = 7.4 Hz), 7.26 (1H, s), 6.87 (1H, brs), 4.66 (2H, d, J = 5.5 Hz), 2.11 (3H, s) ppm and ^{13}C NMR ($CDCl_3$, 125 MHz) δ 170.3, 160.2, 151.9, 128.8, 128.5, 127.4, 124.1, 121.4, 36.9, 22.9 ppm; HRESIMS *m/z* 217.0979 $[M+H]^+$ (calcd for $C_{12}H_{13}N_2O_2$, 217.0972). (Notebook ID: RPN-1-88-1 and RPN-3-123-1)

Synthesis of compound 3.7-F_3. To 15 mg (71 μmol) of **3.17** in a reaction vial, under N_2 atmosphere, were added 2 drops of pyridine, 20 μL trifluoroacetic anhydride, and 1 mL dry CH_2Cl_2. The mixture was stirred at room temperature for 1 h. An additional 1 mL of CH_2Cl_2 was

added to the vial and the contents were washed with 2 mL sat. $NaHCO_3$ and 2 mL brine. The resultant organic layer was dried over anhydrous $MgSO_4$. Upon removal of the solvent *in vacuo*, 16.6 mg of crude yellow oily residue was obtained. The residue was purified by RP HPLC (Phenomenex Luna C_{18}, 250 x 10 mm, 5 μm particle size, 100 Å; eluted with H_2O/CH_3CN containing 0.1% formic acid at 2.75 mL/min using the following gradient: 10-100% CH_3CN over 18 min, and washed at 100% CH_3CN for 12 min) to obtain compound **3.7-F$_3$** (t_R 17.5 min, 3.3 mg, 12 μmol, 17% yield) as an off-white powder. Majority of the starting material remained unreacted, presumably due to degradation of the trifluoroacetic anhydride reagent, which was not purified prior to use. Reaction was not optimized because **3.7-F$_3$** was obtained in sufficient quantity for various experiments.

Compound 3.7-F$_3$: off-white powder; ^{1}H NMR ($CDCl_3$, 500 MHz) δ 7.61 (2H, dd, J = 7.1, 1.2 Hz), 7.43 (2H, t, J = 7.0 Hz), 7.43 (1H, brs), 7.36 (1H, t, J = 7.3 Hz), 7.28 (1H, s), 4.73 (2H, d, J = 5.2 Hz) ppm and ^{13}C NMR ($CDCl_3$, 125 MHz) δ 157.8, 157.3 (q, J = 37.0 Hz), 152.7, 129.0, 128.9, 127.2, 124.3, 121.7, 115.7 (q, J = 287.2 Hz), 37.1 ppm; HRESIMS m/z 271.0687 $[M+H]^+$ (calcd for $C_{12}H_{10}F_3N_2O_2$, 271.0689). (Notebook ID: RPN-4-7-5)

Compound 3.8: white amorphous solid; ^{1}H (CD_3OD, 500 MHz) and ^{13}C NMR (CD_3OD, 125 MHz), Table 7; HRESIMS m/z 328.1184 $[M+H]^+$ (calcd for $C_{18}H_{18}NO_5$, 328.1180). Other spectroscopic data were not acquired due to degradation of the compound. (Notebook ID: RPN-1-57-1 and RPN-1-79-1)

Compound 3.9: yellow amorphous solid; ^{1}H (CD_3OD, 500 MHz) and ^{13}C NMR (CD_3OD, 125 MHz), Table 8; HRESIMS m/z 310.1062 $[M+H]^+$ (calcd for $C_{18}H_{16}NO_4$, 310.1074). Other spectroscopic data were not acquired due to degradation of the compound. (Notebook ID: RPN-1-57-5)

3-Formylindole 3.10: white amorphous solid; ^{1}H NMR ($CDCl_3$, 500 MHz) δ 9.90 (1H, s), 8.17 (1H, d, J = 7.3 Hz), 8.11 (1H, s), 7.49 (1H, d, J = 7.9 Hz), 7.29 (1H, td, J = 7.2, 1.4 Hz), 7.25 (1H, td, J = 7.4, 1.1 Hz) ppm; ESIMS m/z 146.2 $[M+H]^+$; ^{1}H NMR data was consistent with literature reports.[123] (Notebook ID: RPN-1-86-1)

3-Cyanoindole 3.11: white amorphous solid; ^{1}H NMR (CD_3OD, 500 MHz) δ 7.94 (1H, s), 7.64 (1H, d, J = 7.7 Hz), 7.51 (1H, d, J = 8.1 Hz), 7.28 (1H, td, J = 7.1, 1.4 Hz), 7.24 (1H, td, J = 7.1, 1.1 Hz) ppm; ^{13}C NMR (CD_3OD, 125 MHz) δ 137.0, 134.5, 128.5, 124.7, 122.9, 119.6, 117.3, 113.6, 86.2 ppm; ESIMS m/z 143.2 $[M+H]^+$; ^{1}H and ^{13}C NMR data was consistent with literature reports.[124] (Notebook ID: RPN-1-89-1)

Reaction of compound 3.6 with MTPA-Cl. To a solution of 1.5 mg (8.0 μmol) of compound **3.6** in 0.5 mL dry CH_2Cl_2 in a reaction vial were added 50 μL (0.62 mmol) pyridine, and 20 μL (0.11 mmol) (*R*)-(-)-α-methoxy-α-(trifluoromethyl)phenylacetyl chloride. The reaction vial was capped and its contents were shaken and allowed to sit overnight. A 20 μL (0.16 mmol) aliquot of 3-(*N*,*N*-dimethylamino)-propylamine was added to the reaction vial and the mixture was allowed to sit for 10 min. Addition of 1 mL *tert*-butyl methyl ether and 1 mL water was followed by separation of the organic and aqueous layers. The aqueous layer was extracted again with 1 mL *tert*-butyl methyl ether and the combined organic layers were washed with 1 mL 1N HCl, 1 mL sat. $NaHCO_3$ and 1 mL brine, in succession. The resultant organic layer was dried over anhydrous $MgSO_4$ and the solvent removed *in vacuo* to afford the (*S*)-ester **3.12** (2.3 mg, 5.7 μmol, 71 % yield). The (*R*)-ester **3.13** (1.8 mg, 4.5 μmol, 56 % yield) was produced in a similar fashion using (*S*)-(+)-α-methoxy-α-(trifluoromethyl)phenylacetyl chloride instead of the (*R*)-derivatizing reagent. [Note the configuration changes because of CIP priority rules.]

Compound 3.12: white amorphous solid; ^{1}H NMR ($CDCl_3$, 500 MHz) δ 9.17 (N*H*, brs), 7.70-7.64 (3H, m), 7.48-7.39 (5H, m), 7.21 (1H, ddd, J = 8.0, 6.5, 1.5 Hz), 6.02 (1H, dd, J = 6.6, 2.8 Hz), 3.75 (1H, dd, J = 16.6, 6.6 Hz), 3.70 (3H, s), 2.98 (1H, dd, J = 16.6, 2.8 Hz) ppm; ESIMS m/z 426.2 $[M+Na]^+$ (Notebook ID: RPN-1-58-1)

Compound 3.13: white amorphous solid; ^{1}H NMR ($CDCl_3$, 500 MHz) δ 9.21 (N*H*, brs), 7.71-7.65 (3H, m), 7.48-7.41 (5H, m), 7.22 (1H, ddd, J = 8.0, 5.7, 2.3 Hz), 5.88 (1H, dd, J = 6.6, 3.0 Hz), 3.77 (1H, dd, J = 16.5, 6.7 Hz), 3.63 (3H, s), 3.17 (1H, dd, J = 16.5, 3.0 Hz) ppm; ESIMS m/z 426.2 $[M+Na]^+$ (Notebook ID: RPN-1-58-2)

Reduction of compounds 3.12 and 3.13. To 1 mg (2.5 μmol) of **3.12** in a reaction vial were added 1 mL CH_3CN and 1 mg (2.7 μmol) $CeCl_3.7H_2O$ and the mixture cooled in an ice bath. Three small portions of $NaBH_4$, 1 mg (26.4 μmol) in total, were added to the vial and the reaction mixture was stirred for 15 min at 0^{o}C. The vial was removed from the ice bath and the contents stirred for another 15 min before the reaction was quenched by addition of 2 drops of 1N HCl. After addition of 1 mL H_2O, two 1 mL portions of *tert*-butyl methyl ether were used to extract the organic product. The combined organic layers were washed with 1 mL sat. $NaHCO_3$ solution and 1 mL sat. NaCl solution, and dried over anhydrous Na_2SO_4. Solvent was removed *in vacuo* to afford compound **3.14**, which, by ^{1}H NMR analysis, appeared as a single diastereomer amidst other impurities. Following RP HPLC (Phenomenex Luna C_{18}, 150 x 4.6 mm, 5 μm particle size, 100 Å pore size; eluted with H_2O/CH_3CN at 0.7 mL/min using a linear gradient of 10%-100% CH_3CN over 8 min and at 100% CH_3CN for the next 7 min) of the mixture, the single diastereomer of **3.14** (t_R 11.8 min, 0.5 mg, 1.2 μmol, 50% yield) was isolated. Compound **3.13** was reduced and purified in a similar fashion to yield the single diastereomer of compound **3.15** (t_R 11.9 min, 0.4 mg, 1.0 μmol, 40% yield).

Compound 3.14: white amorphous solid; ^{1}H NMR ($CDCl_3$, 500 MHz) δ 8.12 (N*H*, brs), 7.59-7.55 (2H, m), 7.47 (1H, d, J = 7.7 Hz), 7.45-7.41 (3H, m), 7.37 (1H, d, J = 8.3 Hz), 7.21 (1H, ddd, J = 8.3, 7.1, 1.2 Hz), 7.12 (1H, ddd, J = 8.1, 7.1, 1.2 Hz), 5.65 (1H, ddd, J = 7.9, 4.8, 3.3 Hz), 5.40 (1H, m), 3.59 (3H, s), 3.57 (1H, ddd, J = 15.2, 7.8, 1.3 Hz), 3.16 (O*H*, brs), 2.89 (1H, dd, J = 15.2, 4.7 Hz) ppm; ESIMS m/z 428.2 $[M+Na]^+$ (Notebook ID: RPN-1-68-1)

Compound 3.15: white amorphous solid; ^{1}H NMR ($CDCl_3$, 500 MHz) δ 8.10 (N*H*, brs), 7.58-7.54 (2H, m), 7.47 (1H, d, J = 7.7 Hz), 7.45-7.41 (3H, m), 7.36 (1H, d, J = 8.2 Hz), 7.20 (1H, m), 7.12 (1H, m), 5.68 (1H, ddd, J = 7.7, 4.5, 3.1 Hz), 5.32 (1H, m), 3.59 (3H, s), 3.59 (1H, ddd, J = 15.1, 7.7, 1.3 Hz), 3.18 (O*H*, brs), 2.94 (1H, dd, J = 15.2, 4.6 Hz) ppm; ESIMS m/z 428.2 $[M+Na]^+$ (Notebook ID: RPN-1-69-2)

Preparation of agar plates for growth of fungal culture. A solution of Hutner's trace elements was prepared by mixing 80 mL of a solution containing 1.00 g iron(II) sulfate heptahydrate and 10.00 g EDTA with 80 mL of a solution containing 4.40 g zinc(II) sulfate heptahydrate, 2.20 g boric acid, 1.00 g manganese(II) chloride tetrahydrate, 0.32 g cobalt(II) chloride hexahydrate, 0.32 g copper(II) sulfate pentahydrate and 0.22 g ammonium molybdate tetrahydrate. The Hutner's solution was diluted to 200 mL and the final pH adjusted to 6.5 with the addition of aqueous solution of potassium hydroxide. In a 2L Erlenmeyer flask were added 6.00 g sodium nitrate, 0.52 g potassium chloride, 0.52 g magnesium sulfate heptahydrate, 1.52 g potassium phosphate (monobasic), 10.00 g dextrose, 15.00 g Difco agar and suspended in 1 L water. The mixture in the Erlenmeyer flask was treated in an autoclave following the addition of 1 mL solution of Hutner's trace elements. Upon completion of the autoclave procedure, 50 mg of chloramphenicol was added to the flask containing the agar medium. Immediately after dissolution of the antibiotic, media was poured on to 40 agar plates, which were allowed to cool

overnight in a laminar flow hood, sealed to prevent exposure to the atmosphere and stored at 2 – 8 ^{o}C until further use.

Isolation and growth of fungal culture. Cyanobacterial-fungal cell conjugates from an HCC1088 culture were streaked on an agar plate using an inoculating loop. The colonies were allowed to grow over 5 days, after which they were inoculated again on a new agar plate. After 4 days of growth on the new agar plate, the contents of the plate (agar medium and the fungal cell colonies) were transferred into a 4 L Erlenmeyer flask containing 2 L of minimal medium with 50 mg/L chloramphenicol. The minimal medium for fungal growth was prepared using the same ratios of agar medium nutrients (*vide supra*) except for Difco agar. The fungal culture was allowed to grow for 1 month, after which it was harvested for extraction.

Extraction of fungal metabolites. The biomass was filtered and extracted three times with 350 mL ethyl acetate each. Removal of solvent *in vacuo* afforded 735 mg of the cell extract. The culture broth filtrate was also extracted three times with 400 mL ethyl acetate each, and the removal of solvent yielded 215 mg of the media extract.

7.4 Extraction and Purification of Metabolites from *Areca catechu*

Biological material. Young *Areca catechu* nuts and *Piper betle* leaves were obtained from a local convenience store in Honolulu. The areca nuts were cut into halves, scooped out of the husks, and freeze-dried for storage. Other variants of the nuts were obtained as ground dried powder from Guam.

Cell cultures. Jurkat, U937 and HL-60 cell lines were maintained in RPMI 1640 medium (Clontech) supplemented with 10% fetal bovine serum (FBS). RBL-2H3 cells (WT and

M1) were cultured in DMEM medium (Clontech) with 10% fetal bovine serum (FBS). All cells were cultured at 37 °C, 5% CO_2, and 95% humidity.

Fura-2AM based calcium bioassay. The effect of various extracts and chemicals was assessed using a high-throughput kinetic plate reader instrument (Hamamatsu FDSS-7000EX). Cells that grow in suspension (Jurkat, U937 and HL-60) were incubated with the loading medium for one hour then plated in 96-well plates at a density of 100,000 cells/well before measurement. Adherent cells RBL-2H3 (WT and M1) were pre-plated overnight at a density of 60,000 cells/well, and then loaded in the same way. The loading medium is composed of the culture medium supplemented with 2 mM Probenecid, 0.1 % Pluronic and 2 μM Fura-2-AM. Bath solutions contained in mM: 140 NaCl, 0 or 2 $CaCl_2$, 2 $MgCl_2$, 10 glucose, and 10 Hepes (pH 7.2 with NaOH). Stock solutions of extracts and all the tested chemicals were prepared in DMSO. DMSO control was then included in all experiments to monitor the solvent effect.

Preliminary extractions. Chopped young, wet *Areca catechu* nuts (~ 10 g each) were extracted three times (25 mL each) in acetone, dichloromethane, methanol, ethanol and a mixture of chloroform, methanol and water (12:5:3). Solvent was removed *in vacuo*, affording 1.623 g, 0.132 g, 1.560 g, 1.719 g and 1.656 g of crude extract, respectively. The crude extracts were dissolved in 6 mL of aqueous methanol (1:1) and partitioned three times (6 mL each) with chloroform. Upon removal of solvent, aqueous and chloroform fractions of each crude extract were obtained. Based on Ca-mobilizing activity data of crude extracts and their fractions in three different cell lines (Jurkat, U937 and RBL-2H3), acetone was chosen as the optimal solvent for further extractions.

Areca nut husks (~ 20 g) and *Piper betle* leaves (~ 4 g) were also extracted three times (25 mL each) in a mixture of chloroform, methanol and water (12:5:3). Solvent was removed from the combined extracts to afford 0.276 g and 0.352 g of crude husk extract and crude leaf extract, respectively.

Variable pH extractions. Aqueous solutions of pH 4.0, 7.0 and 10.0 were prepared using hydrochloric acid and sodium carbonate. In three separate flasks, 3.0 g each of lyophilized Areca nuts were mixed with 20 mL solutions at the three pH levels. The flasks were stirred overnight using a mechanical shaker. To each flask, 60 mL ethanol was added and sonicated for 30 min. The extract was filtered and the nut residue was extracted two additional times using the same protocol. The combined extract was evaporated to a third of the volume using a rotary evaporator, and then partitioned four times between chloroform and water. Solvent was removed from each fraction to obtain lipophilic and hydrophilic extracts.

Extraction and fractionation of *Areca catechu* nuts. Lyophilized *Areca catechu* nuts (21.0 g) were extracted in acetone three times (400 mL each) and solvent was removed from the combined extract *in vacuo*, affording 3.051 g of crude extract. The crude extract was dissolved in water (50 mL), partitioned three times (50 mL each) with chloroform, and the solvent evaporated, affording 2.445 g of aqueous extract and 0.459 g of chloroform extract. A portion of the aqueous extract (0.700 g) was dissolved in 2.5 mL of a mixture of acetonitrile and water (15:85), filtered using a Whatman syringe filter (0.45 micron), and fractionated using RP HPLC (Phenomenex Gemini C_{18}, 250 x 21.2 mm, 5 μm particle size, 110 Å; eluted with water and acetonitrile (each with 0.1% formic acid) at 12.4 mL/min using the following gradient: 15% CH_3CN (0-10 min), 15-20% CH_3CN (10-15 min), 20% CH_3CN (15-25 min), 20-30% CH_3CN (25-30 min), 30% CH_3CN (30-40 min), 30-50% CH_3CN (40-45 min), 50% CH_3CN (45-50 min),

50-100% CH_3CN (50-55 min) and washed with 100% CH_3CN for additional 15 min.) The first 40 fractions were collected at 1.5 min intervals and solvent was removed using a centrifugal concentrator. Fraction 11 contained catechin (**4.5**, t_R 16 min, 110 mg, 1.8% yield, > 90% purity by ^1H NMR).

Catechin 4.5: white powder; ^1H NMR (CD_3OD, 500 MHz) δ 6.83 (1H, d, J = 1.9 Hz), 6.76 (1H, d, J = 8.2 Hz), 6.71 (1H, dd, J = 8.2, 2.0 Hz), 5.92 (1H, d, J = 2.3 Hz), 5.85 (1H, d, J = 2.3 Hz), 4.56 (1H, d, J = 7.5 Hz), 3.97 (1H, td, J = 7.9, 5.4 Hz), 2.84 (1H, dd, J = 16.2, 5.5 Hz), 2.50 (1H, dd, J = 16.1, 8.2 Hz) ppm; HRESIMS m/z 291.0864 $[M+H]^+$ (calcd for $C_{15}H_{15}O_6$, 291.0869). (Notebook ID: RPN-3-107-6, RPN-3-113-11 and RPN-3-140-11)

Dialysis of extracts and fractions. Samples were dissolved in water and loaded onto cellulose dialysis tubing, manufactured by either Fisherbrand (19 mm x 12.1 mm; nominal molecular weight cutoff 3.5 kDa) or Sigma Aldrich (43 mm x 27 mm; molecular weight cutoff 10.4 kDa). The dialysis tubing loaded with sample was placed in a chamber filled with distilled water, and stirred on a shaker. Water was replaced in the outer chamber every 12 h for a total of four times and the solvents were removed from the solutions in the dialysis tubing and the outer chamber to afford fractions of higher and lower molecular weights.

MALDI-MS analysis of dialyzed aqueous extract. A 1.0 mg sample of dialyzed aqueous extract (RPN-3-145-2) was dissolved in 1 mL 50:50 LCMS grade MeCN:H_2O. A 10 µL aliquot of the solution was mixed with 10 µL aliquot of 50:50 LCMS grade containing 0.1% trifluoroacetic acid. A 1 µL aliquot of this solution was spotted on the MALDI plate, followed by 1 µL of matrix solution (α-cyano-4-hydroxycinnamic acid or 2,5-dihydroxybenzoic acid). MALDI-MS was performed on the Bruker Ultra Flex III using Flex Control v. 3.4.

Hydrolysis of dialyzed aqueous extract. A 36 mg sample of a dialyzed aqueous extract (RPN-3-144-2) in a capped reaction vial was treated with 3 mL of 2*N* NaOH at 60 ^{o}C for 15 min. After cooling the mixture in an ice bath, the pH was adjusted to 6.5 using 4*N* HCl. The resulting solution was extracted with 10 mL hexanes to remove any lipids and the hexanes layer was discarded. Subsequent extractions with 10 mL ethyl acetate were performed twice and the solvent removed *in vacuo* to afford 4.5 mg residue. The aqueous layer was dried down to produce 503 mg of residue, which included salts produced from the basic hydrolysis and subsequent neutralization with acid.

Methylation of dialyzed aqueous extract. This reaction was carried out using dry solvents and reagents in a nitrogen atmosphere using balloons. A 5 mg sample of the dialyzed aqueous extract (RPN-3-145-2) was dissolved in 3 mL methanol. A 2 mL solution containing 500 μL trimethylsilyldiazomethane (2.0 M in hexanes) in toluene was prepared and half the solution was added to the methanolic solution of the dialyzed Areca extract. The mixture was stirred at room temperature for 5 h, upon which the remainder of the trimethylsilyldiazomethane solution was added. The reaction continued for 24 h with stirring. Solvents were removed *in vacuo* to afford 6 mg of crude product. ^{1}H NMR analysis of the crude product showed a complex mixture of components. While new singlets in the 3-4 ppm region of the ^{1}H NMR spectrum were visible, it was extremely difficult to estimate the degree of methylation.

Size exclusion chromatography of dialyzed aqueous extract. A 10 mg/mL solution of the dialyzed aqueous extract (RPN-3-145-2) was prepared in water and subjected to size exclusion chromatography on a Superose 12 10/300 GL column (GE HealthCare Life Sciences; 10 x 300 mm, 11 μm median particle size) with a mobile phase consisting of 0.05 M phosphate and 0.15 M NaCl at pH 7.2. The flow rate was 1.0 mL/min and a photodiode array detector was

used to monitor the progress of the chromatographic separation. A calibration curve was prepared from a standard mixture consisting of blue dextran (t_R 8.3 min), bovine serum albumen (t_R 13.4 min), carbonic anhydrase (t_R 15.1 min), RNase A (t_R 16.2 min), aprotinin (t_R 17.4 min) and methyl cobalamin (t_R 19.1 min).

Attempts to polymerize catechin. In separate vials, 25 mg of catechin was dissolved in 10 mL of three different solvents – 15% CH_3CN in H_2O, 15% CH_3CN in H_2O with 0.1% formic acid, and 30% CH_3CN in H_2O with 0.1% formic acid. The solutions were left to sit and from each vial, 2 mL aliquots were removed at four different time points (1 d, 2 d, 5 d, 10 d), solvent removed *in vacuo* and the residue analyzed by ^1H NMR spectroscopy for any signs of polymerization.

HPLC purification of dialyzed aqueous extract. A 2 mg portion of the dialyzed aqueous extract (RPN-3-145-2) was dissolved in 1 mL of a mixture of acetonitrile and water (15:85), filtered using a Whatman syringe filter (0.45 micron), and purified using HPLC (Phenomenex silica, 250 x 10 mm, 10 μm particle size, 100 Å; eluted with mixed solvent systems A (82% dichloromethane/14% methanol/2% acetic acid/2% water) and B (96% methanol/2% acetic acid/2% water) at 4 mL/min using the following gradient: 0.0-11.7% B (0-20 min), 11.7-25.6% B (20-50 min), 25.6-87.8% B (50-55 min), 87.8% B (55-65 min), 87.8-0.0% B (65-70 min); UV detection at 280 nm). These conditions replicated those described in the literature for purification of proanthocyanidin oligomers and polymers.[180] Fraction at retention time 54-56 min was collected and solvent removed *in vacuo* to afford 0.7 mg of the presumed polymeric (n > 10) proanthocyanidin sample.

7.5 Extraction and Isolation of Metabolites from Other Organisms

Isolation of Callyspongynic Acid from the Sponge 12-Maui-38

Extraction and fractionation of 12-Maui-38. A 1 g sample of freeze-dried biomass of the sponge 12-Maui-38 was cut into small pieces and extracted overnight three times with 1:1 CH_3OH:CH_2Cl_2 (15 mL each). The combined extract solutions were evaporated to afford 69.5 mg of the crude extract. The crude extract was partitioned using a solid phase extraction procedure resulting in the isolation of 3.7 mg of the 75% methanol fraction.

HPLC purification of callyspongynic acid. The 75% methanol fraction was separated by RP HPLC (Phenomenex Luna C8(2), 250 x 10 mm, 5 μm particle size, 100 Å; eluted with water and acetonitrile (each with 0.1% formic acid) at 2.75 mL/min using the following gradient: 50-80% CH_3CN (0-15 min), 80-100% CH_3CN (15-30 min), 100% CH_3CN (30-40 min); photodiode array detection) to afford callyspongynic acid (**5.1**, t_R 24.0 min, 1.2 mg, 0.12% yield, > 95% purity by ^{1}H NMR).

Callyspongynic acid 5.1: white amorphous solid; $[\alpha]_D^{21}$ -1.4 (*c* 0.5, EtOH); ^{1}H NMR ($CDCl_3$, 500 MHz) δ 5.91 (1H, dtd, *J* = 15.3, 6.6, 1.2 Hz), 5.61 (1H, ddt, *J* = 15.3, 6.2, 1.5 Hz), 4.85 (1H, d, *J* = 5.7 Hz), 2.58 (1H, d, *J* = 2.0 Hz), 2.36 (4H, m), 2.25 (8H, m), 2.16 (2H, m), 2.08 (2H, m), 1.69 (2H, p, *J* = 7.0 Hz), 1.64 (2H, p, *J* = 7.0 Hz), 1.61 (2H, m), 1.50 (6H, m), 1.41 (4H, m) ppm; ^{13}C NMR ($CDCl_3$, 125 MHz) δ 156.2, 134.3, 128.5, 91.7, 83.1, 80.3, 80.3, 79.6, 79.3, 77.5, 76.6, 74.1, 72.7, 65.7, 65.3, 62.8, 31.7, 28.5, 28.4, 28.2, 28.2, 28.0, 28.0, 27.8, 27.0, 19.1, 18.7, 18.5, 18.3, 17.9, 17.9, 17.9 ppm; HRESIMS *m*/*z* 469.2734 $[M–H]^–$ (calcd for $C_{32}H_{37}O_3$, 469.2748). Spectroscopic data were generally consistent with literature values.[181] (Notebook ID: RPN-1-97-1)

Isolation of β-Sitosterol from the Sponge 13-Maui-52

Extraction and fractionation of 13-Maui-52. A 79 g sample of freeze-dried biomass of the sponge 13-Maui-52 was broken into small pieces and extracted overnight three times with 1:1 CH_3OH:CH_2Cl_2 (700 mL each). The combined extract solutions were evaporated to afford 6.710 g of the crude extract. An 890 mg portion of the crude extract was partitioned using a solid phase extraction procedure resulting in the isolation of 104.7 mg of the 100% methanol fraction.

HPLC purification of *β*-sitosterol. The 100% methanol fraction was separated by HPLC (Phenomenex Luna Silica, 250 x 10 mm, 10 μm particle size, 100 Å; eluted with ethyl acetate and hexanes at 3.0 mL/min using the following gradient: 15% ethyl acetate (0-10 min), 15-40% ethyl acetate (10-25 min), 40-100% ethyl acetate (25-30 min), 100% ethyl acetate (30-40 min); UV detection at 280 nm) to afford *β*-sitosterol (**4.18**, t_R 22.3 min, 3.6 mg, 0.03% yield, > 95% purity by ^{1}H NMR).

***β*-Sitosterol 4.18**: white amorphous powder; ^{1}H NMR ($CDCl_3$, 500 MHz) δ 5.35 (1H, m), 3.52 (1H, tt, J = 6.3, 4.8 Hz), 2.31-2.21 (2H, m), 1.99 (2H, m), 1.83 (4H, m), 1.68 (2H, m), 1.60-1.42 (8H, m), 1.38-1.23 (6H, m,), 1.18-0.97 (5H, m), 1.00 (3H, s), 0.92 (3H, d, J = 6.6 Hz), 0.85 (3H, t, J = 7.4 Hz), 0.83 (3H, d, J = 7.1 Hz), 0.80 (3H, d, J = 6.9 Hz), 0.67 (3H, s) ppm; ^{13}C NMR ($CDCl_3$, 125 MHz) δ 140.7, 121.7, 71.8, 56.7, 56.0, 50.1, 46.0, 42.3, 42.3, 39.7, 37.2, 36.5, 36.2, 33.9, 31.9, 31.9, 31.6, 28.9, 28.2, 26.3, 24.3, 23.0, 21.1, 19.6, 19.4, 18.9, 18.8, 12.3, 11.8 ppm; HRESIMS *m*/*z* 415.3949 $[M+H]^+$ (calcd for $C_{29}H_{51}O$, 415.3934). Spectroscopic data were consistent with literature reports.[193] (Notebook ID: RPN-3-43-3)

Isolation of Psammaplysin A from the Sponge 14-Maui-05

Extraction and fractionation of 14-Maui-05. A 40 g sample of freeze-dried biomass of the sponge 14-Maui-05 was broken into small pieces and extracted overnight three times with 4:1 CH_3OH:CH_2Cl_2 (300 mL each). The combined extract solutions were evaporated to afford 5.950 g of the crude extract. A liquid-liquid partitioning between hexanes, dichloromethane and aqueous methanol afforded 1.784 g of the dichloromethane fraction. A 325 mg portion of the dichloromethane fraction was further partitioned using a solid phase extraction procedure resulting in the isolation of 57.5 mg of the 75% methanol fraction.

HPLC purification of psammaplysin A. The 75% methanol fraction was separated by RP HPLC (Phenomenex Luna C18, 250 x 10 mm, 5 μm particle size, 100 Å; eluted with acetonitrile and water (each with 0.1% formic acid) at 2.8 mL/min using the following gradient: 10-100% CH_3CN (0-15 min), 100% CH_3CN (15-30 min), 100-10% CH_3CN (30-35 min), 10% CH_3CN (35-45 min); detection using a photodiode array detector) to afford psammaplysin A (**5.2**, t_R 11.7 min, 2.7 mg, 0.04% yield, > 95% purity by ^{1}H NMR).

Psammaplysin A 5.2: white crystalline solid; ^{1}H NMR (CD_3OD, 500 MHz) δ 7.53 (2H, s), 7.13 (1H, s), 4.98 (1H, s), 4.07 (2H, t, J = 5.9 Hz), 3.63 (3H, s), 3.61 (2H, t, J = 7.0 Hz), 3.38 (1H, d, J = 16.1 Hz), 3.14 (2H, t, J = 7.3 Hz), 3.05 (1H, d, J = 15.9 Hz), 2.89 (2H, t, J = 7.5 Hz), 2.13 (2H, p, J = 6.2 Hz) ppm; ^{13}C NMR (CD_3OD, 125 MHz) δ 160.6, 158.7, 153.5, 149.8, 146.7, 137.2, 134.3, 120.8, 119.5, 104.5, 104.3, 80.4, 72.1, 59.3, 41.4, 38.2, 37.9, 33.3, 30.5 ppm; ESIMS m/z 729.9 $[M+H]^+$ (calcd for $C_{21}H_{24}Br_4N_3O_6$, 729.8). Spectroscopic data were consistent with literature reports.[182] (Notebook ID: RPN-3-53-2)

Isolation of Fischerellins and Loliolide from the Cyanobacterium CN-16-1

Biological Material. CN-16-1 (*Hapalosiphon* sp.), originally collected from the Western Caroline Islands in Palau, was obtained from the cyanobacterial collection housed at the University of Hawaii at Manoa. The strain was cultured in twelve 20 L carboys containing BG-11 media with MOPS buffer, under continuous illumination and aeration for 4 weeks. Cells were filtered and lyophilized to obtain 18.60 g of dry biomass.

Extraction and fractionation of CN-16-1. The entire freeze-dried biomass (18.60 g) was extracted overnight three times with 1:1 CH_3OH:CH_2Cl_2 (400 mL each). The combined extract solutions were evaporated to afford 3.22 g of the crude extract. Modified Kupchan partitioning afforded 0.990 g of the hexanes fraction and 0.583 g of the dichloromethane fraction. A 207 mg portion of the hexanes fraction was further partitioned using a solid phase extraction procedure resulting in the isolation of 86.4 mg of the 100% methanol fraction. Likewise, solid phase extraction of a 294 mg portion of the dichloromethane resulted in isolation of 21.0 mg of the 25% methanol fraction and 7.0 mg of the 50% methanol fraction.

HPLC purification of fischerellin A and fischerellin B. A 16 mg aliquot of the 100% methanol fraction obtained from partitioning of the hexanes fraction was separated by RP HPLC (Phenomenex Luna C18, 150 x 4.6 mm, 5 μm particle size, 100 Å; eluted with methanol and water at 0.5 mL/min using the following gradient: 85% CH_3OH (0-15 min), 85-100% CH_3OH (15-35 min), 100% CH_3OH (35-45 min); detection using a photodiode array detector) to afford fischerellin B (**5.4**, t_R 24.6 min, 0.1 mg, 0.003% yield) and fischerellin A (**5.3**, t_R 27.3 min, 0.4 mg, 0.01% yield). Both fischerellin A and fischerellin B contained unidentified impurities (% purity undetermined).

Fischerellin A 5.3: amorphous white solid; mixture of conformers; ^{1}H NMR ($CDCl_3$, 500 MHz) δ 9.94/9.67 (1H, brs/brs), 6.24 (1H, m), 5.49 (1H, d, J = 15.3 Hz), 3.90-3.80 (1H, m), 3.71-3.52 (2H, m), 2.92/2.91 (3H, s), 2.52-2.43 (1H, m), 2.30 (2H, t, J = 7.0 Hz), 2.13 (2H, m), 1.63-1.51 (4H, m), 1.48-1.44 (2H, m), 1.46 (3H, d, J = 7.3 Hz), 1.40 (3H, d, J = 7.2 Hz), 1.38-1.30 (4H, m), 1.33/1.30 (3H, d/d, J = 6.9 Hz/7.0 Hz), 0.89 (3H, t, J = 7.3 Hz) ppm; HRESIMS m/z 409.2866 $[M+H]^+$ (calcd for $C_{26}H_{37}N_2O_2$, 409.2850). ^{1}H NMR data were consistent with literature reports.[183] (Notebook ID: RPN-2-24-3)

Fischerellin B 5.4: amorphous white solid; ^{1}H NMR ($CDCl_3$, 500 MHz) δ 6.23 (1H, dt, J = 15.7, 7.2 Hz), 5.49 (1H, brd, J = 15.1 Hz), 2.76 (1H, m), 1.20 (3H, d, J = 6.7 Hz), 0.90 (3H, t, J = 7.3 Hz) ppm (other signals were obscured by impurities); HRESIMS m/z 300.2318 $[M+H]^+$ (calcd for $C_{20}H_{30}NO$, 300.2322). (Notebook ID: RPN-2-24-2)

HPLC purification of loliolide. The 25% and 50% methanol fractions obtained from the dichloromethane fraction were combined and separated by RP HPLC (Phenomenex Luna C18, 250 x 10 mm, 5 μm particle size, 100 Å; eluted with methanol and water at 2.75 mL/min using the following gradient: 30% CH_3OH (0-5 min), 30-40% CH_3OH (5-15 min), 40% CH_3OH (15-20 min), 40-50% CH_3OH (20-25 min), 50-75% CH_3OH (25-30 min), 75% CH_3OH (30-35 min), 75-100% CH_3OH (35-40 min), 100% CH_3OH (40-55 min); detection using a photodiode array detector) to afford loliolide (**5.5**, t_R 27.2 min, 1.0 mg, 0.01% yield) with other unidentified impurities (% purity undetermined).

Loliolide 5.5: colorless oil; ^{1}H NMR (CD_3OD, 500 MHz) δ 5.74 (1H, s), 4.21 (1H, p, J = 3.4 Hz), 3.52 (1H, s), 2.41 (1H, ddd, J = 13.5, 2.7, 2.6 Hz), 1.98 (1H, ddd, J = 14.4, 2.8, 2.4 Hz), 1.75 (3H, s), 1.73 (1H, dd, J = 14.4, 3.9 Hz), 1.52 (1H, dd, J = 14.5, 3.6 Hz), 1.45 (3H, s), 1.26 (3H, s) ppm; ^{13}C NMR (CD_3OD, 125 MHz) δ 185.7, 113.3, 89.0, 67.2, 47.9, 46.4, 37.1,

31.0, 27.4, 26.9 ppm; HRESIMS *m/z* 219.0981 $[M+Na]^+$ (calcd for $C_{11}H_{16}NaO_3$, 219.0992). Spectroscopic data were consistent with literature reports.[194] (Notebook ID: RPN-2-35-2)

Extraction Isolation of Metabolites from the Fungal Culture

Preparation of agar plates for growth of fungal culture. (See section 7.3)

Isolation and growth of fungal culture. (See section 7.3)

Extraction of fungal metabolites. (See section 7.3)

HPLC separation of fungal cell extract. A 75 mg/mL solution of fungal cell extract was prepared in ethyl acetate and subjected to RP HPLC (Phenomenex Luna C_{18}, 250 x 10 mm, 5 μm particle size, 100 Å; eluted with H_2O/CH_3CN containing 0.1% formic acid at 2.75 mL/min using the following gradient: 10-100% CH_3CN over 18 min, and washed at 100% CH_3CN for 12 min), affording several fractions that were collected based on signals detected by a photodiode array detector. Among these, the fraction eluting at 20.1 min afforded 1.3 mg of compound **5.6** (~90% purity by ^1H NMR) from injections totaling 1600 μL. Yield (1.1% of the crude extract) from the biological material was undetermined because the wet biomass was not weighed.

Compound 5.6: amorphous white solid; mixture of conformers; ^1H NMR ($CDCl_3$, 500 MHz) δ 6.95/6.53 (1H, dt/dt, J = 4.4, 2.3 Hz/4.4, 2.3 Hz), 5.43-5.33 (2H, m), 5.29 (1H, m), 3.90-3.82 (2H, m), 3.57/3.47 (1H, q/q, J = 7.0 Hz/7.0 Hz), 2.77/2.64 (2H, ddt/ddt, J = 9.3, 8.0, 2.4 Hz/10.3, 7.6, 2.4 Hz), 2.58-2.32 (2H, 4 sets of overlapping dt, J = 17.5, 7.4 Hz), 1.95 (2H, m), 1.63/1.62 (3H, brs/brs), 1.58-1.51 (2H, m), 1.39/1.38 (3H, d/d, J = 7.0 Hz/7.1 Hz), 1.35-1.26 (2H, m) ppm; ^{13}C NMR ($CDCl_3$, 125 MHz) δ 207.1, 165.6, 130.9, 129.3/128.3, 125.1, 113.1/111.7, 53.3/53.2, 45.9/45.5, 39.2/39.2, 33.4/32.3, 29.7/28.9, 28.9/28.1, 23.0, 17.9, 13.4/13.1 ppm; HRESIMS *m/z* 250.1796 $[M+H]^+$ (calcd for $C_{15}H_{24}NO_2$, 250.1802). Spectroscopic data were consistent with literature reports.[187a] (Notebook ID: RPN-4-9-7)

APPENDICES

Appendix 1. ^{1}H NMR spectrum of ilimaquinone **2.3** in $CDCl_3$ (500 MHz)

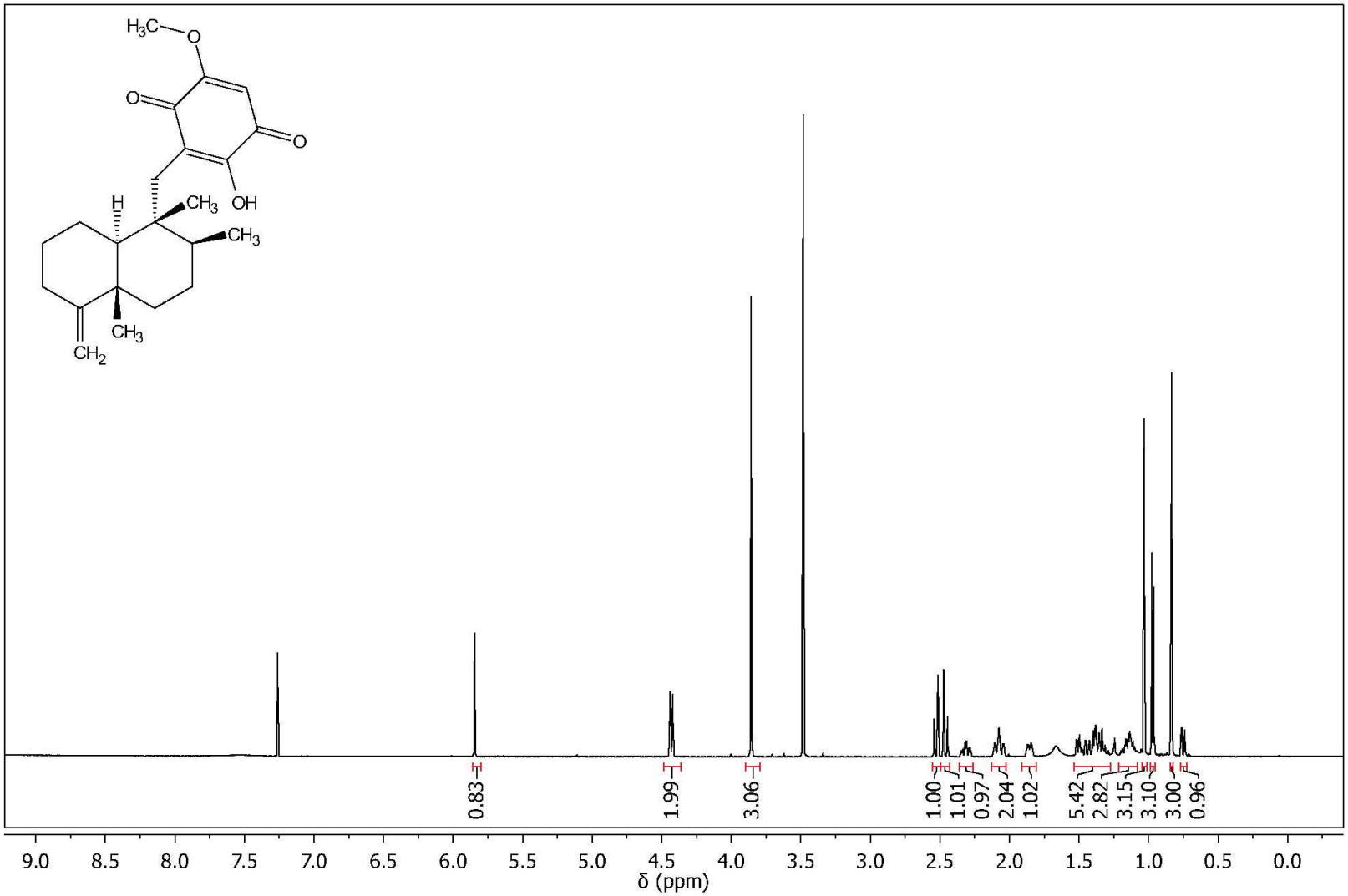

Appendix 2. ^{13}C NMR spectrum of ilimaquinone **2.3** in $CDCl_3$ (125 MHz)

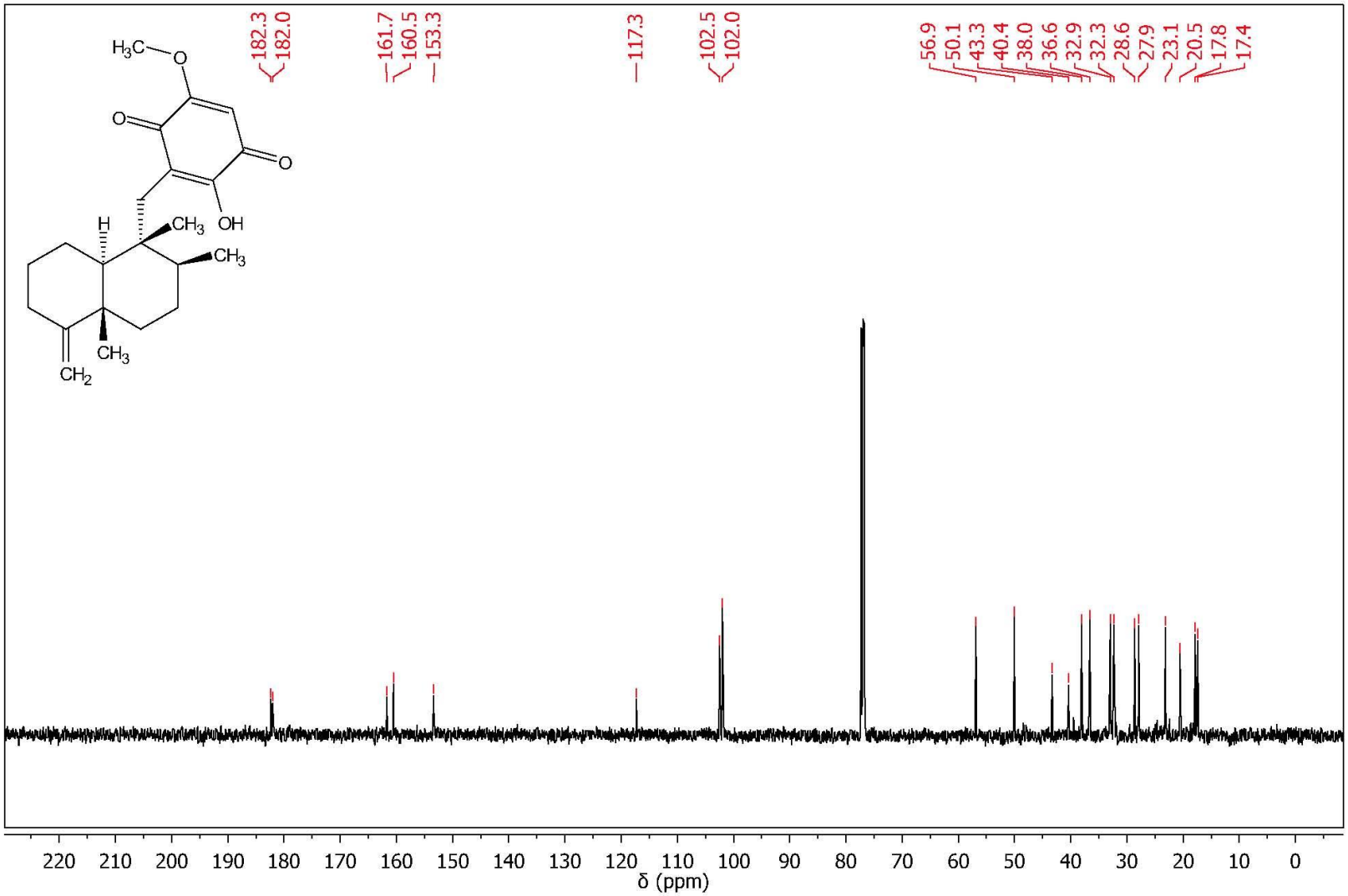

Appendix 3. ^{1}H NMR spectrum of 5-*epi*-ilimaquinone **2.4** in $CDCl_3$ (500 MHz)

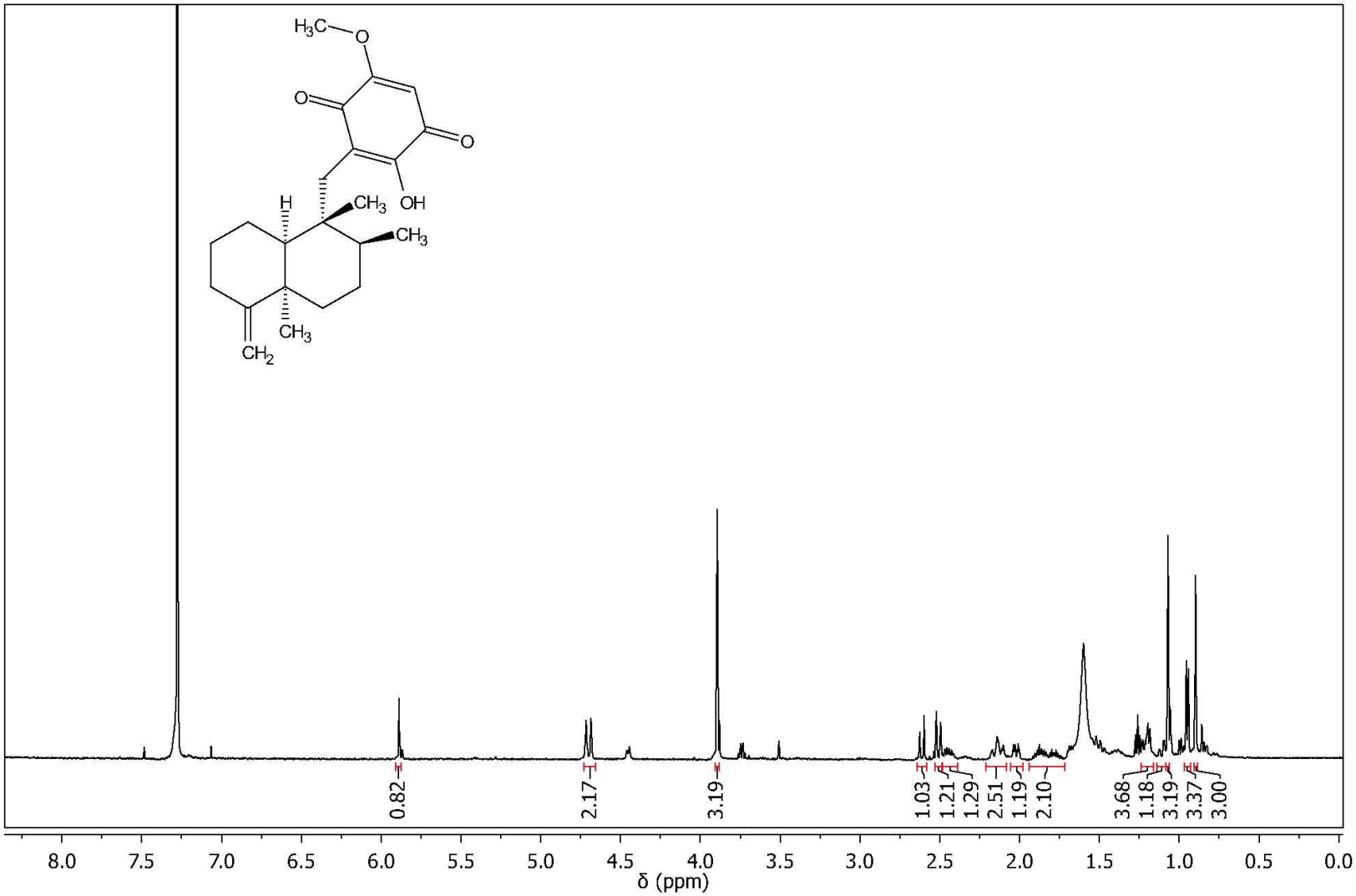

Appendix 4. ^{1}H NMR spectrum of smenospongine **2.5** in $CDCl_3$ (500 MHz)

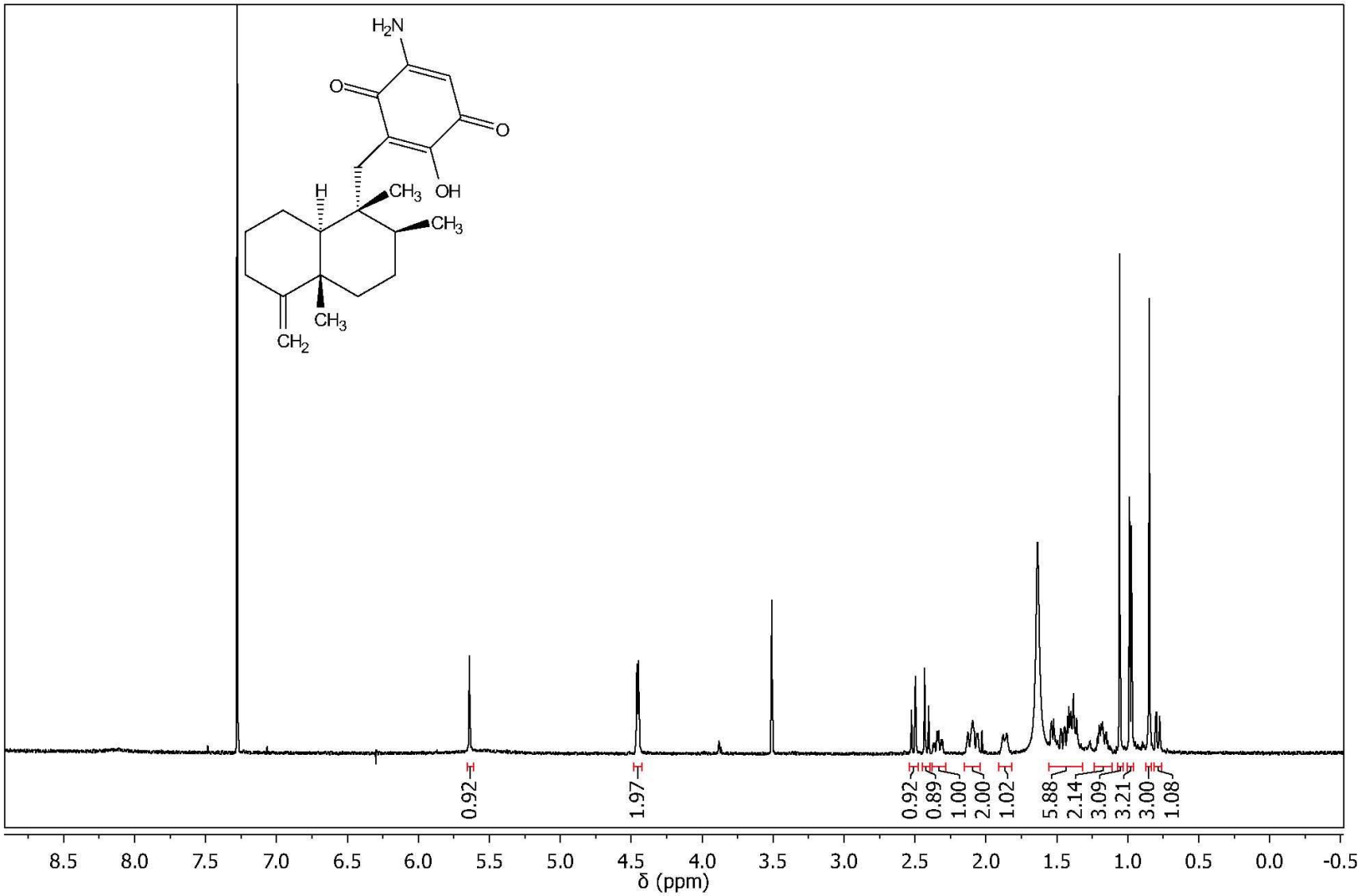

Appendix 5. ^{1}H NMR spectrum of smenospongorine **2.6** in $CDCl_3$ (500 MHz)

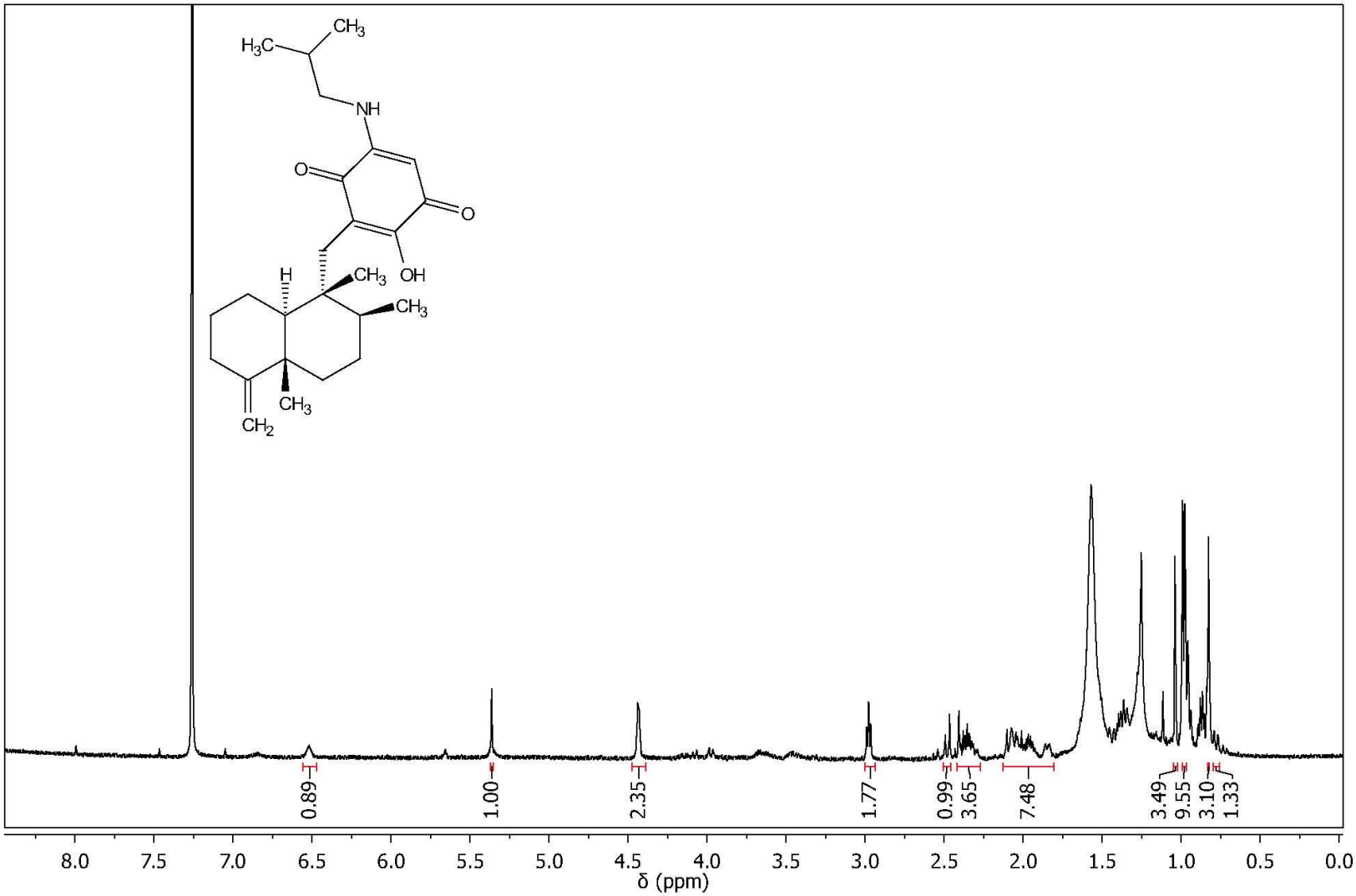

Appendix 6. ^{13}C NMR spectrum of smenospongorine **2.6** in $CDCl_3$ (125 MHz)

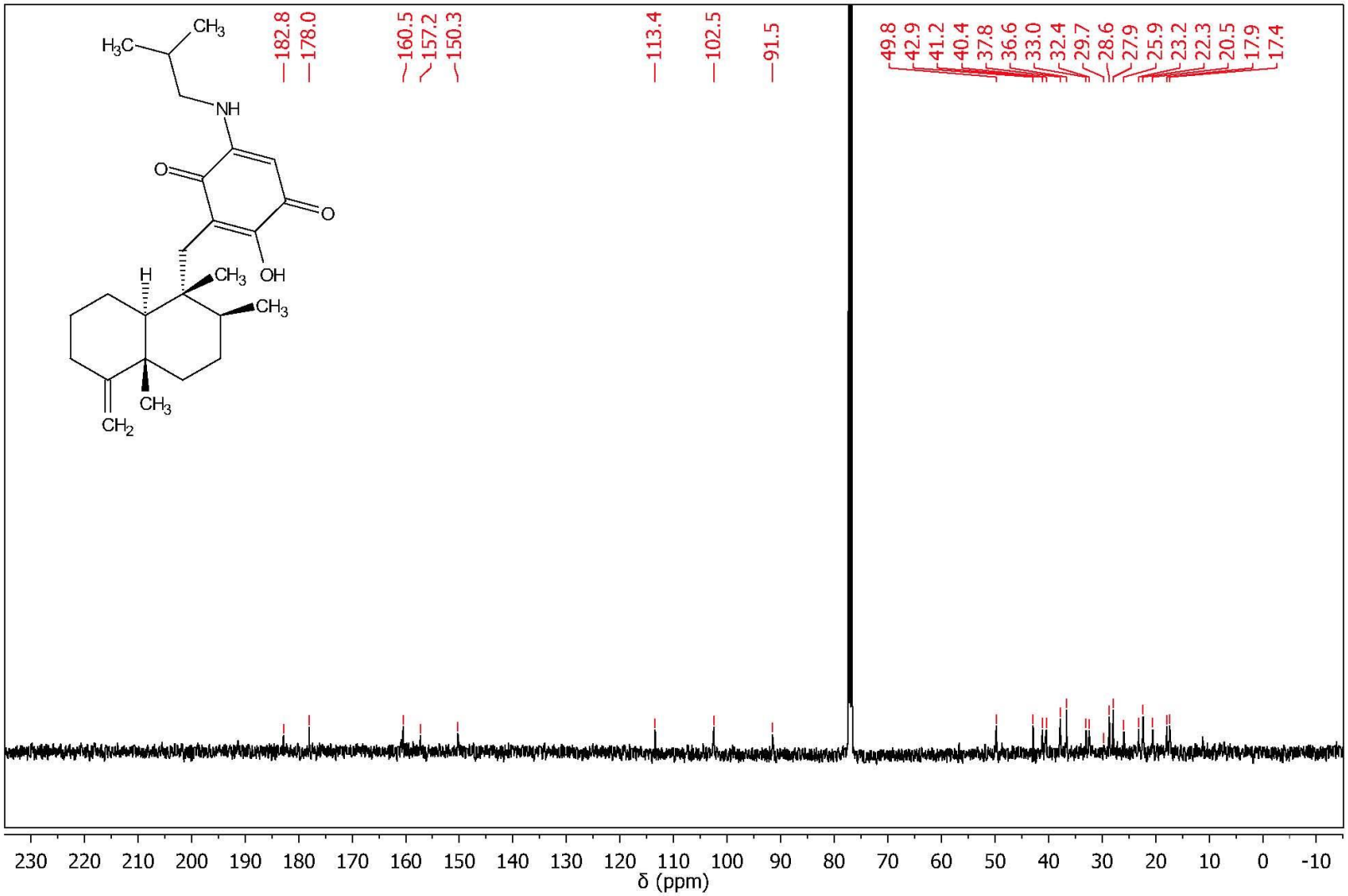

Appendix 7. ^{1}H NMR spectrum of smenospongiarine **2.7** in $CDCl_3$ (500 MHz)

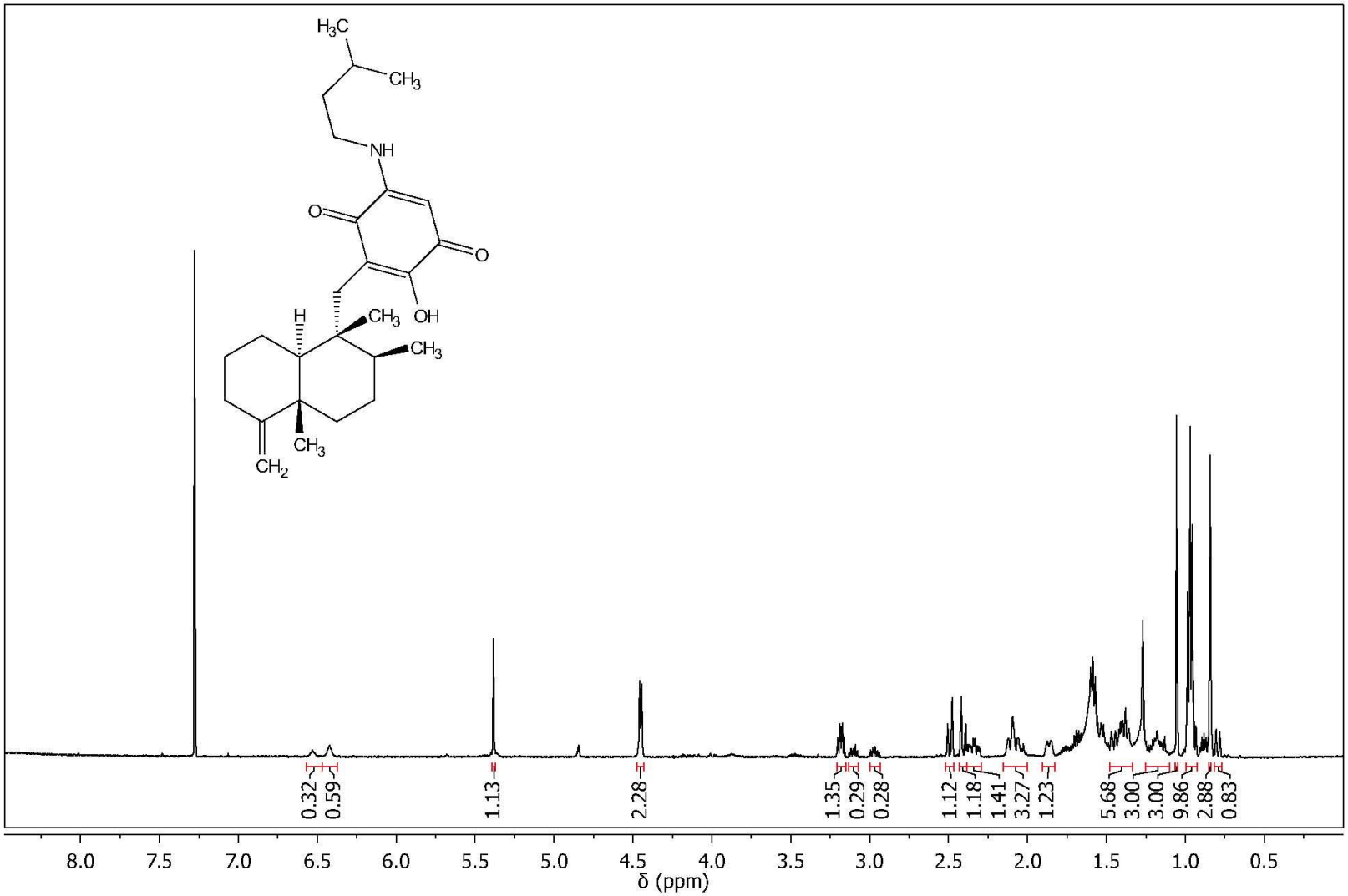

Appendix 8. ^{13}C NMR spectrum of smenospongiarine **2.7** in $CDCl_3$ (125 MHz)

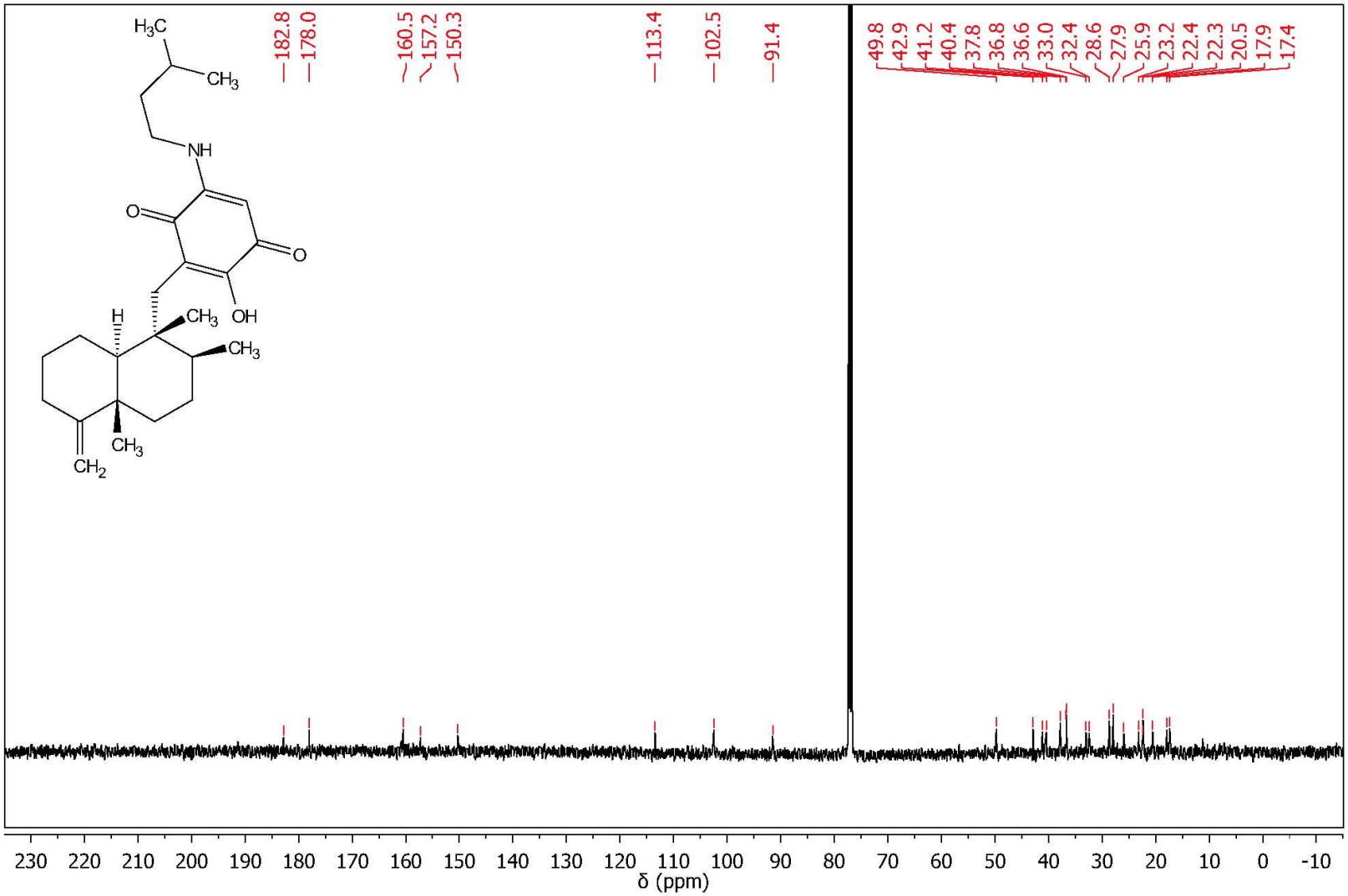

Appendix 9. ^{1}H NMR spectrum of smenospongidine **2.8** in $CDCl_3$ (500 MHz)

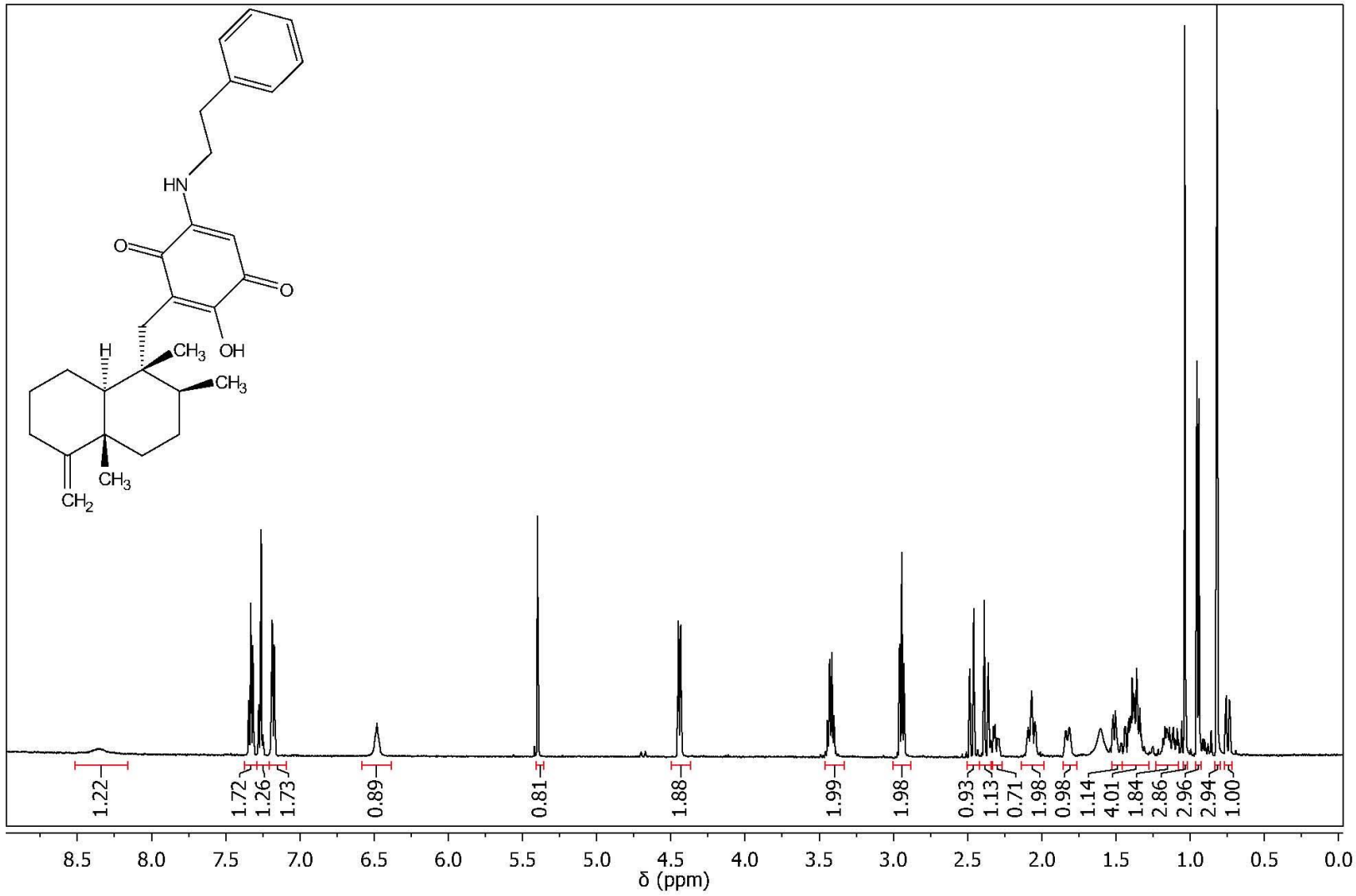

Appendix 10. ^{13}C NMR spectrum of smenospongidine **2.8** in $CDCl_3$ (125 MHz)

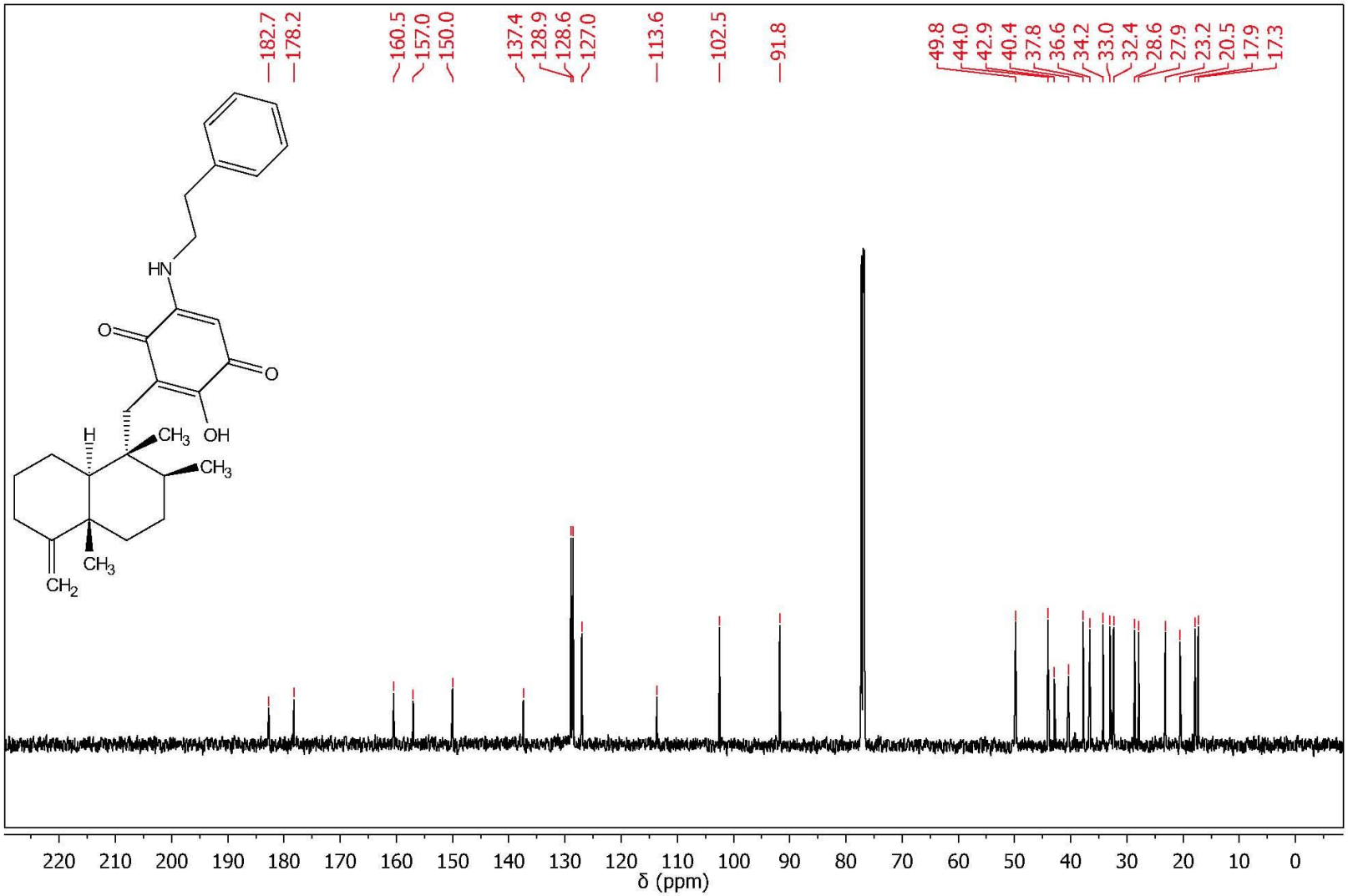

Appendix 11. ^{1}H NMR spectrum of dictyoceratin A **2.9** in $CDCl_3$ (500 MHz)

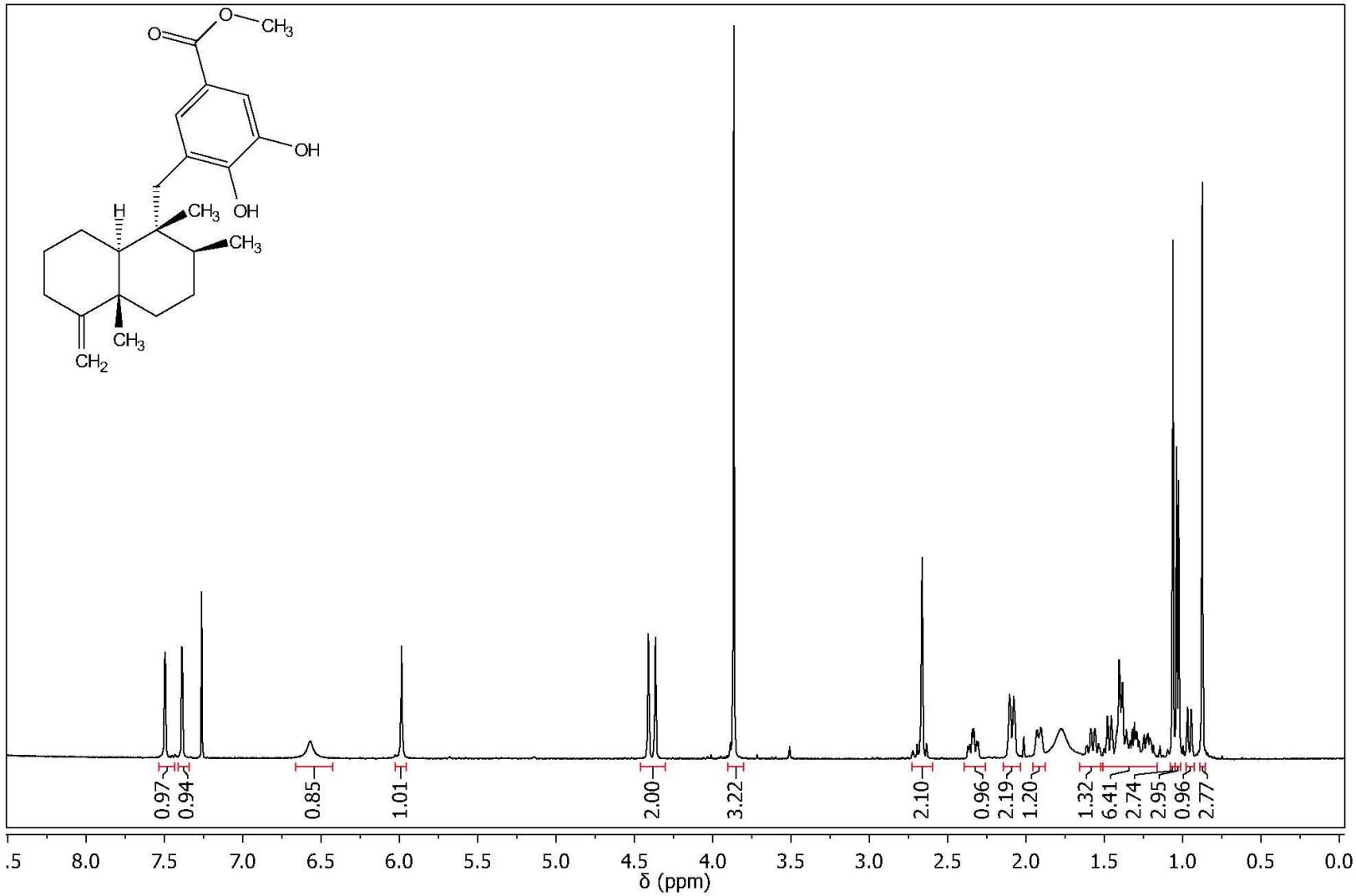

Appendix 12. ^{13}C NMR spectrum of dictyoceratin A **2.9** in $CDCl_3$ (125 MHz)

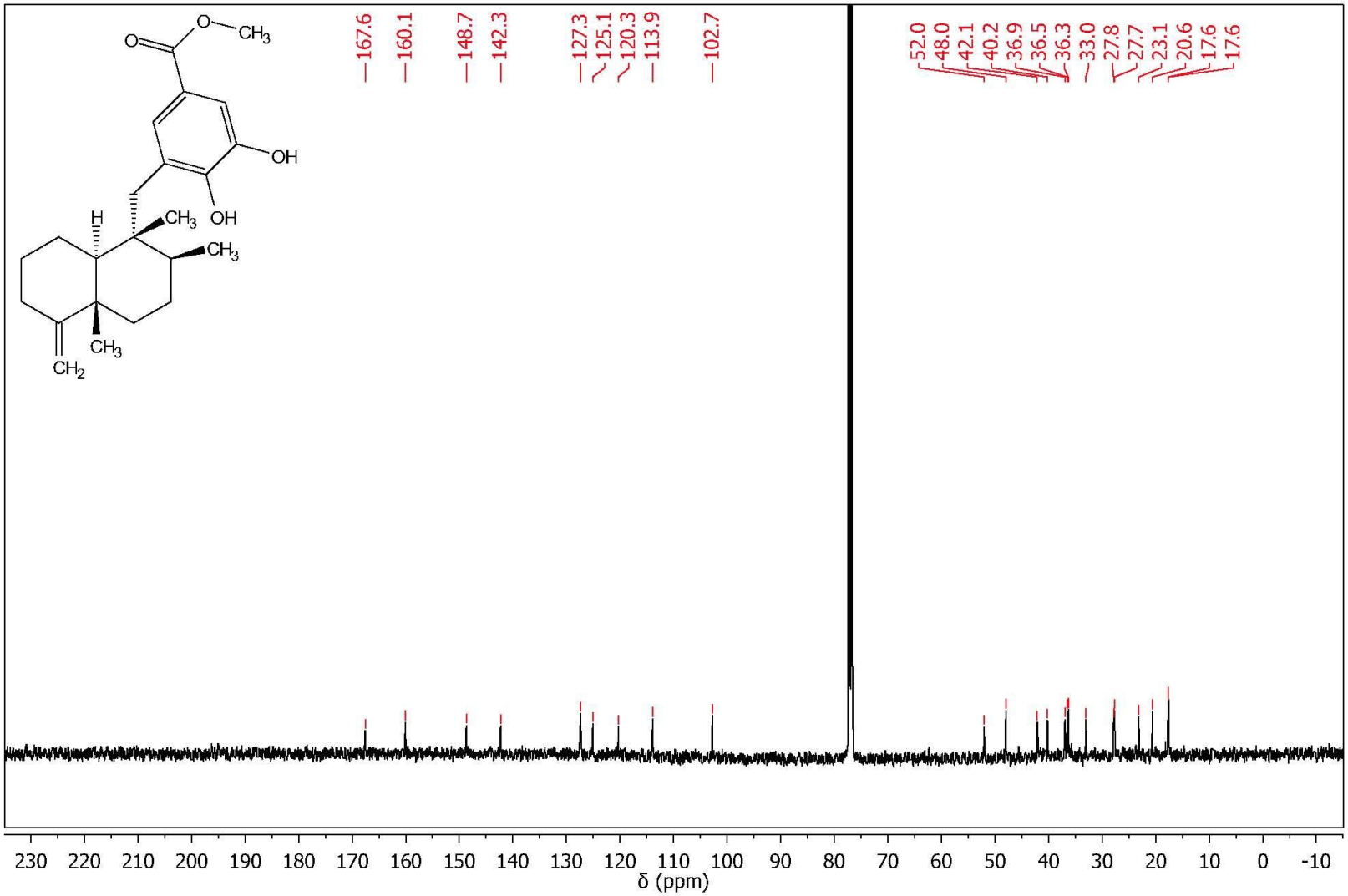

Appendix 13. ^{1}H NMR spectrum of dictyoceratin B **2.10** in $CDCl_3$ (500 MHz)

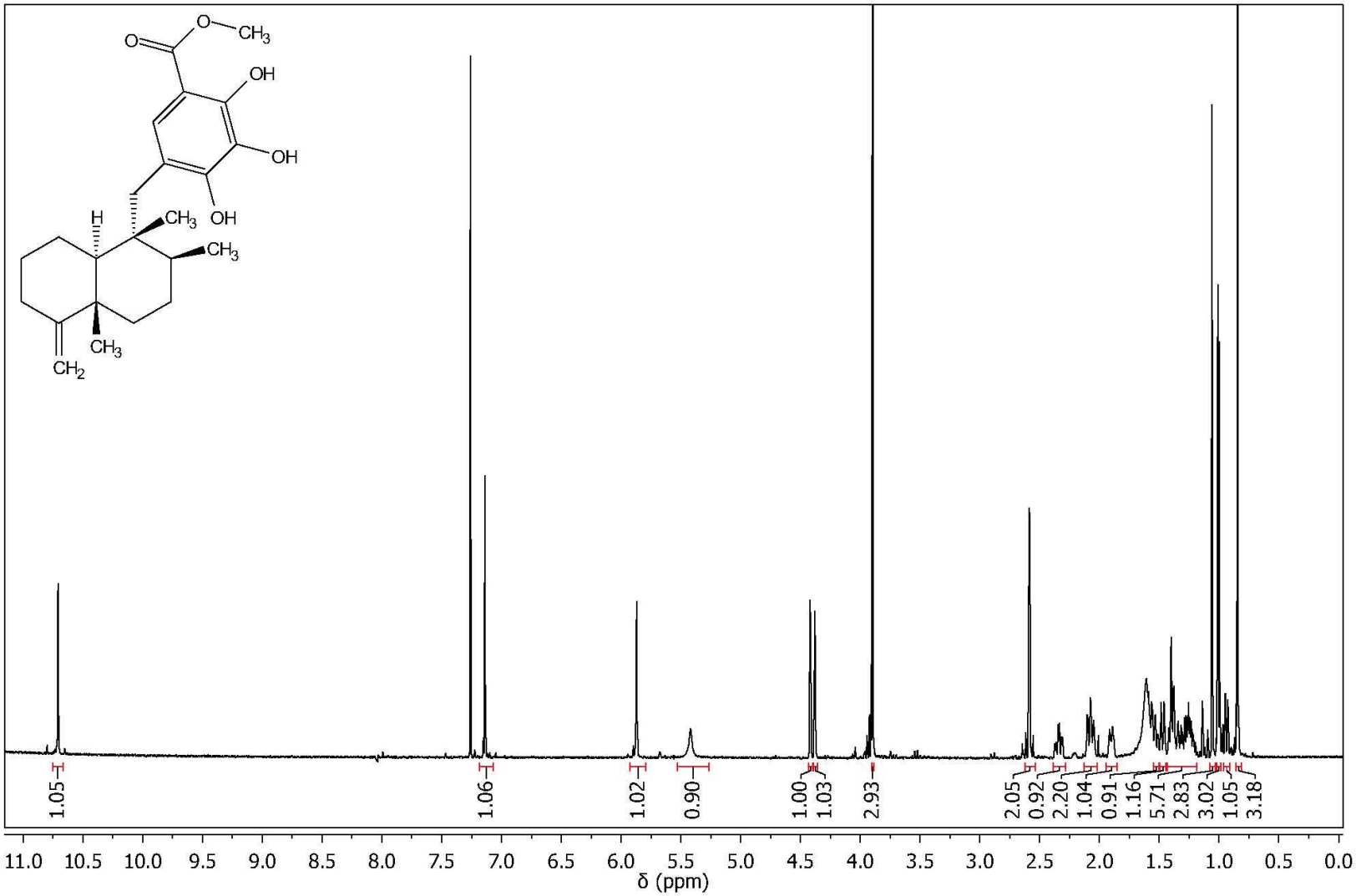

Appendix 14. ^{13}C NMR spectrum of dictyoceratin B **2.10** in $CDCl_3$ (125 MHz)

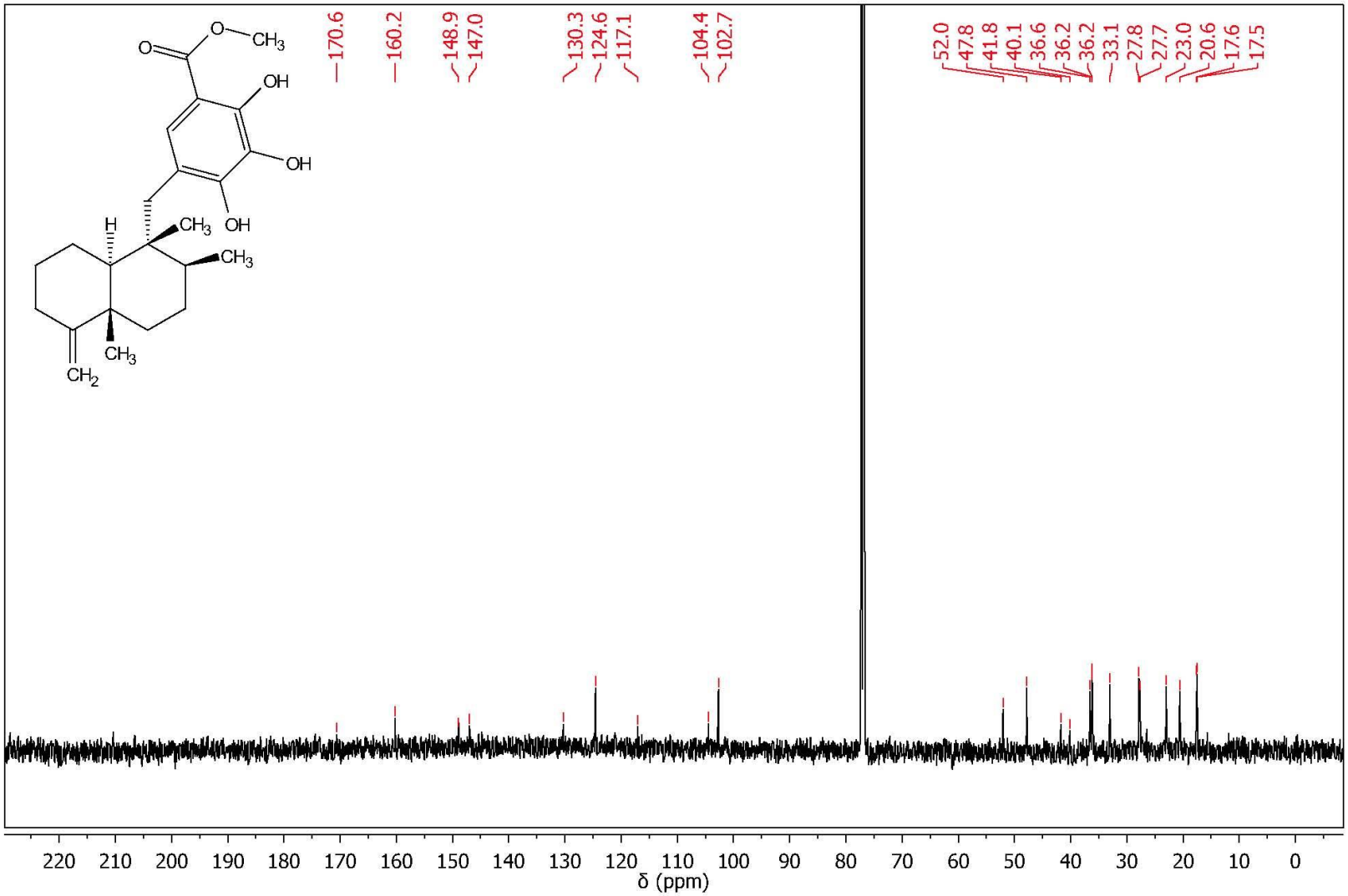

Appendix 15. ^{1}H NMR spectrum of dictyoceratin C **2.11** in $CDCl_3$ (500 MHz)

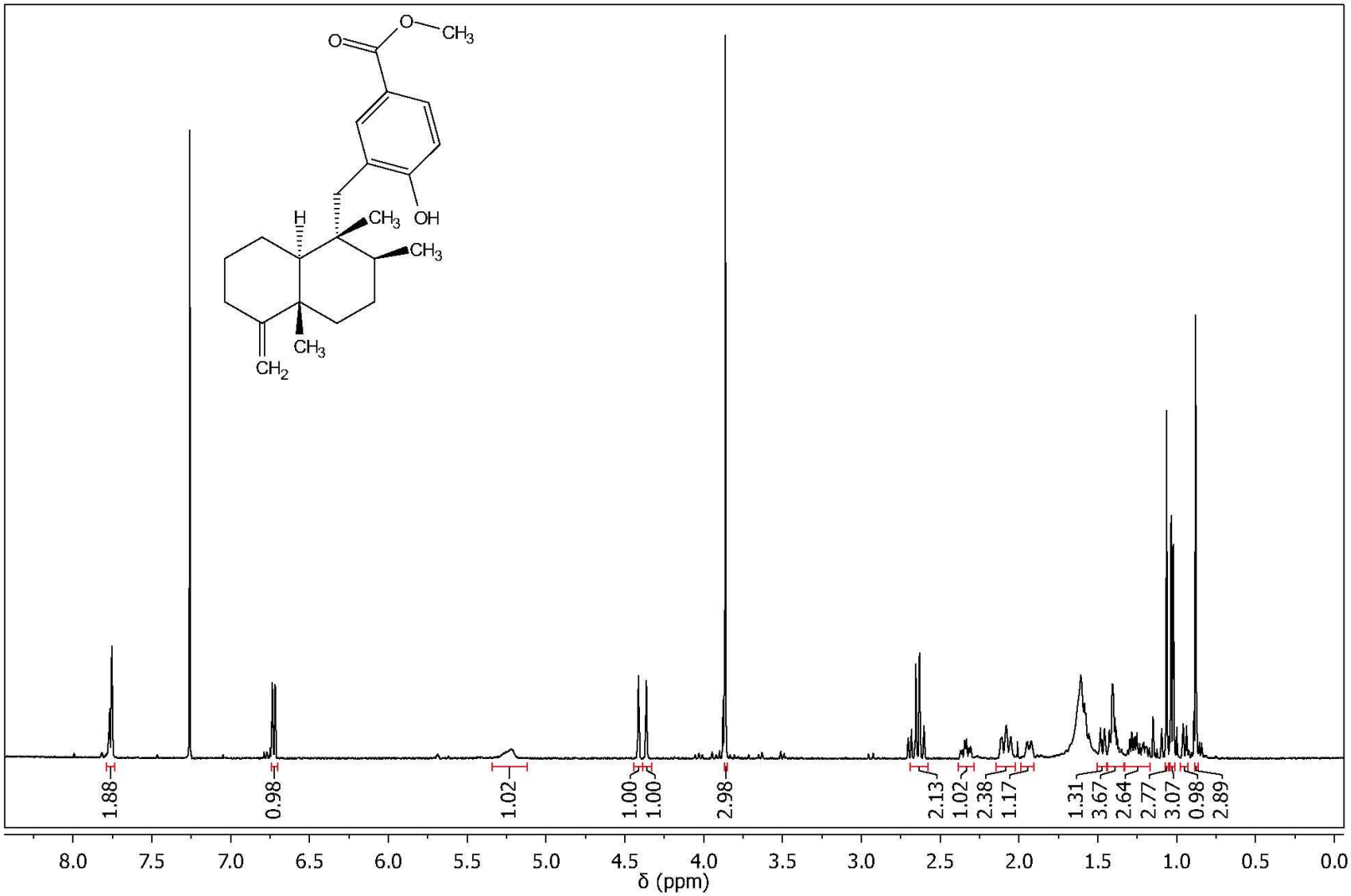

Appendix 16. ^{1}H NMR spectrum of kauamide **2.12** in $CDCl_3$ (500 MHz)

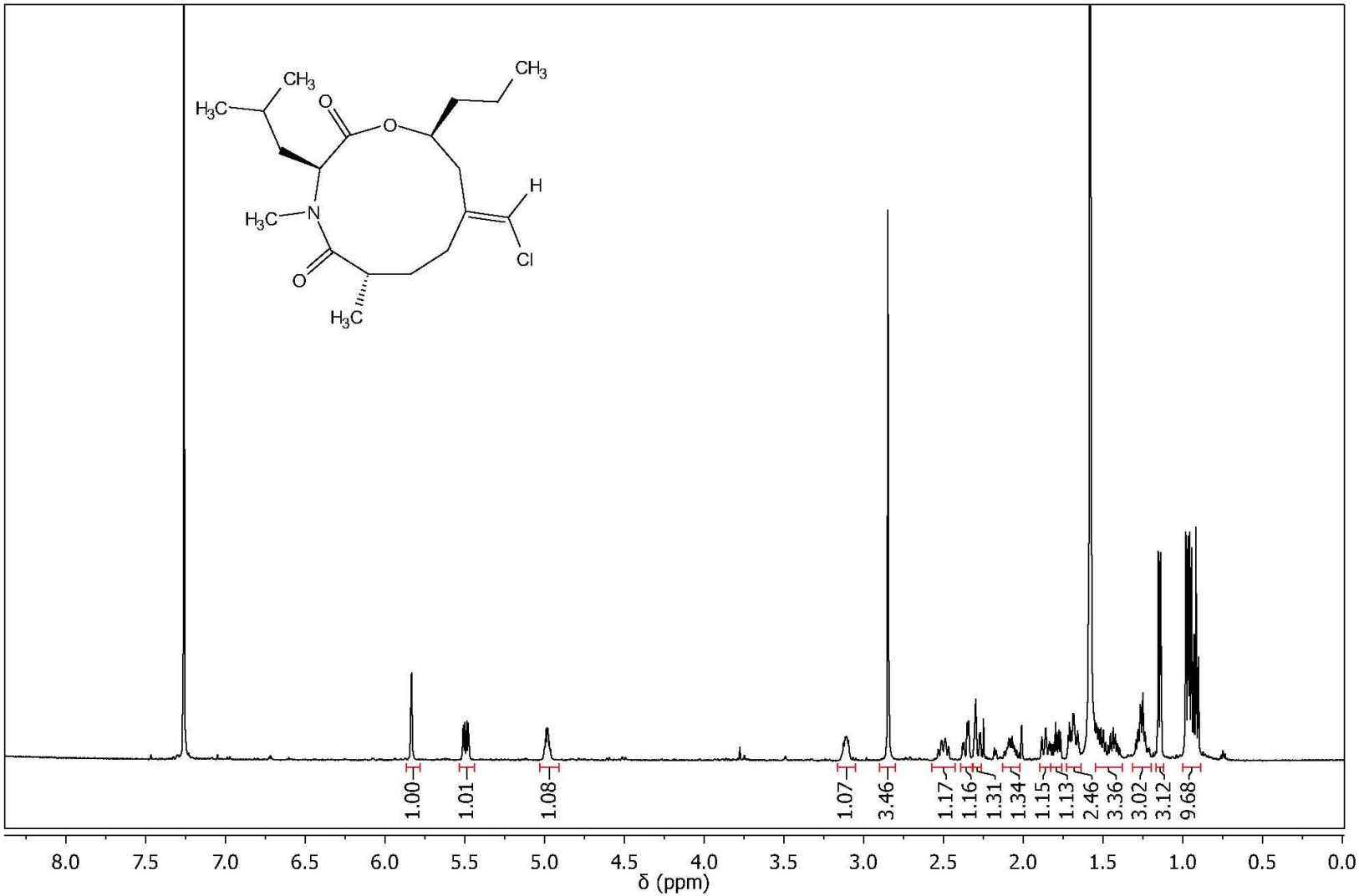

Appendix 17. ^{13}C NMR spectrum of kauamide **2.12** in $CDCl_3$ (125 MHz)

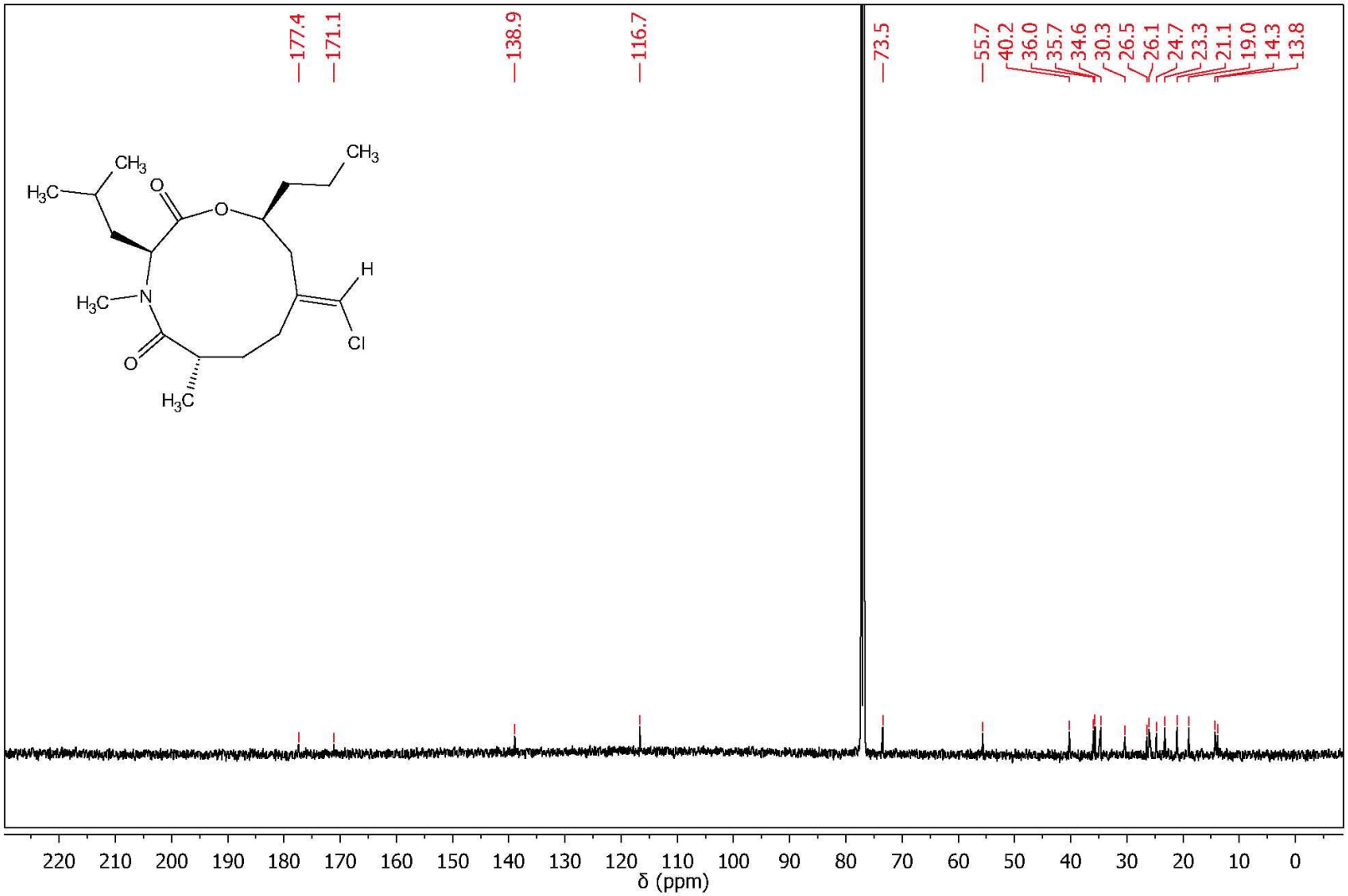

Appendix 18. gCOSY NMR spectrum of kauamide **2.12** in $CDCl_3$ (500 MHz)

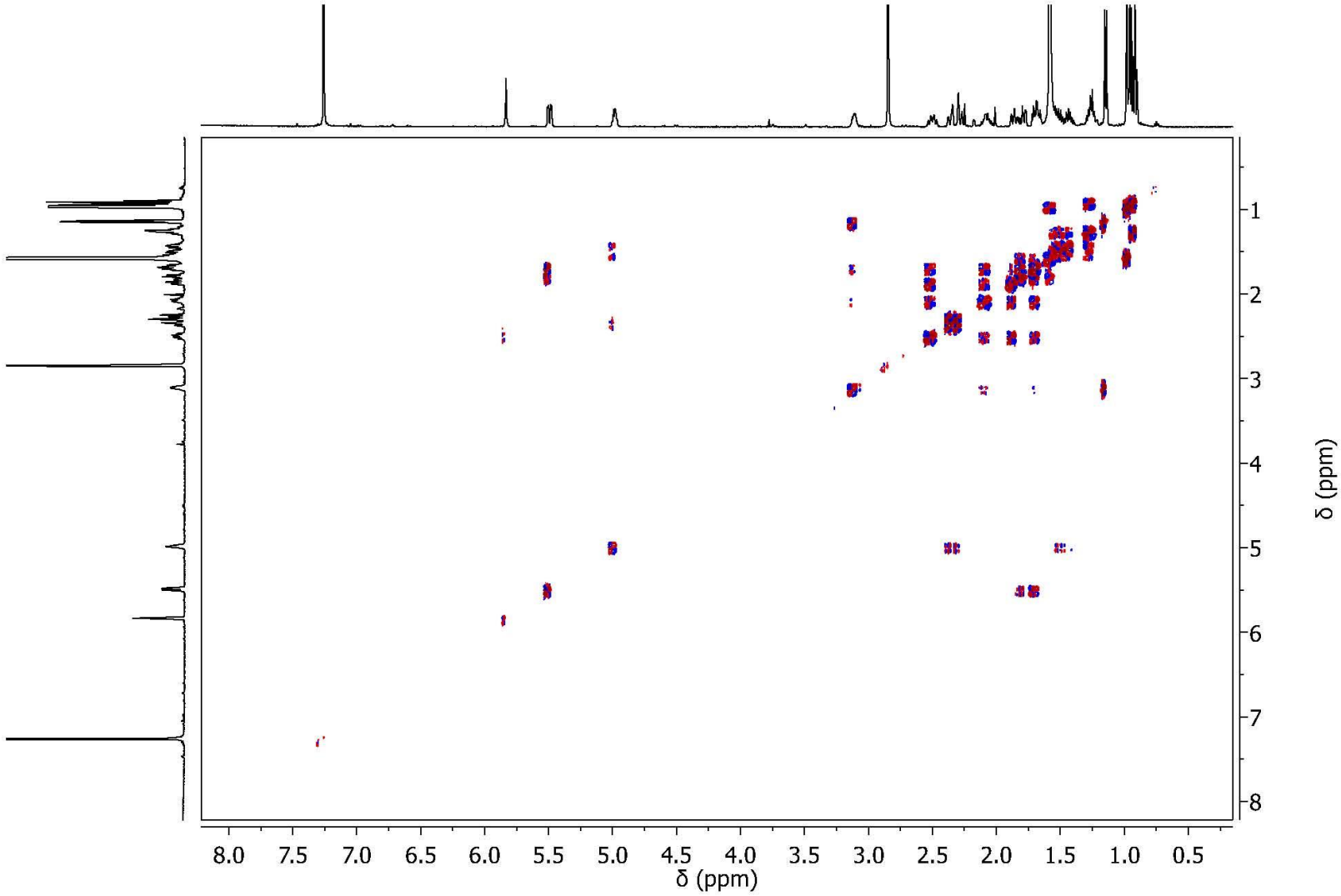

Appendix 19. gHSQC NMR spectrum of kauamide **2.12** in $CDCl_3$ (500 MHz)

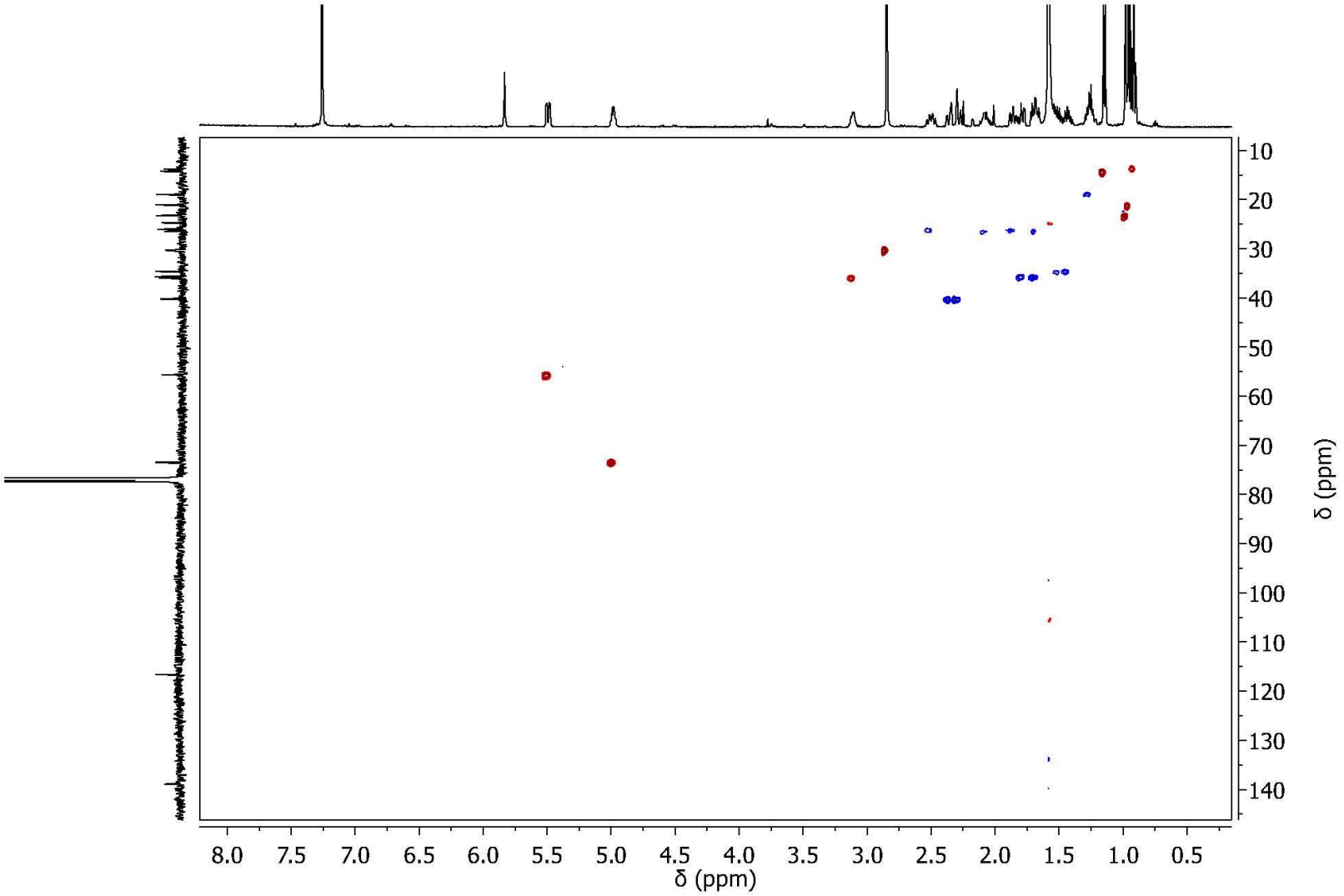

Appendix 20. gHMBC NMR spectrum of kauamide **2.12** in $CDCl_3$ (500 MHz)

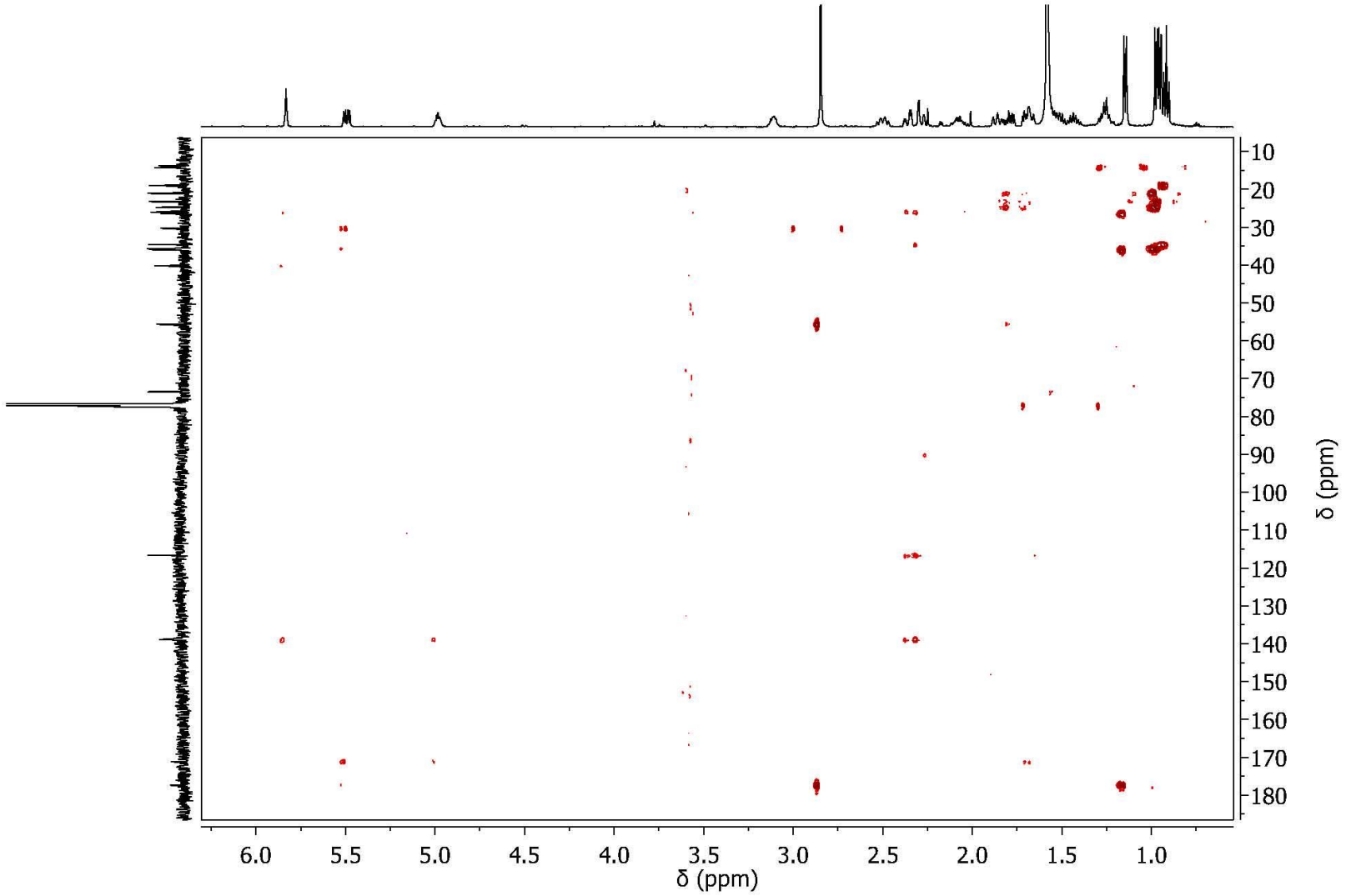

Appendix 21. Advanced Marfey's analysis of the NMeLeu residue of kauamide **2.12**

DL-NMeLeu (Standard) + L-FDLA

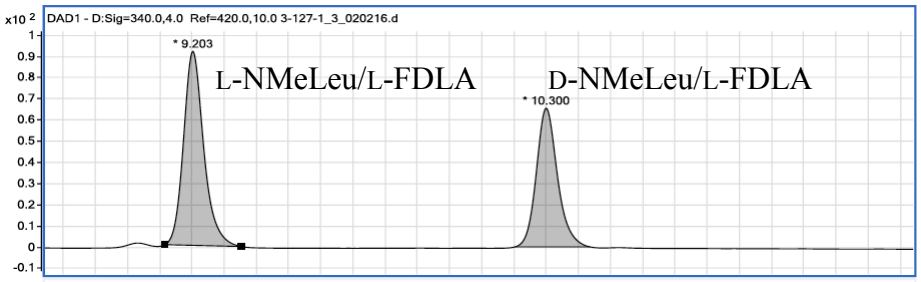

L-NMeLeu (Standard) + L-FDLA

Analyte (NMeLeu from hydrolysis of kauamide) + L-FDLA

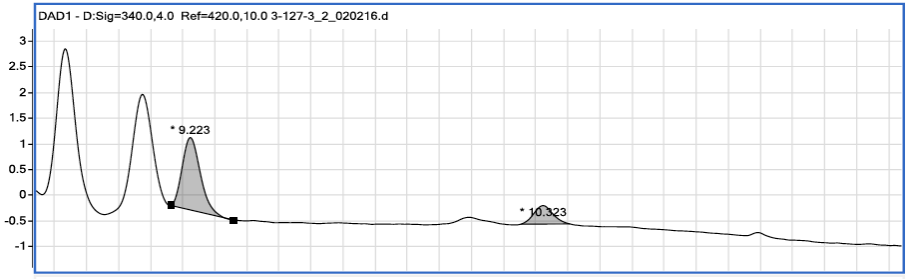

HRMS at 9.2 min

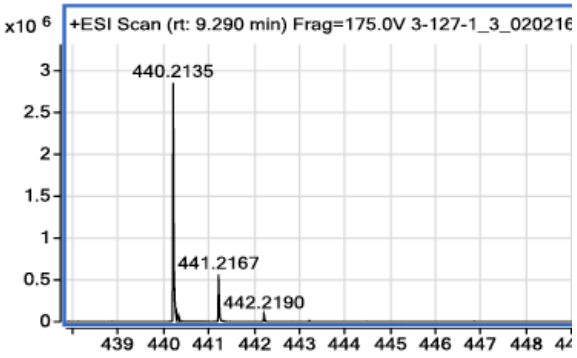

HRMS at 10.3 min

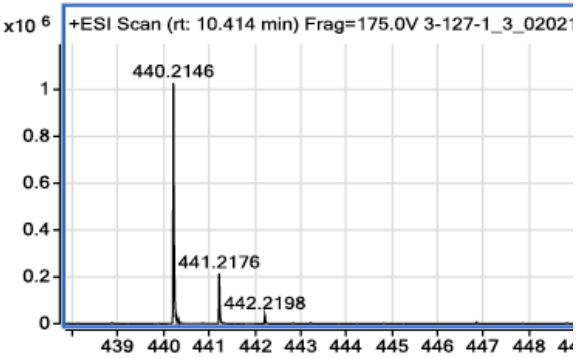

Appendix 22. ^{1}H NMR spectrum of smenospongidinimine **2.24** in $CDCl_3$ (500 MHz)

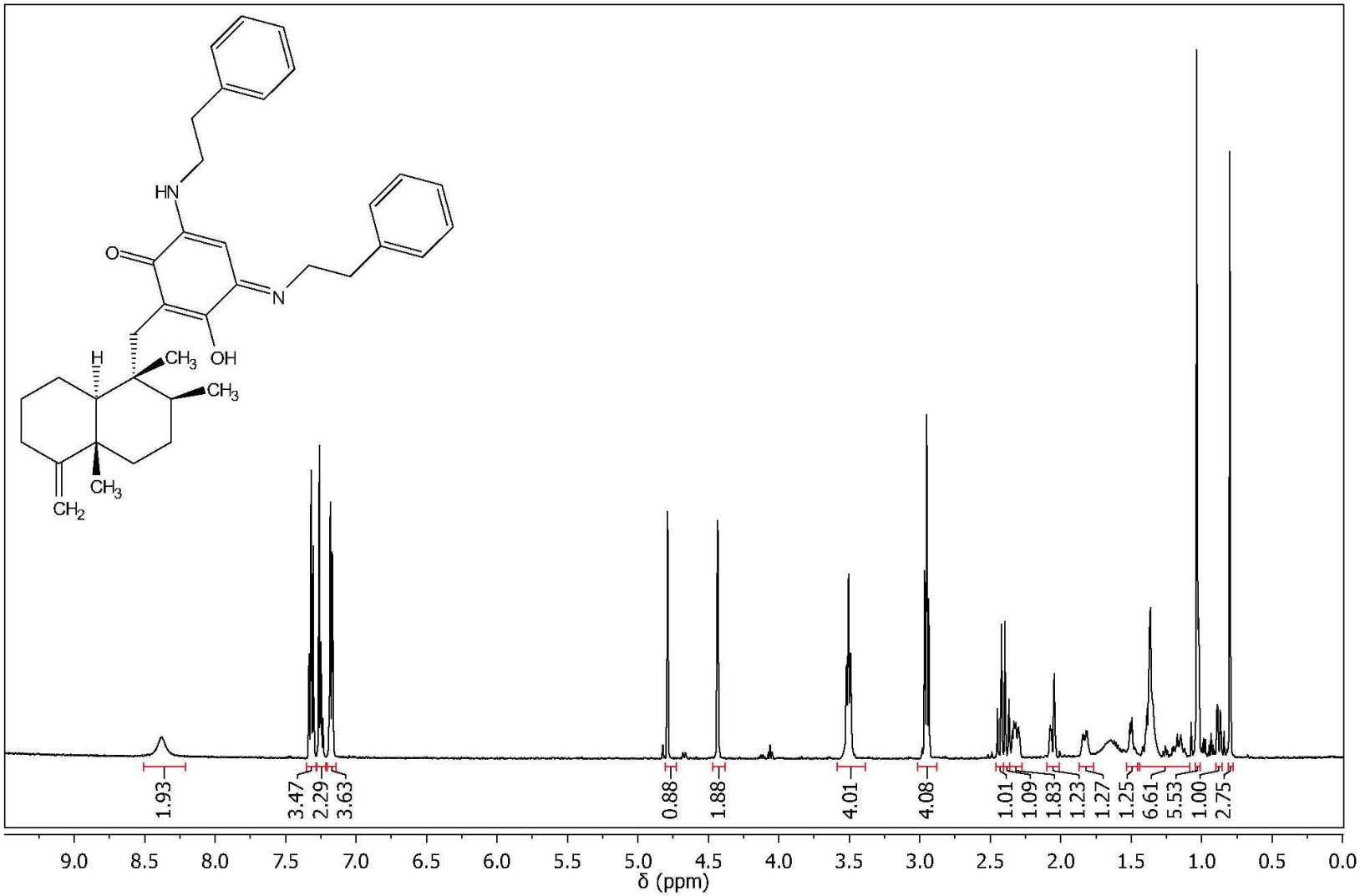

Appendix 23. ^{13}C NMR spectrum of smenospongidinimine **2.24** in $CDCl_3$ (125 MHz)

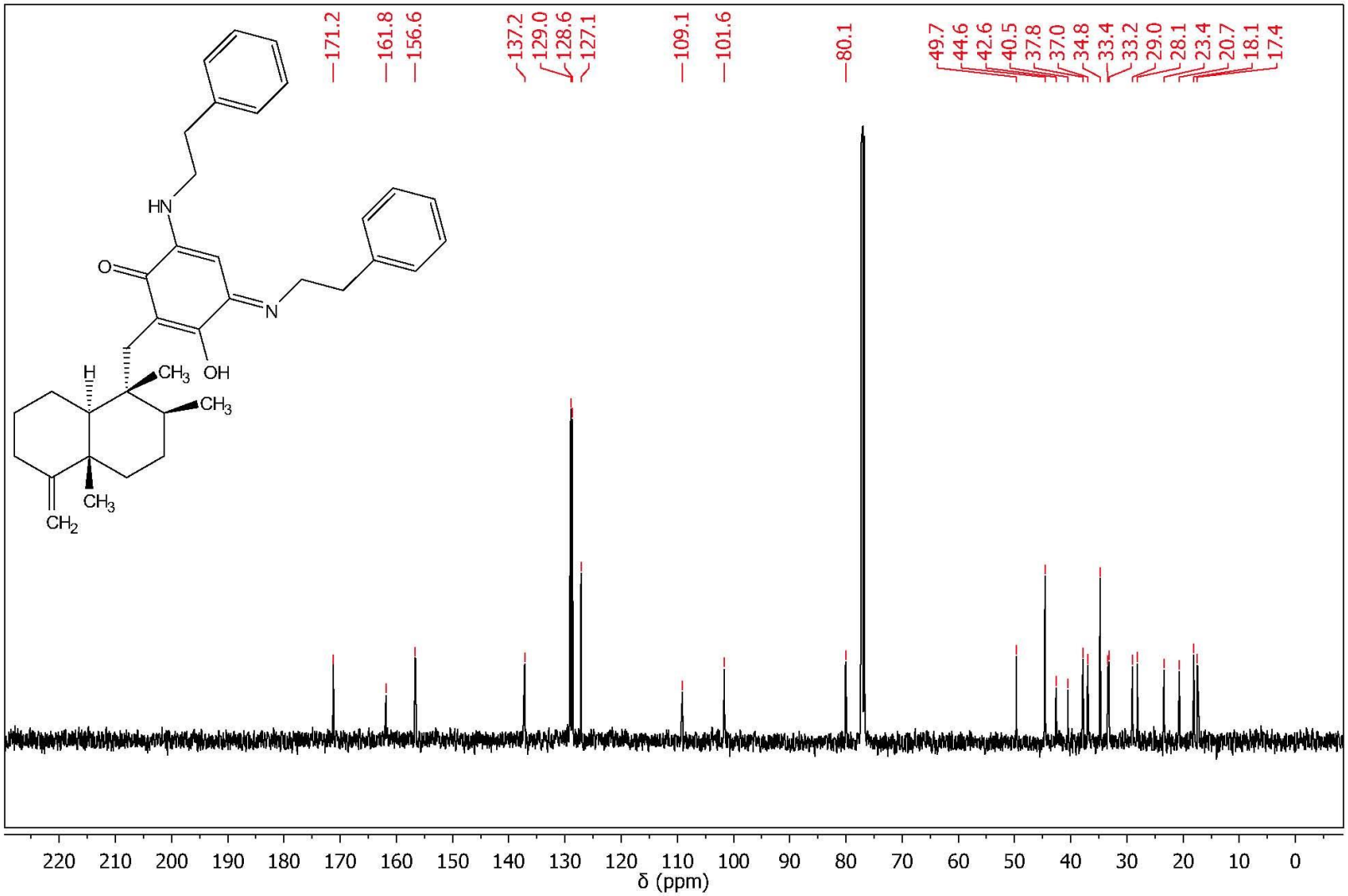

Appendix 24. ^{1}H NMR spectrum of compound **3.6** in DMSO-d_6 (500 MHz)

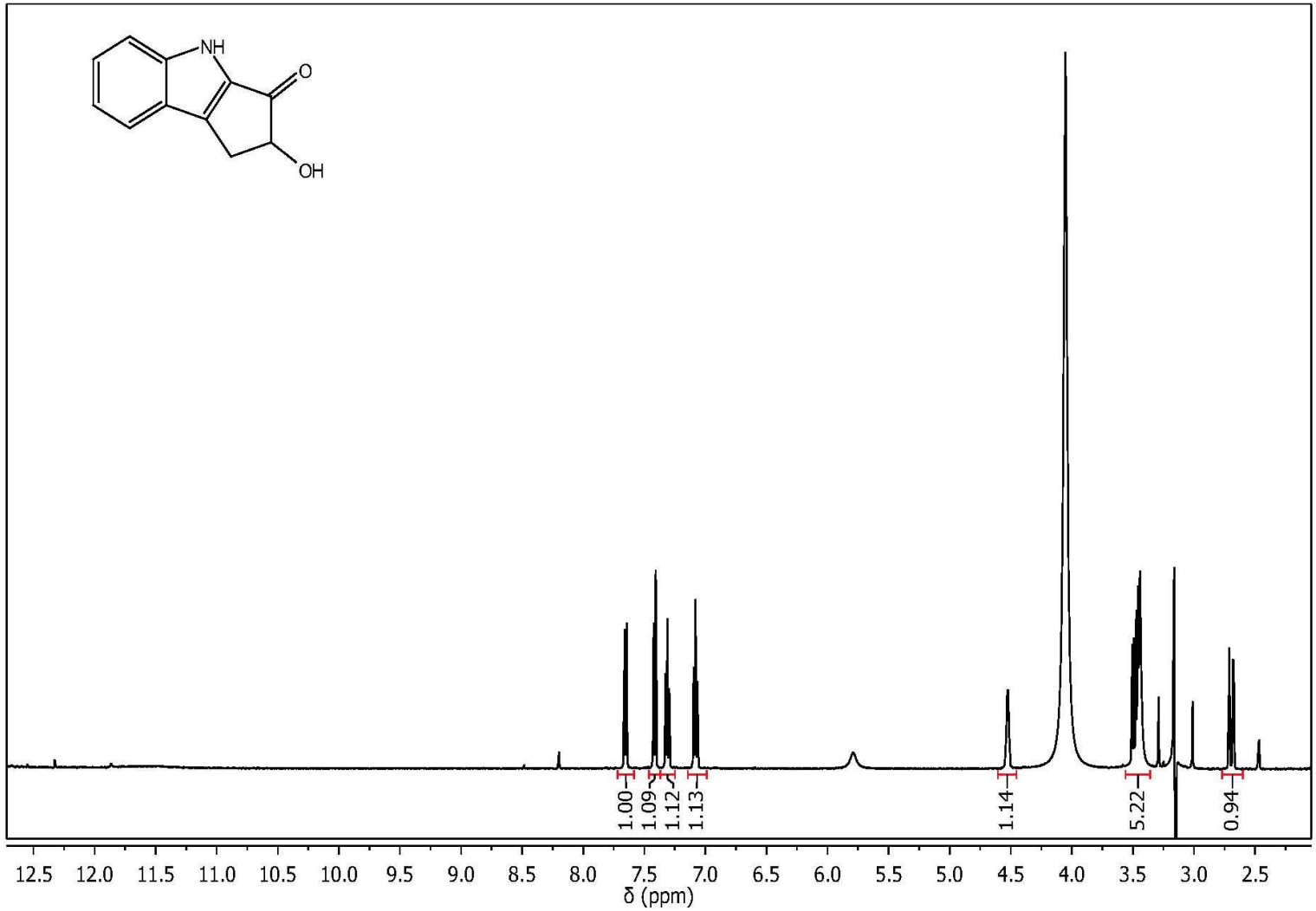

Appendix 25. ^{13}C NMR spectrum of compound **3.6** in DMSO-d_6 (125 MHz)

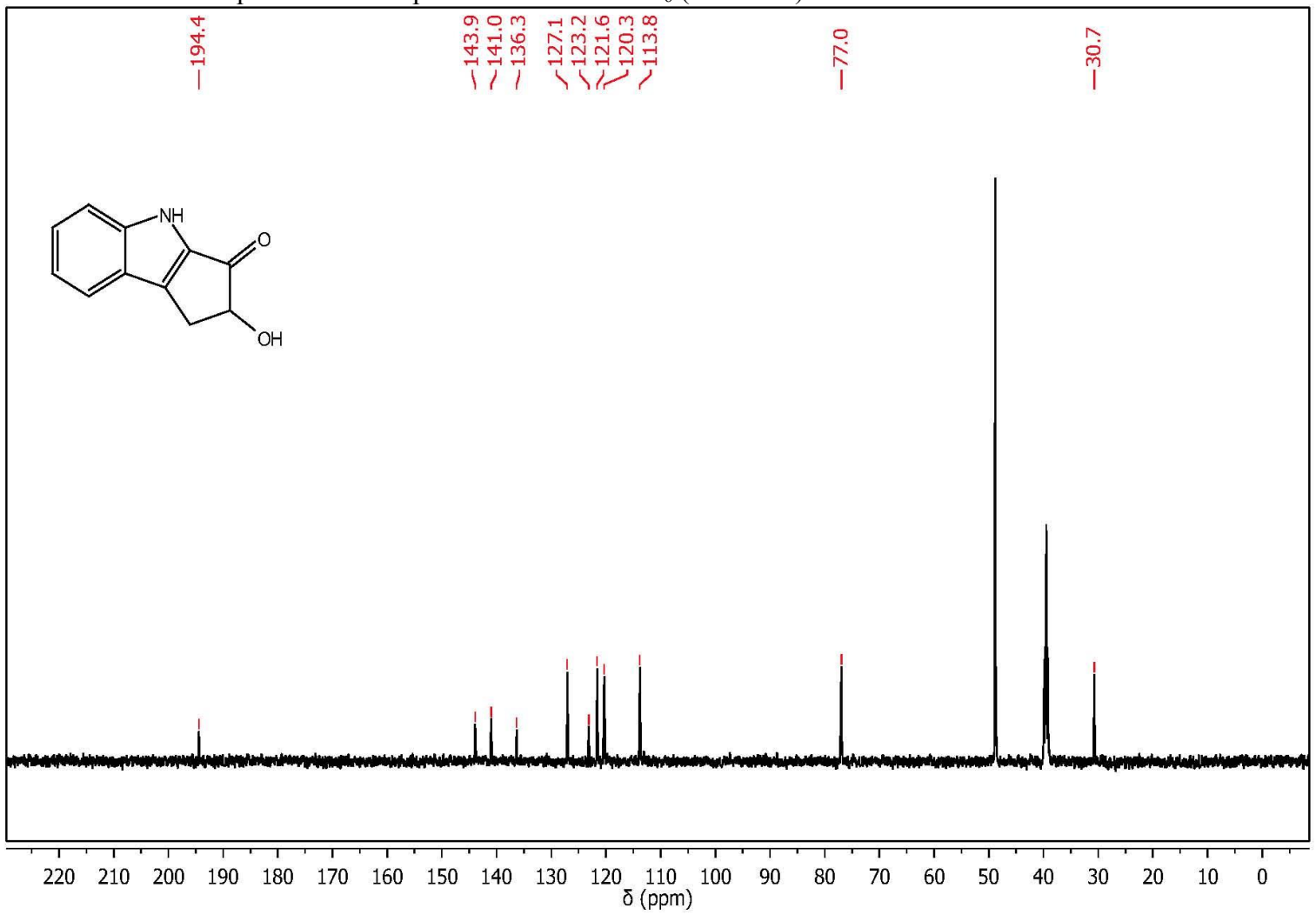

Appendix 26. gCOSY NMR spectrum of compound **3.6** in DMSO-d_6 (500 MHz)

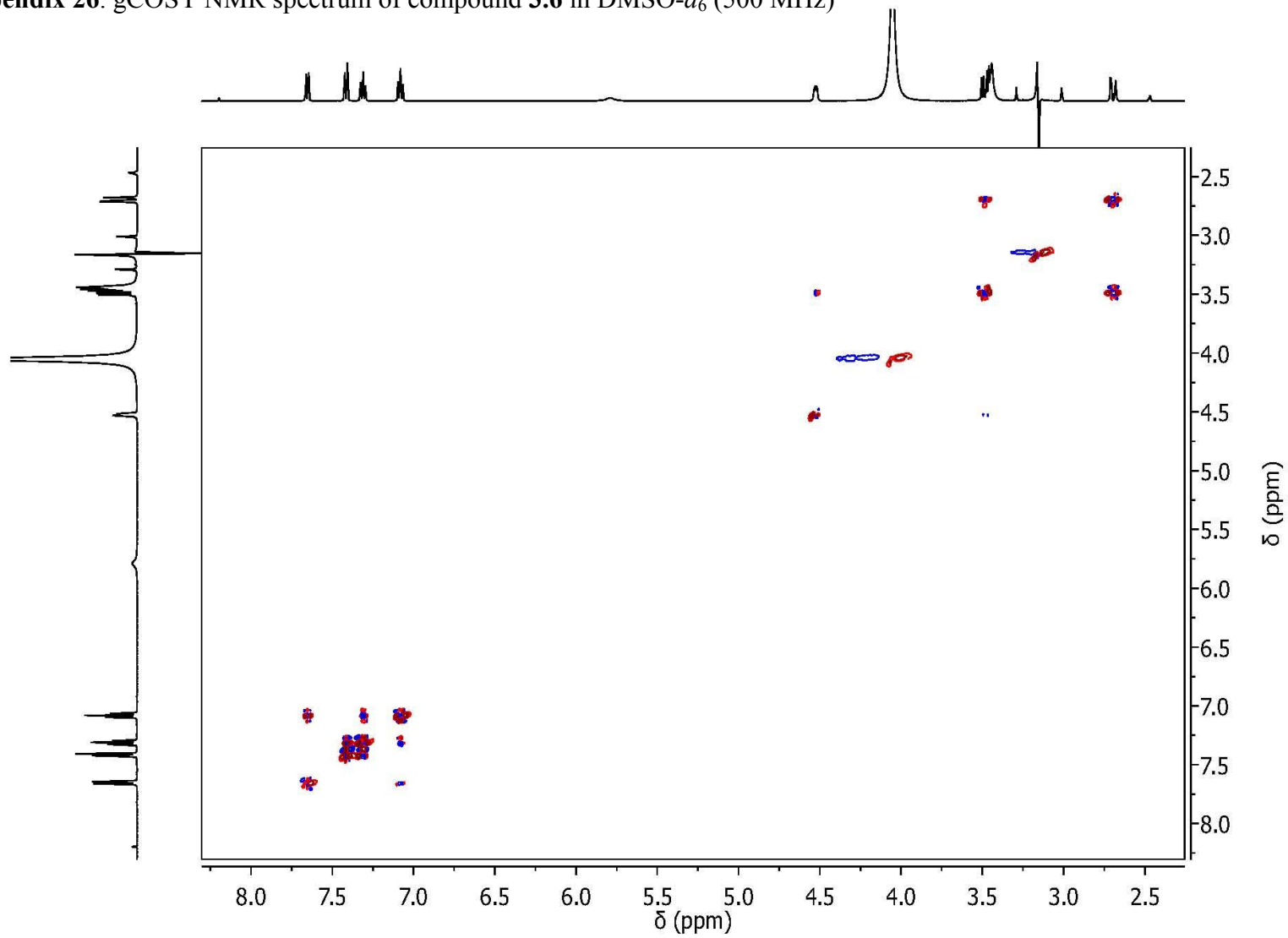

Appendix 27. gHSQC NMR spectrum of compound **3.6** in DMSO-d_6 (500 MHz)

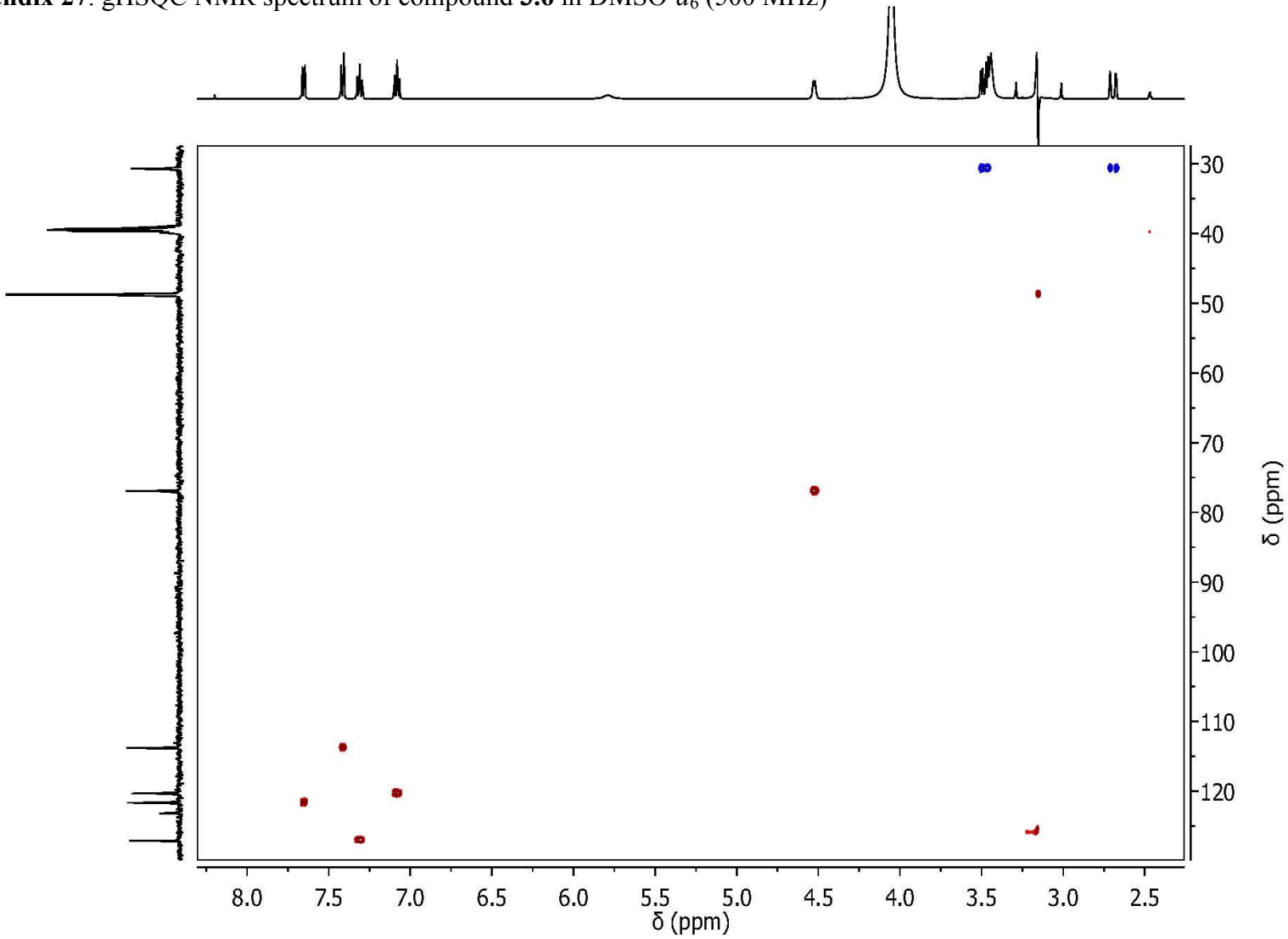

Appendix 28. gHMBC NMR spectrum of compound **3.6** in DMSO-d_6 (500 MHz)

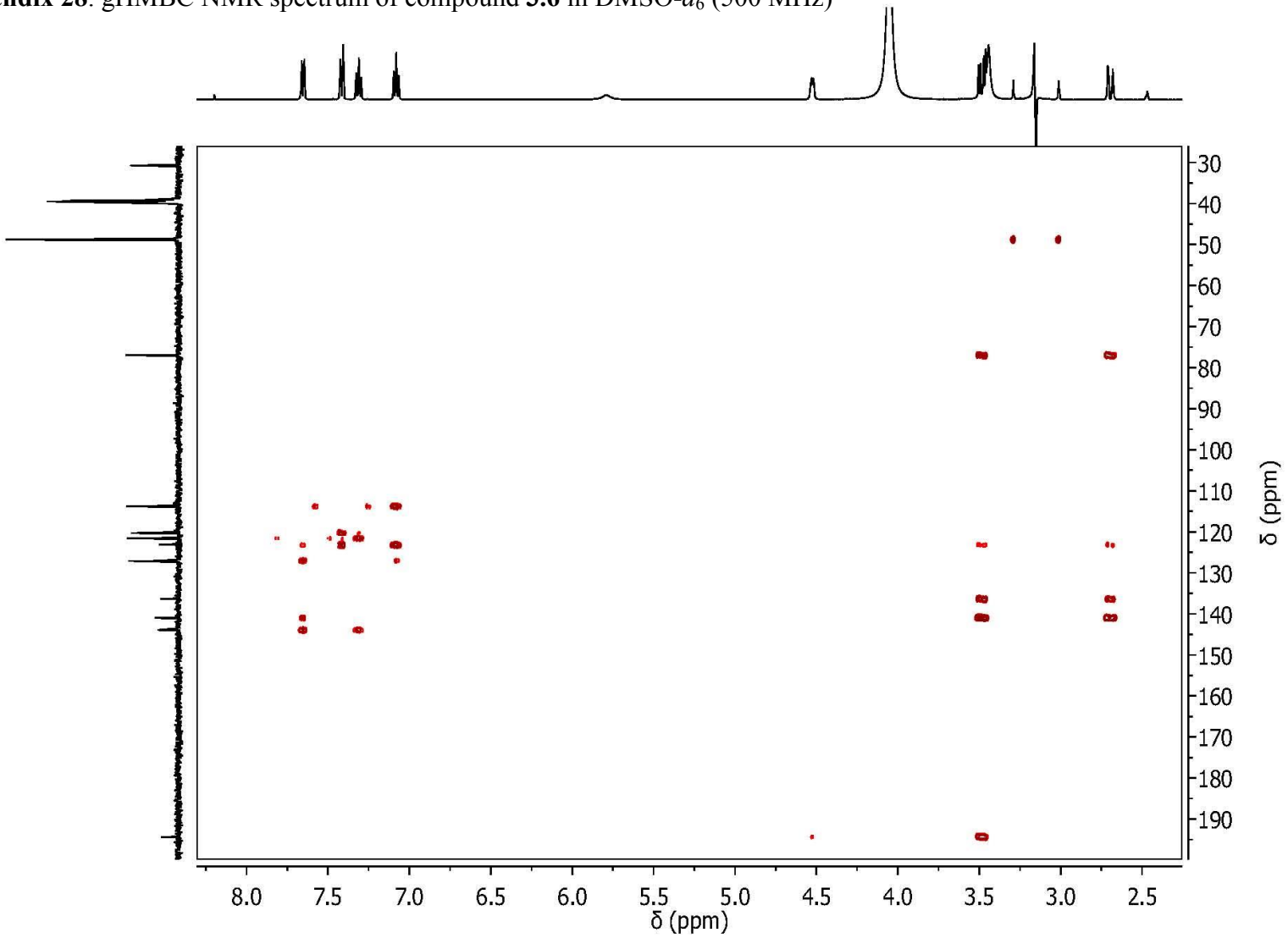

Appendix 29. ^{1}H NMR spectrum of compound **3.6** in CD_3OD (500 MHz)

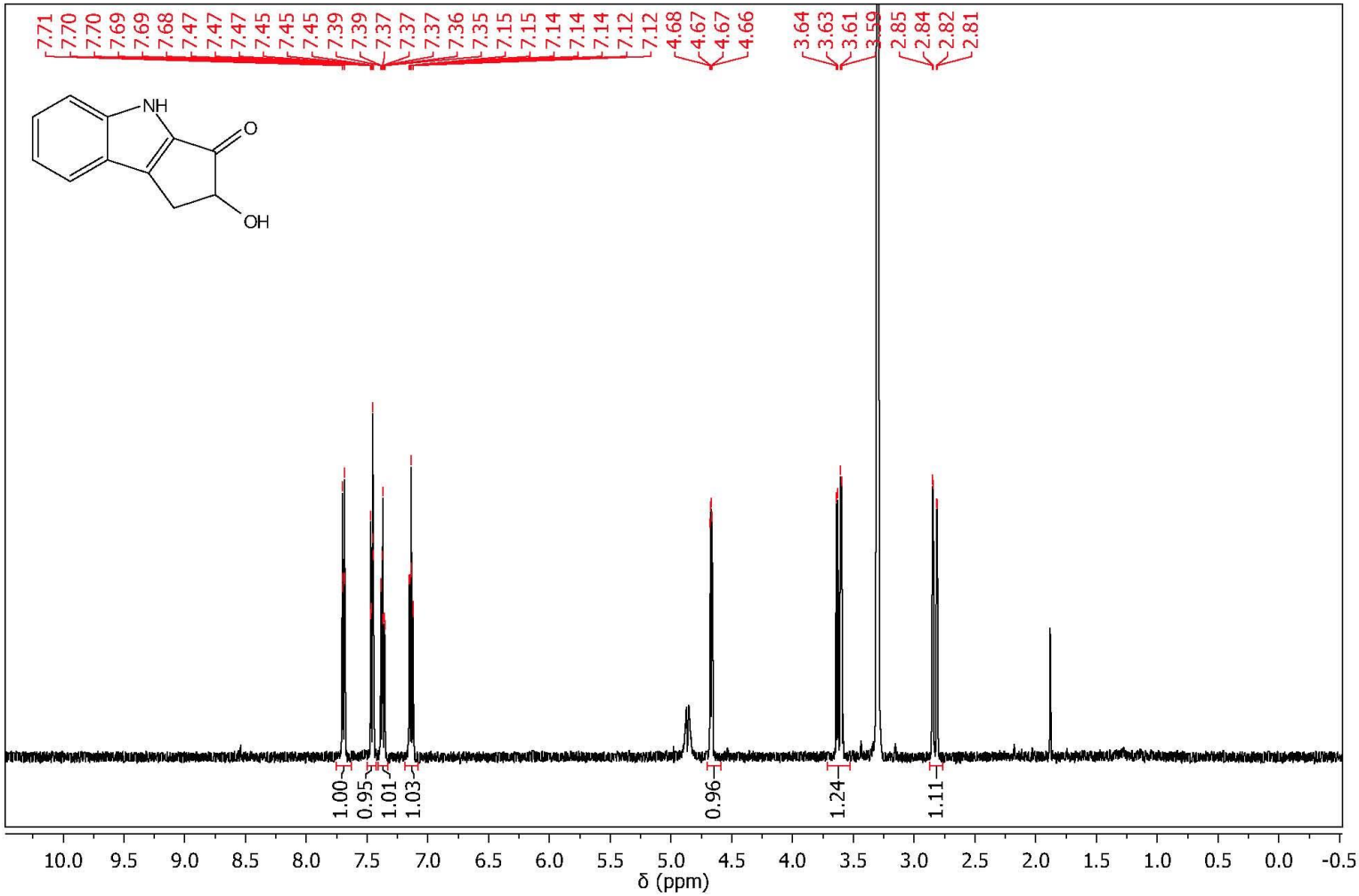

Appendix 30. ^{1}H NMR spectrum of compound **3.7** in $CDCl_3$ (500 MHz)

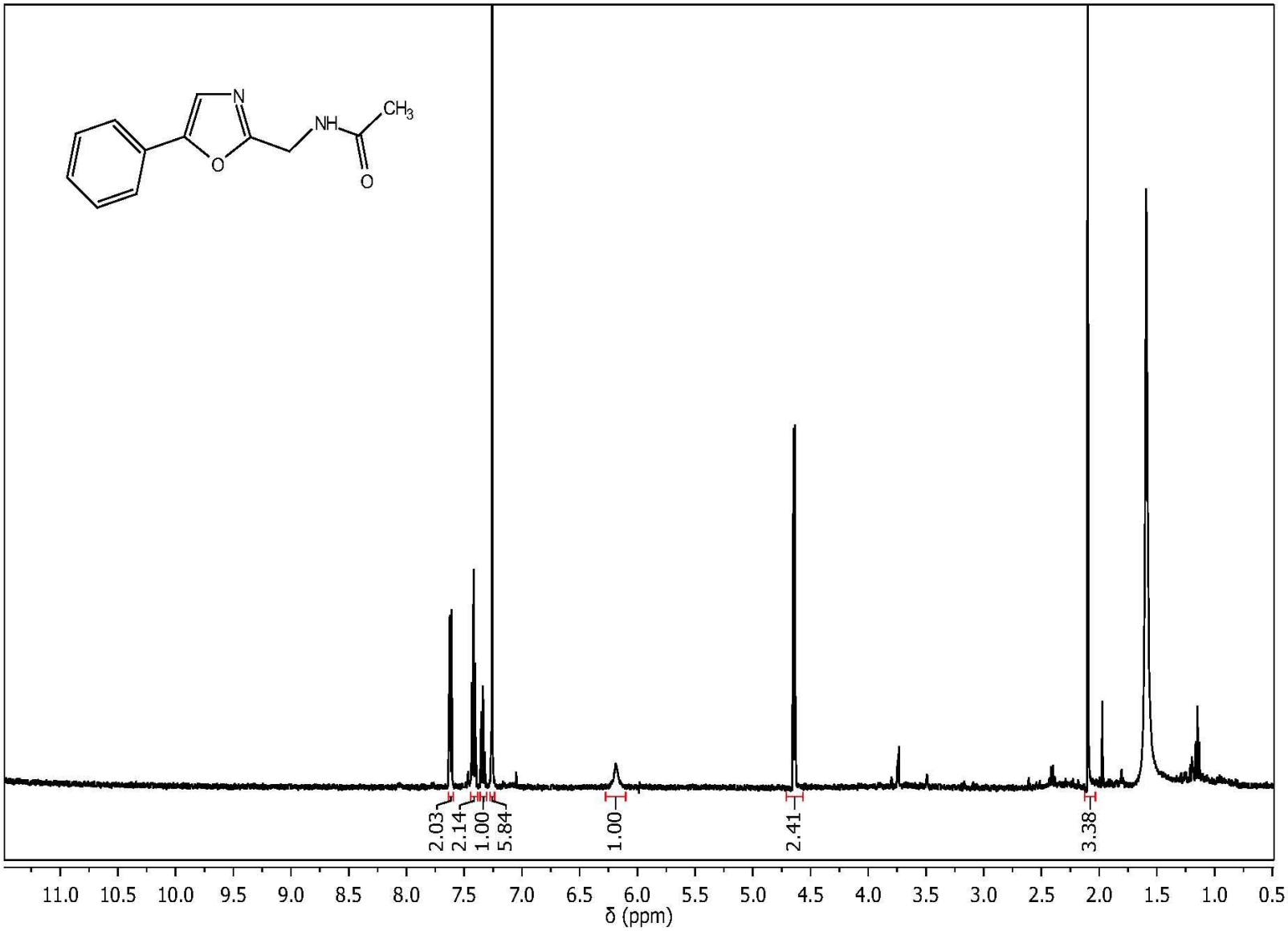

Appendix 31. ^{1}H NMR spectrum of compound **3.7** in CD_3OD (500 MHz)

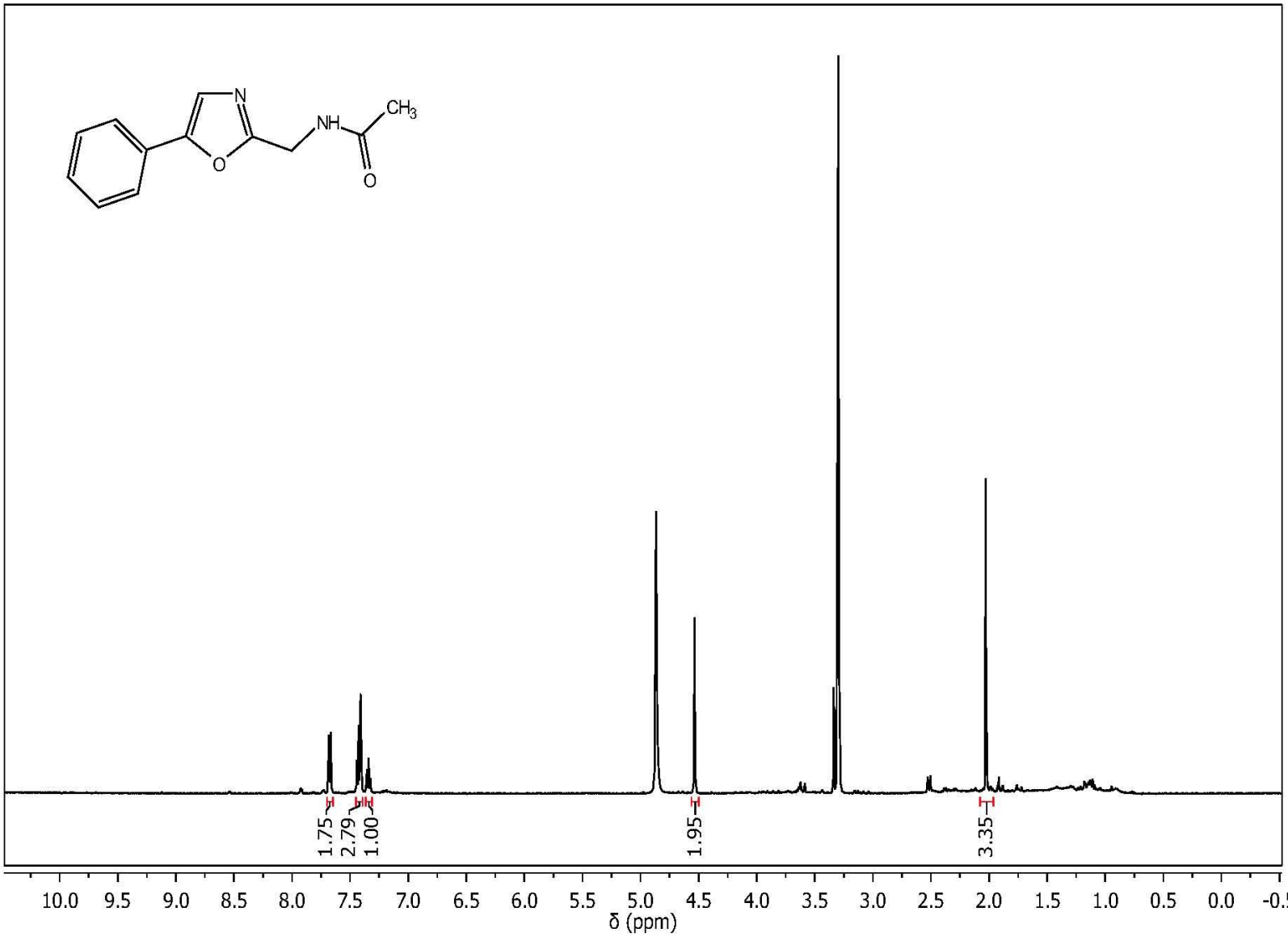

Appendix 32. ^{13}C NMR spectrum of compound **3.7** in $CDCl_3$ (125 MHz)

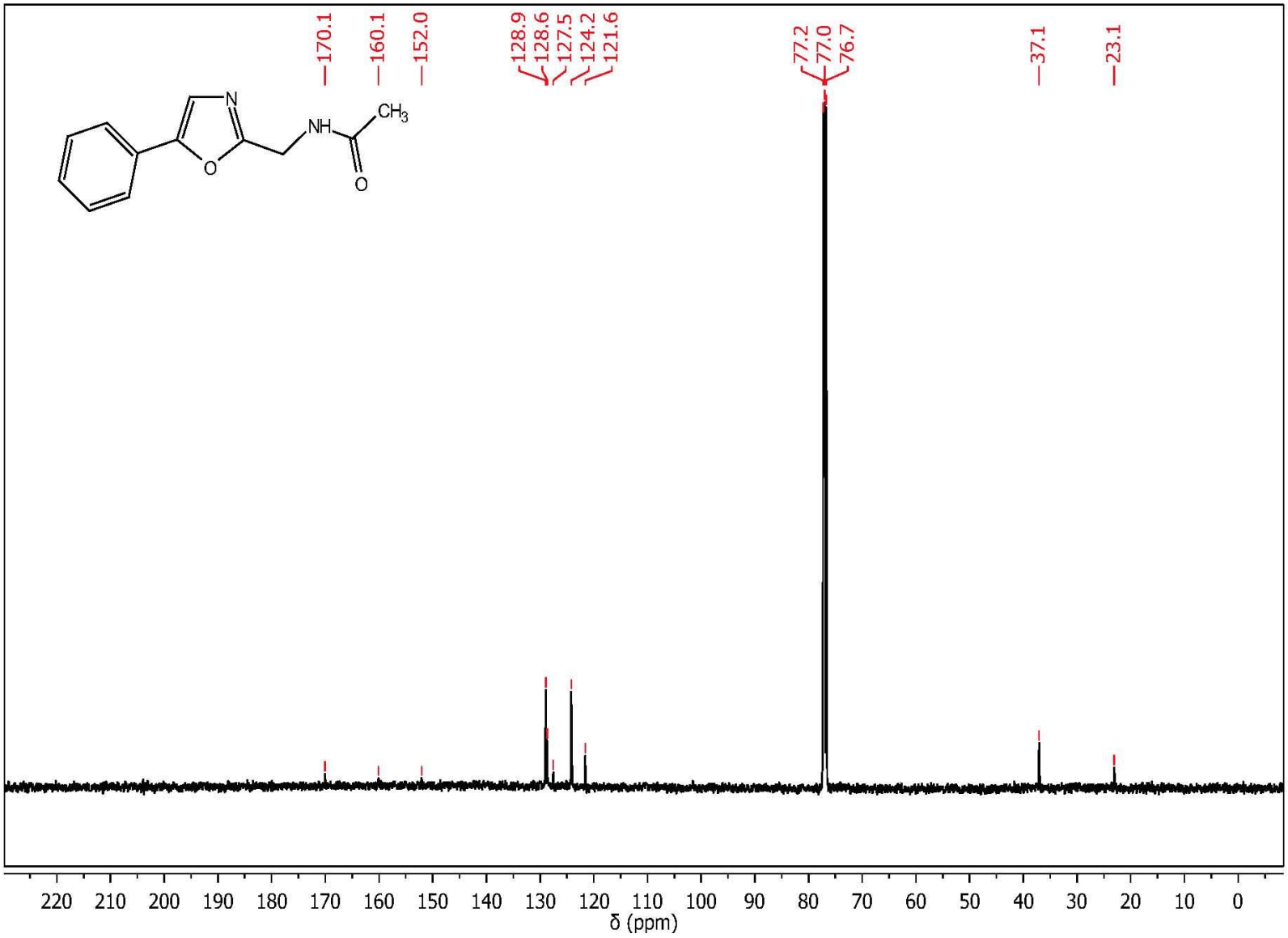

Appendix 33. gHMBC NMR spectrum of compound **3.7** in $CDCl_3$ (500 MHz)

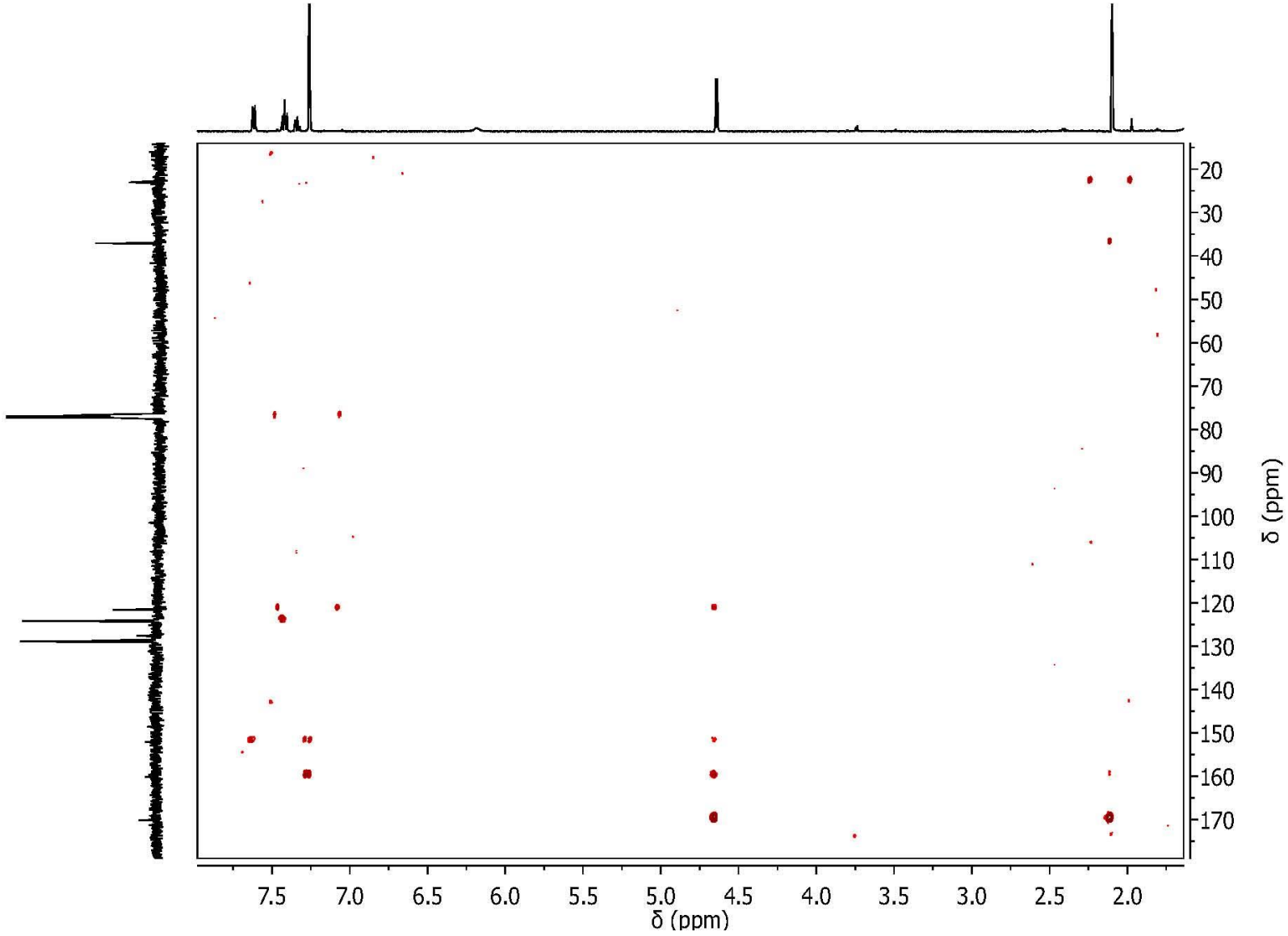

Appendix 34. ^{1}H NMR spectrum of compound **3.8** in CD_3OD (500 MHz)

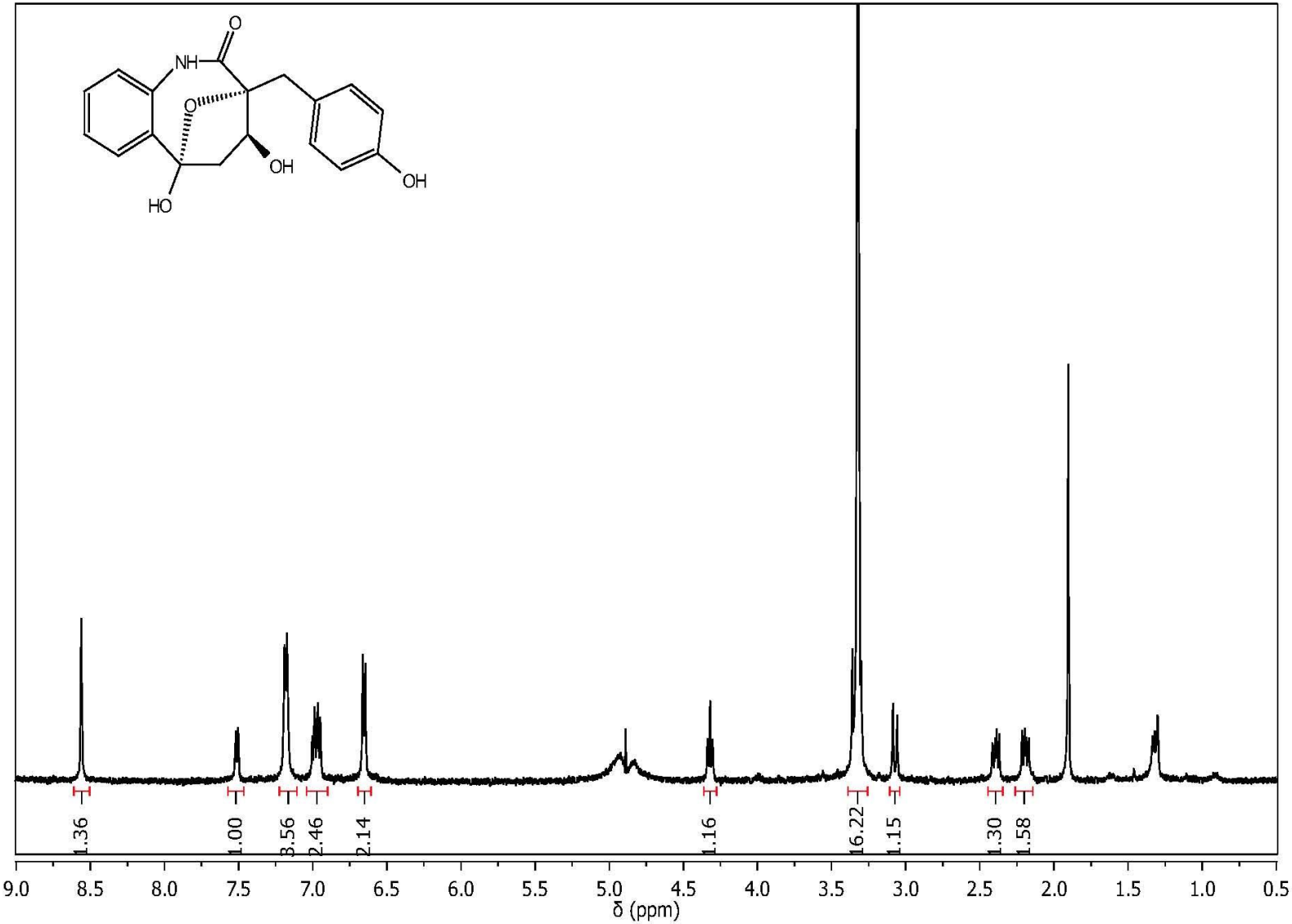

Appendix 35. ^{13}C NMR spectrum of compound **3.8** in CD_3OD (125 MHz)

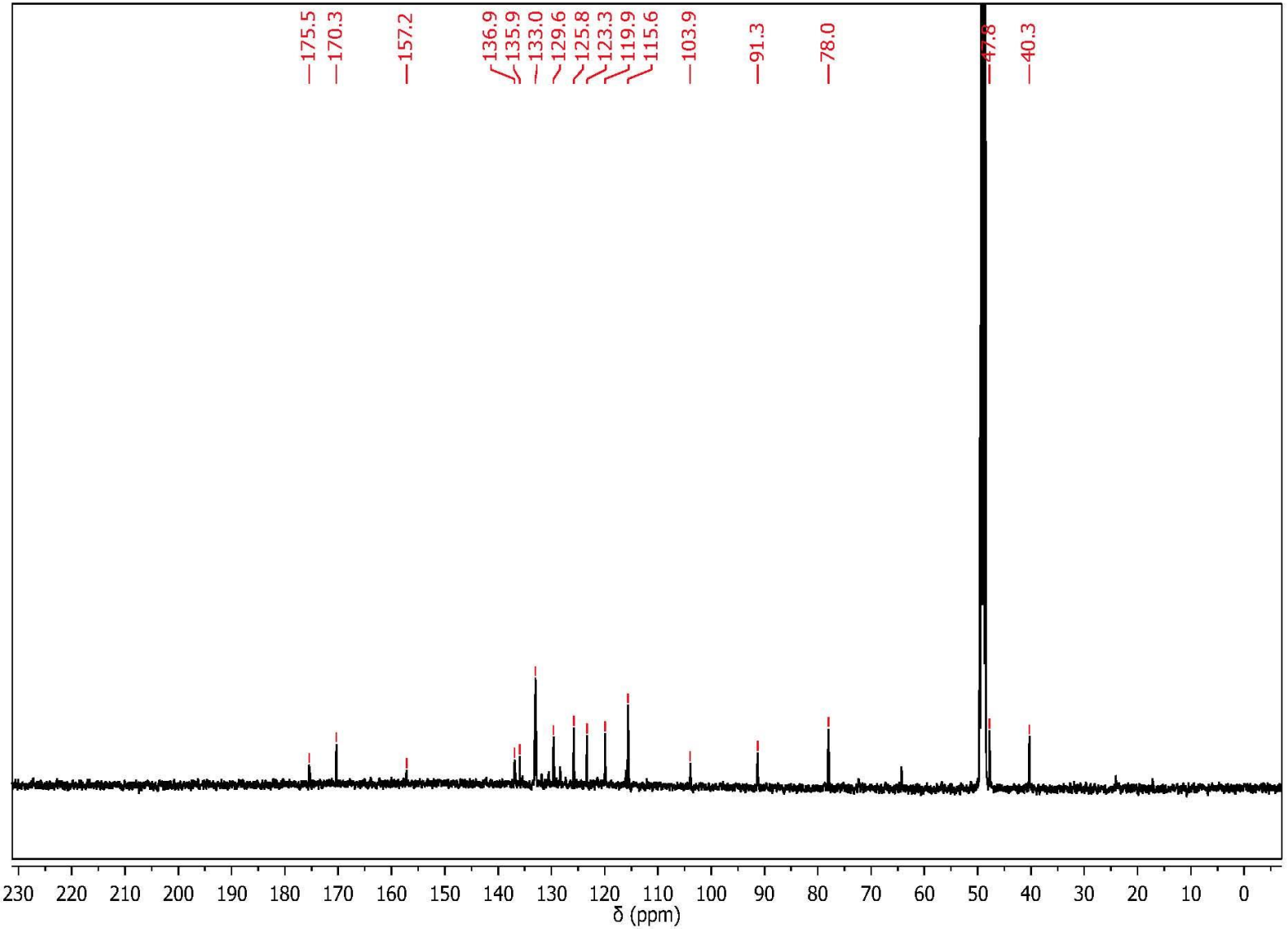

Appendix 36. gCOSY NMR spectrum of compound **3.8** in CD_3OD (500 MHz)

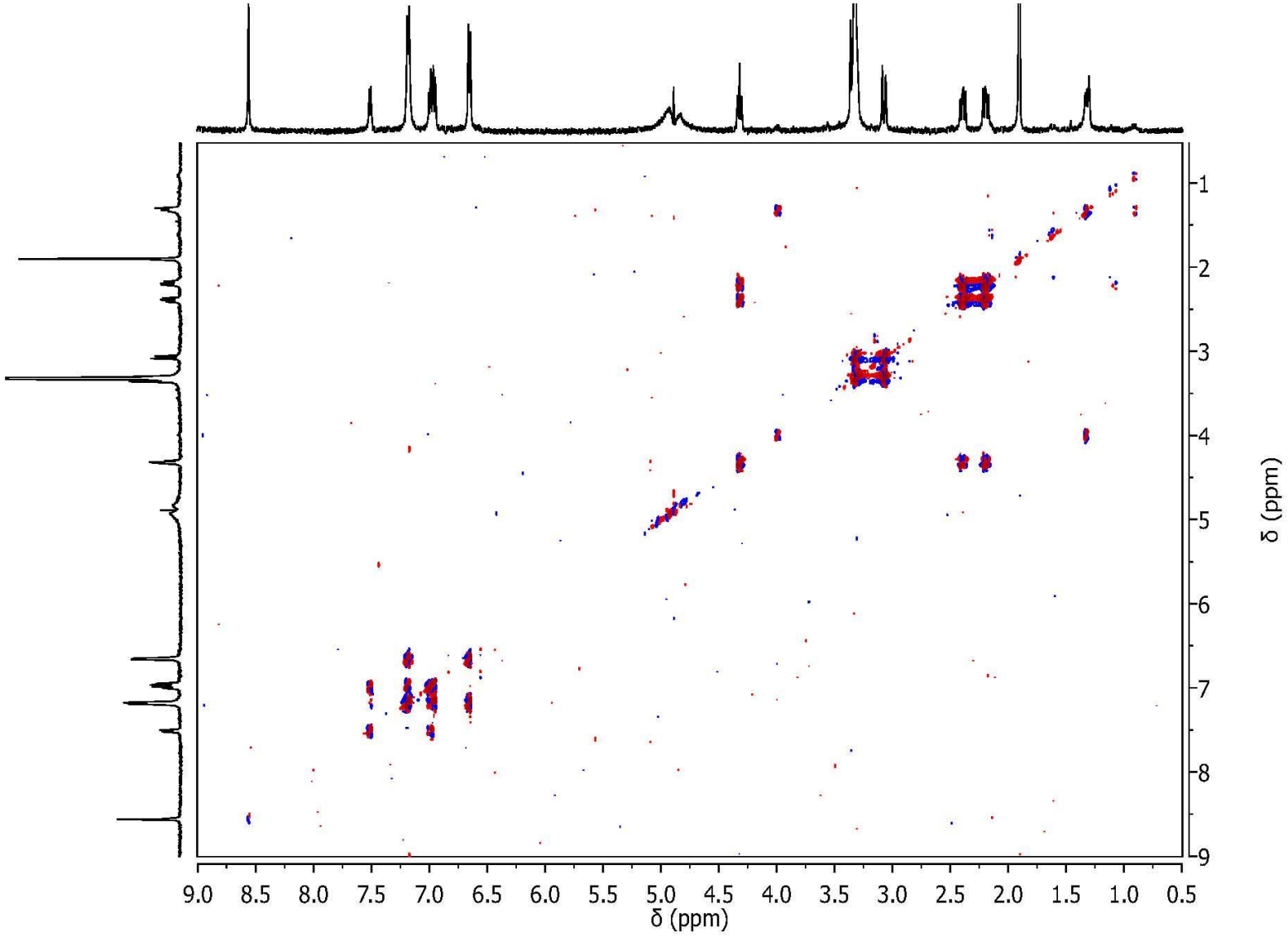

Appendix 37. gHSQC NMR spectrum of compound **3.8** in CD_3OD (500 MHz)

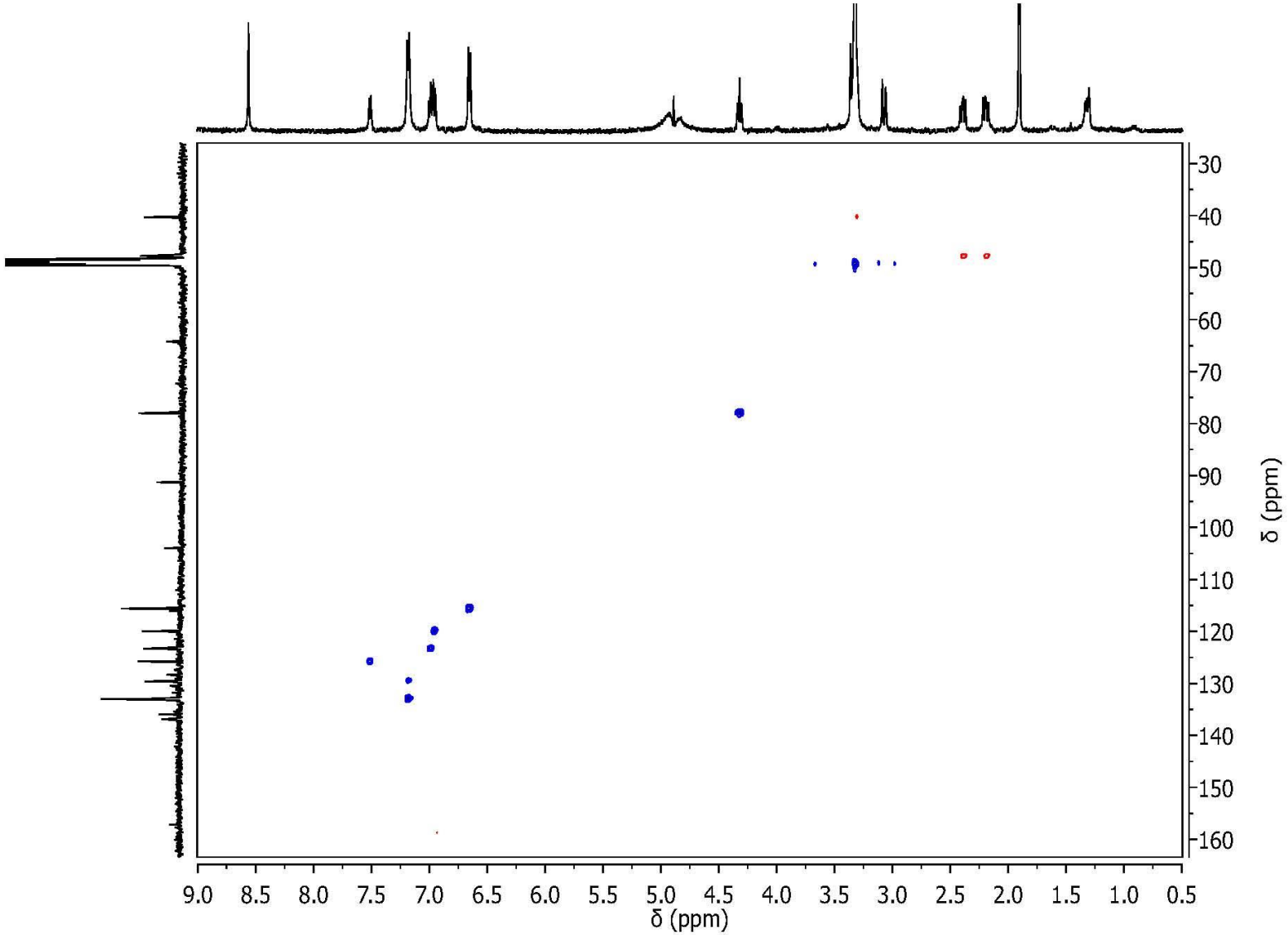

Appendix 38. gHMBC NMR spectrum of compound **3.8** in CD_3OD (500 MHz)

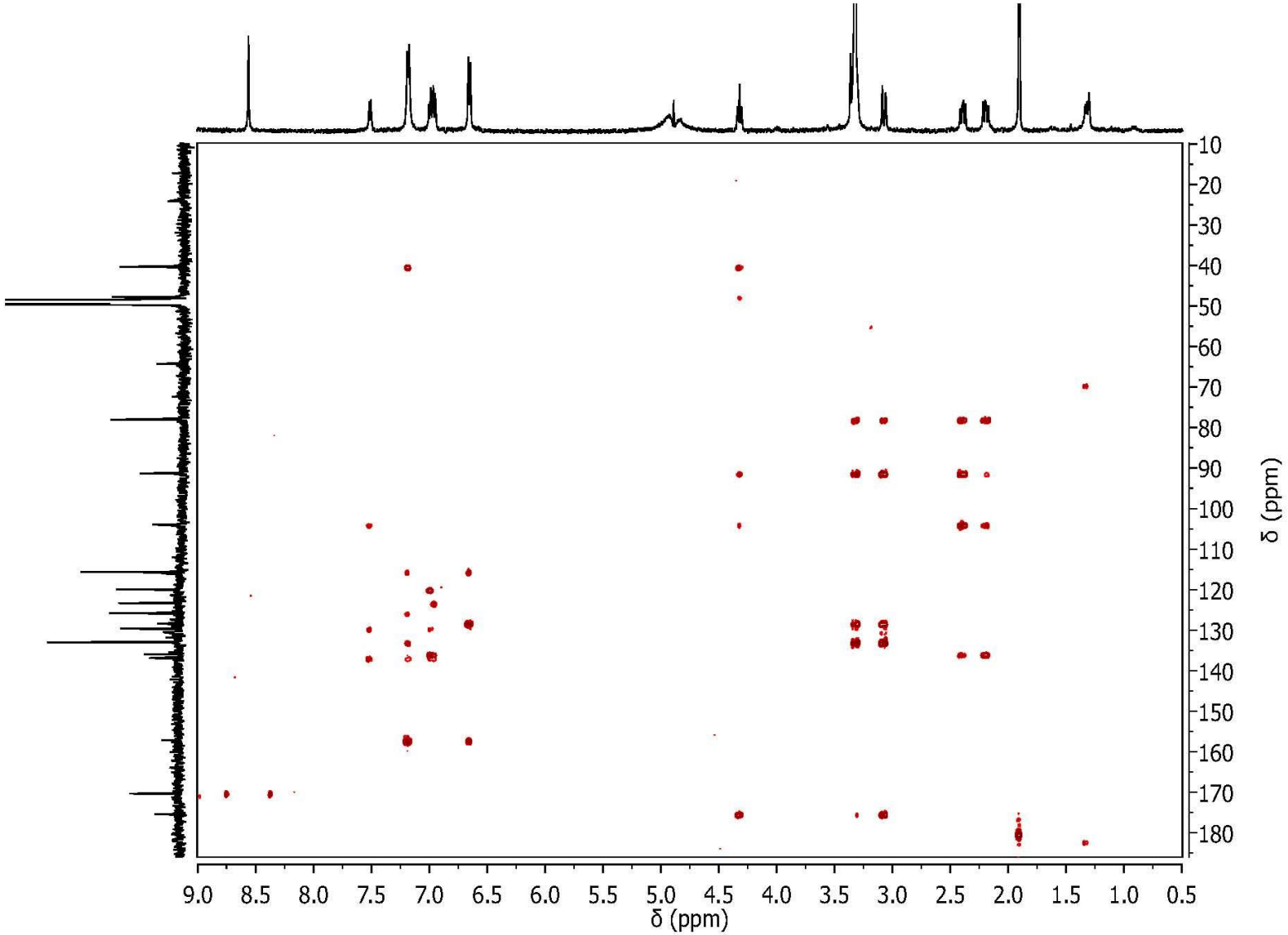

Appendix 39. ^{1}H NMR spectrum of compound **3.9** in CD_3OD (500 MHz)

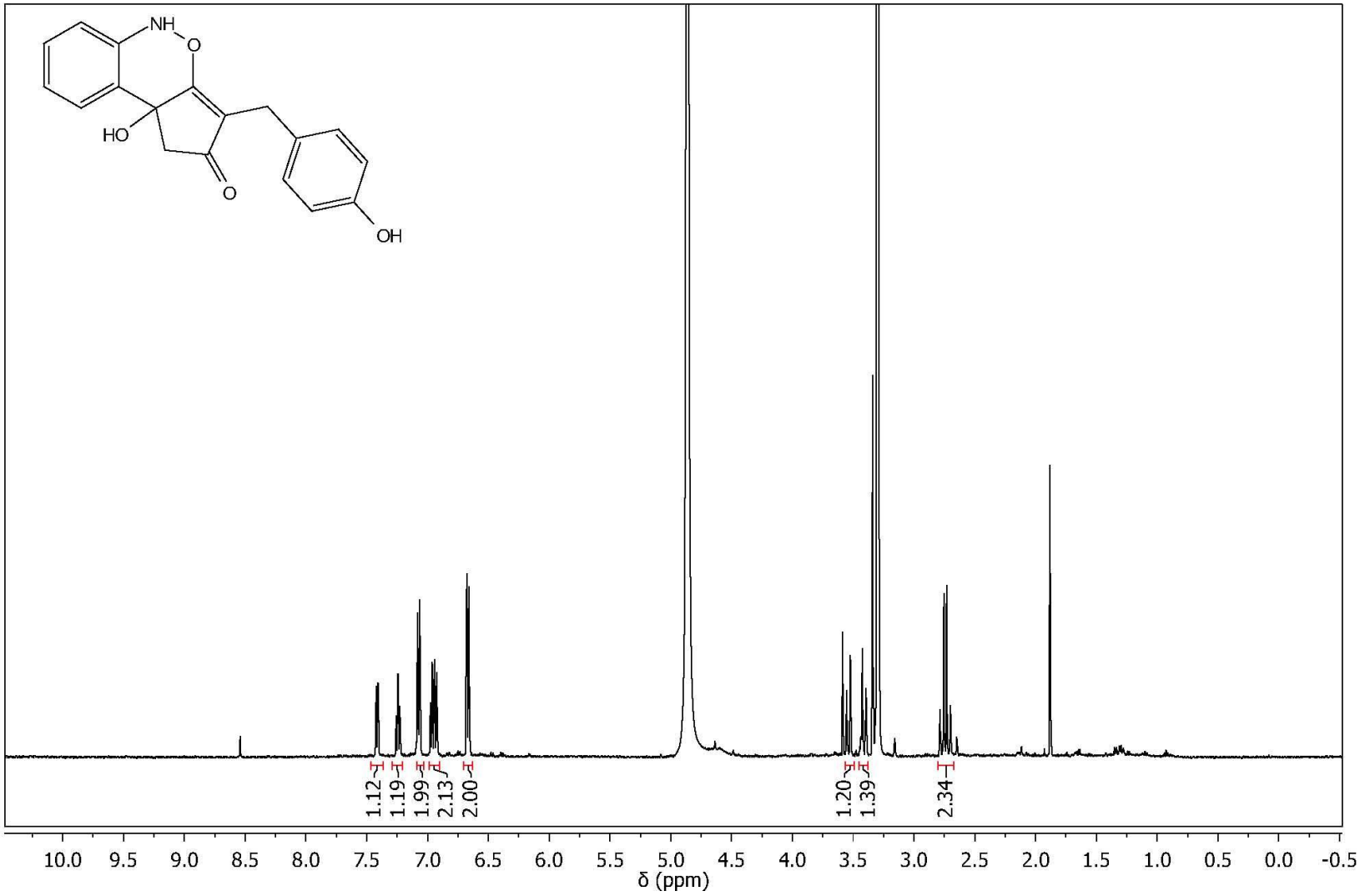

Appendix 40. ^{13}C NMR spectrum of compound **3.9** in CD_3OD (125 MHz)

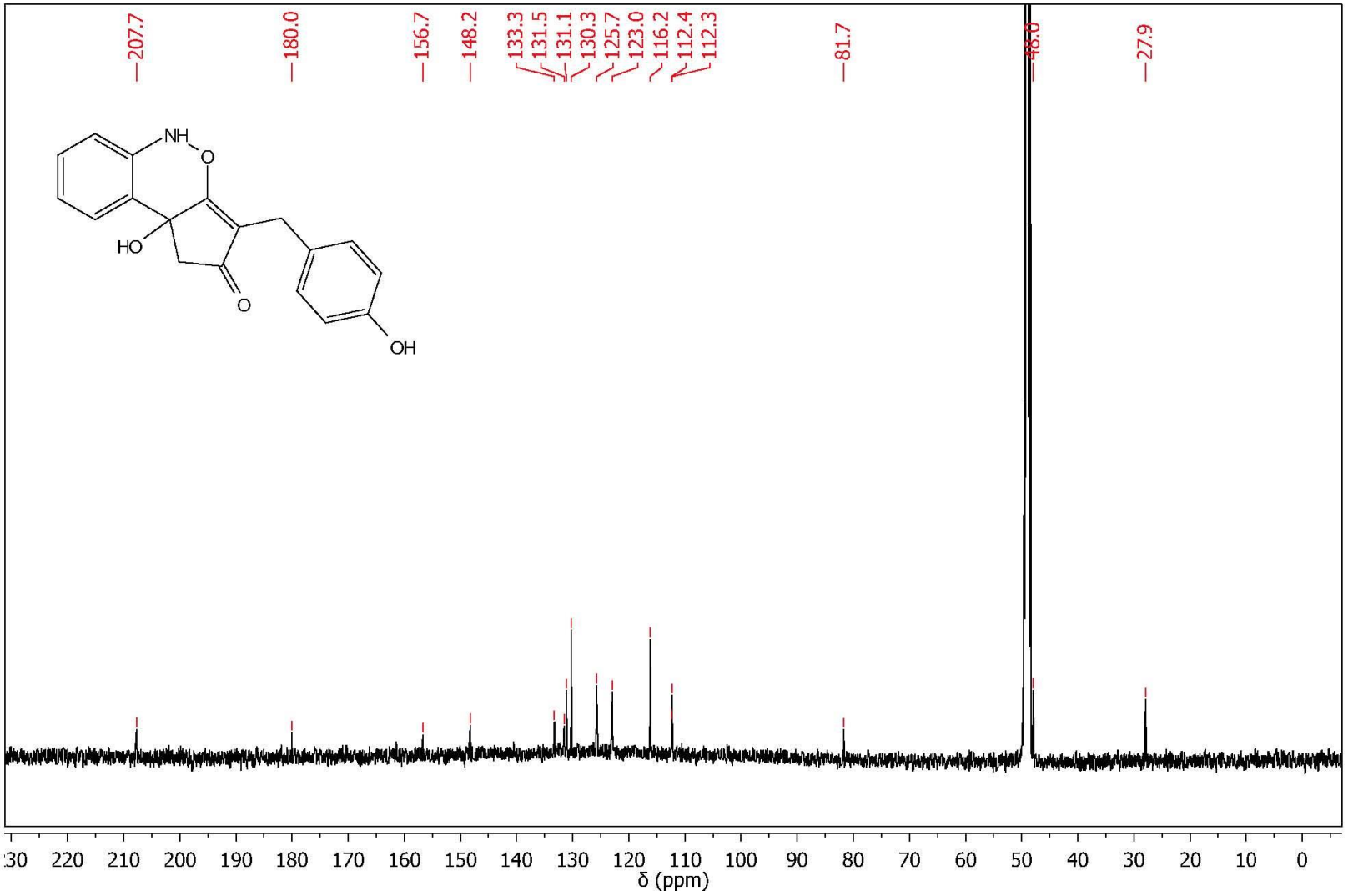

Appendix 41. gHMBC NMR spectrum of compound **3.9** in CD_3OD (500 MHz)

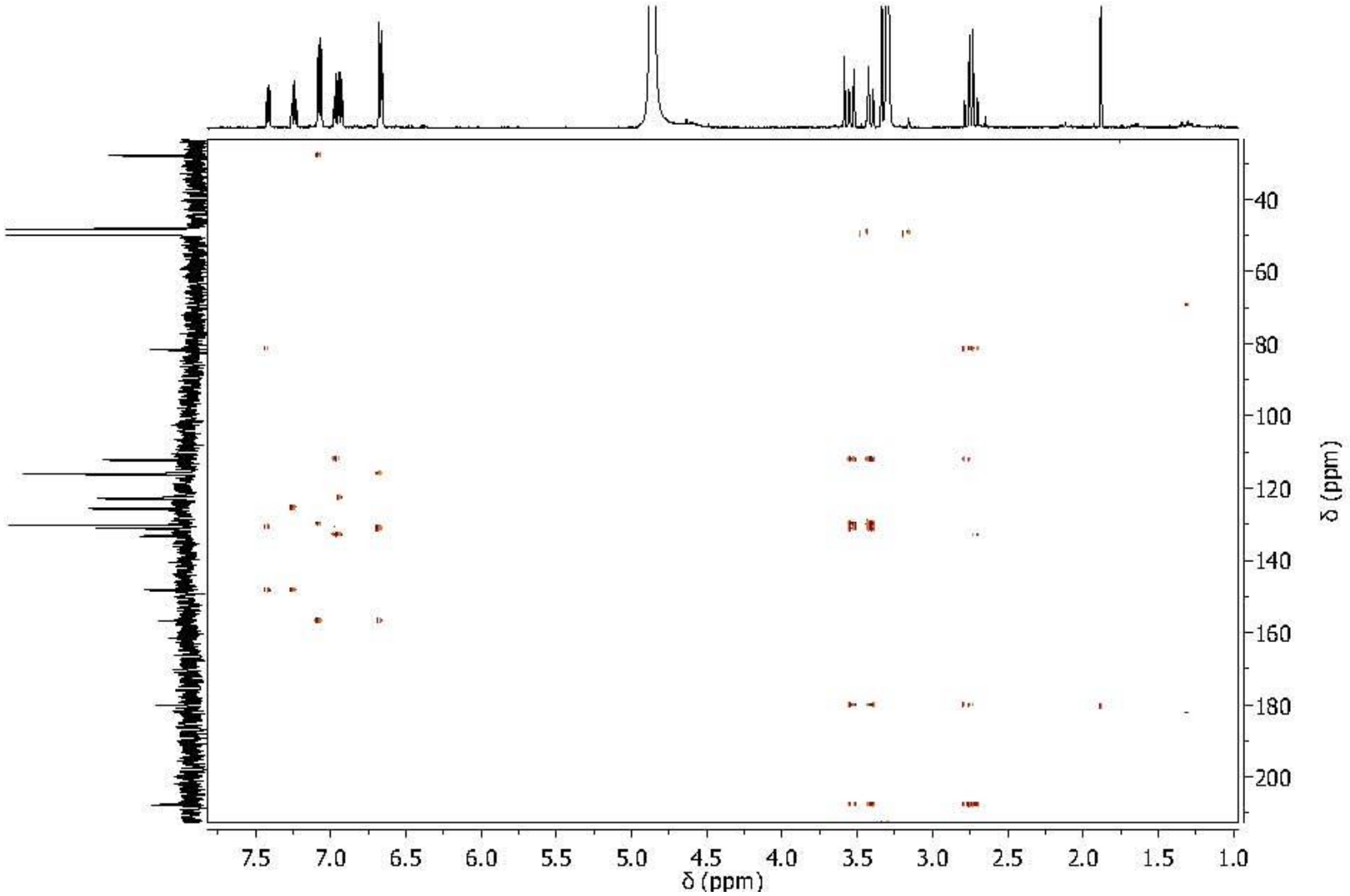

Appendix 42. ^{1}H NMR spectrum of compound **3.10** in CD_3OD (500 MHz)

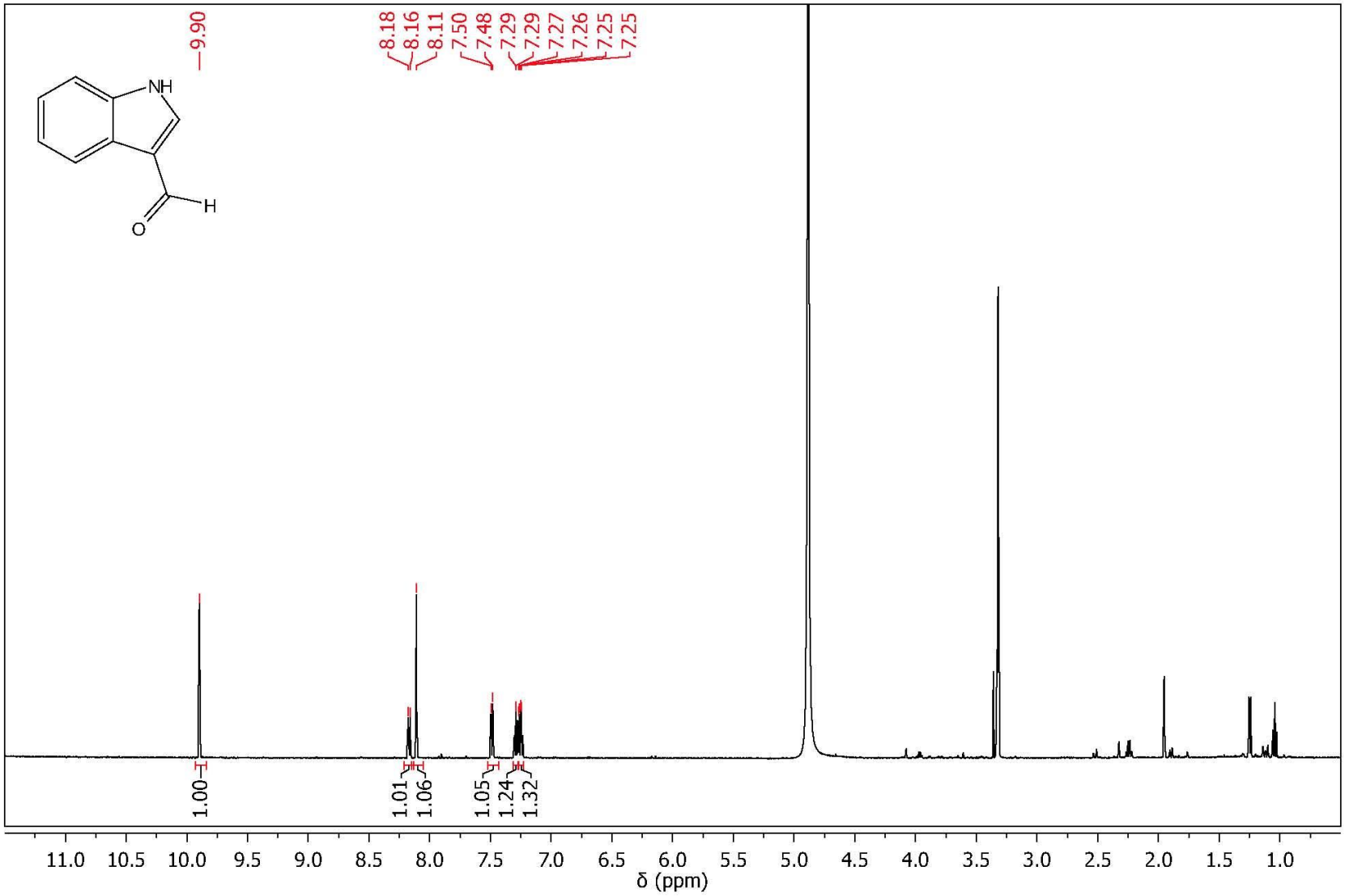

Appendix 43. ^{1}H NMR spectrum of compound **3.11** in CD_3OD (500 MHz)

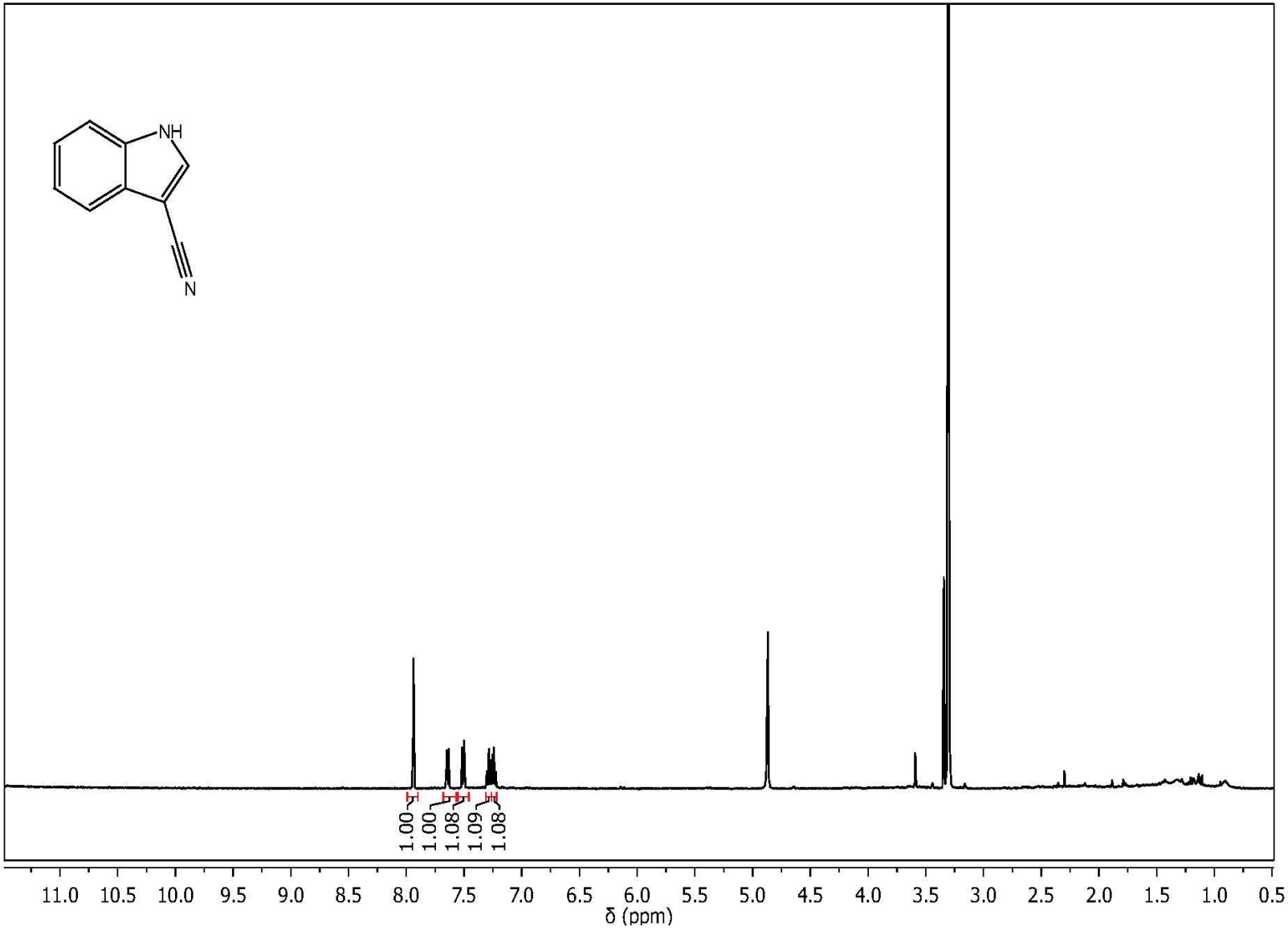

Appendix 44. ^{13}C NMR spectrum of compound **3.11** in CD_3OD (125 MHz)

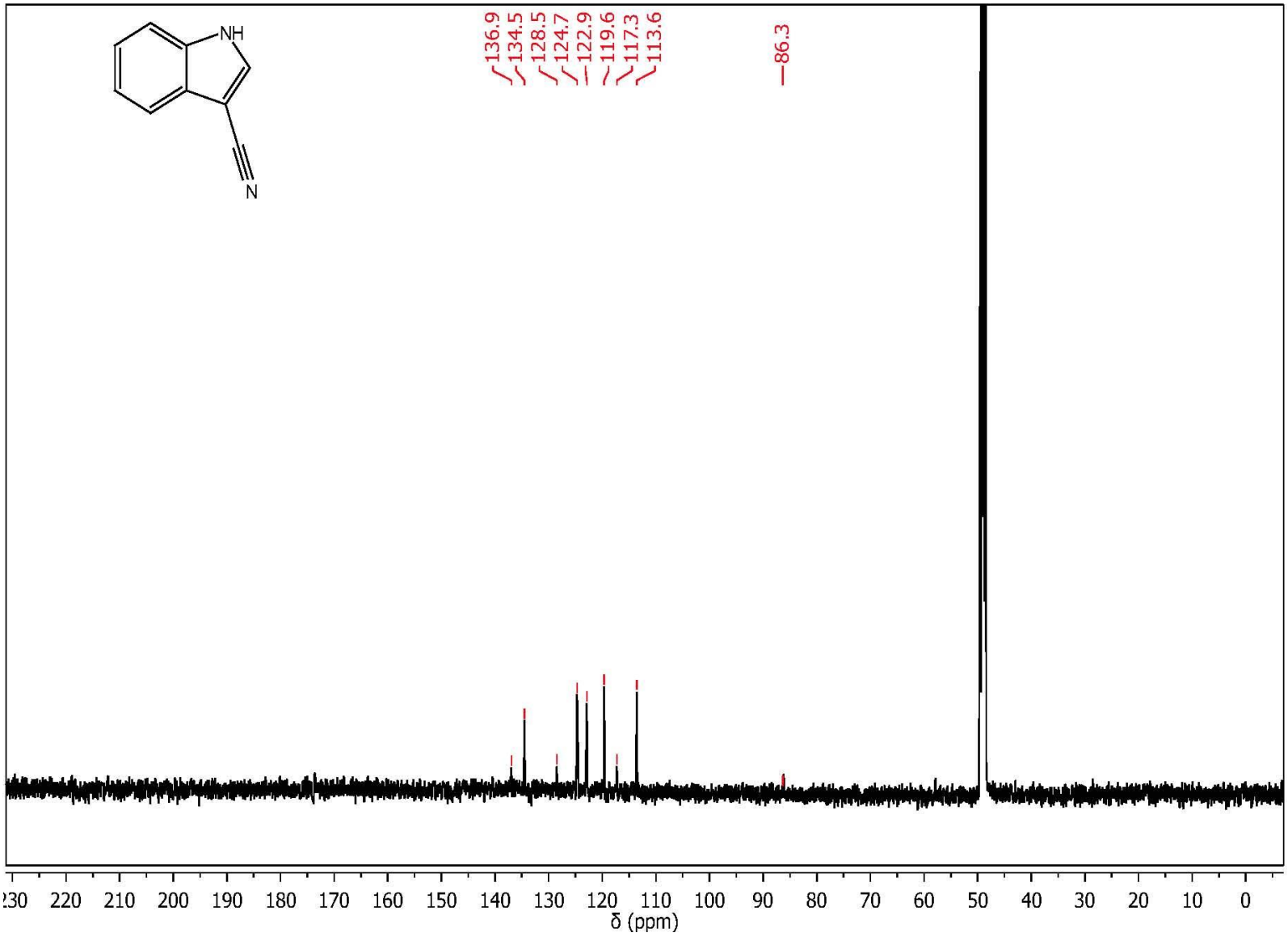

Appendix 45. ^{1}H NMR spectrum of compound **3.12** in CD_3OD (500 MHz)

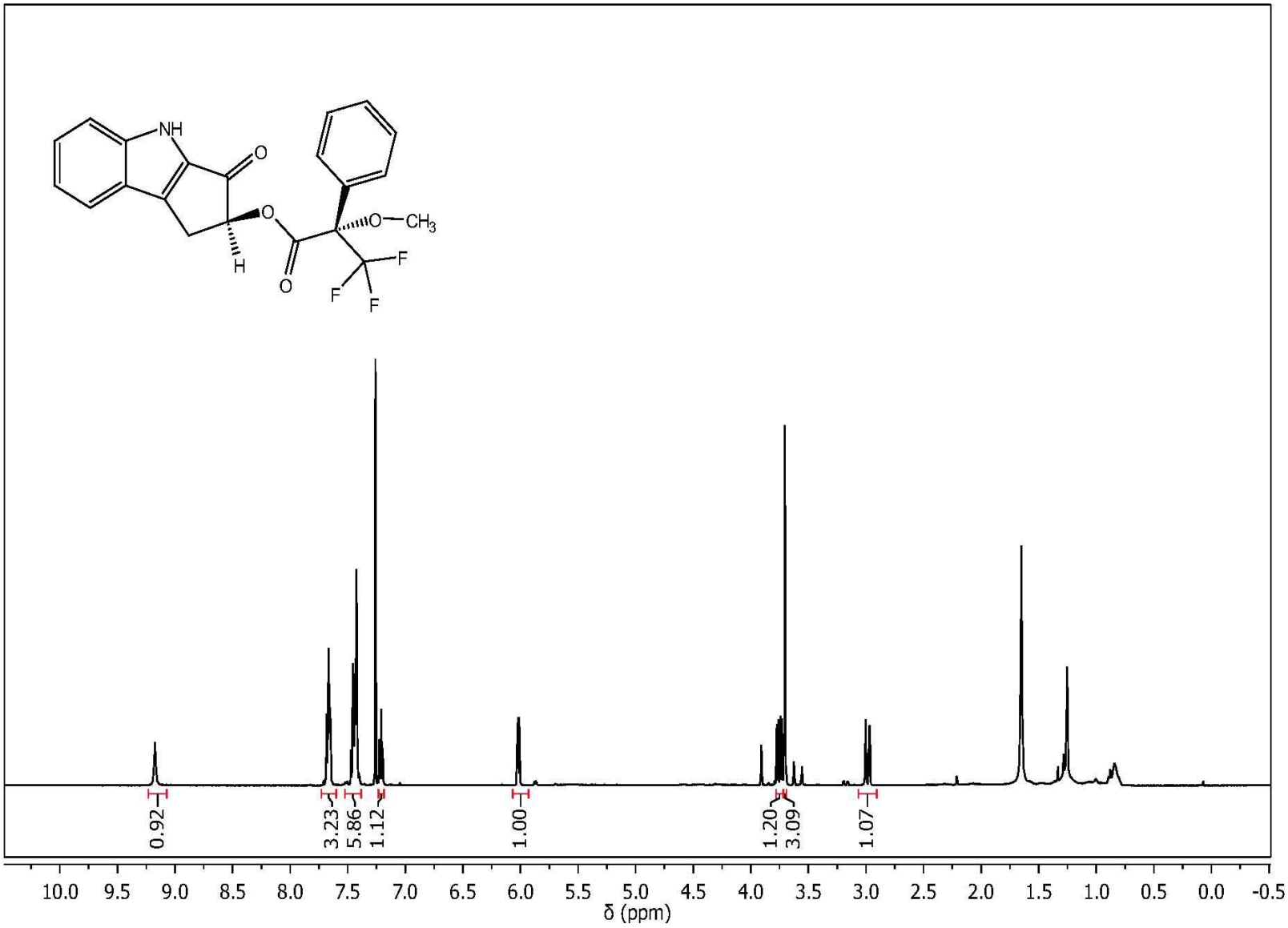

Appendix 46. ^{1}H NMR spectrum of compound **3.13** in CD_3OD (500 MHz)

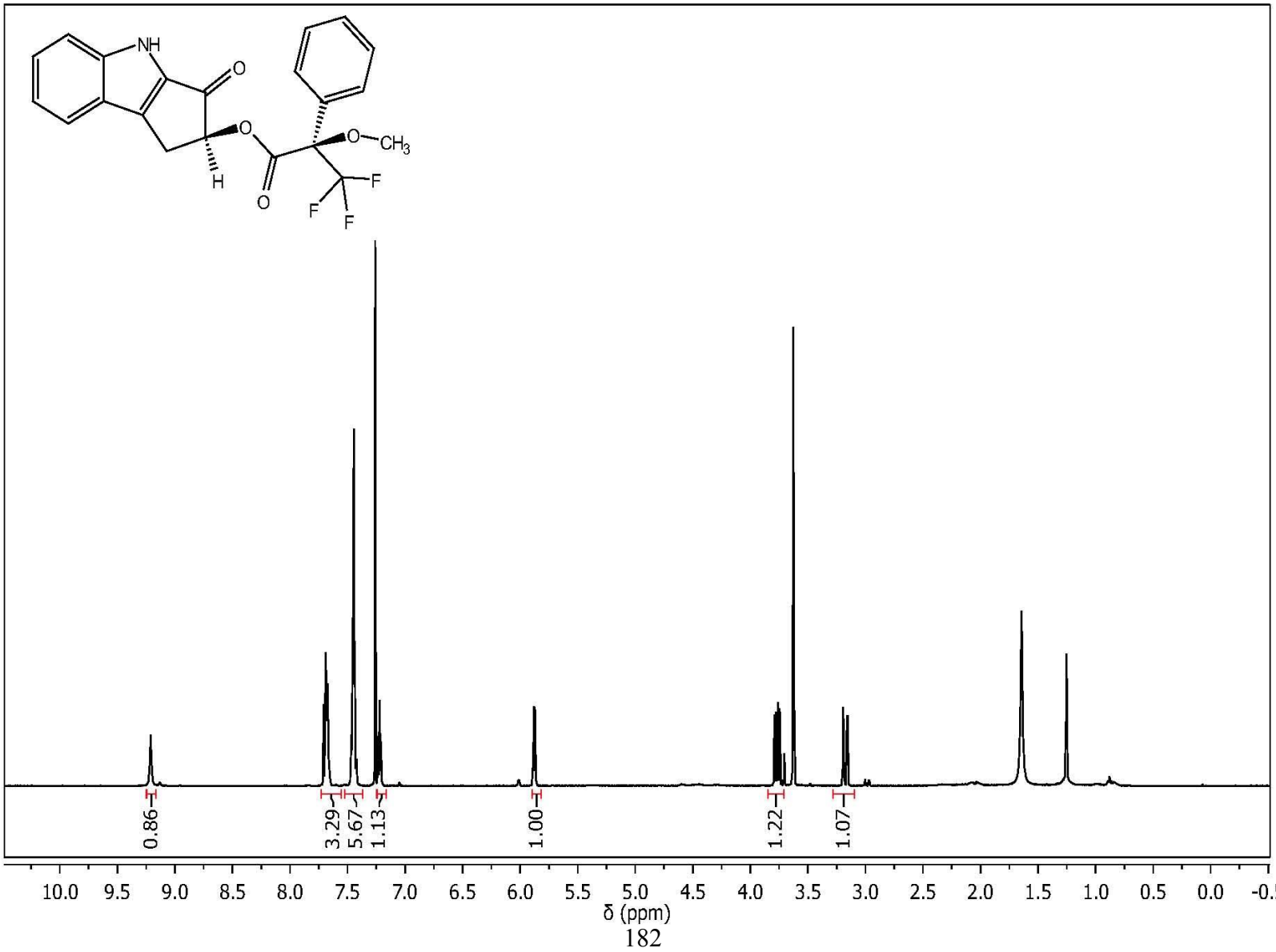

Appendix 47. ^{1}H NMR spectrum of compound **3.14** in CD_3OD (500 MHz)

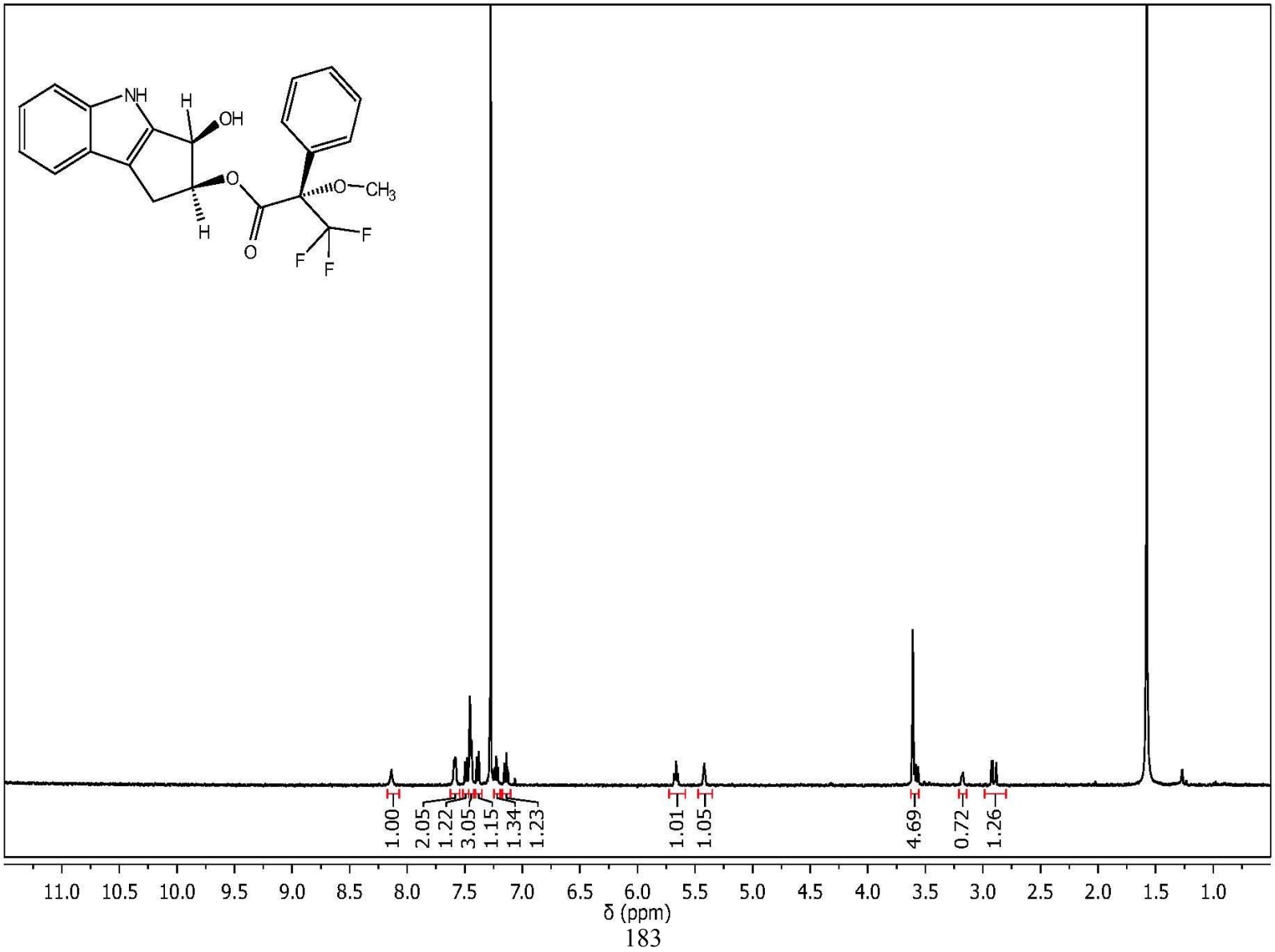

Appendix 48. ^{1}H NMR spectrum of compound **3.15** in CD_3OD (500 MHz)

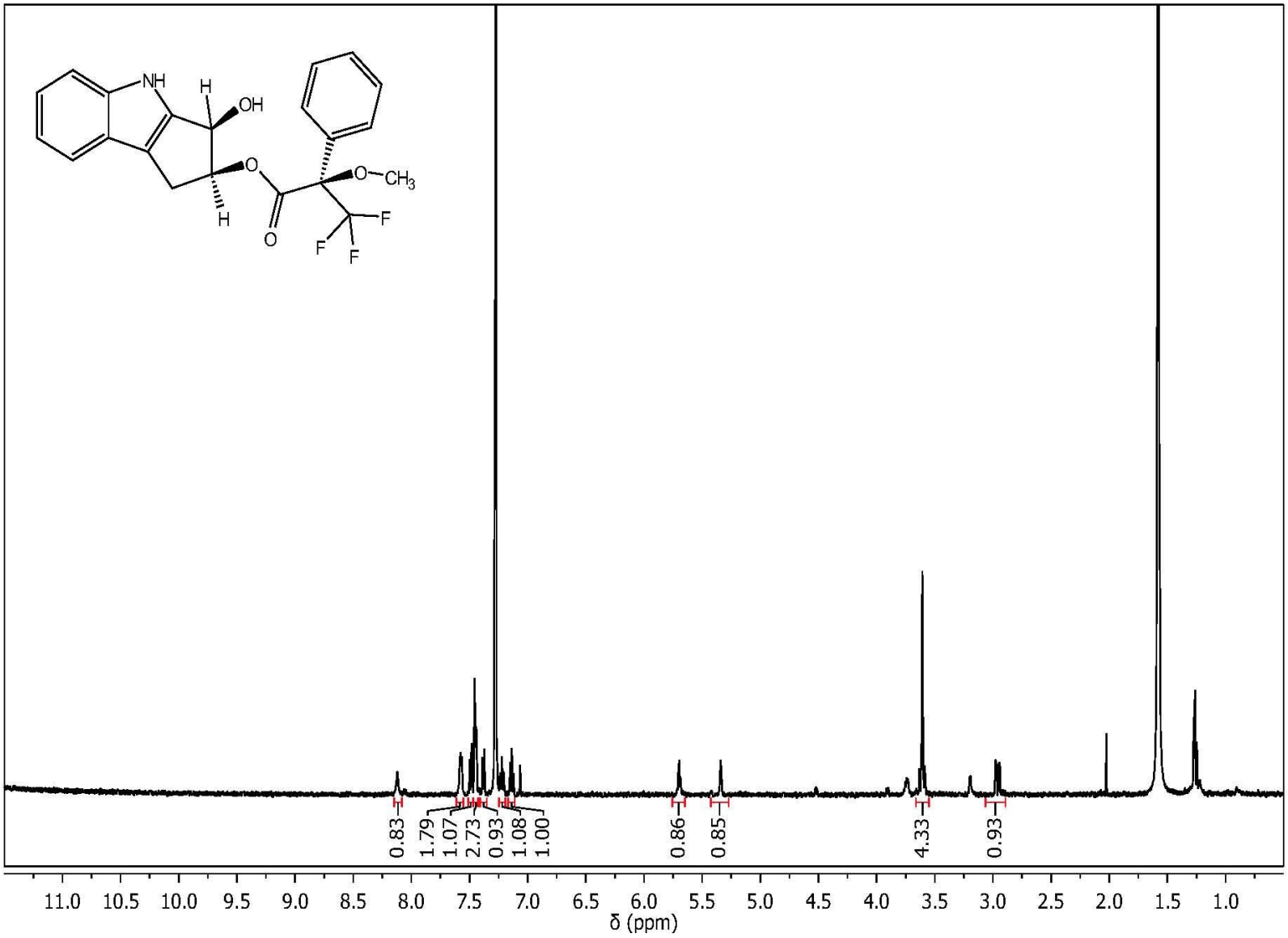

Appendix 49. ^{1}H NMR spectrum of compound **3.7-F$_3$** in $CDCl_3$ (500 MHz)

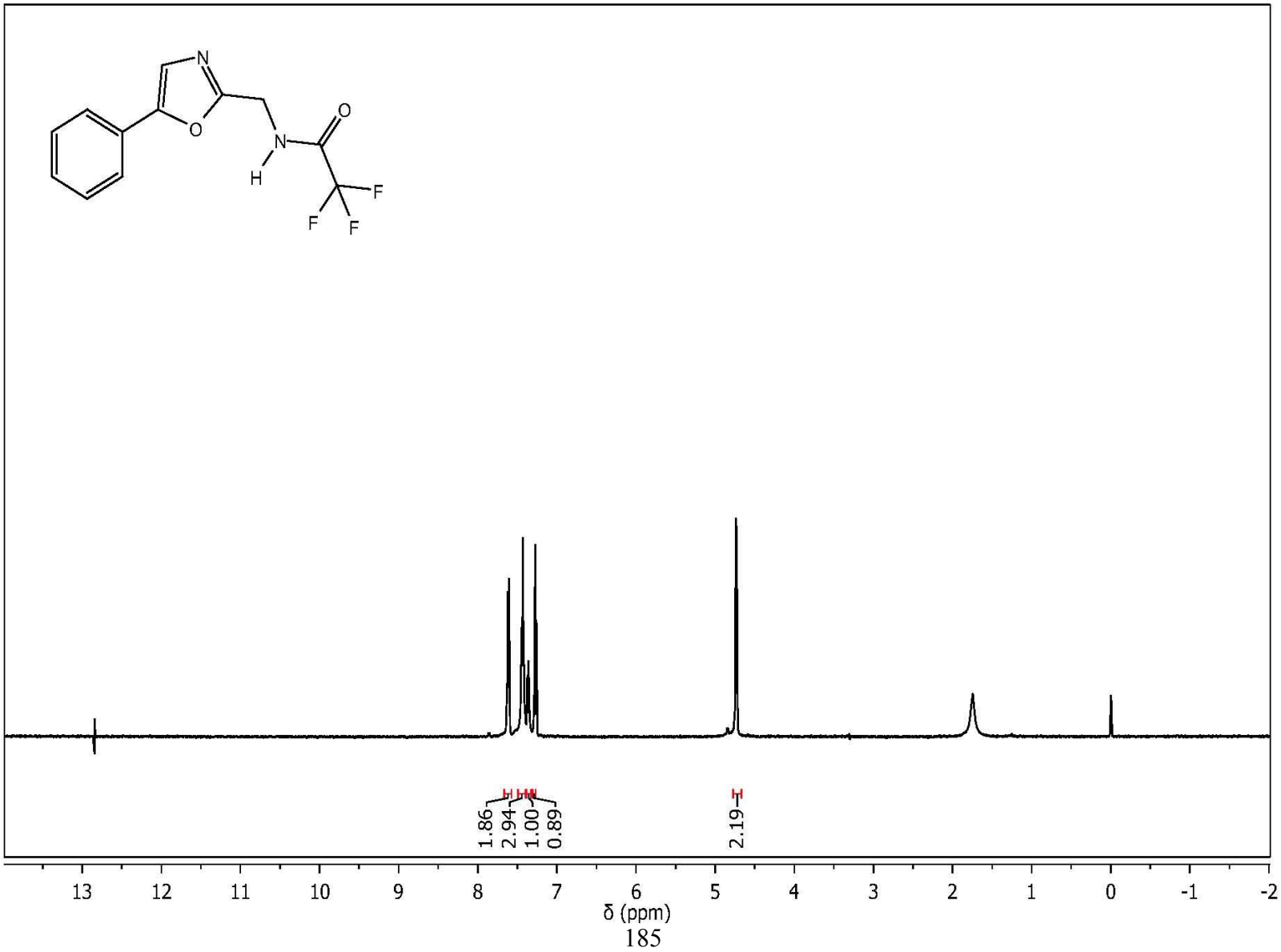

Appendix 50. ^{13}C NMR spectrum of compound **3.7-F$_3$** in $CDCl_3$ (125 MHz)

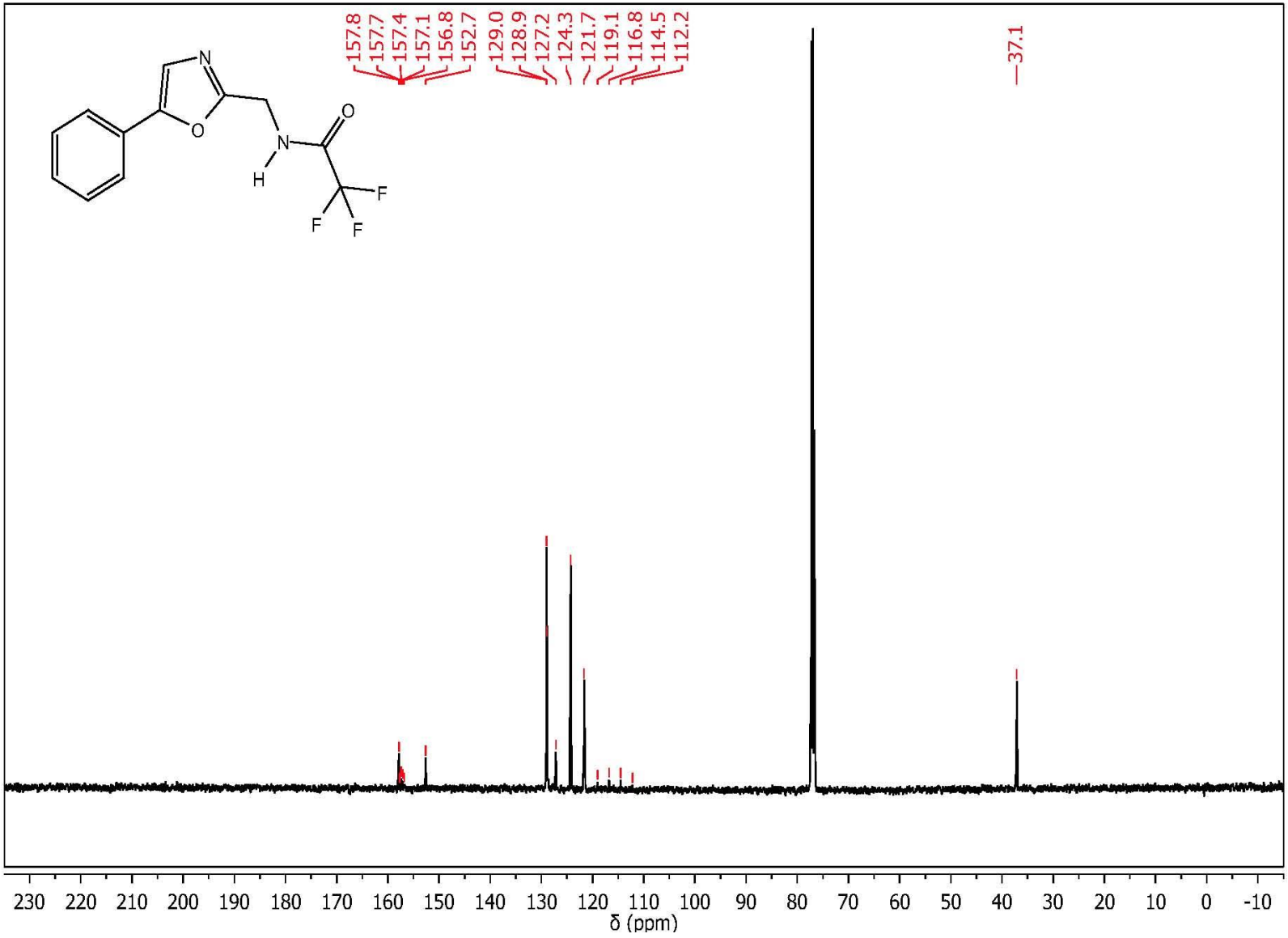

Appendix 51. ^{1}H NMR spectrum of catechin **4.5** in CD_3OD (500 MHz)

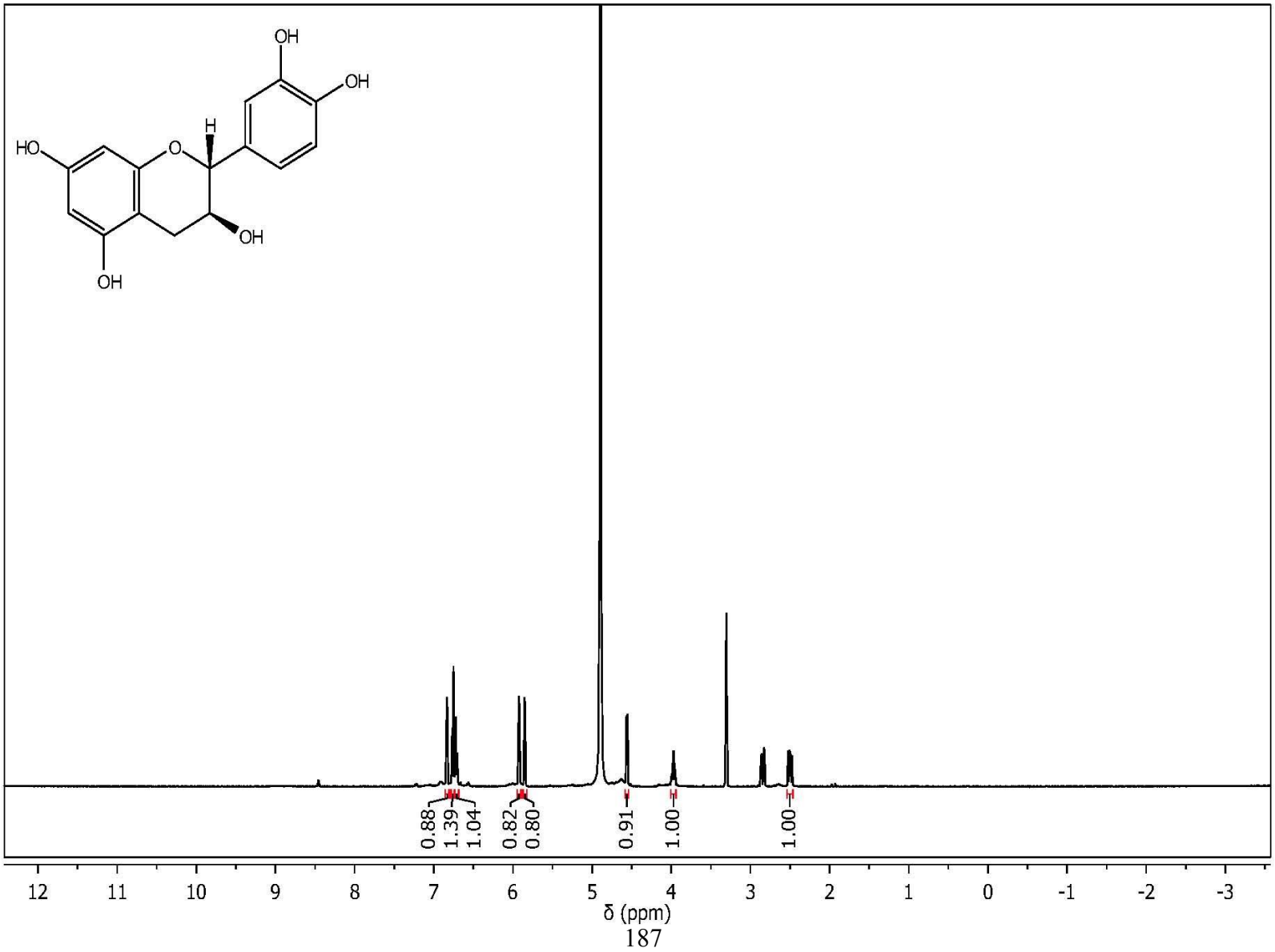

Appendix 52. Stacked ^{1}H NMR spectra from attempts to polymerize catechin **4.5** in 15% acetonitrile in water

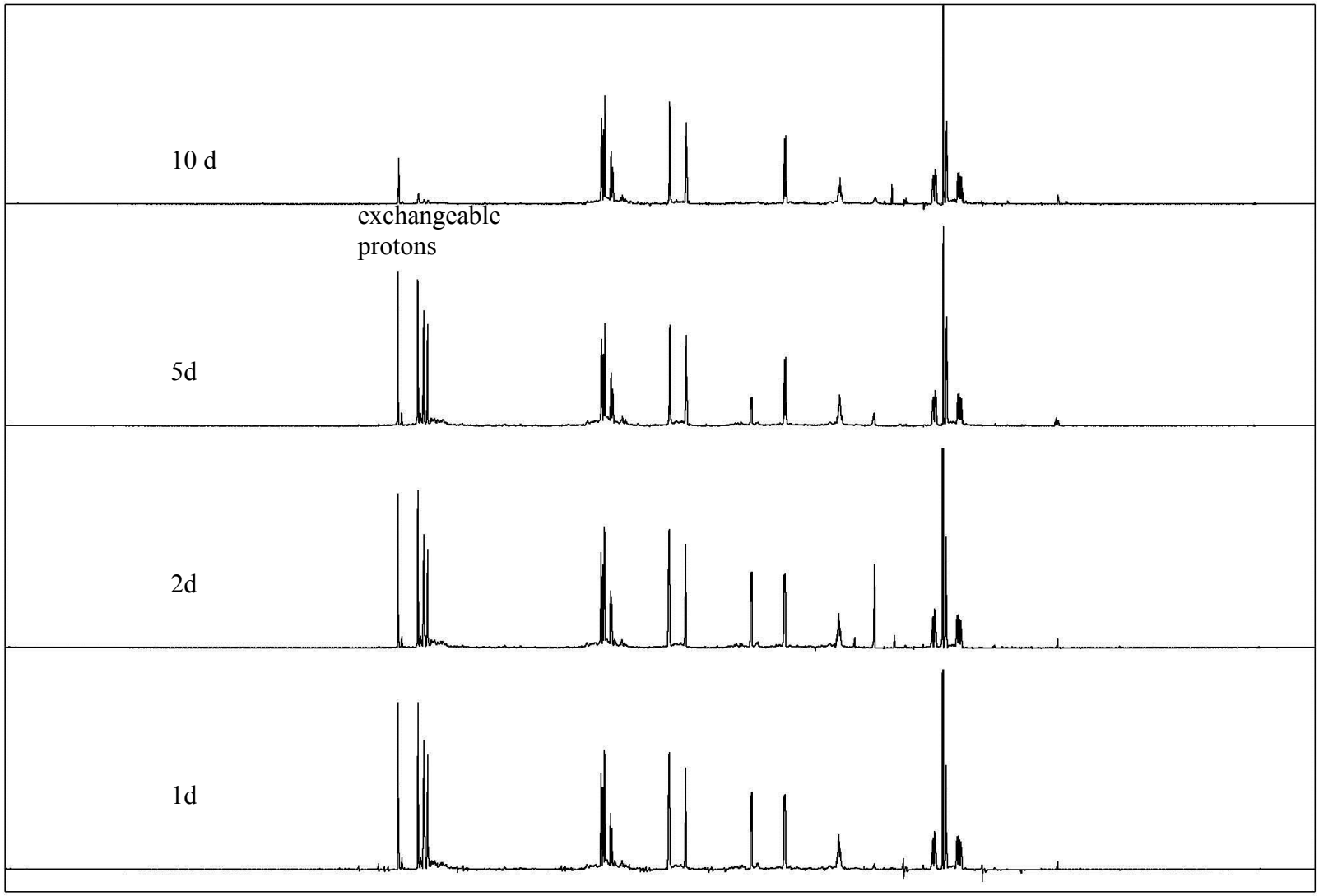

Appendix 53. Stacked ^{1}H NMR spectra from attempts to polymerize catechin **4.5** in 15% acetonitrile in water (with 0.1% formic acid)

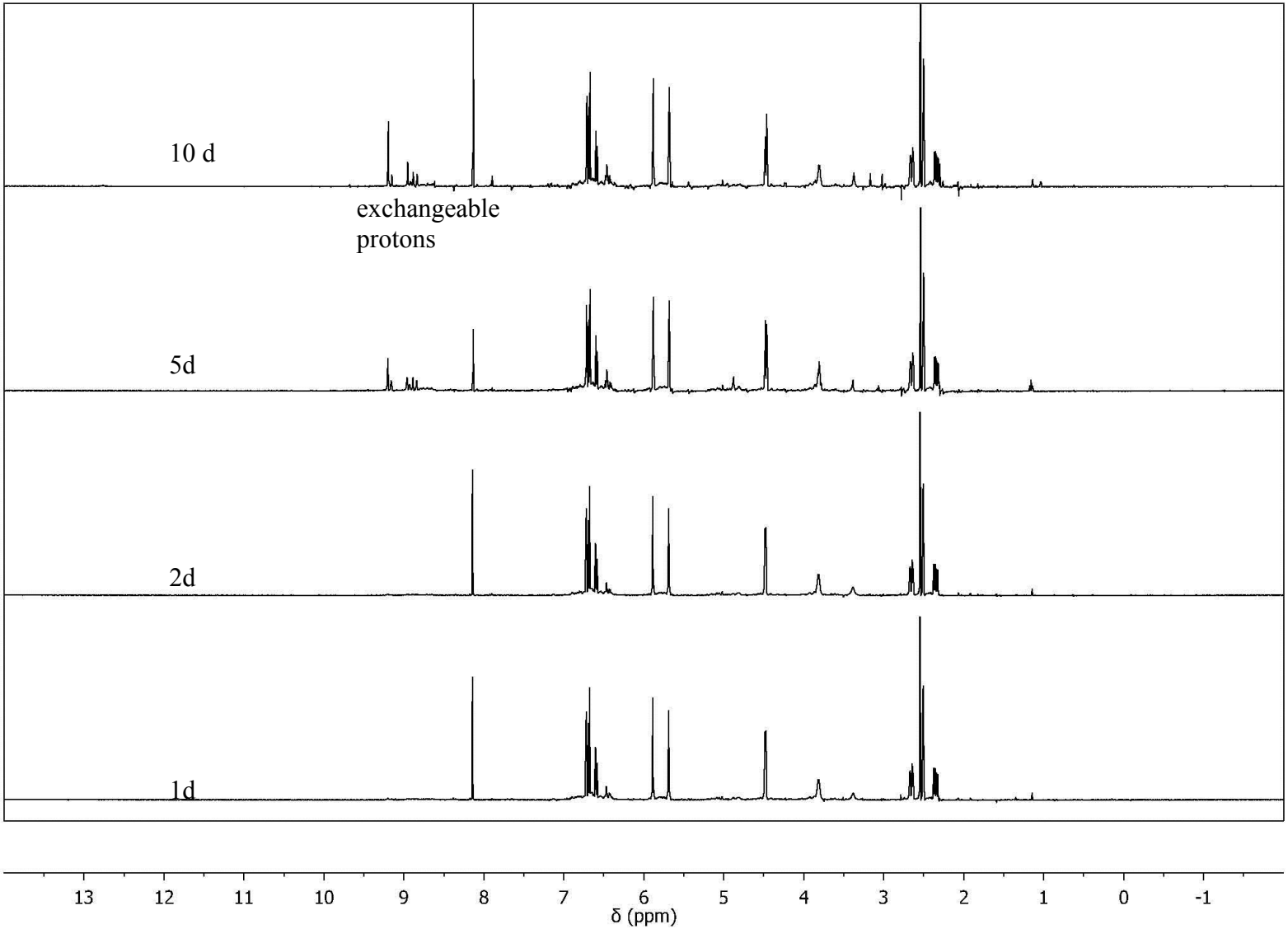

Appendix 54. Stacked ^{1}H NMR spectra from attempts to polymerize catechin **4.5** in 30% acetonitrile in water (with 0.1% formic acid)

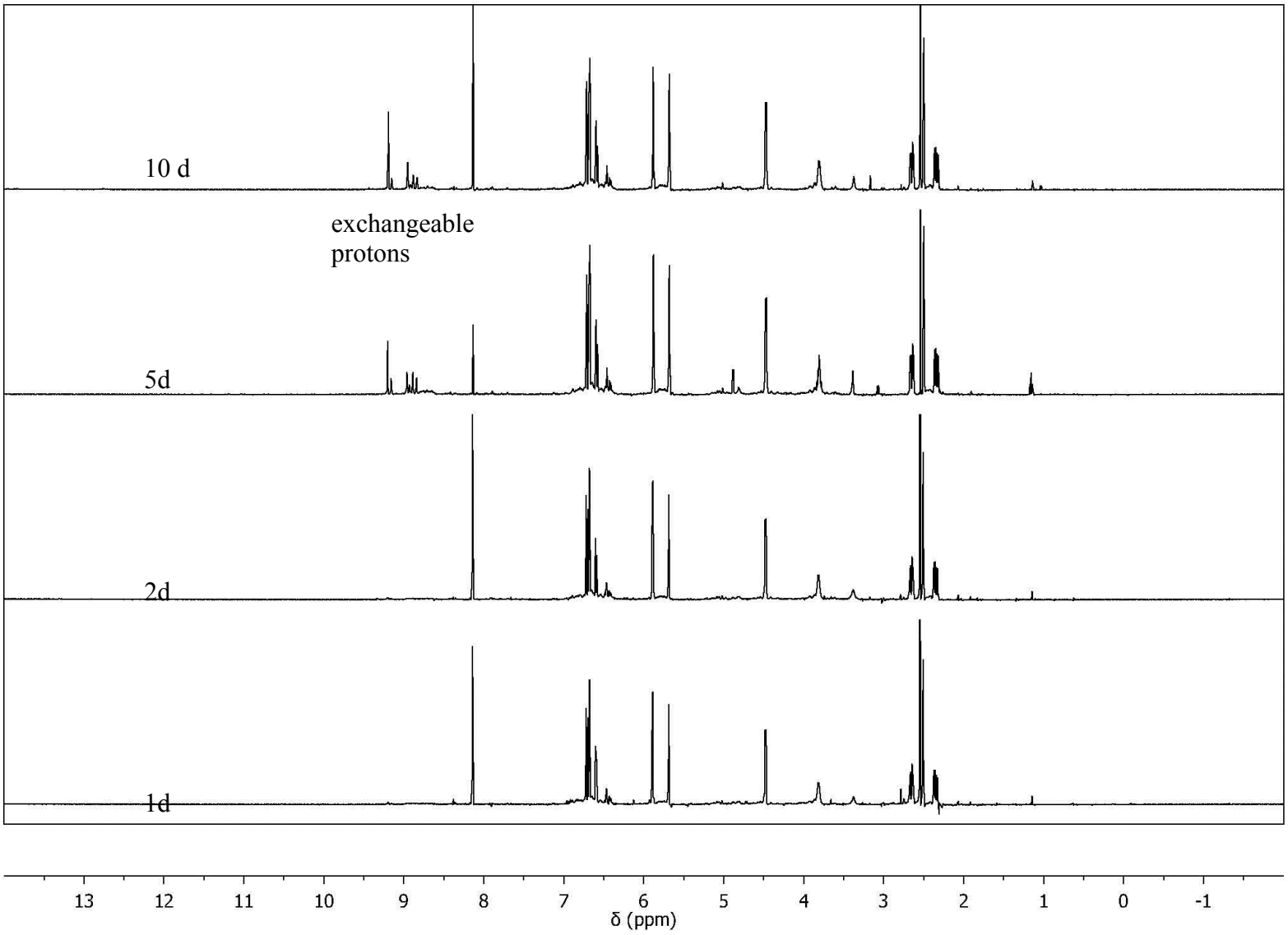

Appendix 55. ^{1}H NMR spectrum after methylation of dialyzed aqueous Areca extract (RPN-3-145-2) in $CDCl_3$ (500 MHz)

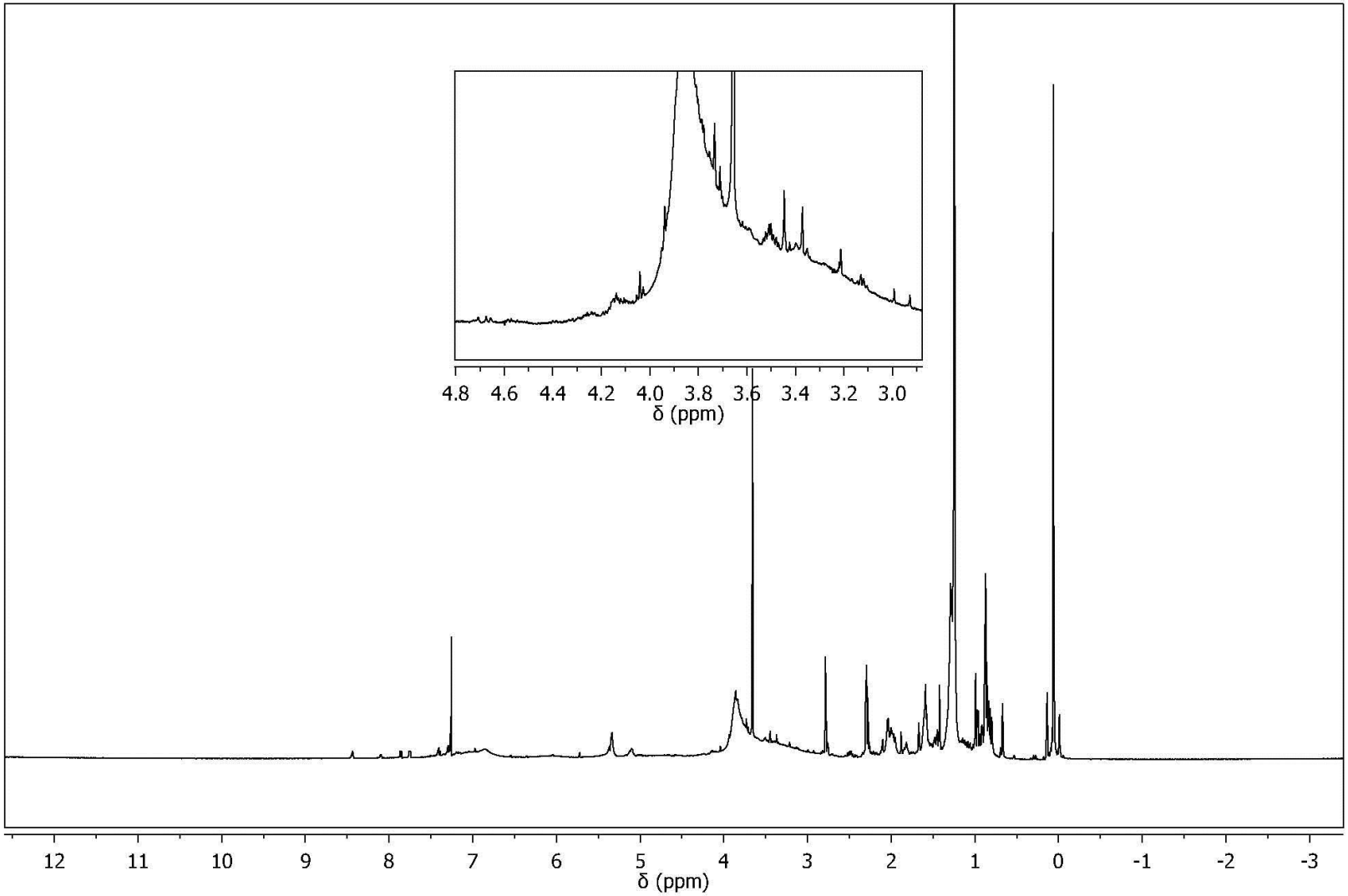

Appendix 56. ^{1}H NMR spectrum of β-sitosterol **4.18** in $CDCl_3$ (500 MHz)

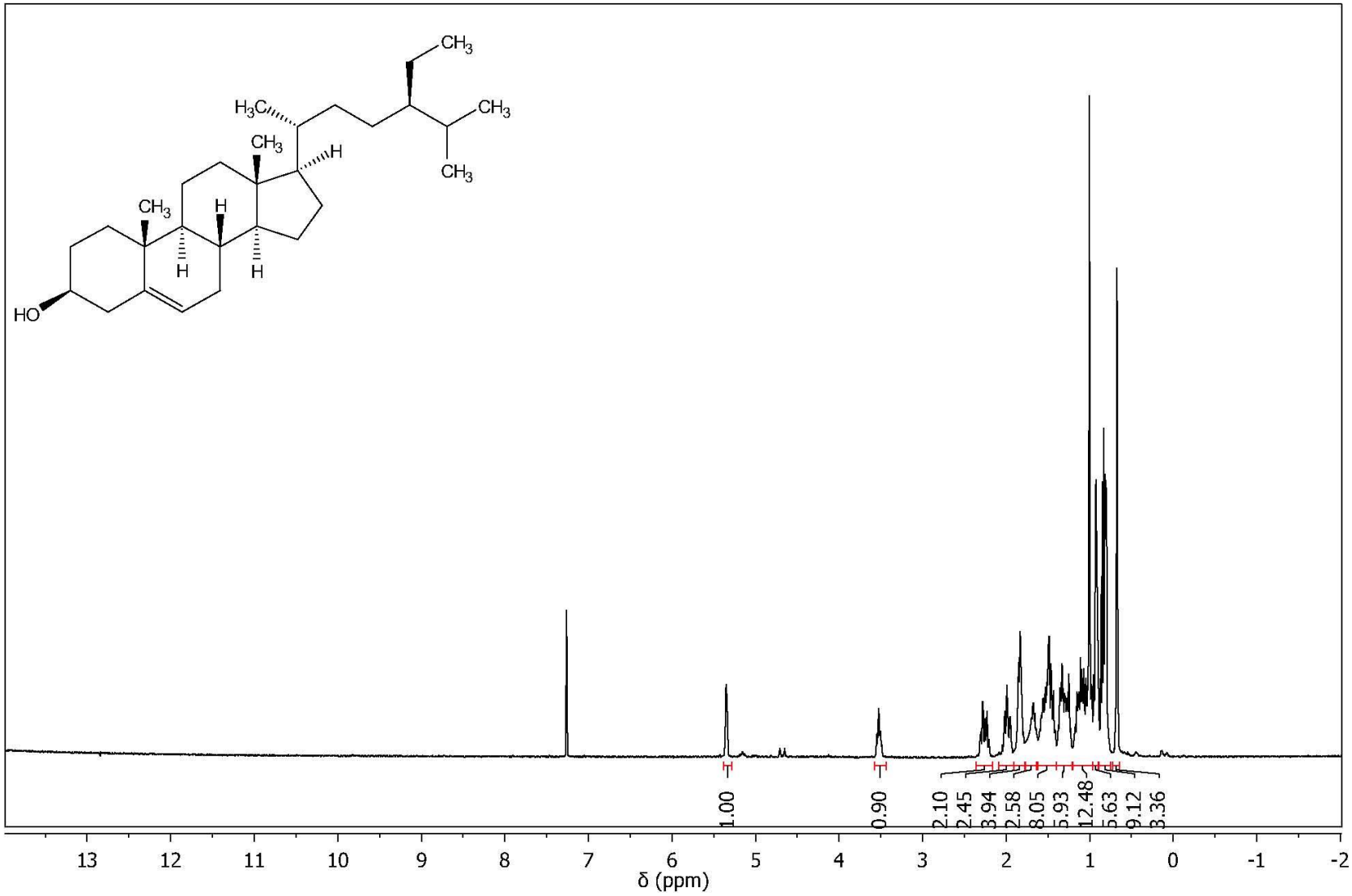

Appendix 57. ^{13}C NMR spectrum of β-sitosterol **4.18** in $CDCl_3$ (125 MHz)

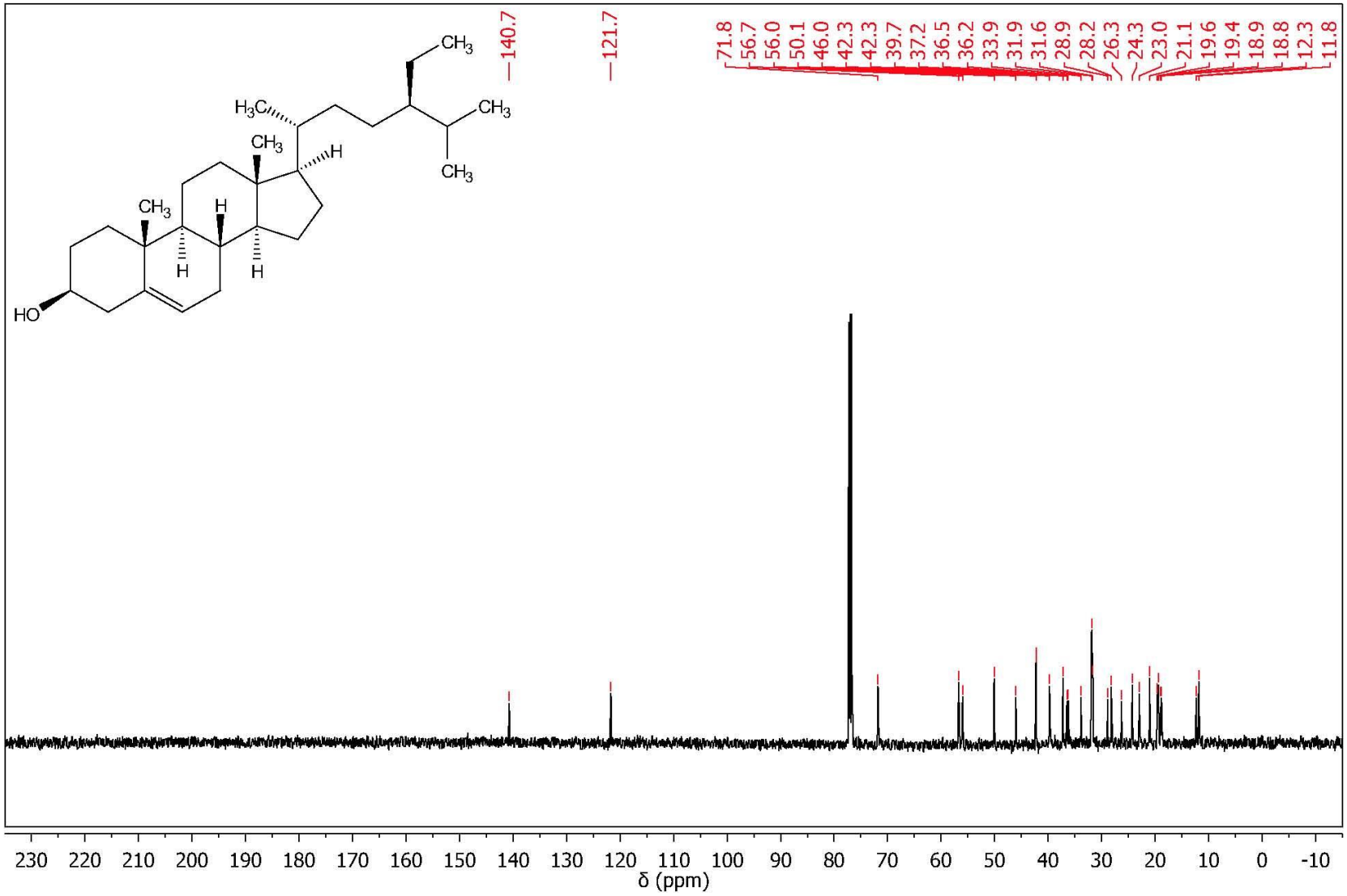

Appendix 58. ^{1}H NMR spectrum of callyspongynic acid **5.1** in $CDCl_3$ (500 MHz)

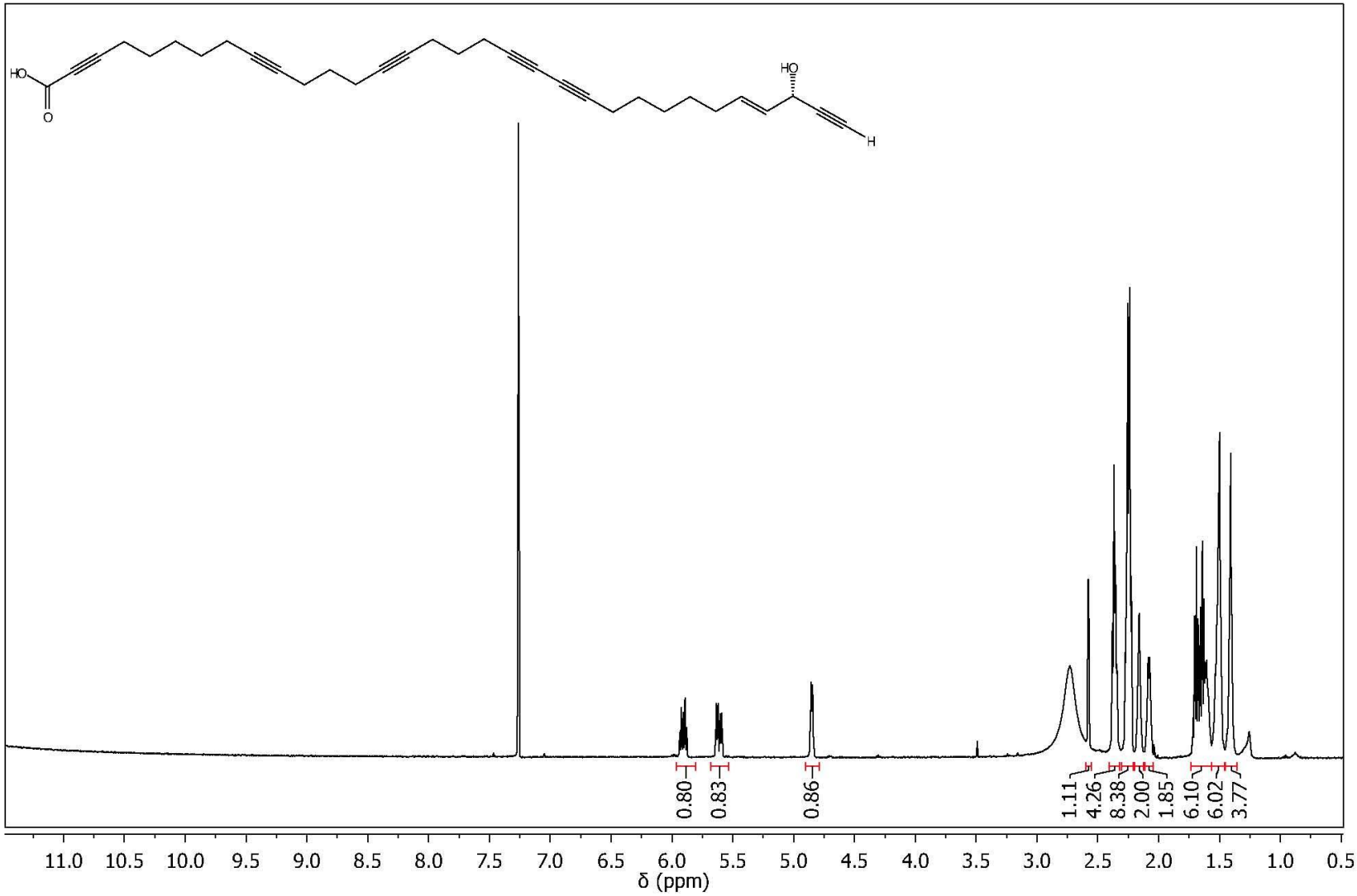

Appendix 59. ^{13}C NMR spectrum of callyspongynic acid **5.1** in $CDCl_3$ (125 MHz)

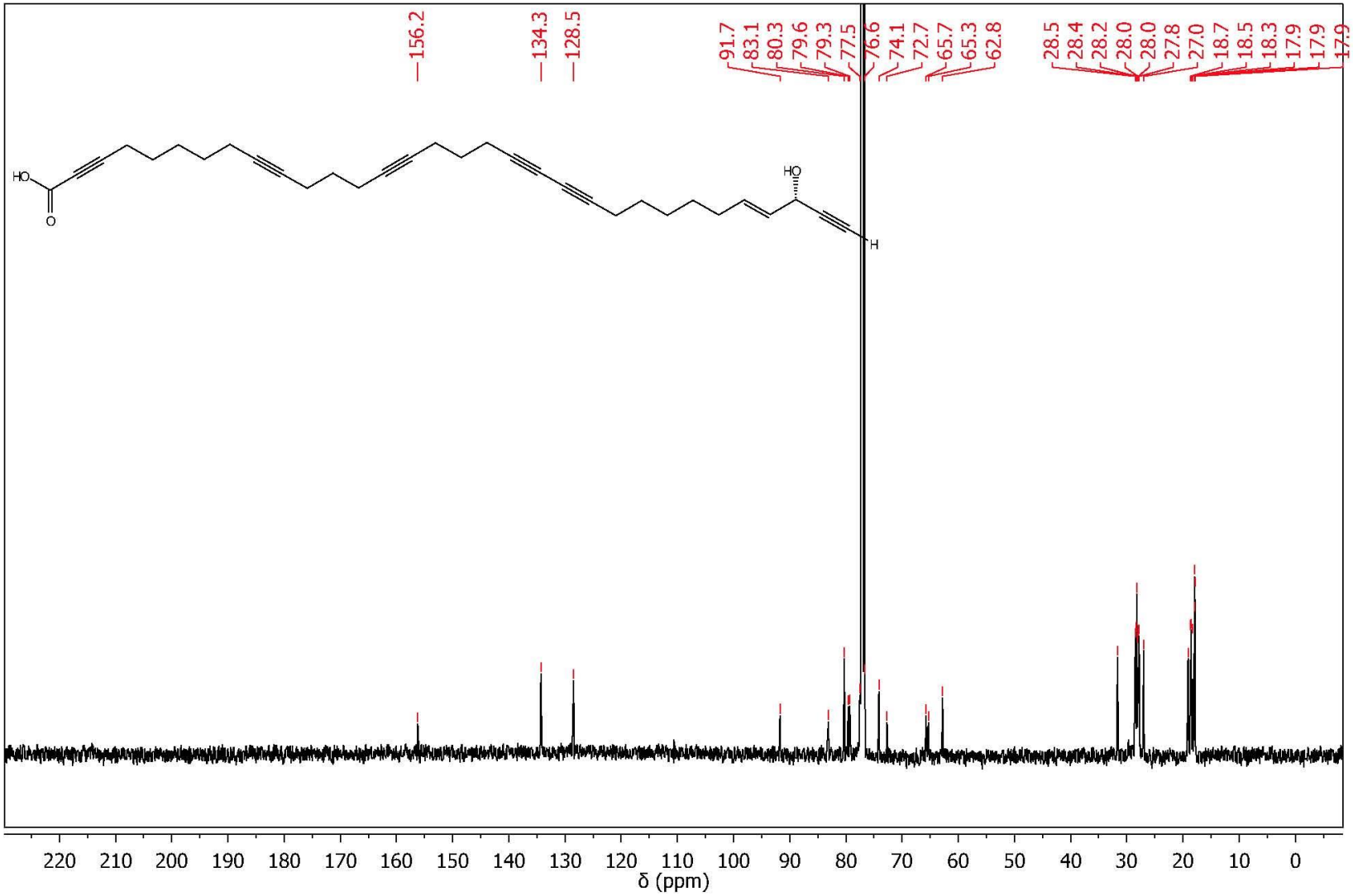

Appendix 60. ^{1}H NMR spectrum of psammaplysin A **5.2** in CD_3OD (500 MHz)

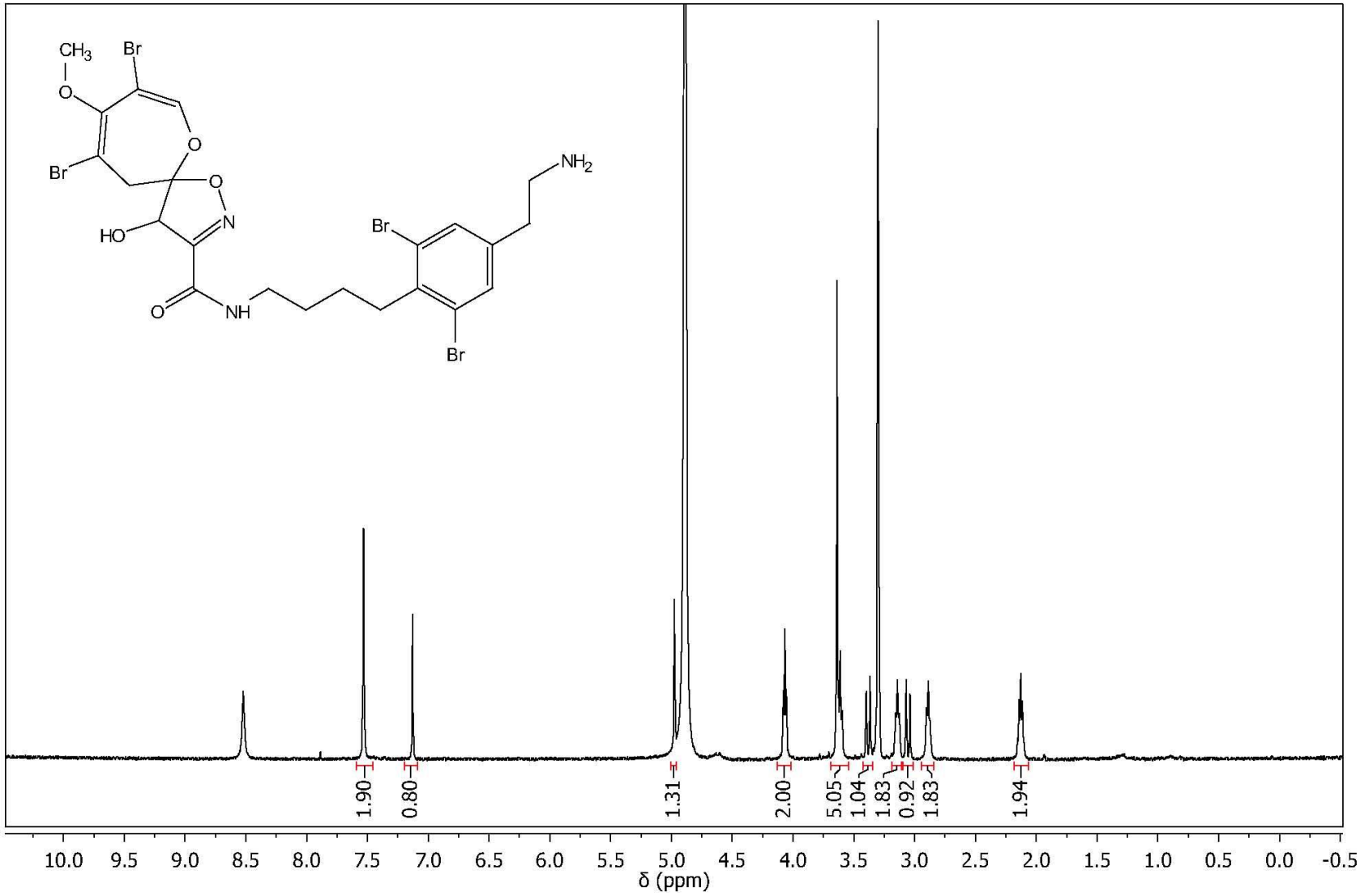

Appendix 61. ^{13}C NMR spectrum of psammaplysin A **5.2** in CD_3OD (125 MHz)

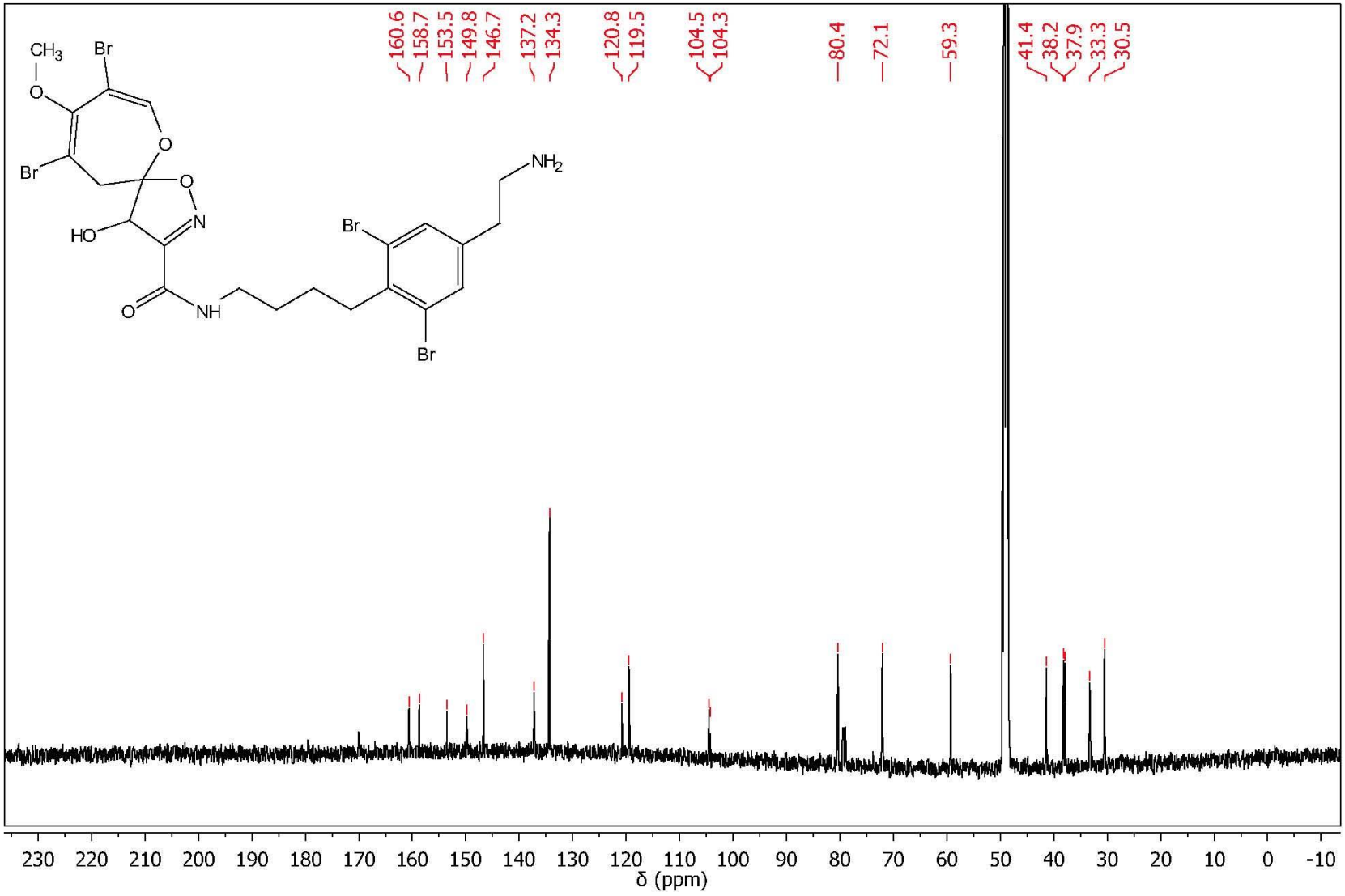

Appendix 62. ^{1}H NMR spectrum of fischerellin A **5.3** in $CDCl_3$ (500 MHz)

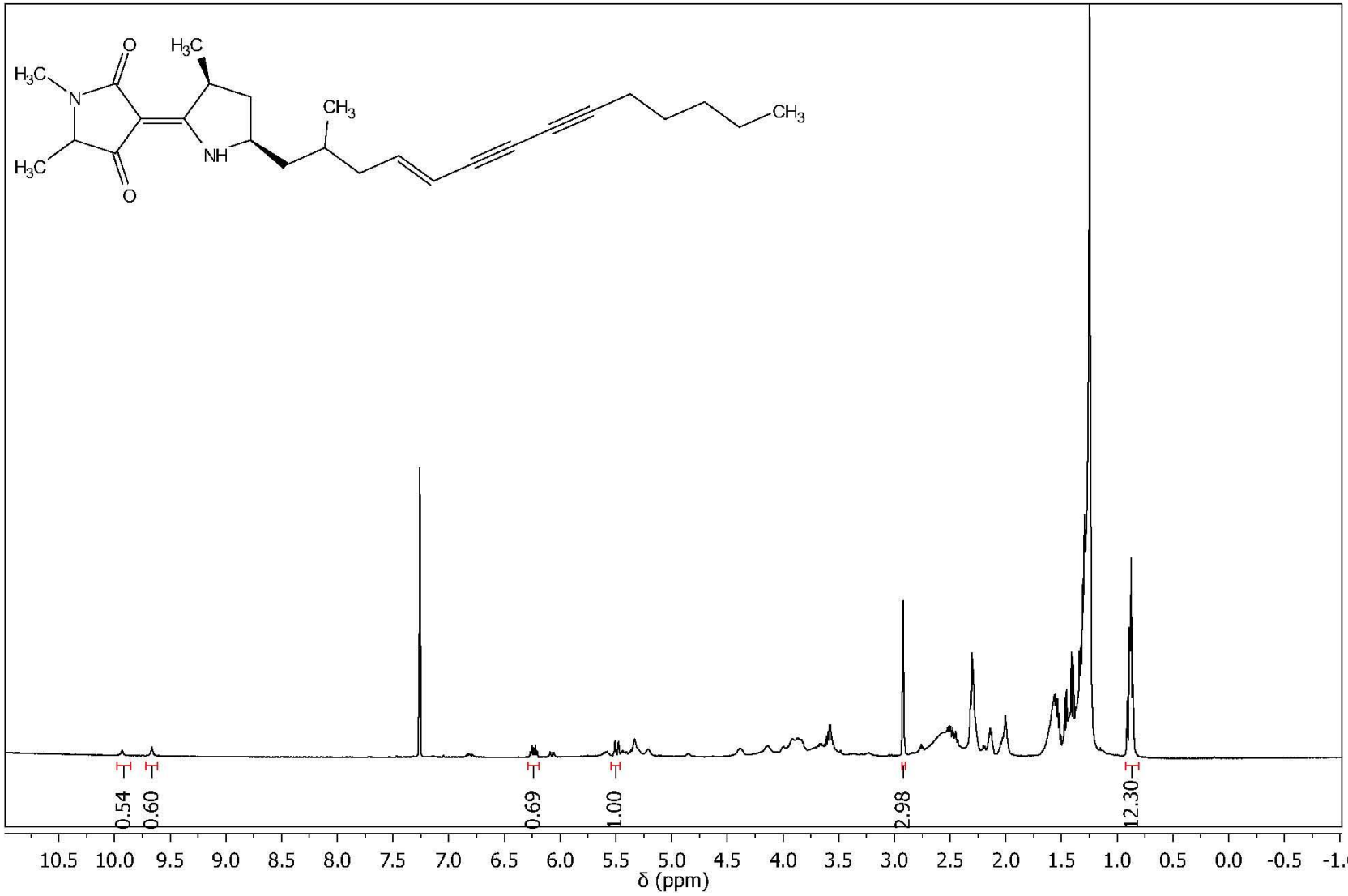

Appendix 63. ^{1}H NMR spectrum of fischerellin B **5.4** in $CDCl_3$ (500 MHz)

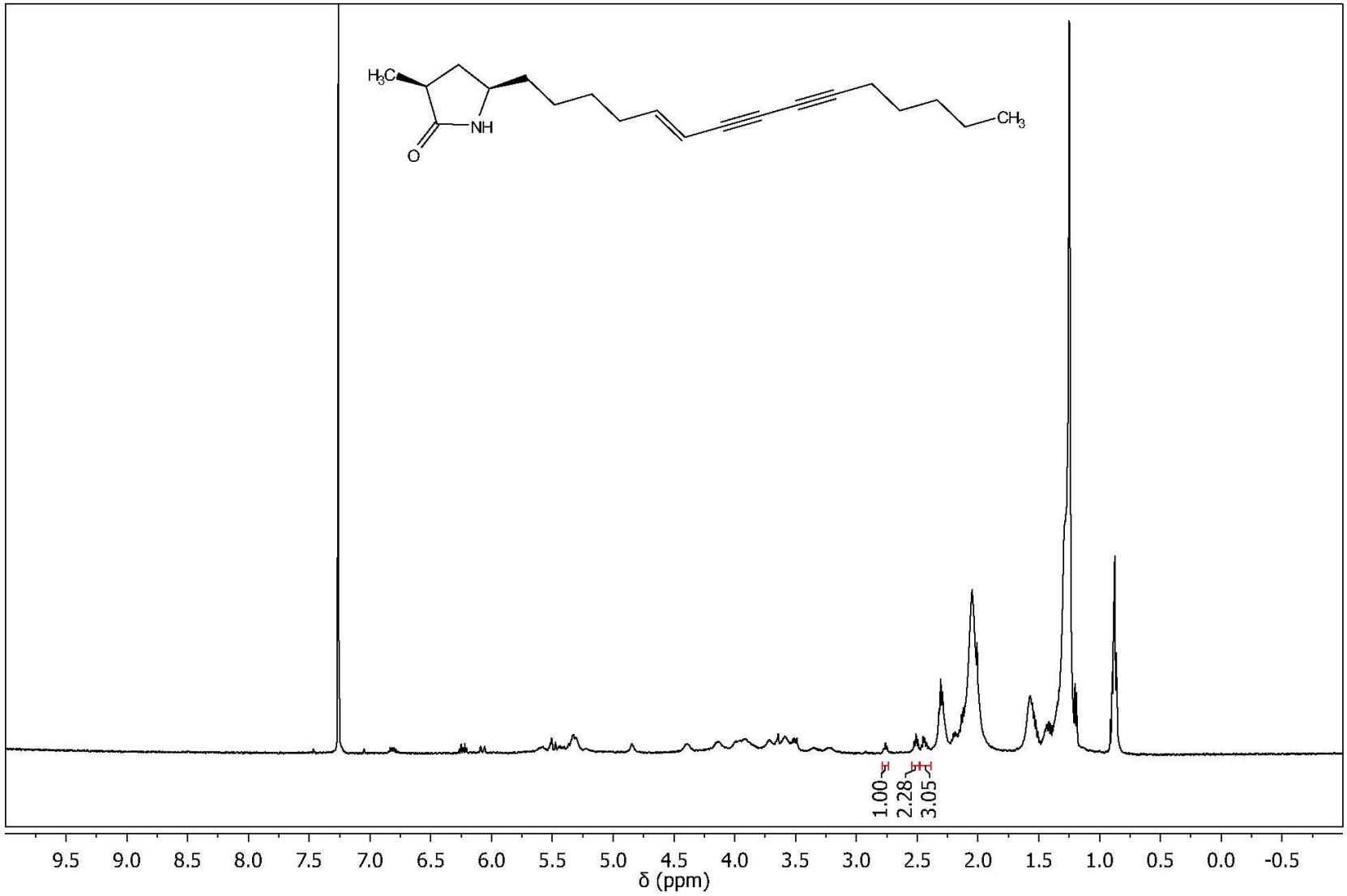

Appendix 64. ^{1}H NMR spectrum of loliolide **5.5** in CD_3OD (500 MHz)

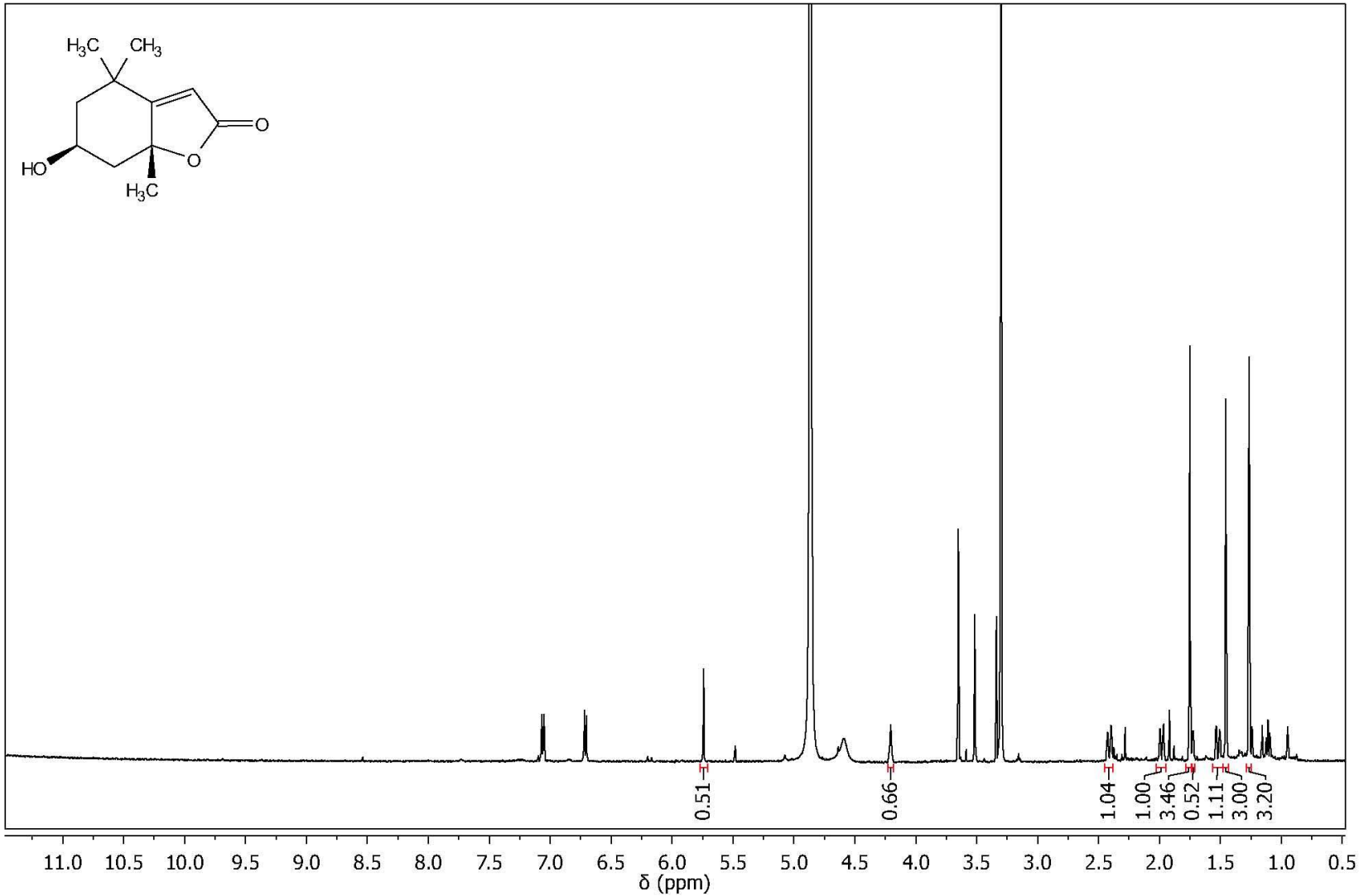

Appendix 65. ^{13}C NMR spectrum of loliolide **5.5** in CD_3OD (125 MHz)

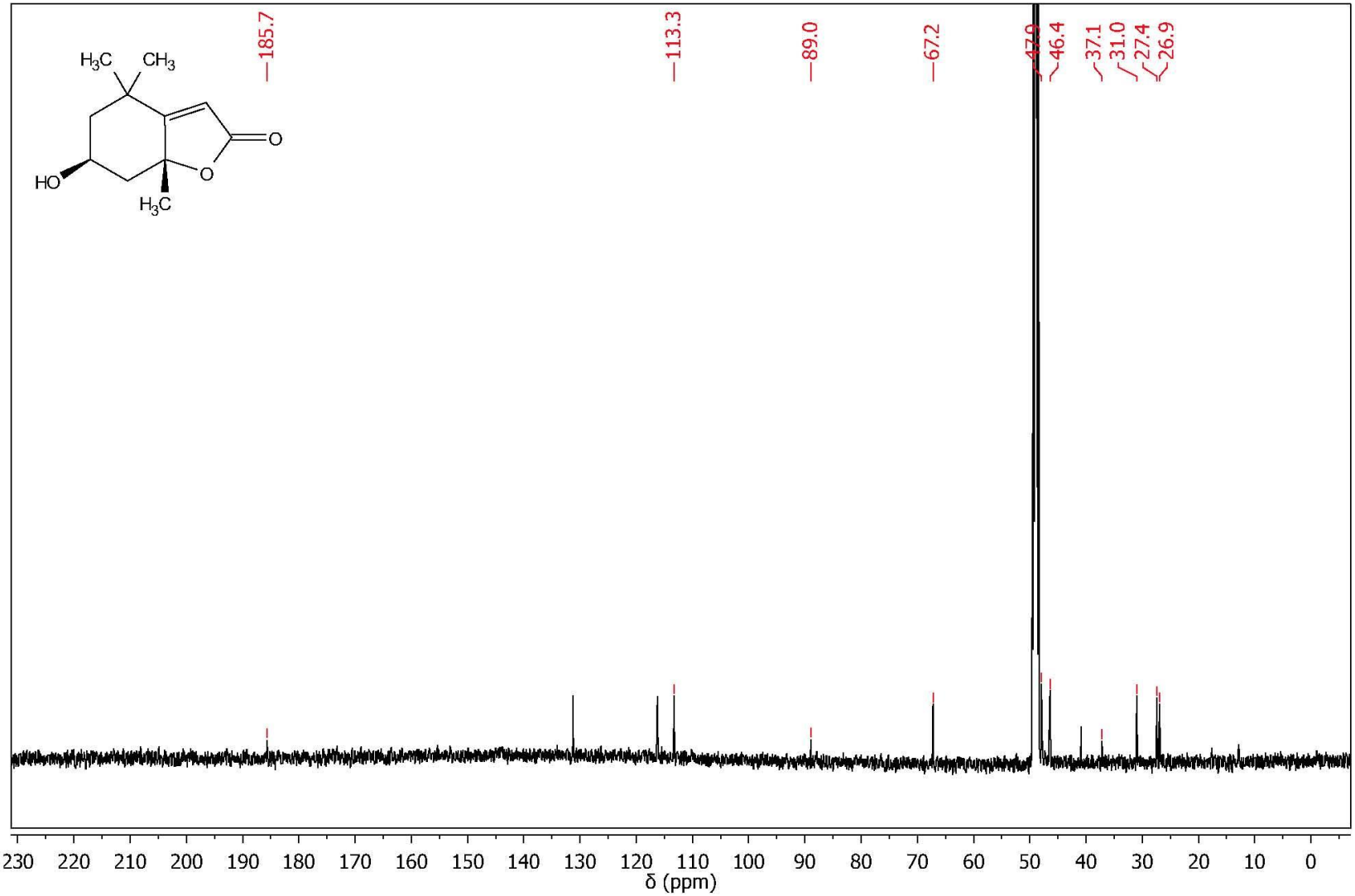

Appendix 66. ^{1}H NMR spectrum of compound **5.6** in $CDCl_3$ (500 MHz)

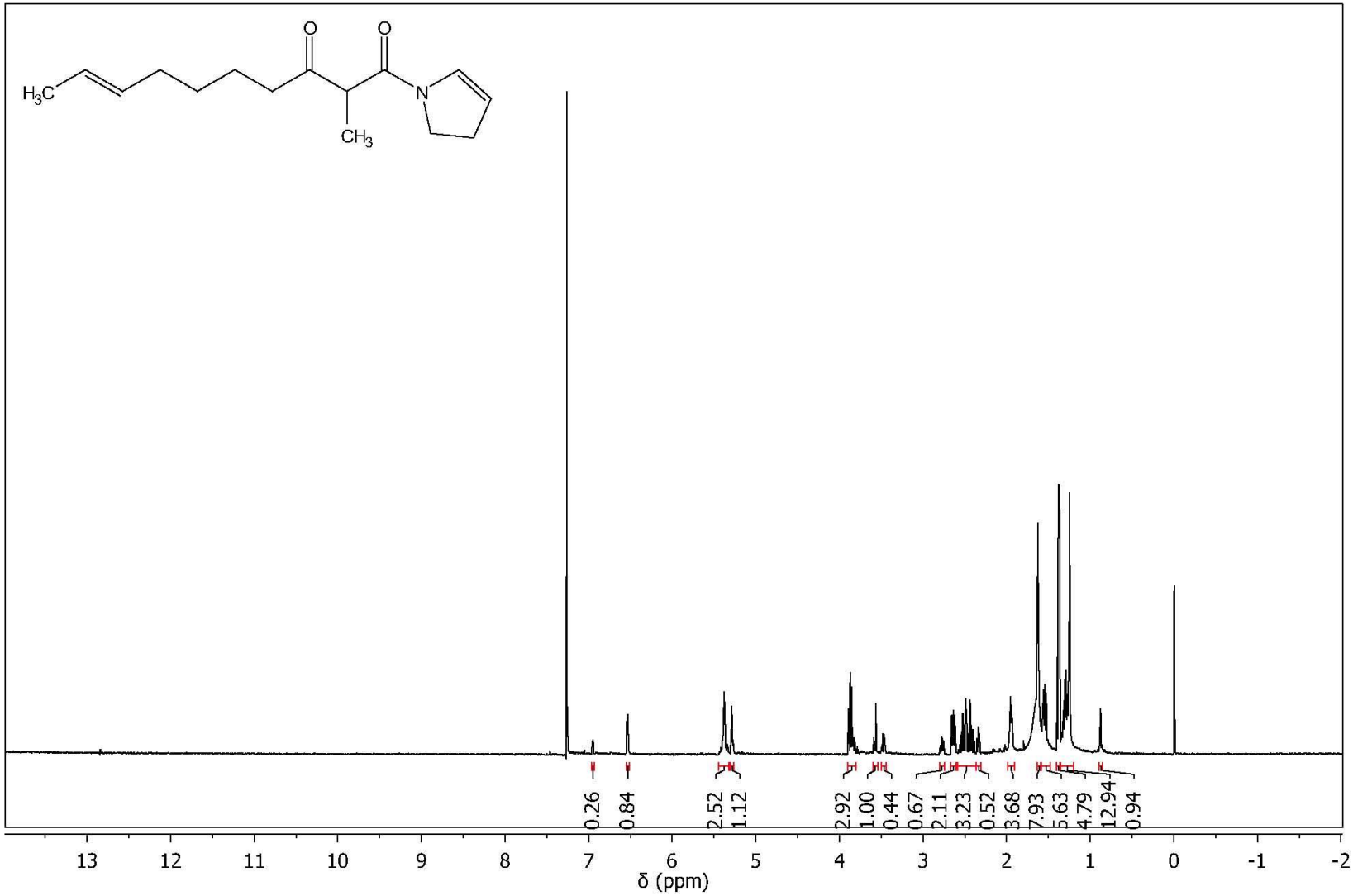

Appendix 67. ^{13}C NMR spectrum of compound **5.6** in $CDCl_3$ (125 MHz)

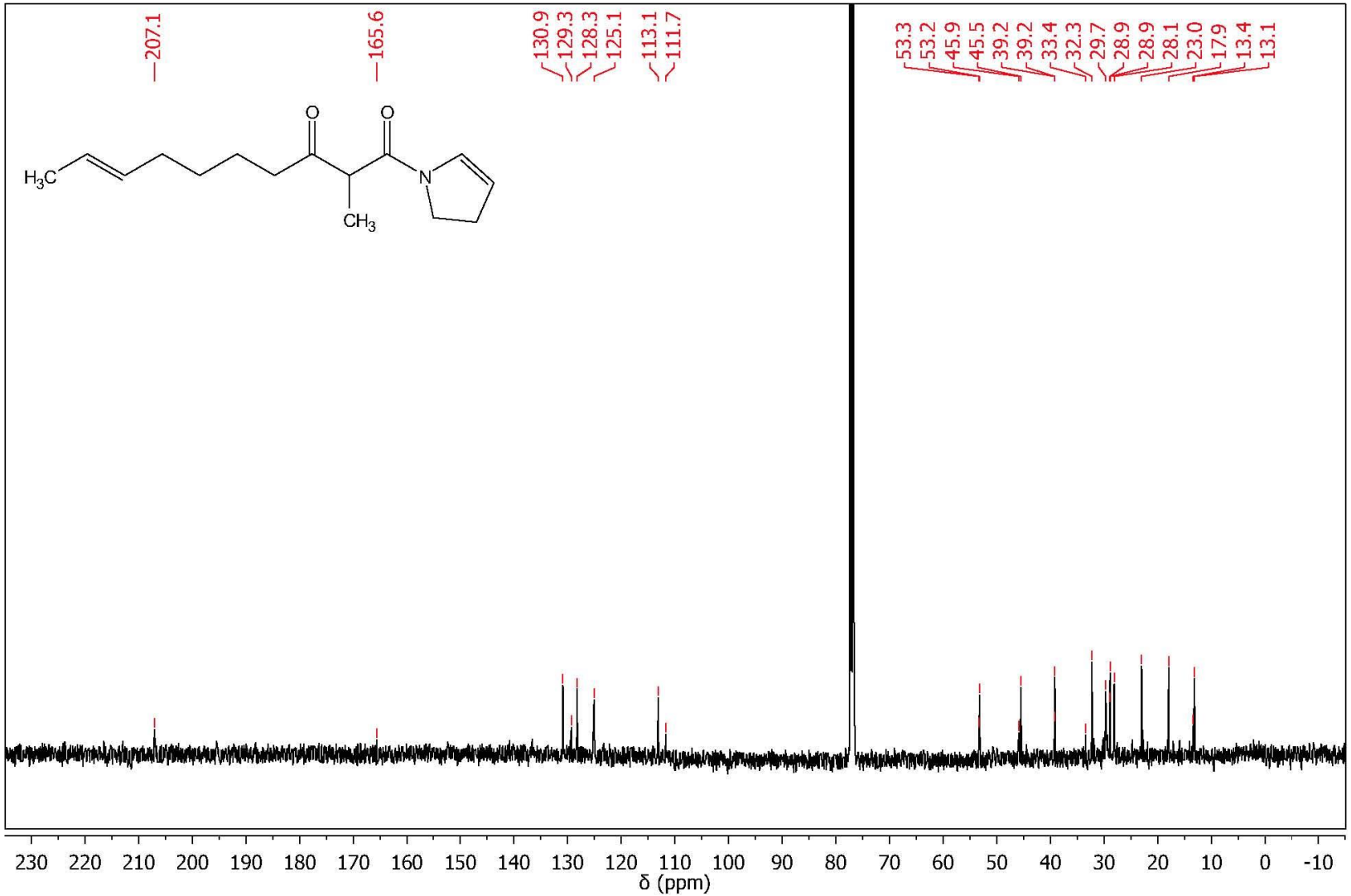

Appendix 68. Biological activity of metabolites isolated from *Dactylospongia elegans*

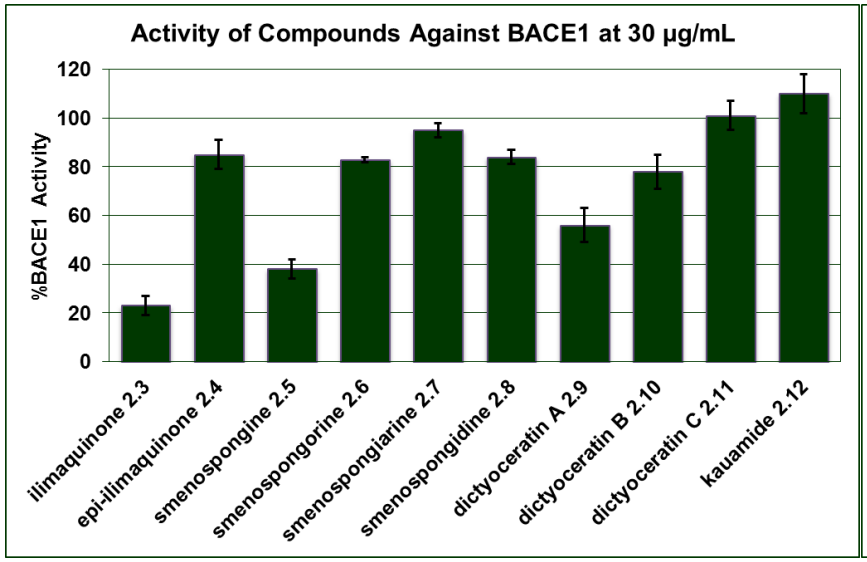

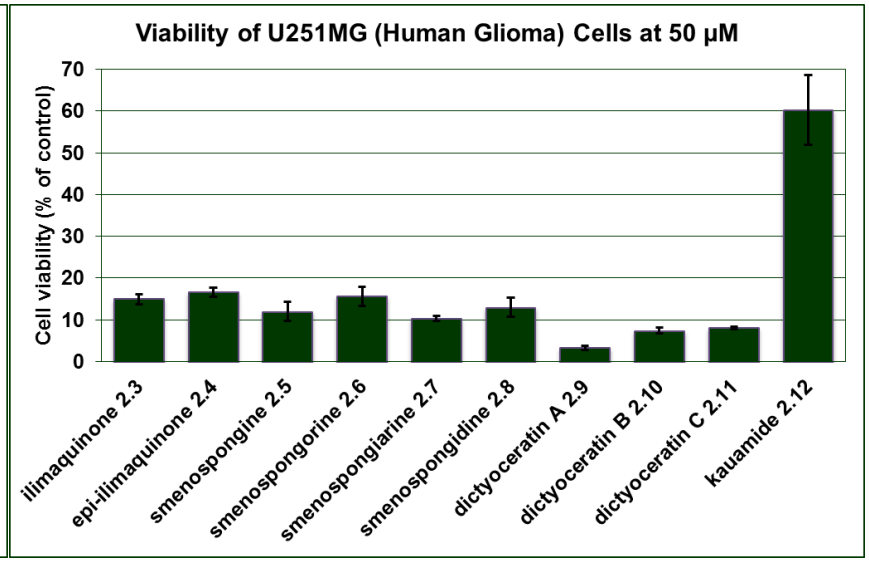

Appendix 69. CC_{50} curves for *Dactylospongia elegans* metabolites against Panc-1 cell line

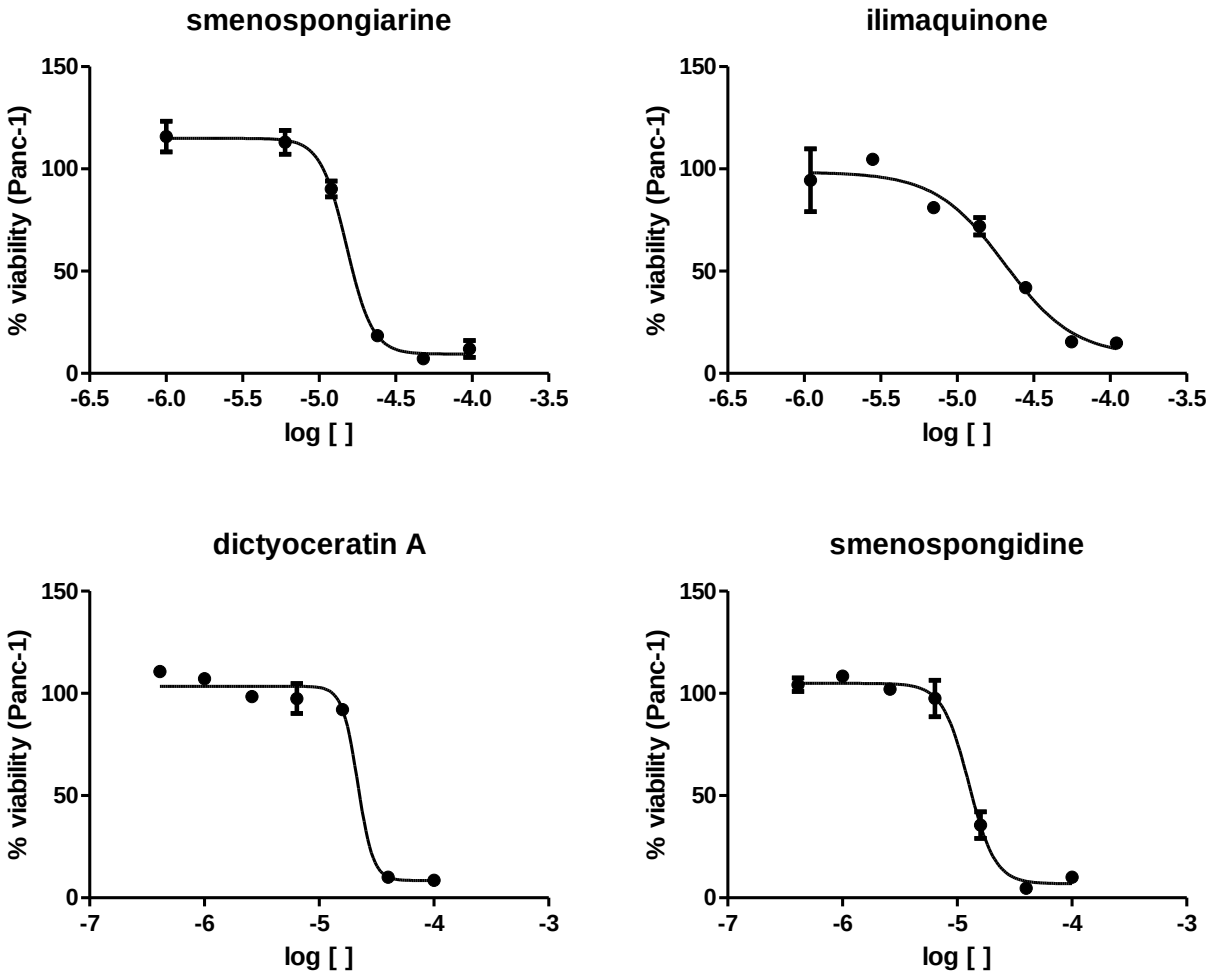

Appendix 70. Boltzmann distribution of conformers of (3*S*,6*S*,11*S*)-**2.19**

Conformer	energy (a.u.)	energy (kcal)	rel energy (kcal)	boltzmann factor	eq mole fraction
18	-1286.7397	-807441.26	0.00	1.000	0.454
16	-1286.7397	-807441.25	0.00	0.995	0.452
4	-1286.7376	-807439.90	1.36	0.101	0.046
2	-1286.7375	-807439.85	1.41	0.093	0.042
20	-1286.7347	-807438.11	3.15	0.005	0.002
19	-1286.7346	-807438.04	3.22	0.004	0.002
5	-1286.7338	-807437.53	3.73	0.002	0.001
17	-1286.7333	-807437.20	4.06	0.001	0.000
15	-1286.7331	-807437.13	4.13	0.001	0.000
9	-1286.7326	-807436.80	4.46	0.001	0.000
14	-1286.7325	-807436.76	4.50	0.000	0.000
12	-1286.7318	-807436.30	4.96	0.000	0.000

Appendix 71. Boltzmann distribution of conformers of (7*S*,9*S*,10*R*)-**3.8**

Conformer	energy (a.u.)	energy (kcal)	rel energy (kcal)	boltzmann factor	eq mole fraction
19	-1126.4073	-706831.18	0.00	1.000	0.220
30	-1126.4072	-706831.11	0.07	0.890	0.196
34	-1126.4071	-706831.01	0.17	0.754	0.166
20	-1126.4070	-706830.95	0.23	0.673	0.148
29	-1126.4068	-706830.85	0.33	0.573	0.126
33	-1126.4067	-706830.77	0.41	0.497	0.109
5	-1126.4038	-706828.97	2.21	0.024	0.005
6	-1126.4037	-706828.88	2.31	0.020	0.004
27	-1126.4034	-706828.71	2.47	0.015	0.003
24	-1126.4031	-706828.53	2.65	0.011	0.003
9	-1126.4030	-706828.49	2.70	0.011	0.002
26	-1126.4030	-706828.43	2.75	0.010	0.002
10	-1126.4027	-706828.30	2.88	0.008	0.002
25	-1126.4026	-706828.22	2.96	0.007	0.001
23	-1126.4026	-706828.20	2.99	0.006	0.001
13	-1126.4022	-706827.94	3.24	0.004	0.001
8	-1126.4021	-706827.90	3.28	0.004	0.001
28	-1126.4020	-706827.86	3.32	0.004	0.001
14	-1126.4020	-706827.85	3.33	0.004	0.001
17	-1126.4020	-706827.84	3.34	0.004	0.001
7	-1126.4019	-706827.79	3.39	0.003	0.001
12	-1126.4019	-706827.75	3.43	0.003	0.001
15	-1126.4018	-706827.74	3.45	0.003	0.001
16	-1126.4018	-706827.70	3.48	0.003	0.001
11	-1126.4016	-706827.58	3.60	0.002	0.001
1	-1126.4015	-706827.54	3.64	0.002	0.000
18	-1126.4014	-706827.48	3.70	0.002	0.000
2	-1126.4014	-706827.46	3.72	0.002	0.000
3	-1126.4011	-706827.24	3.94	0.001	0.000
4	-1126.4010	-706827.24	3.95	0.001	0.000

Appendix 72. Summary of experimental and computed ^{1}H and ^{13}C NMR shifts of all diastereomers of **3.8**

		Computed								
Proton	**Experimental**	**SSR**	**SRR**	**SRS**	**RRR**		**|δSSR-δExp|**	**|δSRR-δExp|**	**|δSRS-δExp|**	**|δRRR-δExp|**
2	6.94	6.65	6.71	6.81	6.84		0.29	0.23	0.13	0.10
3	7.16	7.15	7.17	7.18	7.17		0.01	0.01	0.02	0.01
4	6.97	6.95	6.96	7.01	6.92		0.02	0.01	0.04	0.05
5	7.50	7.50	7.46	7.37	7.20		0.00	0.04	0.13	0.30
8	2.38	2.72	1.72	3.61	2.23		0.34	0.66	1.23	0.15
8	2.18	2.26	2.52	2.20	2.77		0.08	0.34	0.02	0.59
9	4.31	4.57	4.54	5.23	5.37		0.26	0.23	0.92	1.06
12	3.05	3.06	3.10	2.85	3.35		0.01	0.05	0.20	0.30
12	3.30	3.27	3.22	2.94	3.27		0.03	0.08	0.36	0.03
14	7.17	7.29	7.32	7.06	7.15		0.12	0.15	0.11	0.02
15	6.64	6.66	6.69	6.65	6.62		0.02	0.05	0.01	0.02
						ΣABS[Δδ]=	1.17	1.86	3.18	2.63
						MAE=	0.11	0.17	0.29	0.24
Carbon	**Experimental**	**SSR**	**SRR**	**SRS**	**RRR**		**|δSSR-δExp|**	**|δSRR-δExp|**	**|δSRS-δExp|**	**|δRRR-δExp|**
1	136.9	133.3	133.4	143.2	144.8		3.6	3.5	6.3	7.9
2	120.0	117.3	117.6	118.3	117.2		2.7	2.4	1.7	2.8
3	129.6	126.9	127.0	126.0	125.9		2.7	2.6	3.6	3.7
4	123.3	120.1	120.1	120.9	119.6		3.2	3.2	2.4	3.7
5	125.8	124.5	124.8	125.1	119.9		1.3	1.0	0.7	5.9
6	136.0	131.5	130.9	139.5	139.5		4.5	5.1	3.5	3.5
7	104.0	102.3	102.3	99.5	104.9		1.7	1.7	4.5	0.9
8	47.8	50.3	50.3	57.7	51.8		2.5	2.5	9.9	4.0
9	78.0	75.5	75.3	81.4	84.3		2.5	2.7	3.4	6.3
10	91.3	87.5	86.7	88.9	87.0		3.8	4.6	2.4	4.3
11	175.5	173.1	173.8	168.1	176.5		2.4	1.7	7.4	1.0
12	40.3	36.0	35.9	52.0	38.3		4.3	4.4	11.7	2.0
13	128.4	127.3	127.5	126.1	127.6		1.1	0.9	2.3	0.8
14	133.0	130.6	131.1	130.9	130.3		2.4	1.9	2.1	2.7
15	115.6	110.3	110.3	110.6	110.3		5.3	5.3	5.0	5.3
16	157.2	153.5	153.5	154.2	153.4		3.7	3.7	3.0	3.8
						ΣABS[Δδ]=	47.8	47.3	69.9	58.6
						MAE=	3.0	3.0	4.4	3.7

Appendix 73. Boltzmann distribution of conformers of (7*S*,9*S*,10*R*)-**3.18**

Conformer	energy (a.u.)	energy (kcal)	rel energy (kcal)	boltzmann factor	eq mole fraction
33	-1126.3948	-706823.34	0.00	1.000	0.145
3	-1126.3946	-706823.19	0.15	0.776	0.113
36	-1126.3946	-706823.16	0.18	0.738	0.107
8	-1126.3941	-706822.91	0.43	0.483	0.070
6	-1126.3940	-706822.83	0.51	0.425	0.062
30	-1126.3940	-706822.83	0.51	0.422	0.061
4	-1126.3940	-706822.80	0.53	0.406	0.059
35	-1126.3938	-706822.67	0.66	0.326	0.047
1	-1126.3937	-706822.63	0.71	0.302	0.044
5	-1126.3935	-706822.50	0.83	0.245	0.036
22	-1126.3934	-706822.44	0.90	0.220	0.032
2	-1126.3934	-706822.42	0.91	0.213	0.031
24	-1126.3932	-706822.32	1.02	0.178	0.026
25	-1126.3929	-706822.14	1.20	0.131	0.019
15	-1126.3928	-706822.05	1.29	0.113	0.016
19	-1126.3927	-706822.01	1.32	0.107	0.016
11	-1126.3927	-706821.97	1.36	0.100	0.014
39	-1126.3926	-706821.93	1.41	0.092	0.013
26	-1126.3925	-706821.86	1.48	0.082	0.012
38	-1126.3924	-706821.81	1.53	0.075	0.011
12	-1126.3924	-706821.81	1.53	0.075	0.011
21	-1126.3923	-706821.72	1.62	0.065	0.009
20	-1126.3918	-706821.46	1.88	0.042	0.006
34	-1126.3915	-706821.26	2.08	0.030	0.004
23	-1126.3915	-706821.25	2.09	0.029	0.004
14	-1126.3914	-706821.17	2.17	0.026	0.004
17	-1126.3913	-706821.11	2.23	0.023	0.003
10	-1126.3913	-706821.09	2.25	0.022	0.003
29	-1126.3912	-706821.08	2.25	0.022	0.003
18	-1126.3912	-706821.06	2.28	0.021	0.003
13	-1126.3912	-706821.02	2.31	0.020	0.003
9	-1126.3911	-706820.97	2.37	0.018	0.003
31	-1126.3909	-706820.86	2.48	0.015	0.002

Appendix 74. Summary of experimental and computed ^{1}H and ^{13}C NMR shifts of all diastereomers of **3.18**

		Computed							
Proton	**Experimental**	**SSR**	**SRR**	**SRS**	**RRR**	**|δSSR-δExp|**	**|δSRR-δExp|**	**|δSRS-δExp|**	**|δRRR-δExp|**
2	6.94	6.72	6.72	6.72	6.70	0.22	0.22	0.22	0.24
3	7.16	7.15	7.16	7.14	7.14	0.01	0.00	0.02	0.02
4	6.97	6.65	6.64	6.64	6.63	0.32	0.33	0.33	0.34
5	7.50	7.28	7.30	7.28	7.26	0.22	0.20	0.22	0.24
8	2.18	2.62	2.22	2.24	2.41	0.44	0.04	0.06	0.23
8	2.38	2.42	3.04	2.81	2.73	0.04	0.66	0.43	0.35
9	4.31	4.31	4.35	4.38	4.39	0.00	0.04	0.07	0.08
12	3.05	3.33	3.26	3.31	3.24	0.28	0.21	0.26	0.19
12	3.30	3.25	3.43	3.27	3.37	0.05	0.13	0.03	0.07
14	7.17	7.25	7.32	7.26	7.26	0.08	0.15	0.09	0.09
15	6.64	6.74	6.71	6.73	6.73	0.10	0.07	0.09	0.09
						ΣABS[Δδ]=	1.77	2.06	1.83	1.93
						MAE=	0.16	0.19	0.17	0.18

Carbon	**Experimental**	**SSR**	**SRR**	**SRS**	**RRR**	**|δSSR-δExp|**	**|δSRR-δExp|**	**|δSRS-δExp|**	**|δRRR-δExp|**
1	136.9	144.2	144.3	144.2	144.4	7.3	7.4	7.3	7.5
2	120.0	113.7	113.7	113.7	113.7	6.3	6.3	6.3	6.3
3	129.6	128.7	128.7	128.7	128.7	0.9	0.9	0.9	0.9
4	123.3	113.8	113.7	113.7	113.7	9.5	9.6	9.6	9.6
5	125.8	123.6	124.1	124.1	124.2	2.2	1.7	1.7	1.6
6	136.0	115.7	115.0	115.3	115.3	20.3	21.0	20.7	20.7
7	104.0	109.8	111.0	110.0	110.0	5.8	7.0	6.0	6.0
8	47.8	41.6	44.6	41.8	42.2	6.2	3.2	6.0	5.6
9	78.0	70.4	70.4	70.3	71.1	7.6	7.6	7.7	6.9
10	91.3	88.0	89.7	87.7	87.9	3.3	1.6	3.6	3.4
11	175.5	172.3	173.4	172.2	172.1	3.2	2.1	3.3	3.4
12	40.3	31.9	30.7	32.1	32.3	8.4	9.6	8.2	8.0
13	128.4	125.3	126.0	125.3	125.5	3.1	2.4	3.1	2.9
14	133.0	129.8	129.9	129.8	129.9	3.2	3.1	3.2	3.1
15	115.6	111.1	110.9	111.1	111.0	4.5	4.7	4.5	4.6
16	157.2	154.0	153.8	154.0	153.9	3.2	3.4	3.2	3.3
						ΣABS[Δδ]=	95.0	91.5	95.3	93.8
						MAE=	5.9	5.7	6.0	5.9

Appendix 75. Boltzmann distribution of conformers of **3.9**

Conformer	energy (a.u.)	energy (kcal)	rel energy (kcal)	boltzmann factor	eq mole fraction
1	-1049.9375	-658845.67	0.00	1.000	0.089
6	-1049.9375	-658845.65	0.02	0.959	0.085
4	-1049.9374	-658845.61	0.06	0.898	0.080
2	-1049.9374	-658845.59	0.09	0.866	0.077
7	-1049.9374	-658845.58	0.09	0.863	0.076
12	-1049.9373	-658845.51	0.17	0.757	0.067
24	-1049.9371	-658845.39	0.28	0.625	0.055
25	-1049.9369	-658845.26	0.41	0.501	0.044
14	-1049.9368	-658845.22	0.45	0.470	0.042
15	-1049.9365	-658845.04	0.63	0.343	0.030
18	-1049.9365	-658845.01	0.66	0.326	0.029
40	-1049.9365	-658844.99	0.68	0.319	0.028
26	-1049.9365	-658844.99	0.68	0.316	0.028
28	-1049.9364	-658844.97	0.70	0.307	0.027
17	-1049.9363	-658844.86	0.81	0.255	0.023
19	-1049.9361	-658844.75	0.92	0.210	0.019
43	-1049.9360	-658844.72	0.95	0.201	0.018
13	-1049.9360	-658844.72	0.95	0.200	0.018
29	-1049.9360	-658844.70	0.97	0.194	0.017
16	-1049.9360	-658844.67	1.00	0.185	0.016
20	-1049.9358	-658844.57	1.10	0.156	0.014
44	-1049.9356	-658844.45	1.22	0.127	0.011
37	-1049.9355	-658844.41	1.26	0.118	0.010
38	-1049.9354	-658844.32	1.35	0.102	0.009
21	-1049.9352	-658844.21	1.46	0.085	0.008
45	-1049.9352	-658844.21	1.46	0.085	0.008
27	-1049.9352	-658844.19	1.48	0.083	0.007
33	-1049.9350	-658844.10	1.58	0.070	0.006
11	-1049.9350	-658844.09	1.58	0.069	0.006
32	-1049.9349	-658844.03	1.64	0.063	0.006
30	-1049.9348	-658843.95	1.72	0.055	0.005
47	-1049.9348	-658843.92	1.75	0.052	0.005
9	-1049.9348	-658843.92	1.75	0.052	0.005
36	-1049.9347	-658843.91	1.76	0.051	0.005
10	-1049.9347	-658843.91	1.76	0.051	0.005
23	-1049.9346	-658843.85	1.82	0.046	0.004

Appendix 76. Summary of experimental and computed ^{1}H and ^{13}C NMR shifts of **3.9**

No.	δ_C, Exp.	δ_C, Comp.	|δComp-δExp|	δ_H, Exp.	δ_H, Comp.	|δComp-δExp|
1	148.2	142.5	5.7			
2	112.3	117.9	5.6	6.93	7.21	0.28
3	131.1	127.5	3.6	7.24	7.40	0.16
4	123.0	125.1	2.1	6.96	7.30	0.34
5	125.7	123.2	2.5	7.41	7.48	0.07
6	133.3	128.9	4.4			
7	81.7	70.7	11.0			
8	48.0	46.6	1.4	2.77	3.21	0.44
				2.72	2.69	0.03
9	207.7	199.4	8.3			
10	112.4	116.5	4.1			
11	180.0	177.1	2.9			
12	27.9	26.3	1.6	3.30	3.39	0.09
				3.05	3.23	0.18
13	131.6	131.1	0.5			
14	130.3	127.3	3.0	7.07	7.13	0.06
15	116.1	111.2	4.9	6.67	6.64	0.03
16	156.6	153.1	3.5			
		ΣABS[Δδ]=	73.0			1.77
		MAE=	4.0			0.15

REFERENCES

1. Newman, D. J.; Cragg, G. M., Natural Products as Drugs and Leads to Drugs: The Historical Perspective. In *Natural Product Chemistry for Drug Discovery*, The Royal Society of Chemistry: 2009; pp 3-27.

2. (a) Derosne, J. F. *Ann. Chim.* **1803,** *45*, 257-258; (b) Sertuerner, F. *Ann. Phys.* **1817,** *55*, 56-89.

3. Pelletier, P. J.; Caventou, J. B. *Ann. Chim. Phys.* **1818**, 323-336.

4. Pelletier, P. J.; Caventou, J. B. *Ann. Chim. Phys.* **1820,** *15*, 289-318.

5. Robiquet, P. J. *Ann. Chim. Phys.* **1832,** *51*, 225-267.

6. Mein, H. F. *Ann. Pharm.* **1833,** *6*, 67-72.

7. Giseke, A. L. *Arch. Pharm.* **1827,** *20*, 97-111.

8. Ladenburg, A. *Ber. Dtsch. Chem. Ges.* **1886,** *19*, 2578-2583.

9. Fleming, A. *Br. J. Exp. Pathol.* **1929,** *10*, 226-236.

10. Schatz, A.; Bugle, E.; Waksman, S. A. *Proc. Soc. Exp. Biol. Med.* **1944,** *55*, 66-69.

11. Jambor, W. P.; Steinberg, B. A.; Suydam, L. O. *Antibiot. Annu.* **1955,** *3*, 574-578.

12. Hazen, E. L.; Brown, R. *Proc. Soc. Exp. Biol. Med.* **1951,** *76*, 93-97.

13. Newman, D. J.; Cragg, G. M. *J. Nat. Prod.* **2016,** *79*, 629-661.

14. Noble, R. L.; Beer, C. T.; Cutts, J. H. *Ann. N. Y. Acad. Sci.* **1958,** *76*, 882-894.

15. Wani, M. C.; Taylor, H. L.; Wall, M. E.; Coggon, P.; McPhail, A. T. *J. Am. Chem. Soc.* **1971,** *93*, 2325-2327.

16. Wall, M. E.; Wani, M. C.; Cook, C. E.; Palmer, K. H.; McPhail, A. T.; Sim, G. A. *J. Am. Chem. Soc.* **1966,** *88*, 3888-3890.

17. Nitta, K.; Yokokura, T.; Sawada, S.; Kunimoto, T.; Tanaka, T.; Uehara, N.; Baba, H.; Takeuchi, M.; Miyasaka, T.; Mutai, M. *Gan To Kagaku Ryoho* **1987,** *14*, 850-857.

18. Bergmann, W.; Feeney, R. J. *J. Org. Chem.* **1951,** *16*, 981-987.

19. Sakai, R.; Higa, T.; Jefford, C. W.; Bernardinelli, G. *J. Am. Chem. Soc.* **1986,** *108*, 6404-6405.

20. (a) Sigel, M. M.; Wellham, L. L.; Lichter, W.; Dudeck, L. E.; Gargus, J. L.; Lucas, L. H. Food-Drugs From the Sea, Washington DC, Jr., H. W. Y., Ed. Marine Technology Society: Washington DC, 1969; pp 281-294; (b) Rinehart, K. L.; Holt, T. G.; Fregeau, N. L.; Stroh, J. G.; Keifer, P. A.; Sun, F.; Li, L. H.; Martin, D. G. *J. Org. Chem.* **1990,** *55*, 4512-4515.

21. McIntosh, M.; Cruz, L. J.; Hunkapiller, M. W.; Gray, W. R.; Olivera, B. M. *Arch. Biochem. Biophys.* **1982,** *218*, 329-334.

22. Feling, R. H.; Buchanan, G. O.; Mincer, T. J.; Kauffman, C. A.; Jensen, P. R.; Fenical, W. *Angew. Chem., Int. Ed.* **2003,** *42*, 355-357.

23. Pettit, G. R.; Kamano, Y.; Herald, C. L.; Fujii, Y.; Kizu, H.; Boyd, M. R.; Boettner, F. E.; Doubek, D. L.; Schmidt, J. M.; Chapuis, J.-C.; Michel, C. *Tetrahedron* **1993,** *49*, 9151-9170.

24. Pettit, G. R.; Herald, C. L.; Doubek, D. L.; Herald, D. L.; Arnold, E.; Clardy, J. *J. Am. Chem. Soc.* **1982,** *104*, 6846-6848.

25. Luesch, H.; Moore, R. E.; Paul, V. J.; Mooberry, S. L.; Corbett, T. H. *J. Nat. Prod.* **2001,** *64*, 907-910.

26. (a) Davidson, S. K.; Allen, S. W.; Lim, G. E.; Anderson, C. M.; Haygood, M. G. *Appl. Environ. Microbiol.* **2001,** *67*, 4531-4537; (b) Sudek, S.; Lopanik, N. B.; Waggoner, L. E.; Hildebrand, M.; Anderson, C.; Liu, H.; Patel, A.; Sherman, D. H.; Haygood, M. G. *J. Nat. Prod.* **2007,** *70*, 67-74.

27. (a) Oh, D. C.; Kauffman, C. A.; Jensen, P. R.; Fenical, W. *J. Nat. Prod.* **2007,** *70*, 515-520; (b) Cueto, M.; Jensen, P. R.; Kauffman, C.; Fenical, W.; Lobkovsky, E.; Clardy, J. *J. Nat. Prod.* **2001,** *64*, 1444-1446.

28. Patterson, G. M. L.; Bolis, C. M. *J. Phycol.* **1997,** *33*, 54-60.

29. (a) Newman, D. J.; Cragg, G. M. *J. Nat. Prod.* **2007,** *70*, 461-477; (b) Newman, D. J.; Cragg, G. M. *J. Nat. Prod.* **2012,** *75*, 311-335.

30. Singh, N.; Guha, R.; Giulianotti, M.; Pinilla, C.; Houghten, R.; Medina-Franco, J. L. *J. Chem. Inf. Model.* **2009,** *49*, 1010-1024.

31. McArdle, B. M.; Quinn, R. J. *ChemBioChem* **2007,** *8*, 788-798.

32. McArdle, B. M.; Campitelli, M. R.; Quinn, R. J. *J. Nat. Prod.* **2006,** *69*, 14-17.

33. In *Dictionary of Natural Products*, CRC Press: Boca Raton, FL, 2017.

34. In *Dictionary of Marine Natural Products*, Blunt, J.; Munro, M., Eds. CRC Press: Boca Raton, FL, 2016.

35. Harvey, A. L.; Edrada-Ebel, R.; Quinn, R. J. *Nat. Rev. Drug Discovery* **2015,** *14*, 111-129.

36. Sharma, V.; Sarkar, I. N. *J. Am. Med. Inform. Assoc.* **2013,** *20*, 668-679.

37. Williams, P.; Kigoshi, H.; Kita, M. 8th US-Japan Symposium: 21st Century Innovations in Natural Products, Honolulu, HI, Honolulu, HI, 2016.

38. Chellat, M. F.; Raguž, L.; Riedl, R. *Angew. Chem., Int. Ed.* **2016,** *55*, 6600-6626.

39. Irwin, K. K.; Renzette, N.; Kowalik, T. F.; Jensen, J. D. *Virus Evol.* **2016,** *2*, 1-10.

40. Newman, D. J.; Cragg, G. M., Natural Products as Drugs and Leads to Drugs: An Introduction and Perspective as of the End of 2012. In *Natural Products in Medicinal Chemistry*, Wiley-VCH Verlag GmbH & Co. KGaA: 2014; pp 1-42.

41. (a) Kim, E.; Moore, B. S.; Yoon, Y. J. *Nat. Chem. Biol.* **2015,** *11*, 649-659; (b) Unsin, C. E.-M.; Rajski, S. R.; Shen, B., The Role of Genetic Engineering in Natural Product-Based Anticancer Drug Discovery. In *Natural Products and Cancer Drug Discovery*, Koehn, F. E., Ed. Springer New York: New York, NY, 2013; pp 175-191.

42. Heide, L. *Biotechnol. Adv.* **2009,** *27*, 1006-1014.

43. Luo, Y.; Cobb, R. E.; Zhao, H. *Curr. Opin. Biotechnol.* **2014,** *0*, 230-237.

44. Nielsen, J. C.; Grijseels, S.; Prigent, S.; Ji, B.; Dainat, J.; Nielsen, K. F.; Frisvad, J. C.; Workman, M.; Nielsen, J. *Nat. Microbiol.* **2017,** *2*, 1-9.

45. Dalisay, D. S.; Molinski, T. F. *J. Nat. Prod.* **2010,** *73*, 679-682.

46. Wang, M.; Carver, J. J.; Phelan, V. V.; Sanchez, L. M.; Garg, N.; Peng, Y.; Nguyen, D. D.; Watrous, J.; Kapono, C. A.; Luzzatto-Knaan, T.; Porto, C.; Bouslimani, A.; Melnik, A. V.; Meehan, M. J.; Liu, W.-T.; Crüsemann, M.; Boudreau, P. D.; Esquenazi, E.; Sandoval-Calderón, M.; Kersten, R. D.; Pace, L. A.; Quinn, R. A.; Duncan, K. R.; Hsu, C.-C.; Floros, D. J.; Gavilan, R. G.; Kleigrewe, K.; Northen, T.; Dutton, R. J.; Parrot, D.; Carlson, E. E.; Aigle, B.; Michelsen, C. F.; Jelsbak, L.; Sohlenkamp, C.; Pevzner, P.; Edlund, A.; McLean, J.; Piel, J.; Murphy, B. T.; Gerwick, L.; Liaw, C.-C.; Yang, Y.-L.; Humpf, H.-U.; Maansson, M.; Keyzers, R. A.; Sims, A. C.; Johnson, A. R.; Sidebottom, A. M.; Sedio, B. E.; Klitgaard, A.; Larson, C. B.; Boya P, C. A.; Torres-Mendoza, D.; Gonzalez, D. J.; Silva, D. B.; Marques, L. M.; Demarque, D. P.; Pociute, E.; O'Neill, E. C.; Briand, E.; Helfrich, E. J. N.; Granatosky, E. A.; Glukhov, E.; Ryffel, F.; Houson, H.; Mohimani, H.; Kharbush, J. J.; Zeng, Y.; Vorholt, J. A.; Kurita, K. L.; Charusanti, P.; McPhail, K. L.; Nielsen, K. F.; Vuong, L.; Elfeki, M.; Traxler, M. F.; Engene, N.; Koyama, N.; Vining, O. B.; Baric, R.; Silva, R. R.; Mascuch, S. J.; Tomasi, S.; Jenkins, S.; Macherla, V.; Hoffman, T.; Agarwal, V.; Williams, P. G.; Dai, J.; Neupane, R.; Gurr, J.; Rodríguez, A. M. C.; Lamsa, A.; Zhang, C.; Dorrestein, K.; Duggan, B. M.; Almaliti, J.; Allard, P.-M.; Phapale, P.; Nothias, L.-F.; Alexandrov, T.; Litaudon, M.; Wolfender, J.-L.; Kyle, J. E.; Metz, T. O.; Peryea, T.; Nguyen, D.-T.; VanLeer, D.; Shinn, P.; Jadhav, A.; Müller, R.; Waters, K. M.; Shi, W.; Liu, X.; Zhang, L.; Knight, R.; Jensen, P. R.; Palsson, B. Ø.; Pogliano, K.; Linington, R. G.; Gutiérrez, M.; Lopes, N. P.; Gerwick, W. H.; Moore, B. S.; Dorrestein, P. C.; Bandeira, N. *Nat. Biotechnol.*

2016, *34*, 828-837.

47. *2017 Alzheimer's Disease: Facts and Figures*; Washington DC, 2017; pp 1-86.

48. (a) Hardy, J. A.; Higgins, G. A. *Science* **1992,** *256*, 184-185; (b) Selkoe, D. J.; Hardy, J. *EMBO Mol. Med.* **2016,** *8*, 595-608.

49. Vassar, R. *Alzheimer's Res. Ther.* **2014,** *6*, 1-14.

50. (a) Yu, H.; Jove, R. *Nat. Rev. Cancer* **2004,** *4*, 97-105; (b) Johnston, P. A.; Grandis, J. R. *Mol. Interv.* **2011,** *11*, 18-26.

51. Yano, K.; Liaw, P. C.; Mullington, J. M.; Shih, S.-C.; Okada, H.; Bodyak, N.; Kang, P. M.; Toltl, L.; Belikoff, B.; Buras, J.; Simms, B. T.; Mizgerd, J. P.; Carmeliet, P.; Karumanchi, S. A.; Aird, W. C. *J. Exp. Med.* **2006,** *203*, 1447-1458.

52. Sepsis and Cancer. https://www.sepsis.org/sepsis-and/cancer/.

53. Anand, R.; Dhingra, C.; Prasad, S.; Menon, I. *J. Cancer Res. Ther.* **2014,** *10*, 499-505.

54. Hung, S. L.; Lin, Y. J.; Chien, E. J.; Liu, W. G.; Chang, H. W.; Liu, T. Y.; Chen, Y. T. *J. Periodontal Res.* **2007,** *42*, 393-401.

55. *SciFinder*, Chemical Abstracts Service: Columbus, OH, 2017.

56. *MarinLit*, Royal Society of Chemistry: London, UK, 2017.

57. Laatsch, H. *AntiBase*, Wiley-VCH Verlag GmbH & Co.: University of Gottingen, Germany, 2012.

58. Blunt, J.; Munro, M. *AntiMarin*, University of Canterbury, New Zealand, 2011.

59. (a) Alzheimer, A.; Stelzmann, R. A.; Schnitzlein, H. N.; Murtagh, F. R. *Clin. Anat.* **1995,** *8*, 429-431; (b) Alzheimer, A. *Allg. Z. Psychiat.* **1907,** *64*, 146-148.

60. Goedert, M.; Spillantini, M. G. *Science* **2006,** *314*, 777-781.

61. Grundke-Iqbal, I.; Iqbal, K.; Tung, Y. C.; Quinlan, M.; Wisniewski, H. M.; Binder, L. I. *Proc. Natl. Acad. Sci. U. S. A.* **1986,** *83*, 4913-4917.

62. Alzheimer's Disease Medications Fact Sheet. 2015; pp 1-4.

63. Naqvi, T.; Lim, A.; Rouhani, R.; Singh, R.; Eglen, R. M. *J. Biomol. Screen.* **2004,** *9*, 398-408.

64. Williams, P.; Sorribas, A.; Liang, Z. *Curr. Alzheimer Res.* **2010,** *7*, 210-213.

65. Levy, D. E.; Darnell Jr., J. E. *Nat. Rev. Mol. Cell Biol.* **2002,** *3*, 651-662.

66. Furtek, S. L.; Backos, D. S.; Matheson, C. J.; Reigan, P. *ACS Chem. Biol.* **2016,** *11*, 308-318.

67. Johnston, P. A.; Grandis, J. R. *Molecular interventions* **2011,** *11*, 18-26.

68. (a) Frank, D. A. *Cancer Lett.* **2007,** *251*, 199-210; (b) Leeman, R. J.; Lui, V. W.; Grandis, J. R. *Expert Opin. Biol. Ther.* **2006,** *6*, 231-241; (c) Germain, D.; Frank, D. A. *Clin. Cancer Res.* **2007,** *13*, 5665-5669; (d) Seethala, R. R.; Gooding, W. E.; Handler, P. N.; Collins, B.; Zhang, Q.; Siegfried, J. M.; Grandis, J. R. *Clin. Cancer Res.* **2008,** *14*, 1303-1309.

69. Wong, A. L. A.; Hirpara, J. L.; Pervaiz, S.; Eu, J.-Q.; Sethi, G.; Goh, B.-C. *Expert Opin. Invest. Drugs* **2017,** *26*, 883-887.

70. Li, Y.; Hadden, C.; Cooper, A.; Ahmed, A.; Wu, H.; Lupashin, V. V.; Mayeux, P. R.; Kilic, F. *Sci. Rep.* **2016,** *6*, 1-13.

71. Griffiths, G. S.; Grundl, M.; Allen, J. S., 3rd; Matter, M. L. *J. Cell. Physiol.* **2011,** *226*, 2287-2296.

72. Vähätupa, M.; Prince, S.; Vataja, S.; Mertimo, T.; Kataja, M.; Kinnunen, K.; Marjomäki, V.; Uusitalo, H.; Komatsu, M.; Järvinen, T. A. H.; Uusitalo–Järvinen, H. *Invest. Ophthalmol. Visual Sci.* **2016,** *57*, 4898-4909.

73. May, R. M. *Science* **1988,** *241*, 1441-1449.

74. Yin, Z.; Zhu, M.; Davidson, E. H.; Bottjer, D. J.; Zhao, F.; Tafforeau, P. *Proc. Natl. Acad. Sci. U. S. A.* **2015,** *112*, E1453-E1460.

75. (a) Stone, M. J.; Williams, D. H. *Mol. Microbiol.* **1992,** *6*, 29-34; (b) Proksch, P. *Toxicon* **1994,** *32*, 639-55.

76. Blunt, J. W.; Copp, B. R.; Keyzers, R. A.; Munro, M. H. G.; Prinsep, M. R. *Nat. Prod. Rep.* **2015,** *32*, 116-211.

77. Andersen, R. J. *Biochem. Pharmacol.* **2017,** *139*, 3-14.

78. (a) Calcabrini, C.; Catanzaro, E.; Bishayee, A.; Turrini, E.; Fimognari, C. *Mar. Drugs* **2017,** *15*, 310-343; (b) Mehbub, M.; Lei, J.; Franco, C.; Zhang, W. *Mar. Drugs* **2014,** *12*, 4539-4577; (c) Mayer, A. M. S. Marine Pharmacology. http://marinepharmacology.midwestern.edu/clinPipeline.htm (accessed April 24, 2016).

79. Hirata, Y.; Uemura, D. *Pure Appl. Chem.* **1986,** *58*, 701-710.

80. (a) Capon, R. J.; MacLeod, J. K. *J. Org. Chem.* **1987,** *52*, 5059-5060; (b) Luibrand, R. T.; Erdman, T. R.; Vollmer, J. J.; Scheuer, P. J.; Finer, J.; Clardy, J. *Tetrahedron* **1979,** *35*, 609-612.

81. Carte, B.; Rose, C. B.; Faulkner, D. J. *J. Org. Chem.* **1985,** *50*, 2785-2787.

82. Kondracki, M.-L.; Guyot, M. *Tetrahedron* **1989,** *45*, 1995-2004.

83. Rodríguez, J.; Quiñoá, E.; Riguera, R.; Peters, B. M.; Abrell, L. M.; Crews, P. *Tetrahedron* **1992,** *48*, 6667-6680.

84. Nakamura, H.; Deng, S.; Kobayashi, J. i.; Ohizumi, Y.; Hirata, Y. *Tetrahedron* **1986,** *42*, 4197-4201.

85. (a) Kushlan, D. M.; Faulkner, D. J.; Parkanyi, L.; Clardy, J. *Tetrahedron* **1989,** *45*, 3307-3312; (b) Kwak, J. H.; Schmitz, F. J.; Kelly, M. *J. Nat. Prod.* **2000,** *63*, 1153-1156.

86. (a) Harada, K.-i.; Fujii, K.; Mayumi, T.; Hibino, Y.; Suzuki, M.; Ikai, Y.; Oka, H. *Tetrahedron Lett.* **1995,** *36*, 1515-1518; (b) Marfey, P. *Carlsberg Res. Commun.* **1984,** *49*, 591-596; (c) Fujii, K.; Ikai, Y.; Mayumi, T.; Oka, H.; Suzuki, M.; Harada, K.-i. *Anal. Chem.* **1997,** *69*, 3346-3352.

87. Dale, J. A.; Mosher, H. S. *J. Am. Chem. Soc.* **1973,** *95*, 512-519.

88. Yabuuchi, T.; Kusumi, T. *J. Org. Chem.* **2000,** *65*, 397-404.

89. Willoughby, P. H.; Jansma, M. J.; Hoye, T. R. *Nat. Protocols* **2014,** *9*, 643-660.

90. Dong, L.-B.; Wu, Y.-N.; Jiang, S.-Z.; Wu, X.-D.; He, J.; Yang, Y.-R.; Zhao, Q.-S. *Org. Lett.* **2014,** *16*, 2700-2703.

91. Paterson, I.; Dalby, S. M.; Roberts, J. C.; Naylor, G. J.; Guzmán, E. A.; Isbrucker, R.; Pitts, T. P.; Linley, P.; Divlianska, D.; Reed, J. K.; Wright, A. E. *Angew. Chem., Int. Ed.* **2011,** *50*, 3219-3223.

92. Rodríguez, I.; Genta-Jouve, G.; Alfonso, C.; Calabro, K.; Alonso, E.; Sánchez, J. A.; Alfonso, A.; Thomas, O. P.; Botana, L. M. *Org. Lett.* **2015,** *17*, 2392-2395.

93. Lodewyk, M. W.; Tantillo, D. J. *J. Nat. Prod.* **2011,** *74*, 1339-1343.

94. Willwacher, J.; Heggen, B.; Wirtz, C.; Thiel, W.; Fürstner, A. *Chem. - Eur. J.* **2015,** *21*, 10416-10430.

95. Rychnovsky, S. D. *Org. Lett.* **2006,** *8*, 2895-2898.

96. Grimblat, N.; Sarotti, A. M. *Chem. - Eur. J.* **2016,** *22*, 12246-12261.

97. Smith, S. G.; Goodman, J. M. *J. Am. Chem. Soc.* **2010,** *132*, 12946-12959.

98. Zanardi, M. M.; Suárez, A. G.; Sarotti, A. M. *J. Org. Chem.* **2017,** *82*, 1873-1879.

99. Edwards, D. J.; Marquez, B. L.; Nogle, L. M.; McPhail, K.; Goeger, D. E.; Roberts, M. A.; Gerwick, W. H. *Chem. Biol.* **2004,** *11*, 817-833.

100. Engene, N.; Rottacker, E. C.; Kaštovský, J.; Byrum, T.; Choi, H.; Ellisman, M. H.; Komárek, J.; Gerwick, W. H. *Int. J. Syst. Evol. Microbiol.* **2012,** *62*, 1171-1178.

101. Sumimoto, S.; Iwasaki, A.; Ohno, O.; Sueyoshi, K.; Teruya, T.; Suenaga, K. *Org. Lett.* **2016,** *18*, 4884-4887.

102. (a) Aoki, S.; Kong, D.; Matsui, K.; Rachmat, R.; Kobayashi, M. *Chem. Pharm. Bull.* **2004,** *52*, 935-937; (b) Li, J.; Gu, B.-B.; Sun, F.; Xu, J.-R.; Jiao, W.-H.; Yu, H.-B.; Han, B.-N.; Yang, F.; Zhang, X.-C.; Lin, H.-W. *J. Nat. Prod.* **2017,** *80*, 1436-1445; (c) Nguyen, H. M.; Ito, T.; Win, N. N.; Kodama, T.; Hung, V. Q.; Nguyen, H. T.; Morita, H. *Phytochem. Lett.* **2016,** *17*, 288-292; (d) Oda, T.; Wang, W.; Fujita, A.; Mochizuki, M.; Ukai, K.; Namikoshi, M. *J. Nat. Med.* **2007,** *61*, 434-437; (e) Oda, T.; Wang, W.; Ukai, K.; Nakazawa, T.; Mochizuki, M. *Mar. Drugs* **2007,** *5*, 151-156; (f) Zhang, X.; Xu, H.-Y.; Huang, A.-M.; Wang, L.; Wang, Q.; Cao, P.-Y.; Yang, P.-M. *Chem. Pharm. Bull.* **2016,** *64*, 1036-1042.

103. Ling, T.; Poupon, E.; Rueden, E. J.; Kim, S. H.; Theodorakis, E. A. *J. Am. Chem. Soc.* **2002,** *124*, 12261-12267.

104. Kasting, J. F.; Siefert, J. L. *Science* **2002,** *296*, 1066-1068.

105. (a) Charpy, L.; Casareto, B. E.; Langlade, M. J.; Suzuki, Y. *J. Mar. Biol.* **2012,** *2012*, 1-9; (b) Gademann, K.; Portmann, C. *Curr. Org. Chem.* **2008,** *12*, 326-341; (c) Kehr, J.-C.; Gatte Picchi, D.; Dittmann, E. *Beilstein J. Org. Chem.* **2011,** *7*, 1622-1635; (d) Rippka, R. *Methods Enzymol.* **1988,** *167*, 3-27.

106. (a) Knoll, A. H., Cyanobacteria and Earth History. In *The Cyanobacteria: Molecular Biology, Genetics and Evolution*, Herrero, A.; Flores, E., Eds. Caister Academic Press: Norfolk, United Kingdom, 2008; pp 1-19; (b) Sivonen, K.; Boerner, T., Bioactive Compounds Produced by Cyanobacteria. In *The Cyanobacteria: Molecular Biology, Genetics and Evolution*, Herrero, A.; Flores, E., Eds. Caister Academic Press: Norfolk, United Kingdom, 2008; pp 159-198.

107. (a) Berry, J.; Gantar, M.; Perez, M.; Berry, G.; Noriega, F. *Mar. Drugs* **2008,** *6*, 117-146; (b) Cragg, G. M.; Grothaus, P. G.; Newman, D. J. *Chem. Rev.* **2009,** *109*, 3012-3043.

108. (a) Hader, D. P.; Kumar, H. D.; Smith, R. C.; Worrest, R. C. *Photochem. Photobiol. Sci.* **2007,** *6*, 267-285; (b) Paul, V. J. *Adv. Exp. Med. Biol.* **2008,** *619*, 239-257.

109. (a) Becher, P. G.; Beuchat, J.; Gademann, K.; Jüttner, F. *J. Nat. Prod.* **2005,** *68*, 1793-1795; (b) Gustafson, K. R.; Cardellina, J. H.; Fuller, R. W.; Weislow, O. S.; Kiser, R. F.; Snader, K. M.; Patterson, G. M.; Boyd, M. R. *J. Natl. Cancer Inst.* **1989,** *81*, 1254-1258; (c) Singh, R. K.; Tiwari, S. P.; Rai, A. K.; Mohapatra, T. M. *J. Antibiot.* **2011,** *64*, 401-412.

110. (a) Nunnery, J. K.; Mevers, E.; Gerwick, W. H. *Curr. Opin. Biotechnol.* **2010,** *21*, 787-793; (b) Tidgewell, K.; Clark, B. R.; Gerwick, W. H., 2.06 - The Natural Products Chemistry of Cyanobacteria. In *Comprehensive Natural Products II*, Elsevier: Oxford, 2010; pp 141-188.

111. Cardellina, J. H.; Moore, B. S. *J. Nat. Prod.* **2010,** *73*, 301-302.

112. (a) Burja, A. M.; Banaigs, B.; Abou-Mansour, E.; Grant Burgess, J.; Wright, P. C. *Tetrahedron* **2001,** *57*, 9347-9377; (b) Chen, Q.-Y.; Liu, Y.; Luesch, H. *ACS Med. Chem. Lett.* **2011,** *2*, 861-865.

113. (a) Schwartz, R.; Hirsch, C.; Sesin, D.; Flor, J.; Chartrain, M.; Fromtling, R.; Harris, G.; Salvatore, M.; Liesch, J.; Yudin, K. *J. Ind. Microbiol.* **1990,** *5*, 113-123; (b) Patterson, G. M. L.; Baldwin, C. L.; Bolis, C. M.; Caplan, F. R.; Karuso, H.; Larsen, L. K.; Levine, I. A.; Moore, R. E.; Nelson, C. S.; Tschappat, K. D.; Tuang, G. D.; Furusawa, E.; Furusawa, S.; Norton, T. R.; Raybourne, R. B. *J. Phycol.* **1991,** *27*, 530-536; (c) Trimurtulu, G.; Ohtani, I.; Patterson, G. M. L.; Moore, R. E.; Corbett, T. H.; Valeriote, F. A.; Demchik, L. *J. Am. Chem. Soc.* **1994,** *116*, 4729-4737.

114. Pettit, G. R.; Kamano, Y.; Herald, C. L.; Tuinman, A. A.; Boettner, F. E.; Kizu, H.; Schmidt, J. M.; Baczynskyj, L.; Tomer, K. B.; Bontems, R. J. *J. Am. Chem. Soc.* **1987,** *109*, 6883-6885.

115. Gerwick, W. H.; Proteau, P. J.; Nagle, D. G.; Hamel, E.; Blokhin, A.; Slate, D. L. *J. Org. Chem.* **1994,** *59*, 1243-1245.

116. Tius, M. A. *Tetrahedron* **2002,** *58*, 4343-4367.

117. Dumontet, C.; Jordan, M. A. *Nat. Rev. Drug Discov.* **2010,** *9*, 790-803.

118. FDA Approval for Brentuximab Vedotin. https://www.cancer.gov/about-cancer/treatment/drugs/fda-brentuximabvedotin (accessed 11/27/2017).

119. Ueda, H.; Nakajima, H.; Hori, Y.; Fujita, T.; Nishimura, M.; Goto, T.; Okuhara, M. *J. Antibiot.* **1994,** *47*, 301-310.

120. FDA Approval for Romidepsin. https://www.cancer.gov/about-cancer/treatment/drugs/fda-romidepsin (accessed 11/27/2017).

121. Lau, N.-S.; Matsui, M.; Abdullah, A. A.-A. *Biomed. Res. Int.* **2015,** *2015*, 1-9.

122. Tamura, K.; Nei, M. *Mol. Biol. Evol.* **1993,** *10*, 512-526.

123. Palermo, J. A.; Flower, P. B.; Seldes, A. M. *Tetrahedron Lett.* **1992,** *33*, 3097-3100.

124. Fu, X.; Schmitz, F. J.; Tanner, R. S. *J. Nat. Prod.* **1995,** *58*, 1950-1954.

125. (a) Dale, J. A.; Dull, D. L.; Mosher, H. S. *J. Org. Chem.* **1969,** *34*, 2543-2549; (b) Hoye, T. R.; Jeffrey, C. S.; Shao, F. *Nat. Protocols* **2007,** *2*, 2451-2458.

126. Luche, J. L. *J. Am. Chem. Soc.* **1978,** *100*, 2226-2227.

127. Kuethe, J. T.; Comins, D. L. *J. Org. Chem.* **2004,** *69*, 5219-5231.

128. Moffitt, W.; Woodward, R. B.; Moscowitz, A.; Klyne, W.; Djerassi, C. *J. Am. Chem. Soc.* **1961,** *83*, 4013-4018.

129. Bruhn, T.; Schaumlöffel, A.; Hemberger, Y. *SpecDis version 1.63*, University of Wuerzburg: Germany, 2015.

130. (a) Bouman, T. D.; Moscowitz, A. *J. Chem. Phys.* **1968,** *48*, 3115-3120; (b) Djerassi, C.; Osiecki, J.; Riniker, R.; Riniker, B. *J. Am. Chem. Soc.* **1958,** *80*, 1216-1225.

131. Bouman, T. D.; Lightner, D. A. *J. Am. Chem. Soc.* **1976,** *98*, 3145-3154.

132. Li, S. M. *Nat. Prod. Rep.* **2010,** *27*, 57-78.

133. Schmidt, N. G.; Pavkov-Keller, T.; Richter, N.; Wiltschi, B.; Gruber, K.; Kroutil, W. *Angew. Chem., Int. Ed.* **2017,** *56*, 7615-7619.

134. (a) Ohki, S.; Nagasaka, T. *Chem. Pharm. Bull.* **1971,** *19*, 545-551; (b) Condie, Glenn C.; Bergman, J. *Eur. J. Org. Chem.* **2004,** *2004*, 1286-1297; (c) Ohki, S.; Nagasaka, T. 2-Amino-3-oxocyclopenta[b]indole. JP48014658A, 1973.

135. Pretsch, E.; Bühlmann, P.; Badertscher, M., 13C NMR Spectroscopy. In *Structure Determination of Organic Compounds: Tables of Spectral Data*, Springer Berlin Heidelberg: Berlin, Heidelberg, 2009; pp 1-88.

136. Grimblat, N.; Zanardi, M. M.; Sarotti, A. M. *J. Org. Chem.* **2015,** *80*, 12526-12534.

137. Shibata, K.; Fukuwatari, T. *J. Nutr.* **2012,** *142*, 2227S-2230S.

138. Garo, E.; Starks, C. M.; Jensen, P. R.; Fenical, W.; Lobkovsky, E.; Clardy, J. *J. Nat. Prod.* **2003,** *66*, 423-426.

139. (a) Lin, Y.; Shao, Z.; Jiang, G.; Zhou, S.; Cai, J.; Vrijmoed, L. L. P.; Gareth Jones, E. B. *Tetrahedron* **2000,** *56*, 9607-9609; (b) Chang-Lun, S.; Chang-Yun, W.; Yu-Cheng, G.; Ji-Wen, C.; Dong-Sheng, D.; Zhi-Gang, S.; Yong-Cheng, L. *Lett. Org. Chem.* **2009,** *6*, 387-391.

140. Capon, R. J.; Ratnayake, R.; Stewart, M.; Lacey, E.; Tennant, S.; Gill, J. H. *Org. Biomol. Chem.* **2005,** *3*, 123-129.

141. Kanai, Y.; Fujimaki, T.; Kochi, S.-i.; Konno, H.; Kanazawa, S.; Tokumasu, S. *J. Antibiot.* **2004,** *57*, 24-28.

142. Parrish, S. M. Isolation and Structure Elucidation of New Marine Natural Products Isolated from Hawaiian Invertebrates. Ph.D. dissertation, University of Hawaii at Manoa, 2017.

143. Jaki, B.; Zerbe, O.; Heilmann, J.; Sticher, O. *J. Nat. Prod.* **2001,** *64*, 154-158.

144. Jaki, B.; Orjala, J.; Sticher, O. *J. Nat. Prod.* **1999,** *62*, 502-503.

145. Jaki, B.; Orjala, J.; Heilmann, J.; Linden, A.; Vogler, B.; Sticher, O. *J. Nat. Prod.* **2000,** *63*, 339-343.

146. Volk, R.-B. *Microbiol. Res.* **2008,** *163*, 307-313.

147. Rohrlack, T.; Christiansen, G.; Kurmayer, R. *Appl. Environ. Microbiol.* **2013,** *79*, 2642-2647.

148. Pant, I.; Rao, S. G.; Kondaiah, P. *Sci. Rep.* **2016,** *6*, 1-15.

149. (a) Murphy, K. L.; Herzog, T. A. *Hawai'i J. Med. Public Health* **2015,** *74*, 406-411; (b) Williams, S.; Malik, A.; Chowdhury, S.; Chauhan, S. *Addict. Biol.* **2002,** *7*, 147-154.

150. Brownrigg, H., *Betel Cutters*. Thames and London: London, UK, 1992.

151. (a) Banerjee, A. G.; Bhattacharyya, I.; Vishwanatha, J. K. *Mol. Cancer Ther.* **2005,** *4*, 865-875; (b) Metzger, K.; Angres, G.; Maier, H.; Lehmann, W. D. *Free Radic. Biol. Med.* **1995,** *18*, 185-94.

152. (a) *IARC Monogr. Eval. Carcinog. Risks Hum.* **1985,** *37*, 141-200; (b) Sekkade Kiyingi, K. *Lancet* **1992,** *340*, 1357-1358; (c) Sharan, R. N.; Mehrotra, R.; Choudhury, Y.; Asotra, K. *PLoS One* **2012,** *7*, 1-21.

153. (a) Garcia-Algar, O.; Vall, O.; Alameda, F.; Puig, C.; Pellegrini, M.; Pacifici, R.; Pichini, S. *Arch. Dis. Child. Fetal Neonatal Ed.* **2005,** *90*, F276-F277; (b) Gupta, P. C.; Ray, C. S. *Ann. Acad. Med. Singapore* **2004,** *33*, 31-36; (c) Javed, F.; Bello Correra, F. O.; Chotai, M.; Tappuni, A. R.; Almas, K. *Scand. J. Public Health* **2010,** *38*, 838-844; (d) Taylor, R. F. H.; Al-Jarad, N.; John, L. M. E.; Barnes, N. C.; Conroy, D. M. *Lancet* **1992,** *339*, 1134-1136; (e) Yang, M. J.; Chung, T. C.; Yang, M. J.; Hsu, T. Y.; Ko, Y. C. *J. Toxicol. Environ. Health A* **2001,** *64*, 465-472; (f) Zhang, L. N.; Yang, Y. M.; Xu, Z. R.; Gui, Q. F.; Hu, Q. Q. *J. Zhejiang Univ. Sci. B* **2010,** *11*, 681-689.

154. (a) Haddock, R. L.; Whippy, H. J.; Talon, R. J.; Montano, M. V. *Asian Pac. J. Cancer Prev.* **2009,** *10*, 57-62; (b) Paulino, Y. C.; Novotny, R.; Miller, M. J.; Murphy, S. P. *Hawaii J. Public Health* **2011,** *3*, 19-29; (c) Pobutsky, A. M.; Neri, E. I. *Hawai'i J. Med. Public Health* **2012,** *71*, 23-26.

155. Yang, W. Q.; Wang, H. C.; Wang, W. J.; Wang, Y.; Zhang, X. Q.; Ye, W. C. *Zhong Yao Cai* **2012,** *35*, 400-403.

156. Peng, W.; Liu, Y. J.; Wu, N.; Sun, T.; He, X. Y.; Gao, Y. X.; Wu, C. J. *J. Ethnopharmacol.* **2015,** *164*, 340-356.

157. (a) Jeng, J. H.; Chang, M. C.; Hahn, L. J. *Oral Oncol.* **2001,** *37*, 477-492; (b) Jeng, J. H.; Wang, Y. J.; Chiang, B. L.; Lee, P. H.; Chan, C. P.; Ho, Y. S.; Wang, T. M.; Lee, J. J.; Hahn, L. J.; Chang, M. C. *Carcinogenesis* **2003,** *24*, 1301-1315.

158. Bhide, S. V.; Shivapurkar, N. M.; Gothoskar, S. V.; Ranadive, K. J. *Br. J. Cancer* **1979,** *40*, 922-926.

159. Wary, K. K.; Sharan, R. N. *Int. J. Cancer* **1991,** *47*, 396-400.

160. Chang, L. Y.; Wan, H. C.; Lai, Y. L.; Kuo, Y. F.; Liu, T. Y.; Chen, Y. T.; Hung, S. L. *J. Periodontal Res.* **2009,** *44*, 175-183.

161. Gonda, T. A.; Tu, S.; Wang, T. C. *Cell Cycle* **2009,** *8*, 2005-2013.

162. Ryan, G. B.; Majno, G. *Am. J. Pathol.* **1977,** *86*, 183-276.

163. (a) Doherty, D. E.; Downey, G. P.; Worthen, G. S.; Haslett, C.; Henson, P. M. *Lab. Invest.* **1988,** *59*, 200-213; (b) Gabay, C.; Kushner, I. *N. Engl. J. Med.* **1999,** *340*, 448-454; (c) Melnicoff, M. J.; Horan, P. K.; Morahan, P. S. *Cell. Immunol.* **1989,** *118*, 178-191.

164. Paul, W. E.; Seder, R. A. *Cell 76*, 241-251.

165. Paduch, R.; Kandefer-Szerszen, M.; Piersiak, T. *Oncol. Res.* **2010,** *18*, 419-436.

166. (a) Bhandare, A. M.; Kshirsagar, A. D.; Vyawahare, N. S.; Hadambar, A. A.; Thorve, V. S. *Food Chem. Toxicol.* **2010,** *48*, 3412-3417; (b) Khan, S.; Mehmood, M. H.; Ali, A. N.; Ahmed, F. S.; Dar, A.; Gilani, A. H. *J. Ethnopharmacol.* **2011,** *135*, 654-661.

167. (a) Chiang, S. L.; Chen, P. H.; Lee, C. H.; Ko, A. M.; Lee, K. W.; Lin, Y. C.; Ho, P. S.; Tu, H. P.; Wu, D. C.; Shieh, T. Y.; Ko, Y. C. *Cancer Res.* **2008,** *68*, 8489-8498; (b) Trivedy, C. R.; Craig, G.; Warnakulasuriya, S. *Addict. Biol.* **2002,** *7*, 115-125.

168. McFadzean, I.; Gibson, A. *Br. J. Pharmacol.* **2002,** *135*, 1-13.

169. Rasmussen, U.; Broogger Christensen, S.; Sandberg, F. *Acta Pharm. Suec.* **1978,** *15*, 133-140.

170. Eloff, J. N. *J. Ethnopharmacol.* **1998,** *60*, 1-8.

171. Hung, S. L.; Chen, Y. L.; Wan, H. C.; Liu, T. Y.; Chen, Y. T.; Ling, L. J. *J. Periodontal Res.* **2000,** *35*, 186-193.

172. Ghelardini, C.; Galeotti, N.; Lelli, C.; Bartolini, A. *Farmaco* **2001,** *56*, 383-385.

173. (a) *IARC Monogr. Eval. Carcinog. Risks Hum.* **2004,** *85*, 1-334; (b) Chavan, Y. V.; Singhal, R. S. *J. Sci. Food Agric.* **2013,** *93*, 2580-2589; (c) Joshi, M.; Gaonkar, K.; Mangoankar, S.; Satarkar, S. *Int. Curr. Pharm. J.* **2012**, 128-132.

174. Baran, I.; Katona, E.; Ganea, C. *Pflugers Arch.* **2013,** *465*, 1101-1119.

175. Williams, V. M.; Porter, L. J.; Hemingway, R. W. *Phytochemistry* **1983,** *22*, 569-572.

176. Esatbeyoglu, T.; Jaschok-Kentner, B.; Wray, V.; Winterhalter, P. *J. Agric. Food Chem.* **2011,** *59*, 62-69.

177. Haney, P.; Herting, K.; Smith, S., Molecular weight cut-off (MWCO) specifications and rates of buffer exchange with Slide-A-Lyzer Dialysis Devices and Snakeskin Dialysis Tubing. In *Separation Characteristics of Dialysis Membranes*, ThermoFisher Scientific: https://www.thermofisher.com, 2013.

178. Hammerstone, J. F.; Lazarus, S. A.; Schmitz, H. H. *J. Nutr.* **2000,** *130*, 2086S-2092S.

179. Wang, C. C.; Huang, P. L.; Liu, T. Y.; Jan, T. R. *Toxicol. In Vitro* **2009,** *23*, 1234-1241.

180. Gu, L.; Kelm, M.; Hammerstone, J. F.; Beecher, G.; Cunningham, D.; Vannozzi, S.; Prior, R. L. *J. Agric. Food Chem.* **2002,** *50*, 4852-4860.

181. Nakao, Y.; Uehara, T.; Matsunaga, S.; Fusetani, N.; van Soest, R. W. *J. Nat. Prod.* **2002,** *65*, 922-924.

182. Roll, D. M.; Chang, C. W. J.; Scheuer, P. J.; Gray, G. A.; Shoolery, J. N.; Matsumoto, G. K.; Van Duyne, G. D.; Clardy, J. *J. Am. Chem. Soc.* **1985,** *107*, 2916-2920.

183. Hagmann, L.; Jüttner, F. *Tetrahedron Lett.* **1996,** *37*, 6539-6542.

184. Papke, U.; Gross, E. M.; Francke, W. *Tetrahedron Lett.* **1997,** *38*, 379-382.

185. Hodges, R.; Porte, A. L. *Tetrahedron* **1964,** *20*, 1463-1467.

186. Okunade, A. L.; Wiemer, D. F. *J. Nat. Prod.* **1985,** *48*, 472-473.

187. (a) Cantín, Á.; Moya, P.; Castillo, M.-A.; Primo, J.; Miranda, M. A.; Primo-Yúfera, E. *Eur. J. Org. Chem.* **1999,** *1999*, 221-226; (b) Moya, P.; Cantín, Á.; Castillo, M.-A.; Primo, J.; Miranda, M. A.; Primo-Yúfera, E. *J. Org. Chem.* **1998,** *63*, 8530-8535.

188. Pimenta, E. F.; Vita-Marques, A. M.; Tininis, A.; Seleghim, M. H. R.; Sette, L. D.; Veloso, K.; Ferreira, A. G.; Williams, D. E.; Patrick, B. O.; Dalisay, D. S.; Andersen, R. J.; Berlinck, R. G. S. *J. Nat. Prod.* **2010,** *73*, 1821-1832.

189. Frisch, M. J.; Trucks, G. W.; Schlegel, H. B.; Scuseria, G. E.; Robb, M. A.; Cheeseman, J. R.; Scalmani, G.; Barone, V.; Mennucci, B.; Petersson, G. A.; Nakatsuji, H.; Caricato, M.; Li, X.; Hratchian, H. P.; Izmaylov, A. F.; Bloino, J.; Zheng, G.; Sonnenberg, J. L.; Hada, M.; Ehara, M.; Toyota, K.; Fukuda, R.; Hasegawa, J.; Ishida, M.; Nakajima, T.; Honda, Y.; Kitao, O.; Nakai, H.; Vreven, T.; Montgomery, J. A.; Peralta, J. E.; Ogliaro, F.; Bearpark, M.; Heyd, J. J.; Brothers, E.; Kudin, K. N.; Staroverov, V. N.; Kobayashi, R.; Normand, J.; Raghavachari, K.; Rendell, A.; Burant, J. C.; Iyengar, S. S.; Tomasi, J.; Cossi, M.; Rega, N.; Millam, J. M.; Klene, M.; Knox, J. E.; Cross, J. B.; Bakken, V.; Adamo, C.; Jaramillo, J.; Gomperts, R.; Stratmann, R. E.; Yazyev, O.; Austin, A. J.; Cammi, R.; Pomelli, C.; Ochterski, J. W.; Martin, R. L.; Morokuma, K.; Zakrzewski, V. G.; Voth, G. A.; Salvador, P.; Dannenberg, J. J.; Dapprich, S.; Daniels, A. D.;

Farkas; Foresman, J. B.; Ortiz, J. V.; Cioslowski, J.; Fox, D. J., Gaussian 09, Revision B.01. Wallingford CT, 2009.

190. (a) Cammi, R.; Tomasi, J. *J. Comput. Chem.* **1995,** *16*, 1449-1458; (b) Miertuš, S.; Tomasi, J. *Chem. Phys.* **1982,** *65*, 239-245.

191. (a) Gross, E. K. U.; Dobson, J. F.; Petersilka, M. *Top. Curr. Chem.* **1996,** *181*, 81-159; (b) Runge, E.; Gross, E. K. U. *Phys. Rev. Lett.* **1984,** *52*, 997-1000.

192. Kumar, S.; Stecher, G.; Tamura, K. *Mol. Biol. Evol.* **2016,** *33*, 1870-1874.

193. (a) Shaaban, M.; Abd-Alla, H. I.; Hassan, A. Z.; Aly, H. F.; Ghani, M. A. *Org. Med. Chem. Lett.* **2012,** *2*, 30-41; (b) Zhang, X.; Geoffroy, P.; Miesch, M.; Julien-David, D.; Raul, F.; Aoudé-Werner, D.; Marchioni, E. *Steroids* **2005,** *70*, 886-895.

194. (a) Costa, F. L. P.; Bessa Oliveira de Fernandes, S.; Eccard Fingolo, C.; Boylan, F.; Ferreira de Albuquerque, A. C.; Martins dos Santos Junior, F.; de Amorim, M. *Quantum Matter* **2016,** *5*, 675-679; (b) Valdes, L. J., 3rd *J. Nat. Prod.* **1986,** *49*, 171-171; (c) Panyo, J.; Matsunami, K.; Panichayupakaranant, P. *Pharm. Biol.* **2016,** *54*, 1522-1527.